MICROWAVE CURING OF HYBRID INORGANIC-ORGANIC CERAMERS AND SOME ADDITIONAL STRUCTURAL FEATURES OF THESE MATERIALS.

by

DAVID ERNEST RODRIGUES

DISSERTATION submitted to the Faculty of the

Virginia Polytechnic Institute and State University

in partial fulfillment of the requirements for the degree of

DOCTOR OF PHILOSOPHY

in

MATERIALS ENGINEERING AND SCIENCE

APPROVED:

G. L. WILKES

T. C. WARD

J. E. McGRATH

J. P. WIGHTMAN

J. L. LYTTON

24 JUNE 1991

Blacksburg, Virginia

MICROWAVE CURING OF HYBRID INORGANIC-ORGANIC CERAMERS AND SOME ADDITIONAL STRUCTURAL FEATURES OF THESE MATERIALS.

by

DAVID ERNEST RODRIGUES

G. L. WILKES, Chairman

MATERIALS ENGINEERING AND SCIENCE

(ABSTRACT)

This dissertation reflects the results of probably the very first attempt to cure sol gel ceramers using microwaves. These materials were first prepared in 1985, but were found to take almost two to six days to cure, when stored under ambient conditions. Microwaves have been found to provide a method for circumventing this problem under certain conditions. It was discovered that the more highly phase separated ceramer systems can be cured in twenty minutes when subjected to heating in a microwave field. Curing in a conventional oven, has on the other hand been found to hinder the extent of reaction because the slow initial rate of heating (which allows for evaporation of some of the compatibilizing solvent media) is believed to leave the reactants in a somewhat diffusion limited state.

Dielectric investigations on the ceramer films show the existance of Maxwell Wagner Sillars intefacial polarization which results from charge migration in the ceramer system and also show the possibility of PTMO chain expansion

at higher metal alkoxide contents in these ceramers when cast onto a substrate onto which the film adheres. Finally, structural investigations into the ceramers using SAXS, gives an idea of the fractal dimensions of the scattering phases. These investigations have also proved quite conclusively that there exists a contribution to scattering from the porosity present in the inorganic phase at metal alkoxide contents as low as 40 wt%.

Acknowledgements

The author would first like to thank his advisor Dr. G. L. Wilkes for his advice, patience, guidance and above all for permitting him the freedom to pursue his research in whatever manner he chose to. A large measure of the authors success during the course of his M. S. and Ph. D. was possible mainly because of the interdisciplinary nature of the Polymer Materials Interfaces Laboratories which permitted him to work without hindrance at any of their laboratories on campus. The author would especially like to thank Dr T. C. Ward and the students at his labs for their cooperation and support during the course of his Ph. D.

Thanks are also due to Dr. William Conger and the secretaries Diane P., Sandy, Diane C., Sue and Carol for the immeasurable help rendered to him without which, getting his Ph. D. might have been twice as hard.

The author would also like to thank Dr. A. B. Brennan, Dr. G. A. York, Dr. Graybeal, Ken Baker, Don Brandom, Steve McCartney and other colleagues for their help and for a number of useful discussions that he had with them over the years.

Finally, the author would like to thank his immediate family as well as his Uncle Melville (and his family) whose sacrificies and help, made this course of study in the U. S. A. possible. The author will be ever grateful for their support.

Table of Contents

A BRIEF HISTORY OF CERAMER MATERIALS AND THE RATIONALE FOR PURSUING THIS RESEARCH **1**

INTRODUCTION 5

CHAPTER 1 ..... **9**

LITERATURE REVIEW 9

1-1 HISTORY AND BACKGROUND 9

1-2 WAVEGUIDE THEORY AND MATHEMATICS 15

1-2-1 RECTANGULAR WAVEGUIDES 15

1-2-2 CIRCULAR WAVEGUIDES 25

1-2-3 GENERAL WAVEGUIDE AND CAVITY THEORY 27

1.3 CAVITY PERTURBATION 30

1-4 MICROWAVES AS A HEAT SOURCE 31

1-4-1 INTRODUCTION AND GENERAL THEORY 31

1.5 DEPENDENCE OF HEATING UPON THE STRUCTURE OF MOLECULES 42

1.6 MACROSCOPIC CONSIDERATIONS FOR MICROWAVE HEATING 44

1.7 MICROWAVES AS A HEATING SOURCE FOR REACTIONS 54

1.8 SOL-GEL REACTIONS 61
1.9 AGING OF GELS 69
1.10 CERAMERS: SOME GENERAL STRUCTURAL FEATURES OF PTMO CONTAINING HYBRIDS 71

CHAPTER 2 ..... **76**
EXPERIMENTAL 76
2.1 MATERIALS 76
2.2 MICROWAVE EQUIPMENT 80
2.2.1 CYLINDERICAL CAVITY 80
2.2.2 LUXTRON FIBRE OPTIC TEMPERATURE PROBE 89
2.2.3 RECTANGULAR CAVITY 91
2.2.4 STUB TUNER AND SLIDING SHORT 91
2.3 CHARACTERIZATION METHODS 96
2.3.1 SMALL ANGLE XRAY SCATTERING 96
2.3.2 DYNAMIC MECHANICAL ANALYSIS 97
2.3.3 DIELECTRIC ANALYSIS 97
2.3.4 THERMAL ANALYSIS 98
2.3.5 STRESS STRAIN ANALYSIS 99
2.3.6 SCANNING AND TRANSMISSION ELECTRON MICROSCOPY 99
2.3.7 SWELLING EXPERIMENTS 100
2.3.8 DIELECTRIC NETWORK ANALYSIS 100

CHAPTER 3 ..... **102**
STRUCTURE PROPERTY BEHAVIOR OF TEOS/PTMO CERAMERS CURED IN SOLVENT MEDIA OF N, N DIMETHYLFORMAMIDE AND ISOPROPANOL 102
3.1 BRIEF HISTORY OF THE USE OF N, N DIMETHYLFORMAMIDE IN SOL GEL CHEMISTRY 103
3.1. INTRODUCTION AND OBJECTIVES 104

3.2 EXPERIMENTAL METHODS AND SAMPLE PREPARATION 106
3.3 RESULTS AND DISCUSSION 113
3.3.1 STRESS STRAIN ANALYSIS 113
3.3.2 DYNAMIC MECHANICAL ANALYSIS OF THE DIFFERENTLY CURED CERAMERS . 117
3.3.3 SMALL ANGLE XRAY SCATTERING 127
3.4 AGING BEHAVIOR OF THESE TEOS/PTMO CERAMERS 129
3.4.1 STRESS STRAIN ANALYSIS ON AGED TEOS/PTMO CERAMERS 131
3.4.2 SMALL ANGLE XRAY SCATTERING OF AGED MATERIALS 133
3.4.3 DYNAMIC MECHANICAL ANALYSIS OF THE AGED CERAMERS 137
3.5 EXPERIMENT TO OBTAIN AN ACTUAL IMAGE OF THE MICROWAVE CURED TEOS/PTMO CERAMERS 139
3.5.1 SMALL ANGLE XRAY SCATTERING OF THE TEOS/PTMO CERAMERS AS A FUNCTION OF METAL ALKOXIDE CONTENT 141
3.5.2 TRANSMISSION ELECTRON MICROSCOPY STUDIES OF THESE TEOS/PTMO CERAMERS AS A FUNCTION OF METAL ALKOXIDE CONTENT 142
3.6 CONCLUSIONS 146

CHAPTER 4 ..... **148**
STRUCTURE PROPERTY RELATIONSHIPS IN TEOS/PTMO CERAMERS CURED IN SOLVENT MEDIA OF TETRAHYDROFURAN AND ISOPROPANOL 148
4.1 INTRODUCTION AND OBJECTIVES 149
4.2 SAMPLE PREPARATION PROCEDURES 151
4.3 RESULTS AND DISCUSSION 160
4.3.1 DYNAMIC MECHANICAL ANALYSIS 160
4.3.2 MECHANICAL PROPERTIES 166
4.3.3 SMALL ANGLE XRAY SCATTERING (SAXS) ANALYSIS 171
4.5 CONCLUSIONS 174

CHAPTER 5 ..... **176**

EFFECT OF SOLVENT ON THE TEOS/PTMO REACTION 176

5.1 INTRODUCTION AND OBJECTIVES 176

5.2 EXPERIMENTAL 179

5.3 RESULTS AND DISCUSSION 185

STAGE A 185

5.3.1 MEASUREMENTS MADE ON INDIVIDUAL REACTANTS 185

.STAGE B 189

5.3.2 MEASUREMENTS MADE ON THE REACTION MIXTURE BEFORE THE ADDITION OF ACID 189

5.3.2.1 DIELECTRIC AND TEMPERATURE-TIME HEATING MEASUREMENTS 189

5.3.2.2 DIELECTRIC MEASUREMENTS 194

5.3.2.3 TIME-TEMPERATURE HEATING EXPERIMENTS 196

5.3.3 MEASUREMENTS MADE AFTER THE ADDITION OF ACID CATALYST 197

5.3.3.1 DIELECTRIC MEASUREMENTS 197

5.3.3.2 TEMPERATURE TIME HEATING MEASUREMENTS AFTER THE ADDITION OF ACID 201

5.4 SOLUTION SMALL ANGLE XRAY SCATTERING RESULTS 205

5.5 STRESS STRAIN PROPERTIES OF TEOS/PTMO CERAMER MATERIALS 210

5.6 SMALL ANGLE XRAY SCATTERING ON FILMS 214

5.7 CONCLUSIONS 217

CHAPTER 6 ..... **219**

STRUCTURE PROPERTY RELATIONSHIPS IN MICROWAVE CURED TIOPR/PTMO AND ZROPR/PTMO CERAMERS 219

6.1 INTRODUCTION 219

6.2 RESEARCH AND OBJECTIVES 220

6.3 EXPERIMENTAL 222

6.4 RESULTS AND DISCUSSION 233

6.4.1 MECHANICAL PROPERTIES OF THE TiOPr/PTMO CERAMERS 233
6.4.2 MECHANICAL PROPERTIES OF THE ZrOPr/PTMO CERAMERS 235
6.4.3 DYNAMIC MECHANICAL SPECTROSCOPY FOR THE TiOPr/PTMO CERAMERS .. 237
6.4.4 DYNAMIC MECHANICAL BEHAVIOR OF ZrOPr/PTMO CERAMERS 242
6.4.5 SMALL ANGLE XRAY SCATTERING OF THE TiOPr/PTMO CERAMERS 247
6.4.6 SAXS PROFILES FOR THE ZrOPr/PTMO CERAMERS 249
6.5 CONCLUSIONS 251

CHAPTER 7 ..... **253**
INVESTIGATIONS INTO THE DIELECTRIC PROPERTIES OF CERAMERS 253
7.1 INTRODUCTION 253
7.2 EXPERIMENTAL 255
7.3 RESULTS AND DISCUSSION 257
7.3.1 DIELECTRIC SPECTROSCOPY OF TiOPr/PTMO CERAMERS 257
7.3.1.1 EFFECT OF METAL ALKOXIDE CONTENT 257
7.3.1.2 EFFECT OF METAL ALKOXIDE TYPE 283
7.3.1.3 EFFECT OF SOLVENT ON THE TEOS/PTMO CERAMERS 286
7.3.1.4 EFFECT OF AGEING 297
7.4 THE CASE FOR EXPANDED PTMO CHAINS 301
7.4.1 EFFECT OF METAL ALKOXIDE CONTENT UPON THE CHAIN DIMENSIONS 307
7.4.2 EFFECT OF SOLVENT ON THE CHAIN DIMENSIONS 314
7.5 SUMMARY AND CONCLUSIONS 316

CHAPTER 8 ..... **319**
STRUCTURAL INVESTIGATIONS INTO CERAMERS DURING THE PROCESS OF GELATION 319
8.1 INTRODUCTION 319
8.2 FRACTALS: A BRIEF DISCUSSION ON THEIR FORM, SHAPE AND SIZE 322
8.3 EXPERIMENTAL 325

8.4 RESULTS AND DISCUSSION 328
8.4.1 NATURE OF GROWTH OF THE SILICATE PHASES 328
8.4.1.1 TEOS/PTMO CERAMERS REACTED IN DMF/IPA 328
8.4.2 PHASE MIXING AND POROSITY IN THESE TEOS/PTMO CERAMERS REACTED IN DMF/IPA AS A FUNCTION OF TEOS CONTENT 351
8.5 STRUCTURE OF THE INORGANIC PHASE IN THE TEOS/PTMO CERAMERS REACTED IN THF/IPA 357
8.6 STRUCTURE OF THE INORGANIC PHASE IN THE TiOPr/PTMO CERAMERS 366
8.6.1 STUDY OF THE TiOPr SOL USING SAXS 366
8.6.2 STUDY OF THE TiOPr/PTMO CERAMERS 369
8.7 CONCLUSIONS 376

1.0 CHAPTER 9 381
RECOMMENDATIONS AND FUTURE WORK 381
REFERENCES 386

A BRIEF HISTORY OF CERAMER MATERIALS AND THE RATIONALE FOR PURSUING THIS RESEARCH

This work reflects a beginning on the applications of microwaves to the curing of sol-gel derived hybrid materials called ceramers (1). These hybrid materials were first synthesized in 1985 using tetraethylorthosilicate (TEOS) and silanol terminated polydimethylsiloxane (PDMS) by conventional thermal curing (1). The reaction between the TEOS and the bifunctional PDMS was acid catalyzed. The acid catalyzed TEOS develops into a more linear inorganic species as has been reported by Schaefer et al (2). These ceramer films were typically 5 to 20 mils in thickness and were optically transparent. The films were found to be flexible in general, except when high weight fractions of TEOS was initally used in which case brittleness was noted. The effect of acid level, water level

and oligomer molecular weight on the structure property relationships of these ceramer films were also studied (1). From studies such as these, it was found that these ceramers had a low elastic modulus and a low tensile strength. These were attributed to network defects such as dangling chain ends as well as the generally poorer mechanical properties of PDMS.

In order to facilitate the development of better mechanical properties in these hybrid materials, recourse was taken to the use of isocyanatopropyltriethoxysilane endcapped polytetramethyleneoxide (PTMO) instead of the bifunctional PDMS (1). The presence of trifunctional reactive groups at each end of the PTMO chains helped acheive a higher extent of incorporation of the oligomer into the ceramer network. The films obtained from the reaction between endcapped PTMO and TEOS were also transparent, which indicated the lack of any macrophase separation. These reactions were conducted at room temperature and they took from two to six days to obtain films which could be handled and tested. The oligomer molecular weight was also varied from 650 g/mole to 2900 g/mole and the mechanical properties were found to be dependent upon oligomer molecular weight as well as the the composition ratio of the alkoxide to the PTMO.

Wang subsequently formulated several equivalent ceramer systems in which the metal alkoxide was varied from TEOS to titanium isopropoxide Ti(OPr) and to zirconium isopropoxide Zr(OPr), while the oligomeric component was maintained as endcapped PTMO of M_n = 2000 g/mole. The Ti(OPr)/PTMO and

Zr(OPr)/PTMO ceramers were characterized and studied by Brennan (3). It was found that both titanium isopropoxide and zirconium tetraisopropoxide, which are more reactive than TEOS, produced better mechanical properties. The general morphological features for these titania and zirconia systems were found to be the same as their TEOS based counterparts (3). These reactions like those of the TEOS/PTMO ceramers were also conducted at room temperature. One of the limitations of this approach i. e. curing at room temperature, was the extensive period of time taken for the attainment of a sufficiently high extent of cure so that the sample can be handled and tested. While the time interval between the casting of the sample and subsequent testing of the ceramer film was found to vary depending upon the reactivity of the metal alkoxide, it generally exceeded a period of two days. In order to bring about a quicker turnaround time in the production of ceramer films it was decided to attempt curing at higher temperatures using different approaches. This then became the primary focus of the work documented in this dissertation.

In order to acheive the objective of a quicker sample production time two routes were chosen for elevating the temperature of the reactants. One method consisted of utilizing a conventional convection oven while the other method consisted of heating the sample using electromagnetic waves in the microwave frequency range - the latter method being the principle focus of this dissertation.

Microwaves heat materials by means of direct energy transfer to the dipolar molecules in a material. The heating is therefore dependent upon the strength of permanent or induced dipoles present in the reacting mixture. Many reactions conducted in microwave fields have been enhanced significantly purely as a result of the nature of energy transfer (4). Microwave radiation has further been successfully used to heat materials for several purposes such as the drying of paper and pulp, curing of epoxies, styrene butadiene rubber etc. Attempts to conduct curing reactions in a microwave field have in general been successful as will be seen in chapter 1 and in a number of cases significantly different morphologies have been observed between microwave cured and oven cured materials. In several cases, lower power and reduced curing times were sufficient to attain the desired objectives in material processing with microwaves. Furthermore lower processing temperatures were sometimes found to produce successfully cured materials when microwave radiation was used to heat the reactants. Microwave radiation, however, had not been used to cure metal alkoxide based sol gel materials prior to this investigation. Keeping in mind some of the successful results reported with microwave curing and taking into consideration the extensive period of time required for curing TEOS/PTMO ceramers at room temperature it was decided to attempt the use of microwave radiation as a potential accelerator in the curing process.

INTRODUCTION

Chapter 1 consists of a literature review that deals extensively with the fundamentals behind microwave equipment and microwave principles used in this thesis. A small but nonetheless significant amount of literature exists on the heating of materials and reactions using microwave radiation and an attempt has been made to summarize these. The latter portion of this review is devoted to explaining certain aspects of metal alkoxide based sol gel reactions, which the author will make use of in describing some results in the later chapters of this thesis. Chapter 2 is a detailed description of experimental equipment and apparatus used for experimentation.

The four chapters, viz. 3 - 6, deal with comparisons of the structure-property relationships between microwaved and oven cured materials. In chapter 3, acid catalyzed reactions between TEOS and isocyanatopropyltriethoxysilane endcapped PTMO are conducted in a cosolvent system of N, N dimethylformamide (DMF) and isopropanol (IPA). The ratio of DMF to IPA was 1:1. TEOS constituted 60 wt% of the initial reaction mixture with respect to endcapped PTMO of M_n = 2000 g/mole. The water is added in a stoichiometric amount equivalent of 100wt%. Results obtained from mechanical testing show significantly better mechanical properties for the microwave cured system as

against those seen in the oven cured materials. Several reasons for the better properties of the microwave cured sample are proposed.

Chapter 4 deals with the same reactants utilized in the same proportion as in chapter 3 - the only difference being the use of tetrahydrofuran (THF) in conjunction with IPA as the cosolvent system. These materials show no significant difference in either structure or properties between samples subjected to microwave curing as compared with those cured in a conventional convection oven. However they show a significant difference in structure as well as properties from those documented in chapter 3 despite the fact that the reactants (except for the solvent) are essentially the same. Further there is a significant enhancement of properties brought about by microwave curing versus oven curing in the materials detailed in chapter 3.

To investigate the reasons for these differences a study of the governing factor i. e. effect of solvent, constituted the basis for chapter 5. Most of the research documented in this chapter has been performed on the reactants (TEOS/PTMO) in the solution state. The solvent composition was varied from pure IPA to IPA/DMF ratios of 1:3, 1:1, 3:1 to pure DMF. From this work, it is shown how different solvent ratios affect properties depending upon the method of processing. The results clearly show the effect that the nature of the solvent has upon the final structure and properties of the resulting ceramer films.

In chapter 6 the type of metal alkoxide is the principle variable; TEOS is first replaced with Ti(OPr) and then with Zr(OPr). Both of these latter metal alkoxides are known to be faster reacting than TEOS and hence it was decided to find out whether microwave processing can significantly alter the structure property behavior of these ceramers. In the case of the Zr(OPr)/PTMO systems no water was used except for that available from the acid catalyst. The results obtained from this research prove that water is a necessary element for enhancing the reaction rates utilizing microwave processing.

Chapter 7 represents a change from the preceding four chapters, in that it does not deal with microwaves. Instead deals with the dielectric properties of the (TEOS/PTMO, Ti(OPr)/PTMO and Zr(OPr)/PTMO) ceramer films in the solid state. These investigations show interesting properties based upon the microstructures of the ceramer. Maxwell Wagner Sillars interactions predominate in the highly phase separated materials (TEOS/PTMO reacted in DMF/IPA, Ti(OPr)/PTMO and Zr(OPr)/PTMO ceramers) above 0°C, but do not manifest themselves in the more mixed systems (TEOS/PTMO reacted in THF/IPA).

Chapter 8 deals with xray scattering experiments performed during the course of gelation in the TEOS/PTMO ceramers reacted in THF/IPA and DMF/IPA as well as the TiOPr/PTMO ceramers. Attempts were made to study the fractal dimensions of the scattering particles during the course of film formation (using SAXS).

Chapter 9 suggests future work to be considered on ceramer systems as well as recommendations for furthur verification of some of the proposed results and speculations in this dissertation.

CHAPTER 1

LITERATURE REVIEW

1-1 HISTORY AND BACKGROUND

Electromagnetic waves are generated whenever dipoles are made to oscillate by the application of an alternating electric field. It was J. C. Maxwell who first postulated that all light waves were electromagnetic in nature i. e. the electric vector and the magnetic vector are in phase with one another but the electric flux lines are 90° apart in space as shown in Fig 1.1. Either wave, however,

propagates in a direction at right angles to the flux lines. In other words the electric and magnetic fields are transverse to the direction of propagation. Such a wave is of the TEM (transverse electric, transverse magnetic) type, which occurs only in free space and on a conventional transmission line (not in a wave guide) (1). This is shown in Fig 1.2. Maxwell also calculated that all forms of light irrespective of the frequency travelled at a speed of 3×10^8 m/s in vaccuum. This makes it relatively easy to compute the frequency of light. Since velocity = distance/time, the velocity of an electromagnetic wave in free space is represented by

$$c = \frac{\lambda}{t} = f\lambda \qquad (1)$$

where c is the velocity of light, λ is the wavelength, t is the time and f is the frequency.

Microwave radiation may be defined as one region of the electromagnetic spectrum. The frequency range of microwaves is still open to debate.The microwave frequency band is claimed by some to begin at 890MHz, which is where the ultra-high-frequency(UHF) TV band finishes. Others contend that it begins at 300MHz at the beginning of the UHF band. It is generally accepted amongst the scientific community that microwaves extend from 1 GHz (1 GHz = 10^9Hz) to 1 Terahertz (1 THz = 10^{12}Hz) This provides for a rather large range of wavelengths from 0.03 centimeter at the higher end of the microwave frequency spectrum to 30 centimeter at the lower end of the spectrum. Since

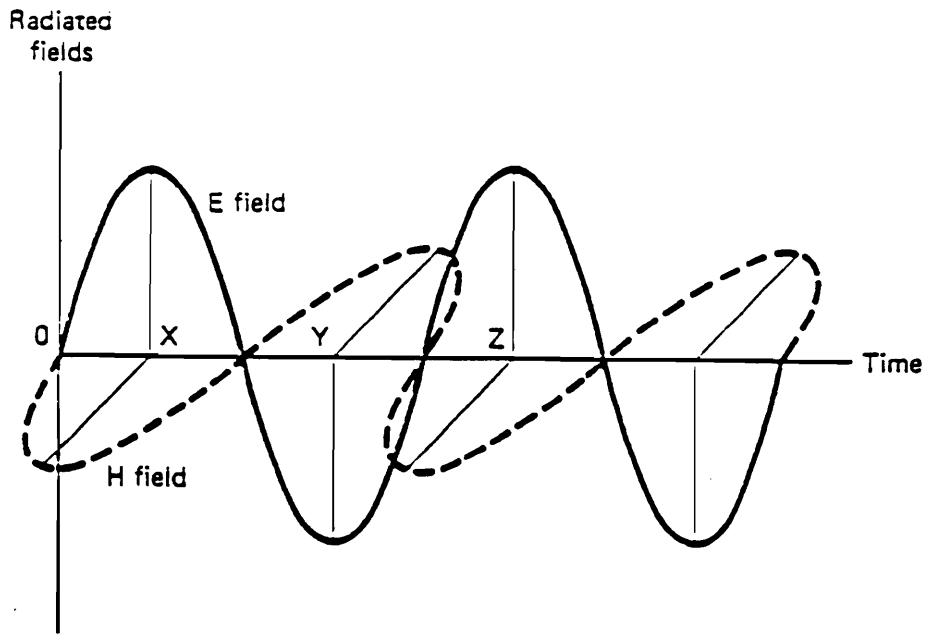


Figure 1.1. Schematic showing electrical and magnetic flux lines in an electromagnetic wave. (1)

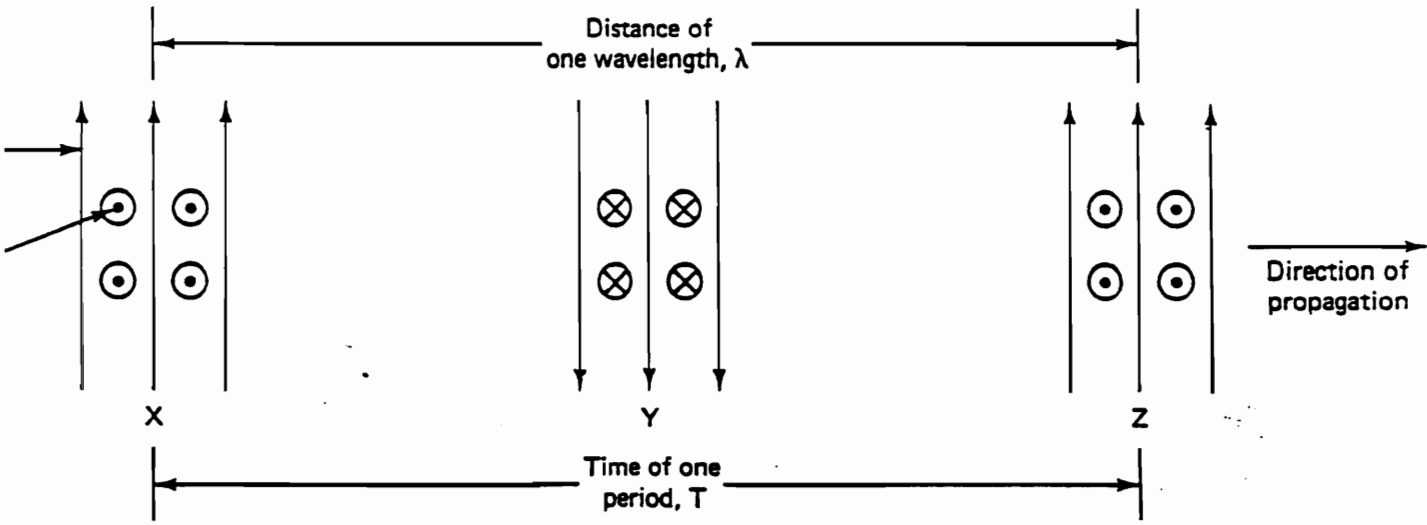


Figure 1.2. Schematic showing electrical and magnetic fields in free space (TEM wave) (1)

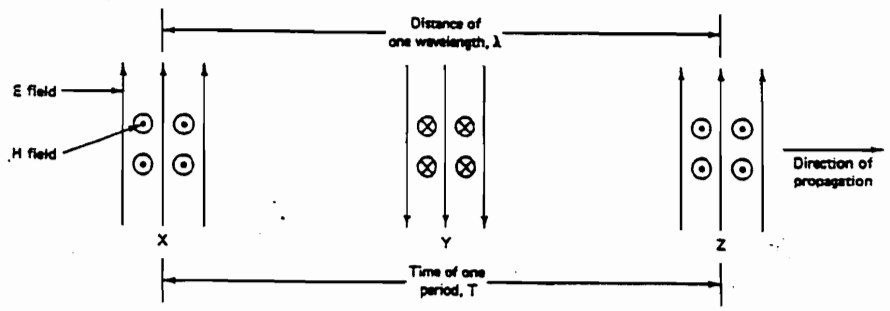


Figure 1.2. Schematic showing electrical and magnetic fields in free space (TEM wave) (1)

microwaves occupy the frequency spectrum from 1 GHz to 1THz equation (1) can be conveniently modified to :

$$\lambda = \frac{30}{f} \qquad (2)$$

where λ = wavelength(cm), f = frequency (GHz)

Since as stated above the microwave band encompasses a large range of frequencies, the microwave band has been further divided into four regions as shown in the Fig 1.3. This classification made specifically by the Industrial Scientific Medical Council serves the purpose of having users not interrupt one another's transmissions. For example the S band is used by radar surface detection systems, while the X band, which employs a frequency of 10GHz, is used by navigational radar. Standard home kitchen microwave ovens use a frequency of 2.45 GHz, which is also in the S band. Microwaves are used for various communication purposes such as satellite transmissions and radar because of their wide bandwidth's, straight line propagation and high antenna directivity (1, 2, 3). They have also been used for as a heating source for drying paper, wood pulp and more recently for conducting reactions and orientational drawing. It is on this latter aspect of heating, that this introduction will be drawn to, since the effect and the consequences arising out of it will eventually be the subject of most of the work presented in this thesis.

Letter designation	Frequency range (GHz)
L	1.12–1.7
S	2.6–3.95
C	3.95–5.85
X[a]	8.2–12.4
K	18.0–26.5

[a] The X band is not connected in any way with x-rays.

Figure 1.3. Table indicates the classification made by the Industrial Scientific Medical Council (1).

1-2 WAVEGUIDE THEORY AND MATHEMATICS

1-2-1 RECTANGULAR WAVEGUIDES

Since microwaves are of a much higher frequency than conventional electric current the method of transmission has to be varied in order to prevent severe dielectric losses. These losses are very high for conventional insulating materials such procelain, Bakelite, Lucite etc. and hence special insulating materials such polyethylene and polytetrafluoroethylene which have dielectric constants below three are typically used. Coaxial cables are often used to transmit microwave energy (1,2). However at high power levels even coaxial cables cannot be used for extensive lengths because of some copper losses and dielectric losses. In order to transmit microwaves over large distances, large hollow rectangular, circular or elliptical sections are used. These sections are typically made of metals and are called waveguides. Waveguides have one distinct disadvantage over other methods of transmission; they are inordinately bulky and take up a large amount of space. The size of a waveguide is dependent upon the frequency of the electromagnetic waves being transmitted. In order for an electromagnetic wave to be transmitted successfully down a rectangular waveguide, the wide dimension 'a' must exceed one half wavelength, corresponding to the frequency of the wave. If

λ_c (in meters) is the cutoff wavelength for a given wide dimension 'a'(in meters) as shown in the Fig 1.4, then

$$a = \frac{\lambda_c}{2} \tag{3}$$

and the cutoff frequency f_c in Hz

$$f_c = \frac{c}{\lambda_c} = \frac{c}{2a} \tag{4}$$

The narrow dimension 'b' is an important factor in determining the power handling capacity of the waveguide. A low value of 'b' may cause the voltage established between the walls to exceed the breakdown potential for the air dielectric and hence arcing may result (1,3).

Energy is transferred down the waveguide in the form of alternating electric (E) and magnetic (H) fields. Separate field patterns exist for the E field and the H field and these obey boundary conditions put forth by Maxwell two of these being:

a)All electrical flux lines must be perpendicular to the walls of the guide.

b)All magnetic flux lines at a wall must run parallel to the surface.

The above established conditions indicate that any electrical flux line at a wall surface would create a surface current in the wall and the line would be eliminated. Similarly a magnetic field having a component perpendicular to the surface would give rise to an eddy current and be eliminated. The

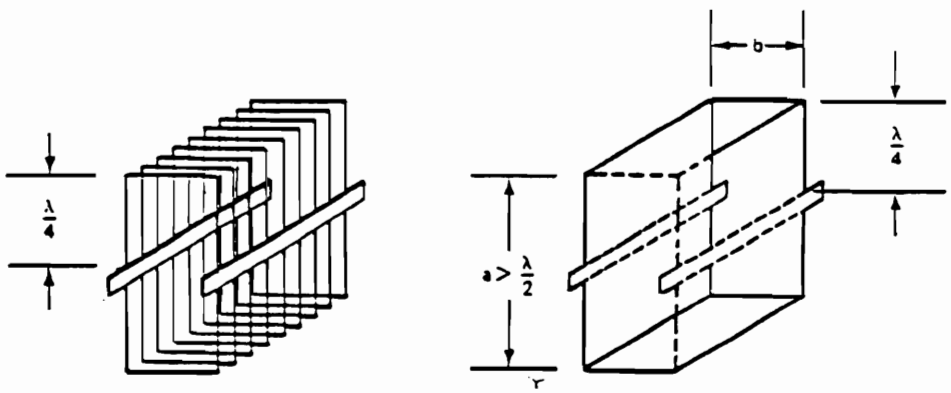


Figure 1.4. Section shows a rectangular waveguide formed by joining quarter waveguide stubs (1).

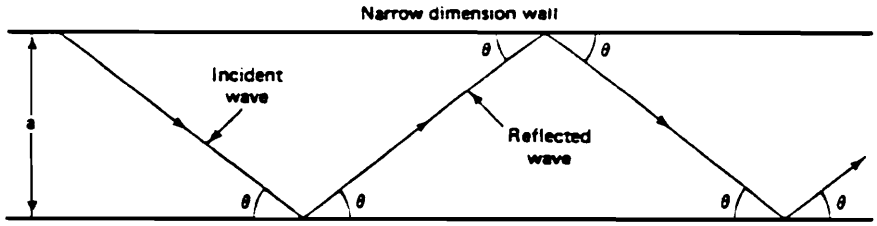


Figure 1.5. Path of electromagnetic wave in a rectangular waveguide (1).

electromagnetic wave does not have the same wavelength in a waveguide as in a vaccuum or free space. The electromagnetic energy progresses down the waveguide by a series of reflections of the internal surface of the narrow dimension as shown in Fig 1.5. The wavelength in a rectangular waveguide is therefore given by

$$\lambda_g = \frac{\lambda}{[1 - (\frac{\lambda}{2a})^2]^{1/2}} \tag{5}$$

where λ_g is the wavelength in the waveguide. In terms of the cutoff frequency f_c, Eq. 5 becomes

$$\lambda_g = \frac{\lambda}{[1 - (\frac{f_c}{f})^2]^{1/2}} \tag{6}$$

Waveguides are normally designed so that a single field pattern or mode is dominant. The mode may be defined as being either transverse electric (TE) or transverse magnetic (TM). In the TE mode all electric flux lines are at right angles to the direction of propagation, so that there are no lines which are parallel to the direction of travel. A dominant TE_{10} is shown in Fig 1.6. The subscripts are used to indicate the field patterns and are usually designated as m, n and p. In the case of a rectangular waveguide the first subscript m is the number of half wave patterns in the wide 'a' dimension while the second subscript n represents the number of half wave patterns in the narrow 'b' dimension. Subscript p represents the number of half wavelengths in the

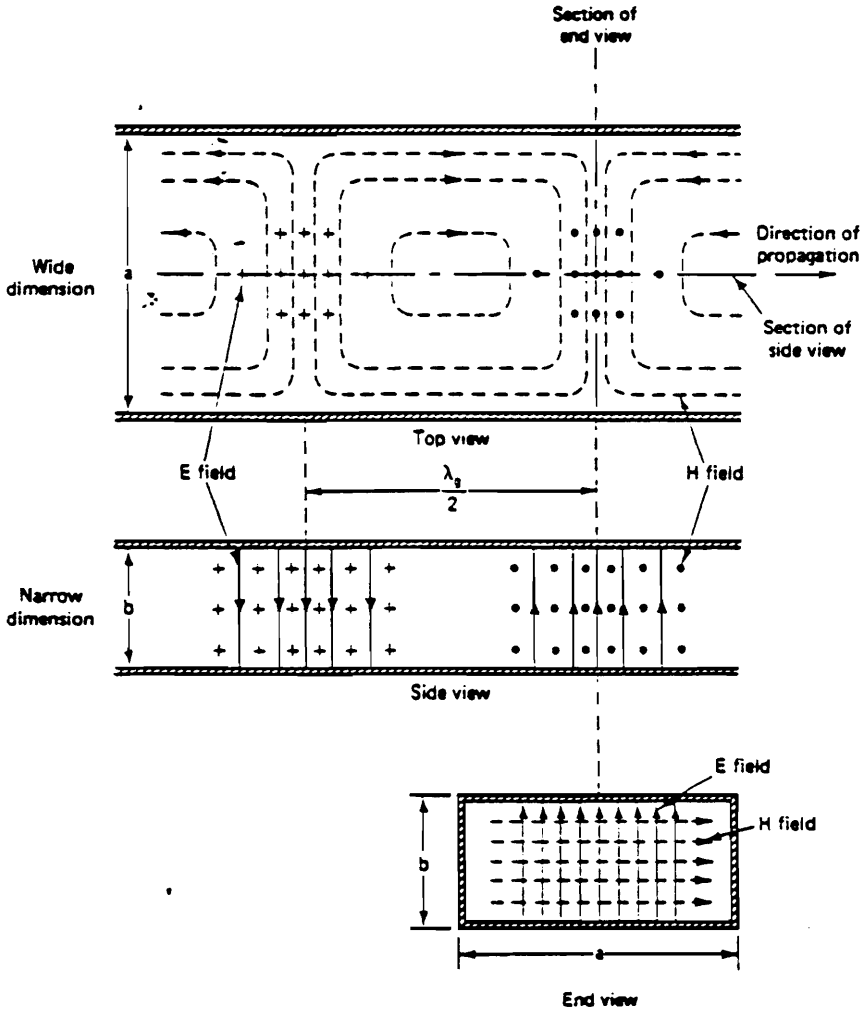


Figure 1.6. Schematic of dominant TE_{10} mode (1).

direction of propagation. For a dominant TM mode the H lines are entirely transverse. The dimensions of the waveguide determine the dominant mode i.e. other modes would require a different size waveguide. Theoretically a given resonator has an infinite number of resonant modes, and each mode corresponds to a definite resonant frequency (3). When the frequency of an impressed signal is equal to a resonant frequency, a maximum amplitude of the standing wave occurs, and the peak energies stored in the electric and magnetic fields are equal. The mode having the lowest resonant frequency is called the dominant frequency.Hence it is possible that if the frequency of the electromagnetic wave is raised above the critical value for the waveguide dimensions, then, the energy introduced into the waveguide can be split between several possible modes. This poses certain problems especially when attempting to dissipate energy in a certain manner from a field or when it is required to join two sections of a waveguide. In the above mentioned cases only the dominant mode will respond leaving the other modes unhindered.

Energy is typically coupled into a waveguide by means of an E probe, H loop or slot (1,4). Some of these are shown in Fig 1.7. The E probe represents capacitive coupling and is similar to an antenna so that when excited by an EM signal in the radio or microwave frequency range, alternating E and H fields are established. An E probe is normally placed in the center of the waveguide's 'a' dimension and one quarter of a wavelength from the from the sealed end of the waveguide. This position contains a maximum density of E lines, so that there is a maximum coupling between the probe and the guide.

The degree of coupling can be varied by adjusting the depth of penetration of the probe in the waveguide (2).

The H loop is usually placed at a position of maximum H field strength. The H loop is normally part of a coaxial cable, the outer part of which is connected to the wall of the waveguide. The inner part is then formed into the loop in the guide and is connected to the internal wall. The degree of coupling is varied by adjusting the loop's plane relative to the direction of the H lines. It should also be emphasized that these methods are also used to facilitate the removal of energy from a waveguide.

Slots can be cut in a waveguide to introduce as well as remove energy from a waveguide. Figure 1.8 shows slots cut in the wall to introduce energy. Radiating slots typically produce a maximum distortion of the wall currents. However, non radiating slots produce very little distortion in the wall currents and hence can be used to insert probes for measuring field strength or temperature in a dielectric being heated in a cavity.

Rectangular waveguides can be converted into resonators or cavities by short circuiting both ends as shown in Fig 1.9. Short circuiting is usually acheived by inserting a sliding short at the opposite end of the cavity. The sliding short is then adjusted to acheive a resonant cavity. Electric and magnetic energy is stored within the cavity, and power can be dissipated in the metallic walls of

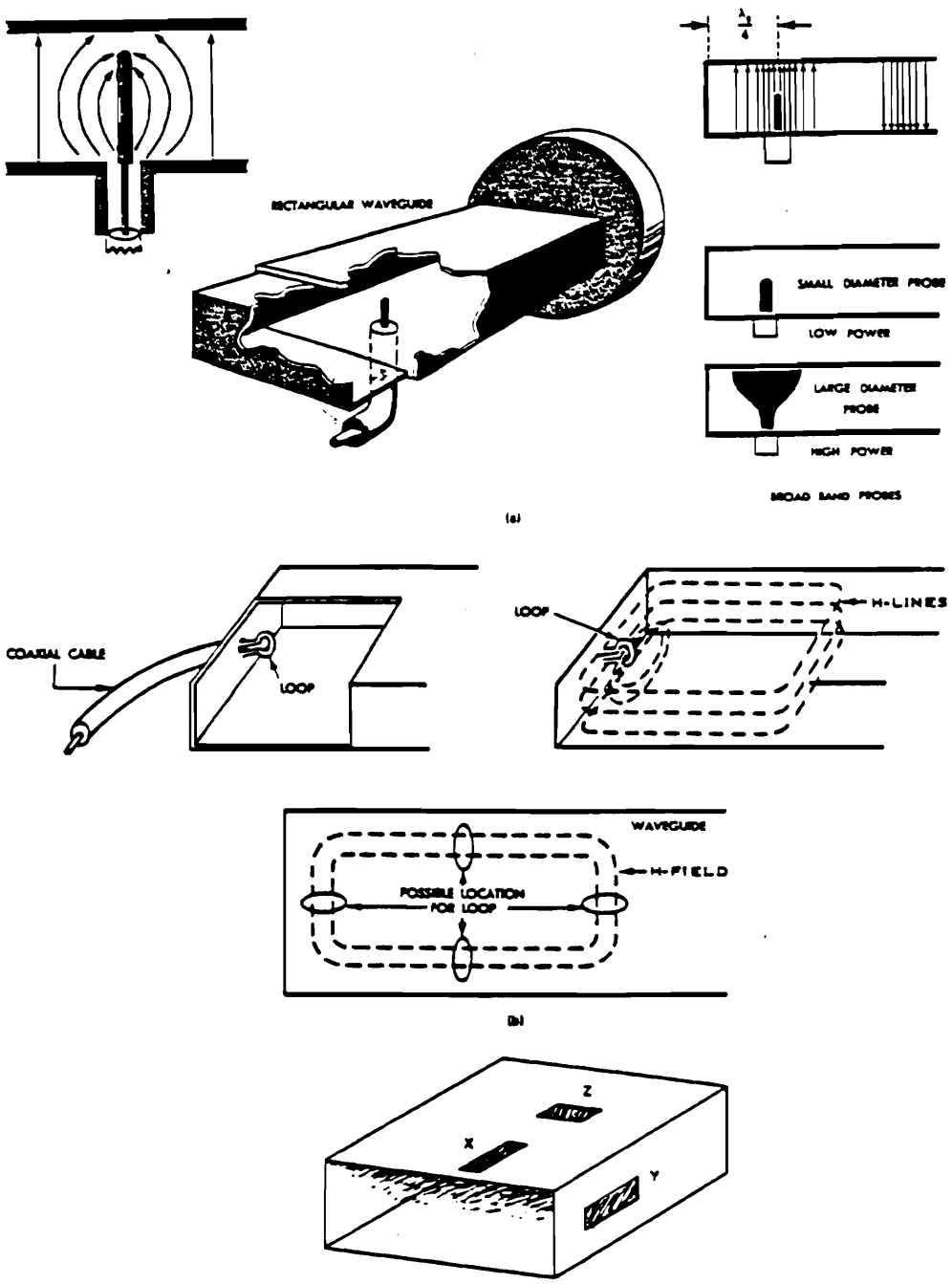


Figure 1.7. Modes of coupling of electromagnetic waves into a waveguide (1) .

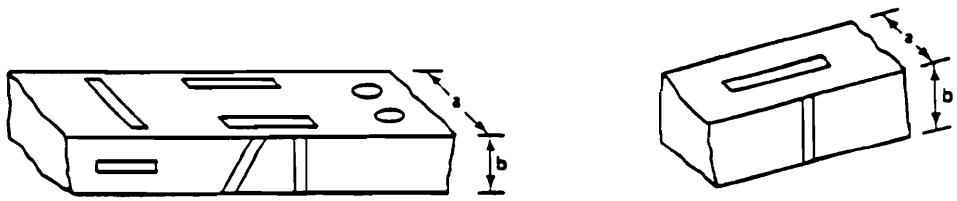


Figure 1.8. Slots in a waveguide to introduce and remove electromagnetic energy.

the cavity as well as the dielectric filling the cavity. The resonant frequency can be calculated by

$$f_r = \frac{0.5}{(\mu\varepsilon)^{1/2}} \left[\left(\frac{m}{a} \right)^2 + \left(\frac{n}{b} \right)^2 + \left(\frac{p}{d} \right)^2 \right]^{1/2} \qquad (7)$$

where 'a','b' and 'd' are the wide dimension, narrow dimension and the length of the cavity respectively.

1-2-2 CIRCULAR WAVEGUIDES

A circular waveguide can be considered to be a coaxial cable with its center conductor removed. Circular waveguides have inherent advantages over their rectangular counterparts in that they can easily negotiate twists and rotations without undergoing severe discontinuity losses (1,4). Microwaves are introduced into the circular cavity in the same manner as a rectangular cavity and the physical dimensions can be adjusted by means of a sliding short to create a resonant frequency. The modes in the cavity can again be classified into TE and TM. On the numbering system, the first subscript indicates the number of full-wave patterns that is encountered as one moves around the circumference, and the second subscript refers to the number of half-wave E patterns across the diameter. For a dominant TE_{11} there is one full wave

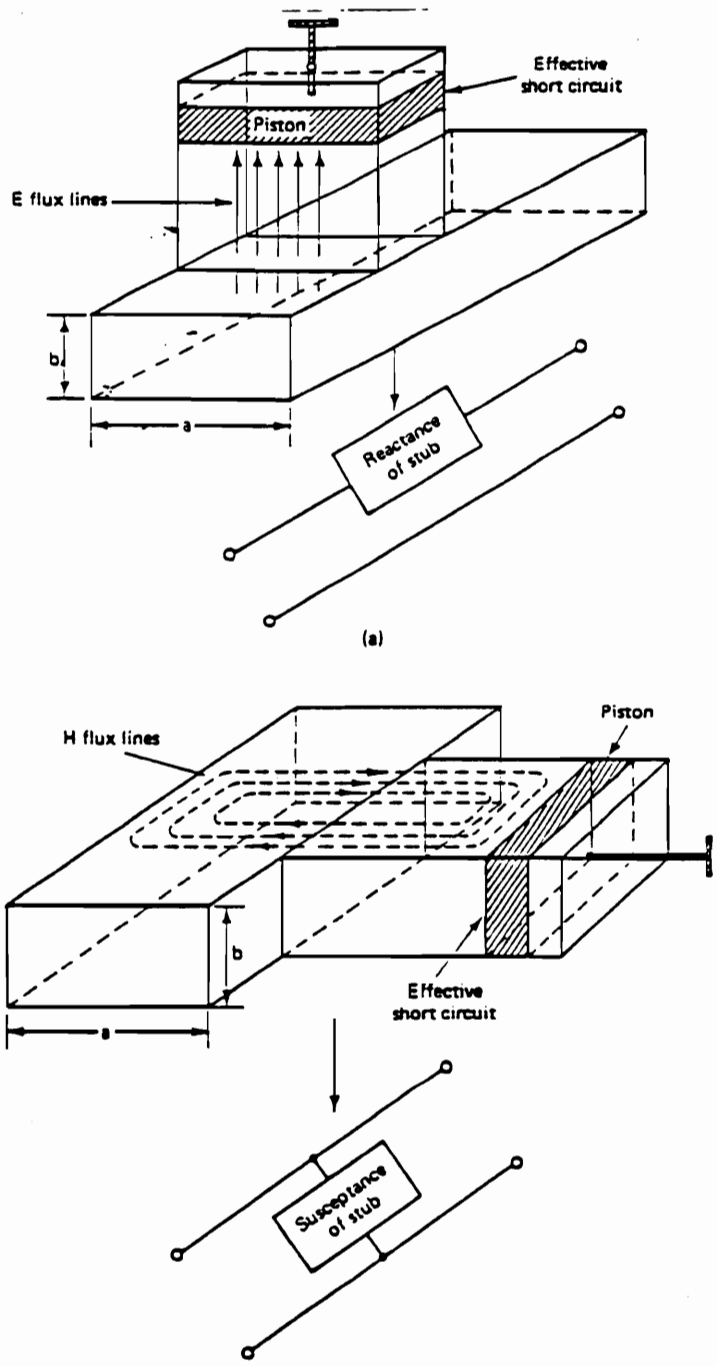


Figure 1.9. Sliding short for creating a resonant cavity.

pattern across the circumference and one half-wave pattern across the diameter as shown in the Fig 1.10. In the circular waveguide the cutoff wavelength is 1.71 times the diameter of the cavity. This makes circular waveguides larger than rectangular waveguides for a given wavelength, which is an inherent drawback. Another inherent disadvantage of this geometry is that the plane of polarization tends to change as we move down the waveguide and hence it is difficult to withdraw energy from the cavity since in order to do so the antenna has to be parallel to the plane of polarization.

1-2-3 GENERAL WAVEGUIDE AND CAVITY THEORY

The quality factor Q_0 of an cavity resonator is a measure of the frequency selectivity of a resonant circuit and is defined as

$$Q_0 = 2\pi \frac{(E_s)}{(E_d)} \tag{7}$$

where E_s is the energy stored per cycle and E_d is the energy dissipated per cycle.

$$Q_0 = \frac{\omega U}{(P_w + P_s)} \tag{8}$$

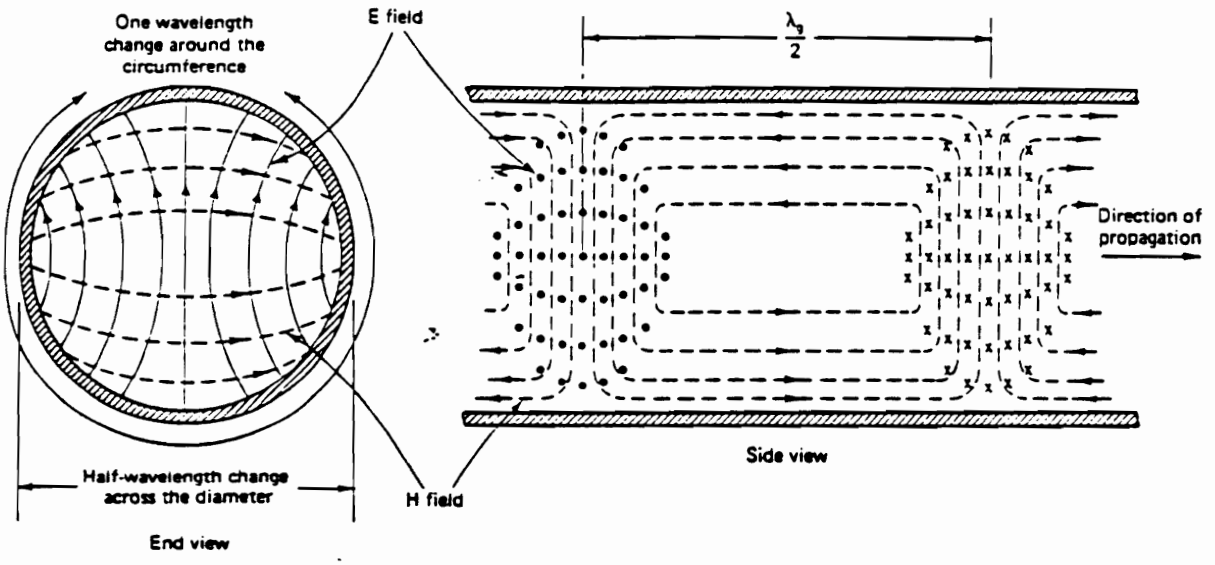


Figure 1.10. Dominant TE_{11} mode in a cylinderical cavity (2).

where ω is the frequency, U relates to the total energy stored in the cavity P_s andP_w are the powers dissipated in the dielectric and the cavity walls respectively. The average power stored in the cavity is given by

$$P_{av} = \frac{1}{2}\omega\varepsilon_0\varepsilon''_{eff}(E \times .E)dV \tag{9}$$

where ε_0 and ε_{eff} are the permittivity of vacuum and the dielectric loss factor of the sample in the cavity respectively. Combining the above two equations we have the quality factor Q_0 for a loaded cavity as

$$\frac{1}{Q} - \frac{1}{Q_0} = \frac{\varepsilon''}{\varepsilon'} \tag{10}$$

In a cavity the degree of standing waves is measured by the voltage standing wave ratio (VWSR) which is measured by E_{max}:E_{min}. E_{max} is the notation for an in-phase condition and E_{min} is the notation for a 180° out-of-phase condition. If V_i and V_r are the incident voltage and reflected voltages respectively then

$$E_{max} = V_i + V_r = V_i(1 + P) \tag{11}$$

$$E_{min} = V_i - V_r = V_i(1 - P) \tag{12}$$

Therefore

$$VWSR, S = \frac{(1+P)}{(1-P)} \tag{13}$$

where P is called the reflection coefficient. If P = 0 (matched line), then S = 1, while if P = 1 (open or short circuited-line), S = infinity. Thus we see that the value of the VWSR can vary from 1 to infinity. On a matched system a value less than 1.2 is normally regarded as acceptable (3).

1.3 CAVITY PERTURBATION

When a **small** sample is inserted into an electromagnetic field, the cavity is said to be perturbed slightly. Use has been made of this perturbation to determine the dielectric properties of the sample (2). This requires measuring a shift in the resonant frequency from the original unperturbed value ω_0 to the new value of ω and the difference of the Q-factor values of the cavity of the sample with and without the sample (1). The dimensions of the sample must be small as compared with the size of the cavity. There are several sample geometries for which cavity perturbation can be carried out. The most important feature of cavity perturbation is the placement of the sample. The sample should be placed so as to preserve symmetry. A simplified representation of the equations are shown in (1) and these will be presented here to maintain the lucidity of this article:

$$\varepsilon = 1 - A\left(\frac{\delta\omega}{\omega_0}\right) \qquad (14)$$

and

$$\varepsilon_{eff}'' = A\left(\frac{1}{2Q_0} - \frac{1}{2Q}\right) \qquad (15).$$

where A is a factor dependent upon the cavity dimensions and sample geometry.

1-4 MICROWAVES AS A HEAT SOURCE

1-4-1 INTRODUCTION AND GENERAL THEORY

Microwave heating as an industrial process is a technique which was originally conceived forty years ago. The advent of the magnetron during World War II presented scientists and engineers in industry and universities with an opportunity to develop a new way of heating materials for scientific uses. The task was quite formidable though, because of a lack of functional equipment and the absence of any reliable data on the dielectric properties of

materials to denote which were suitable candidates for microwave heating. Most of the early work on these properties was pioneered by Von Hippel and co-workers in the forties and fifties (4). Their pioneering work has since been used extensively and still is the most exhaustive documentation of organic and inorganic properties in the radio frequency and microwave region. Since then, research in this area has been expanded by several people notably Coehlo (5), Frohlich (6), Johnk, Harvey and Hasted (8, 9, 10).

When a material is subjected to a direct electric current field the dipoles present in the material tend to align themselves with the applied field. Even when a molecule does not possess a permanent dipole it acquires one by induction when placed in an electric field because of the displacement of charged particles from their equilibrium positions. An induced polarization can arise mainly from the displacement of electrons around the nucleii (electronic polarisation) or due to the relative displacement of atomic nuclei because of the unequal distribution of charge in molecule formation (atomic polarisation) (1,11). Lastly, a source of reorientation polarisation arises from charge build up in interfaces between components in heterogenous systems, termed Maxwell-Wagner polarisation - this behavior is illustrated in Fig 1.11. The molecules however can never fully align themselves with the direction of the applied field because of thermal density fluctuations (thermal agitation) (12). If therefore a local field (E) is applied to an individual dipole as shown in the Fig 1.12 the dipole moment μ is a simple function of the field (assumed linear) giving:

$$\mu = \alpha_t E \tag{16}$$

where α_t is called the polarisability of the medium and may be summed up as

$$\alpha_t = \alpha_e + \alpha_a + \alpha_d + \alpha_{MW} \tag{17}$$

where the subscripts refer to electronic, atomic, dipolar or reorientation and interfacial or Maxwell-Wagner polarisations respectively.

If the applied field is an alternating field, then the molecules will begin to oscillate as the field changes direction. This tendency is demonstrated in the Fig 1.13. The ability of the molecules of the dielectric to keep in phase with the applied alternating field is dependent upon a number of factors such as the strength of the dipole, temperature and frequency of the impressed field. The molecule's inability to keep in phase with a given frequency results in a dielectric loss factor which is proportional to the rise in temperature as will be seen later. This dielectric loss factor ε'' is related to the dielectric constant ε^* through the relationship

$$\varepsilon^* = \varepsilon' - j\varepsilon'' \tag{18}$$

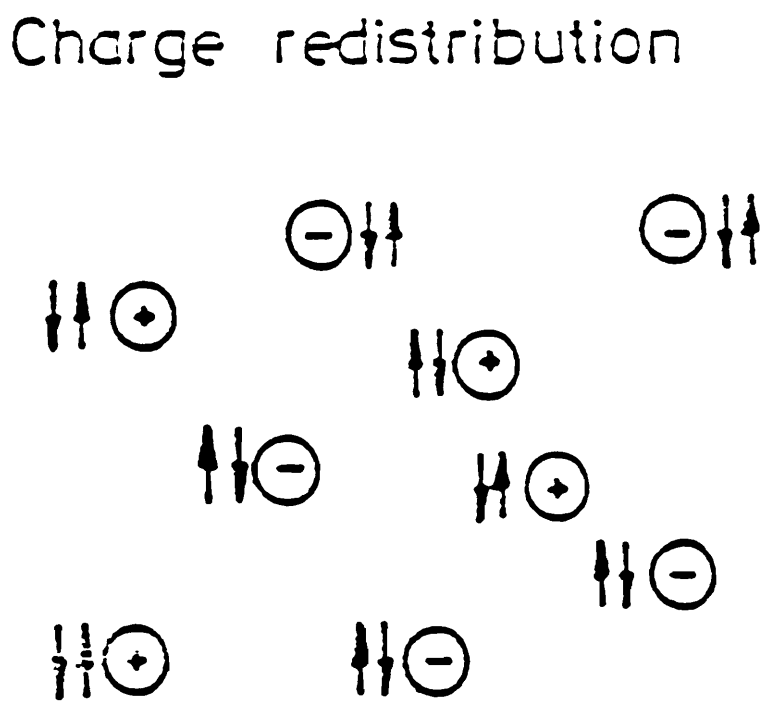


Figure 1.11. Schematic shows polarization due to the Maxwell Wagner effect (2).

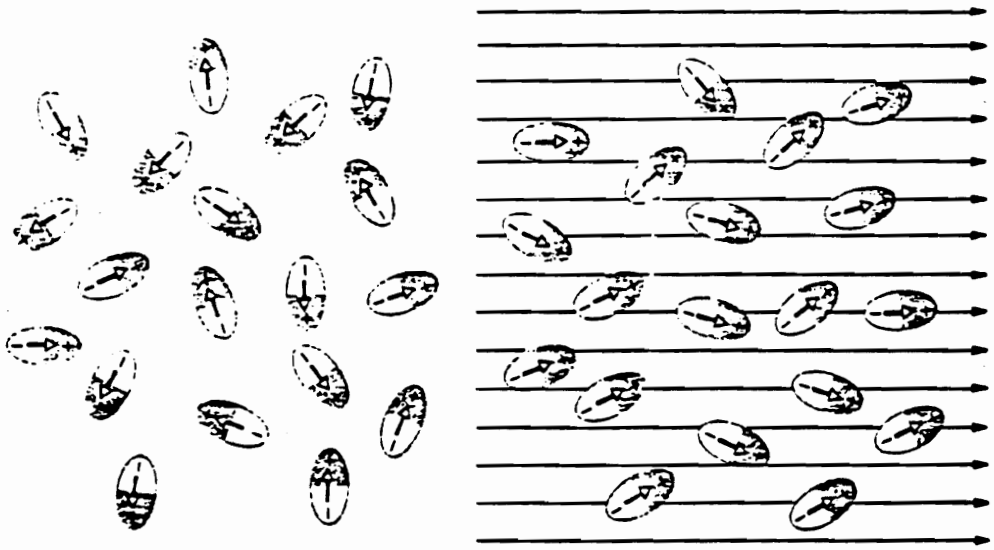


Figure 1.12. Figure shows molecular reorientation when subjected to an applied electromagnetic field.

The actual derivation of the above relationship has been described elsewhere (2,12). The loss factor ε'' can be broken down into its components as in the case of polarisation above. This can be shown as

$$\varepsilon''_{eff}(\omega) = \varepsilon''_{d}(\omega) + \varepsilon''_{e}(\omega) + \varepsilon''_{a}(\omega) + \varepsilon''_{MW}(\omega) + \frac{\sigma}{\varepsilon_0}\omega \qquad (19)$$

where the subscripts are described above and the last term in the expression refers to dielectric loss due to conduction. The loss factors show a frequency dependence which helps simplify analysis because for a given frequency band there is a dominance of one or two loss mechanisms over the others. The frequency dependence of the loss mechanisms has been clearly demonstrated by Hasted (10) who has schematically represented the various contributing mechanisms to the loss factor of a moist material. Since most industrial frequency heating takes in the range of 10^7 to 10^9 Hz, the mechanisms that one should be most likely concerned with are those of dipolar reorientation, Maxwell-Wagner-Sillars (13, 14, 15) interfacial polarisation and d. c. conductivity. Loss mechanisms due to atomic and electronic polarisations, collectively termed distortion polarisations, occur at frequnecies in the infra-red and visible part of the spectrum and as such play no part in the high frequency heating. This is shown in the Fig 1.14. Hence the complex dielectric constant can be now be modified to:

$$\varepsilon^* = \varepsilon' - j\varepsilon''_{eff} \qquad (20)$$

where ε''_{eff} includes the factors which are relevant to high frequency heating. The ratio of the effective loss factor to that of the dielectric constant is called the effective loss tangent, which includes the effects of d. c. conductivity, and is the angle between the total current density vector and the vertical axis in the Fig 1.15 shown below.

The effective loss factor described above depends on the structure of the material as will be discussed later and it is the quantity upon which the ability of a material to heat in a microwave field is dependent. A material that is readily polarisable by a small electric field has a high loss factor and is easy to heat (16). The power absorbed is directly dependent upon the dielectric loss factor and the equation for this is given below:

$$P_a = \omega \varepsilon_0 \varepsilon''_{eff} E^2 V \qquad (21)$$

where P_a is the power absorbed, ω is the frequency, V is the volume in m^3, E is the electric field strength. If the polarising field alternates direction at a high frequency, considerable energy is imparted to each molecule of the material causing the molecule to be agitated as the field alternates each cycle. This agitation gives rise to friction amongst the molecules which in turn causes the material to heat. Since the field penetrates the molecule, heat is generated from within. In a uniform electric field a homogenous material will heat very

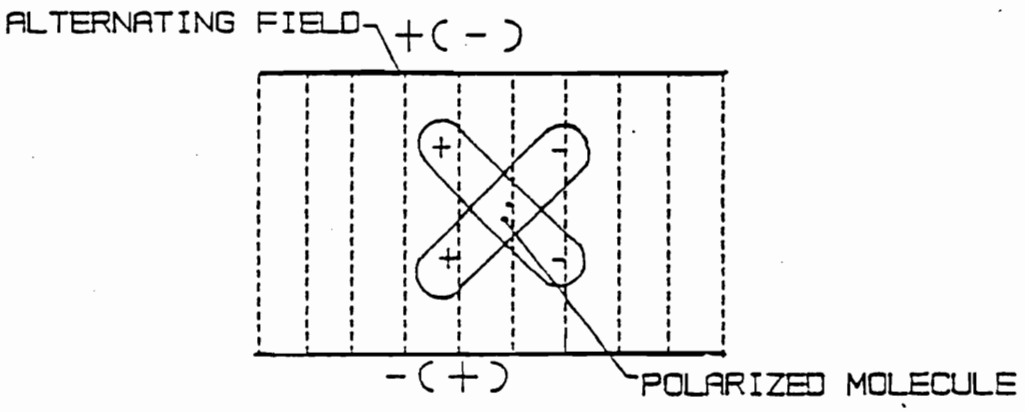


Figure 1.13. Oscillation of a molecule when subjected to an alternating electromagnetic field (16).

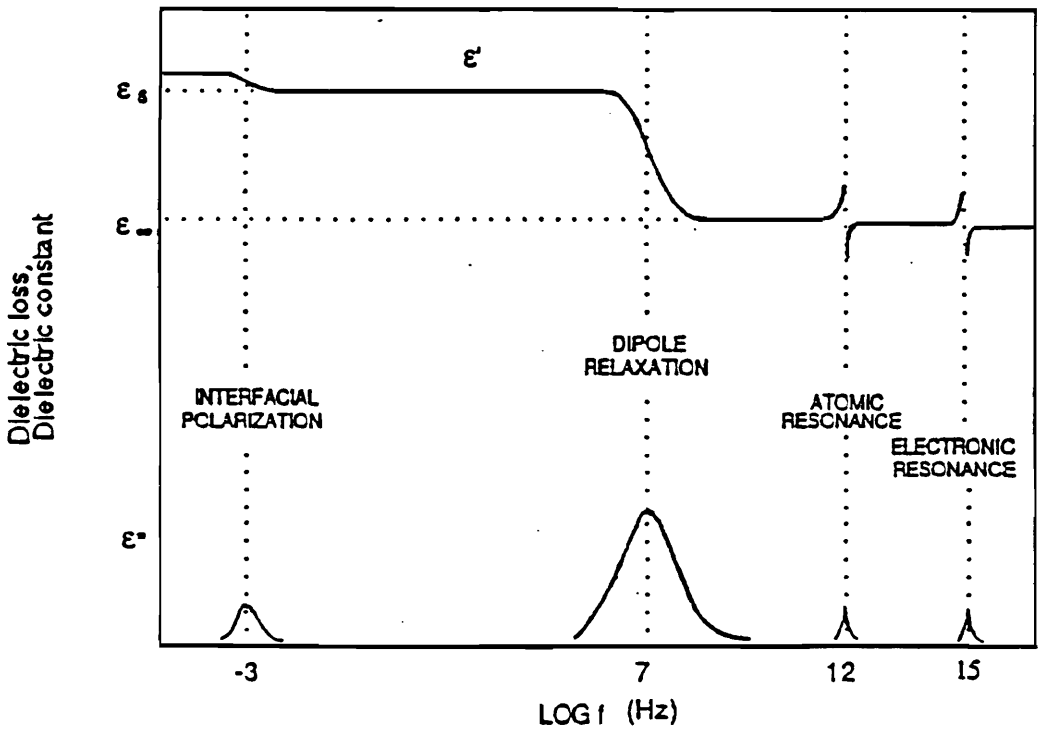


Figure 1.14. Dielectric constant as a function of frequency in the region of dipolar and distortion adsorption (2).

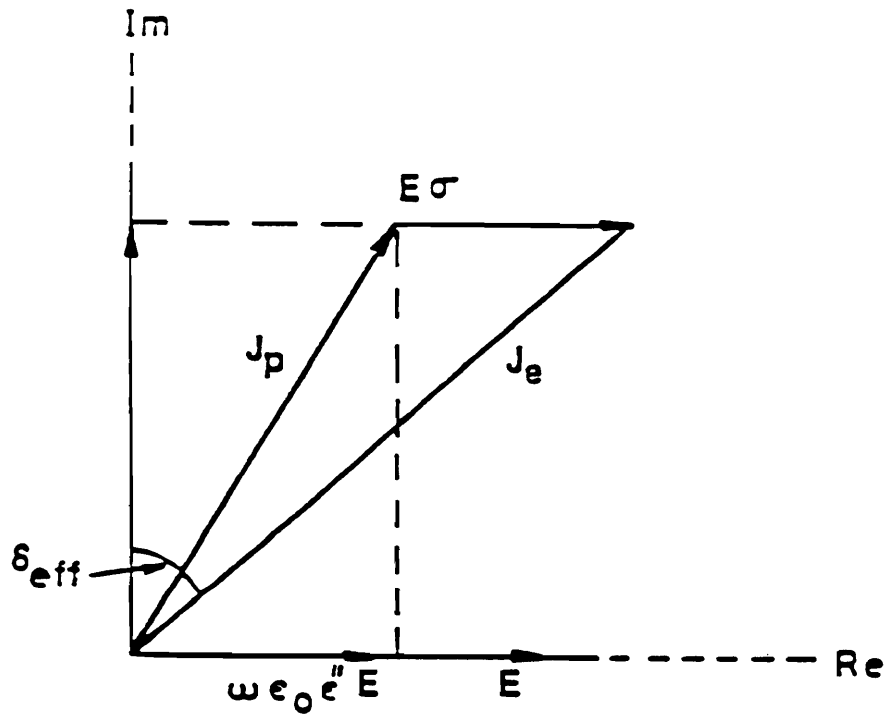


Figure 1.15. Phasor diagram between the external electric field vector, E, and the polarization vector P (2).

uniformly across its cross section since an equal amount of energy is imparted to each molecule. The rate of temperature increase can be calculated from the above equation as follows:

$$P_a = \frac{Q_h}{t} = M_a C_p \frac{(T - T_0)}{t} \qquad (22)$$

where M_a is the mass of material,C_p is the specific heat of the material, T and T_0 are the final and initial temperatures of the material respcetively. Substituting Eq. (22) in Eq. (21) we get

$$\frac{(T - T_0)}{t} = 0.556x10^{-10}\varepsilon'' E^2 \frac{f}{\rho C_p} \qquad (23)$$

From the above equation it can be seen that the temperature rise for a given frequency is dependent upon the dielectric loss factor and the square of the applied electric field. This makes the rate of temperature increase dependent upon the temperature itself since the loss factor is temperature dependent (2, 11, 16).

1.5 DEPENDENCE OF HEATING UPON THE STRUCTURE OF MOLECULES

Microwave heating of materials is dependent upon the lossy characteristics of the material. Thus the microwave heating of materials is selective. This is different from conventional thermal heating, where materials heat by conduction and convection irrespective of their structure. In order for a material to heat in a microwave field it must possess permanent dipoles or ionic or electronic mobility. Molecules, which, in general do not possess charge symmetry have high dipole moments (17). Thus for organic materials including polymers, the possession of nitrile groups, hydroxyl groups, amine groups, epoxide groups provide an opportunity for absorption of microwaves, which consequently result in heating. The concentration of such groups in a mixture of small molecules or in a polymer blend will determine the dielectric loss factor and the rate of heating (11). A. L. McClellan (18) in 1962 collected and published data on those dipoles which had been experimentally verified. The dipole moments were expressed in units of Debye (1 Debye = 10^{-18}esu cm) and were usually determined in the gas phase or in a solution of a non-polar solvent, where at infinite dilution the interaction between polar molecules can be neglected. Urea and sulfone groups have highest dipole moments with a Debye value of over 4. Lactone, amide and nitrile groups are next with values between 3 and 4 Debyes. Isocyanate and ketone groups have

Debye values between 2 and 3. The ether and carbonate groups have the low dipole moments around 1 Debye. The monosubstituted groups such as the hydroxy, ester etc. have Debye values between 1 and 2. It should be noted that there are certain groups of molecules that are microwave transparent. Molecules having a center of charge symmetry such as argon, carbon tetrafluoride (CF_4), methane (CH_4), carbon tetrachloride (CCl_4), propane (C_3H_8) etc. are non-polar and exhibit zero dipole moments. Polymeric materials such as polyethylene, polypropylene, polytetrafluoroethylene etc are microwave transparent and are commonly referred to as 'microwaveable plastics'.

In the case of conductive materials, the net charge due to electrons or ions conducted inside the material gives rise to a conducting current. This conduction of charge in a material gives rise to heating, and the ability of a material to induce charge density is called the dielectric constant (2). Hence for carbon fibers in epoxies there is a higher heating from the interior towards the skin because of the conductivity of charges through the fibres. It should be noted though that in a perfect conductor, there is no heating since the electric field is reflected and therefore no conduction currents are set up in these materials at any frequencies (13). Hence no electromagnetic energy is dissipated even though the conductivity of the perfect conductor is infinite.

1.6 MACROSCOPIC CONSIDERATIONS FOR MICROWAVE HEATING

Though the molecular structure of molecules plays an important role in their capability to absorb microwaves it is important to note that the morphology and conformation of molecules in any given material also determine their capability to heat up when placed in a microwave field. The temperature of the material and its nature (solid glass, liquid and gas) also plays an pivotal role in the value of the dielectric constant and determines the heating capability of the material. In 1929 Debye first theorised that at low frequencies near d. c., the dipoles have ample time to follow the variations of the applied field and the dielectric constant is at its maximum value. With increasing frequency the dipoles were unable to keep pace with the alternating field and hence a loss factor (as described above) was now associated with the molecules. As the frequency is increased further the dipolar or reorientation polarization cannot keep pace with the applied field and hence its contribution to the total polarization decreases significantly. This fall in polarisation significantly increased the loss factor and energy is now drawn from the system and is dissipated as heat.

Debye interpreted this relaxation as dipolar rotation against frictional forces in the medium. Using Stokes theorem, he assumed a spherical dipole and used the following expression for the dipolar relaxation time:

$$\tau = 4\pi r_q^3 \frac{n_v}{k_b} T \qquad (24)$$

where n_v is the viscosity of the medium, r_q is the radius of the dipole and k_b is the Boltzmann constant. This interpretation turned out to be fairly inaccurate, especially in solids where it is impossible to imagine a spherical dipole oscillating in a medium where viscosity is the dominant mechanism. Moreover in a solid where molecules and atoms are bonded together the dipole is subject to the influence of the surrounding dipoles. Debye recognised this shortcoming and later introduced the notion of hindered motion of molecules, wherein he postulated that an activation energy U was necessary for the dipole to attain another equiprobable position. If U was less than k_bT then the dipole would be free to rotate and reorientate. This is likely in a system where the molecules are free to move around and possess very little intermolecular forces of attraction which is the case in most gases. However, von Hippel (4) noted that there are large deviations from this theory when $U >> k_b$ and intermolecular forces dominate. This is so for most solids (including polymers) and viscous liquids. Later Onsager and Kirkwood generated new theories that suitably described the dipolar motions of molecules in simple liquids.

The Onsager theory took recourse to the introduction of a reaction field R in a material, which therefore made the total force F acting on a molecule in a electric field, E, equal to

$$F = G + R \tag{25}$$

where G is the cavity field which is due to the interaction of the dipole of the molecule with the applied field E alone. The total moment of the molecule in the presence of the field is given by

$$m = \mu_0 u + \alpha_c F \tag{26}$$

where μ_0 is the permanent dipole moment of the molecule, 'u' is the unit vector in the direction of the permanent dipole moment and α_c is the deformation polarizability of the molecule. These modifications from the Debye theory give us the Onsager relationship:

$$\mu_0^2 = \frac{3kT}{4\pi N} \frac{(2\varepsilon_r + \varepsilon_u)}{3\varepsilon_r} \left[\frac{3}{(\varepsilon_u + 2)} \right]^2 (\varepsilon_r - \varepsilon_u) \tag{27}$$

The Onsager theory has the disadvantage of not taking into account the orientation correlations between molecules and thus is applicable only to systems of rigid non-associating molecules and hence cannot be applied to condensed phases especially polymer molecules.

Kirkwood (6) introduced a factor g into the relationship derived by Onsager. This factor was introduced emperically and hence gave rise to the modified relationship

$$\frac{[(\varepsilon_r - 1)(2\varepsilon_r + 1)]}{9\varepsilon_r} = \frac{4}{3}\pi N[\alpha_c + \frac{g\mu^2}{3kT}] \qquad (28)$$

'g' is called the Kirkwood correlation function and takes into account short range orientation correlations between molecules. If a reference molecule was surrounded by z nearest neighbours then

$$g = 1 + z\cos\gamma \qquad (29)$$

Since the orientation function is emperically added on it gives rise to an error when g = 1; i.e. the equation does not reduce to the Onsager equation as it should, if orientation correlations were lacking.

The orientation correlation between dipoles in condensed phases was finally evaluated by Frohlich (6) in terms of the limiting values of the dielectric constant. This equation is called the Kirkwood-Frohlich equation and is as follows:

$$\varepsilon_r - \varepsilon_u = \frac{(3\varepsilon_r + \frac{\varepsilon_u}{2\varepsilon_r})4\pi N}{3kT}[\frac{(\varepsilon_u + 2)}{3}]^2 gN\mu^2 \qquad (30)$$

where 'g' is the Kirwood correlation factor as described above and μ is the dipole moment of the isolated molecule. The Kirkwood-Frohlich equation is applicable to the study of the dielectric properties of polymers if the orientation correlation factor is expressed as follows:

$$g = 1 + \frac{1}{N} \Sigma cos\gamma_{ij} \qquad (31)$$

where $\gamma_{ij}$is the angle between the first and the jth unit of one chain (19). N is the number of repeat units in the chain. It is now clear that if all the dipoles are situated along the chain backbone then g = 1, which means that the summation of all the cosines along the backbone is zero. Chain geometry has a strong influence on g values and bond rotational potentials have to considered when calculating the value for a complex structure (20). The Kirkwood-Frohlich modification is however important because it states that in a condensed phase the dipole moment of the molecules or groups interact strongly, resulting in a decrease of the total dipole moment. The value of the orientation factor is dependent on the number and distance of the nearest polar neighbours to the group considered. This modification has important consequences in that it predicts for small molecules in the liquid form and for dilute solutions of polymers, a decrease with increasing temperature. However, for most polar polymers there is in the microwave region an increase in the dielectric loss factor with increasing temperature which is mainly governed by the change in confirmations and the consequent change

in intra and intermolecular energies. For most polymers the dielectric losses at microwave frequencies consists of background losses or the high and low frequency tails of losses which occur outside this region. For example the low frequency tail of losses due to phonon absorption in the far IR can contribute to the losses in the microwave region. Similarly the high frequency tail of relaxation dispersions, which are associated with motion of polar segments of the polymer chain, extend into the microwave region.

Since the conformational motions of polymer units are not fully understood, it is difficult to determine which specific part of the molecule behaves rigidly during thermal motion in a given temperature range. Studies are still being conducted in various places to determine the effect of microwaves on polymers in the solid state, but meanwhile there are several rules of thumb that are worth commenting and elaborating upon. These are as follows:

1) In the case of polymers, for a material to undergo dipolar relaxation at microwave frequencies it is essential that the material be above its glass transition and that $T - T_g$ be as large as possible. This is because of the shift of the T_g (characterized by the α dispersion) to higher temperatures with increasing frequencies (21). However, the lower temperature dispersions such as the β and γ relaxations which have lower activation energies than the α dispersion shift a much faster than the latter. As a result these dispersions tend to merge as the frequency is increased. This merging of dispersions when taken together with the tails of losses occuring at frequencies above and

below the microwave region causes a change in the shape of the loss dispersions. Hence for polymeric glasses it has been determined (11) that there is a critical temperature T_c below which it is imperative that additional power be supplied to the molecules in order to promote heating. In order to promote microwave absorption at low power, the temperature of the material is to be raised above T_c. In doing this the relaxation spectrum for the material is moved into the microwave region. By combining conventional thermal heating with microwaves, the absorption and heating of these materials is significantly improved. Hydrogen bonding plays an important role as in the case, for example of polyamides. Below the T_g the heating rate is very slow, while above the glass transition it is necessary to disrupt the hydrogen bonding to allow for large scale motions of the chains. Studies conducted by Frosinni and Butta (22) on the dielectric properties of polyoxymethylene, polyvinyl acetate, polyvinyl alcohol, polycarbonate and vinyl chloride-vinyl acetate copolymers at microwave frequencies revealed that all relaxation peaks either connected with cooperative motions in the main chain or in side chains (secondary processes) usually disappear; the corresponding relaxation effects however manifest themselves through a progressive increase of losses with increasing temperature which is particularly marked above the T_g. The latter transition inspite of the high frequency, is marked by a change in the slope of the tanδ vs temperature curve which accompanies its onset. This is explained on the basis of a large distribution of relaxation times in the bulk of the polymer and a larger free volume for relaxation of side chains. Chantry et

al (23) studied the dielectric properties of ethylene-vinyl acetate copolymers at microwave frequencies as well as the far infra-red region and postulated that the relaxations in the microwave region were very complex and not of the Debye type alone.

2) In the case of semicrystalline polymers it has been discovered that the presence of crytals significantly alters the dielectric loss to a lower value (11). This considarably reduces heating rates. Amano and Nagakawa (24) have also documented that it is only the amorphous region in a polymer that absorbs energy and contributes to heating. This has also been stated by Nakagawa and Konaka (27, 28). Amrhein noted that absorption in the amorphous materials was much higher than in the corresponding crystalline regions and related this effect due to one phonon absorption in the high frequency i. e. 10^{12} Hz region. Amrhein pointed out to the near equivalence of the dielectric loss and the spectrum of the density of phonon states. However, it should be noted that in certain semiconductor materials (GaAs) molecular resonances have been determined in certain crystals which makes them useful for certain applications in diodes and other electronic applications (1).

3)The mole percent of polar groups in a copolymer chain determine the dielectric properties in a manner dependent upon the constitution of the monomeric units and their ratio (11). For example the effect of the molar ratio of polar groups can be seen as a function of (a) % of CONH (amide) groups in different nylons (b) % of Cl (chloride) groups in poly(vinyl chloride) and

polychloroprene (c) % of COOR (ester) groups in polymethacrylates. The position of these groups is vital to their contribution to the loss factor. For example, units in the backbone are less mobile than those in the side groups and hence the dipole moment contributes less to the first case than in the second.

4)The presence of crosslinks causes the molecular weight to increase and this increases the relaxation times of the dipole segmental loss. The density of the crosslinking determines the magnitude of dielectric loss. Other factors such as branching, stereochemical structure and orientation also have been found to effect the dielectric loss factor.

Microwave heating is not uniform however and can introduce several factors which need to be carefully considered - some of these are:
when a uniform cross section of a dielectric is placed in a uniform microwave field of equal strength in all directions, even heating across the total volume takes place since each molecule sees the same field. However, if the material is a very strong absorber (e. g. water) then the field is attenuated by strong absorption in the first few millimetres of the body of the material. This produces large temperature gradients within the bulk of the material. A similar situation arises when a system of polymeric heterogenous absorbers such as a blend is placed in a uniform field. The material with the higher dielectric absorbs more strongly leading to gradients within the material. Since the dielectric properties of polymers increases with temperature this can lead to

a phenomenon called "thermal runaway" (29) where the temperature of one phase increases causing the loss factor of that constituent to increase. This produces a cascading effect which proceeds until degradation takes place. The effect can also be seen in homogenous materials when placed in a non uniform field. One part of the sample is exposed to a stronger field which produces the cascading effect in that part of the material.

There is a common misconception that microwaves heat from inside outwards. This has been documented by Nakagawa et al (24, 27, 28). This temperature gradient is caused initially by conduction and convection at the surface and not because of greater relaxation of molecules in the bulk than at the surface. However with time it is possible that due to the gradient there may be an increase in dielectric loss factor at the center, which could cause a cascading effect. Because of this effect it is common to subject materials to a combination of thermal and microwaving heating. This produces uniform heating and is actually utilised in the drying of wood pulp (30) and paper (31) and grains (32).

The presence of thermal gradients is not always an inconvenience. They have been used with much benefit in the manufacture of composites (22). The use and development of composites has opened a whole new field to the applications of microwaves. The use of conductive fillers in an insulating matrix has enhanced the status of microwaves as a heating source. The conductive fillers such as carbon fibres, carbon black, metal filings heat rapidly because of conduction and are able to heat the surrounding matrix

material and produce better adhesion and a better overall product. Work done by Raj (34, 35) on the polymerization of epoxy - iron and epoxy - copper composites reveals that the concentration of metal particles as well as the size of the particles play an important role in the efficient curing of the composite. Larger sized particles promote better curing. It was also revealed that a greater strength of electric field caused a higher extent of cure. In both cases the microwave cured sample was found to display higher degrees of cure than the oven cured materials.

1.7 MICROWAVES AS A HEATING SOURCE FOR REACTIONS

There is a only a small body of knowledge developed thus far about the effect of microwaves on reactions. Reactions have been carried with small molecules as well as polymers and in both cases, the claims are similar save for a few exceptions: microwaves generally produce a tremendous increase in the rate of reaction. However the reasons for the increase in the rate of reaction vary and these along with a brief description of the experiments are tabulated below.

Silinski et al (35) studied the synthesis of polyurethane polymers under continuous microwaves at 2.45 GHz. The conversion to heat of the dielectric loss due to the dipolar relaxation of the chemical species is used to activate the crosslinking reaction. The temperature vs time heating curves is divided into three parts i. e. preheating of the resin, exothermal conversion and the cooling period. The dielectric loss is also plotted vs time and it is found that the maximum in the dielectric loss corresponds with the sol to gel transition. The temperature continues to rise beyond this point despite the decrease in the loss factor. The increase in temperature is attributed to the exothermic spread while the decrease in the loss factor is due to the crosslinking which tends to immobilize the polymeric segments. The cooling period has been ascribed to heat transfer following the completion of the curing process so that despite the fact that the dielectric loss remains constant, the temperature decreases. The authors found that a higher initial power caused a higher initial rate of heating and consequently a more rapid transition from sol to gel. The properties of polyurethanes produced under all conditions of initial power showed very little variation in properties from their oven cured counterparts. Thullier et al (36) studied the curing reaction between DGEBA and DDS by studying structures under FTIR and ^{13}C NMR. Pulsed microwaves having an average power of 150 watts were used. The peak power was varied between 300 watts and 2700 watts and the pulse power was changed from 1 to 100 milliseconds. Curing time was set at 30 minutes. The optimal rate of conversion was 62%. Their most interesting observation, however, is the fact

that percent conversion did not scale with temperature, but rather depended upon the efficient transfer of electromagnetic energy to dipolar sites. The authors did not, however, take into consideration the possibility of thermal gradients which could be a plausible explanation for their discovery. The most efficient peak pulse powers was found to be 1500 and 1800 watts. The optimum pulse time was found to be 50 milliseconds. Similar samples heated to 180°C in a conventional convection oven for three hours revealed a 95% conversion. Finally it was also shown that a low pulse rate of 2 milliseconds induced the formation of bis-aliphatic ethers by catalyzing the homopolymerization reaction, while a longer pulse repitition period produced the reaction with amines only.

Van and Gourdenne (37) looked at the curing of epoxies with diaminodiphenylmethane at 2.45 GHz as well as in a conventional oven at 120°C. Another sample was placed in an oven at 60°C and then heated to 120°C. The total time of heating was 60 minutes. The heating curves were analyzed in a manner similar to that of Silinski et al. However, physical testing carried out on the samples in axial compression showed that the elastic modulus for microwave cured samples was 2.7 GPa while the oven cured samples had an elastic modulus of 2.4 GPa. A comparison of curing between pulsed and continuous microwaves (38) shows the development of a higher temperature and dielectric loss when the pulsed source was used. The respective profiles were quite similar indicating that there was no major difference in the mode of cure. The authors explained the development of a

higher temperature in the case of the pulsed microwaves was due to a 'syneresis' effect on the dipole and the flexible chain segments between the source frequency (2.45 GHz) and the pulse frequency (200 Hz). The mechanical properties i. e. the elastic modulus measured in compression show no significant difference. In an extension of this work the authors (39) varied the frequency of pulsing from 20 KHz to 20 Hz. The results were similar i. e. pulsed microwaves can be used to activate crosslinking reactions. By a judicious choice of pulse frequencies reactions can be speeded up when compared with continuous microwaves. This improved efficiency was attributed to a double relaxation (40) which is a combination of dipolar relaxation linked at the level of epoxide and hydroxyl groups to the frequency of the E-M waves, and of the segmental relaxation maintained by the discontinuous emission of electrical energy according to a periodic low frequency law. Lewis et al (41) also studied the curing of epoxy resins using 4,4'- diaminodiphenylsulfone (DDS) and 3,3'-diaminodiphenylsulfone. The cure rate was accelerated, but there was no difference in mechanical properties between microwave and oven cured materials. The authors (42) also performed studies on thermoplastic modified epoxies. The modifier was amine terminated polysulfone. Mechanical properties between oven and microwave cured samples were identical, though a difference was seen in the morphology. The EM processed sample showed a lower degree of phase separation in samples with high loadings and smaller particles at low extents

of loading. These differences were attributed to the differences in viscosity during the cure process which influences the kinetics of phase separation.

Lewis et al (43, 44) also monitored the step growth reaction of benzophenone tetracarboxylic acid of dianhydride (BTDA) and 3,3′-diaminodiphenylsulfone (DDS) in N-methylpyrollidone. Reaction kinetics were studied using FTIR with samples drawn from the aliquot during microwaving. No consideration was given to the fact that the removal of a small volume from the sample holder would affect the electric field strength and hence the curing properties. The activation energy calculated for the process was one half of the value obtained for the oven cured sample. The authors speculated that this increase in the reaction rate might be due to an interaction of the solvent NMP with the amic acid under the influence of the electromagnetic field. The authors also took a new approach to analyze the apparent difference; an approach frequently used in ultrasonics and went on to assume that the activation energy for the two processes i. e. the microwave and oven curing was the same and that the difference in the rates of cure was due to a difference in the interaction between the microwaves and the various dipolar species in the reacting system. The reactive groups being more highly polar would therfore absorb more efficiently than the bulk of the material. The difference in temperature was calculated to be about 50°C between the measured temperature and the temperature at these reactive sites. These localized molecular hot spots were suspected to have caused the increase in the rate of reaction. However, Jabbari (45) who performed a similar experiment on the imidization of

polyamic acid contradicted these results. These experiments though performed under similar conditions were subjected to agitation in order to negate the effects of thermal gradients if any. It was found that the higher the rate of agitation, the lesser the difference in the rate of reactivity between the oven and the microwave cured samples. At a agitation rate of 1700 rpm the difference between the oven and the microwave cured sample is almost negligable. The author consequently explained that Lewis's results were due to the presence of thermal gradients. The author believes that various differences reported in the literature with microwave curing are due to the high initial rate of energy transfer with microwaves as opposed to the energy transfer rate in conventional processing. It should be pointed out that these experiments too suffer from the drawback that there is a) no consideration given to the effect of the change in the electric field strength and consequent increased heating upon withdrawing a small quantity of the sample for analysis b) samples cured in an oven were not subjected to the same agitation as were their microwave cured counterparts; this would help alleviate any discrepencies associated with heat transfer between the two methods of cure.

Curing reactions have also been studied in several elastomers and synthetic rubbers. Lee (46) reported on the curing of silicone based elastomers. The efficiency of microwaving was increased by incorporating bulky polar substituents into the chain backbone or by adding conductive fillers to the bulk of polymer. In both cases it was found that the addition of initiators such as peroxides was necessary to stimulate the reaction. The authors reported more

uniform curing with microwaves than with oven curing as well as energy savings. Several other authors have performed preliminary curing experiments with elastomers and most reports acknowledge faster curing, heating efficiency as well as energy savings (47, 48).

Work done by Gedye et al (49) on reactions involving small molecules shed light on several aspects of reactions not yet described in any detail i. e. the effect of polar solvents during a microwave reaction. The author found that more polar molecules tended to produce much larger extents or reaction. The non polar molecules on the other hand did not facilitate such an extent of conversion because of their inability to absorb microwaves. He suggested that reactions could be optimized by use of the right amount of power, pressure and reaction volume. He claimed that reactions could be speeded upto 1240 times as compared with conventional oven curing.

In conclusion it can be said that microwaves cause heating in molecules depending upon their dielectric loss factors and the temperature of the material. In the case of polymeric molecules heating is not easily predictable because of the fact that there are conformational and configurational factors which cause increases in the dielectric loss factor with temperature especially at microwave frequencies. These increases may be associated with the tails of losses taking place at frequency regimes above and below the microwave region. The presence of crystallinity in materials also causes significant decreases in the rate of heating. Thermal runaway also gives rise to

tremendous unpredictability in measured heating rates. It is therefore pertinent to make use of as small sample sizes possible when measuring temperature increases.

In the case of reactions, most seem to indicate an increase in the rate of reaction with the use of microwaves. The number of explanations for this enhancement seem as numerous as the experiments performed. This is not surprising, considering the fact that the field is relatively new and experimental conditions are in a relative stage of development.It underscores, if anything, the need for more analytical equipment which can operate in a microwave field without perturbing the field or the reaction. One claim which seems unanimous is that pulsed waves can increase the rate of a reaction when the rate of pulsing is similar to the relaxation time of the chain segments.

1.8 SOL-GEL REACTIONS

A typical sol gel reaction consists of the hydrolysis and condensation a metal alkoxide with either an acidic or basic catalyst. The reactions are similar for other metal alkoxides such as titanium isopropoxide, aluminum sec-butoxide, zirconium isopropoxide etc. All of these undergo hydrolysis and condensation to yield their respective oxides as is indicated with the silicate system shown

below. The rates of reaction and the respective structures formed depend on a large number of parameters such as the catalyst used, solvents used for compatibilization, metal alkoxides or combinations thereof, cure temperatures etc. Since a majority of the work contained in this dissertation will deal with the effects of different kinds of solvents on the properties of ceramers and their interactions with microwaves, it is therefore pertinent that a large portion of this overview will deal extensively with the structures produced by the use of various solvent media during reactions. This section will focus on some work which will be pertinent to the last chapters in this dissertation.

The sol gel technique for silicates consists of hydrolysing and condensing a tetrafunctional silicon alkoxide such as TEOS, TMOS (tetramethylorthosilicate) using an acidic or basic catalyst (50). Three reactions can be used to describe the sol gel process.

Hydrolysis

$$\equiv Si - OR + H_2O \rightleftharpoons \equiv Si - OH + ROH$$

A) Alcohol Condensation

$$\equiv Si - OR + HO - Si\equiv \rightleftharpoons \equiv Si - O - Si\equiv + ROH$$

B) Water Condensation

$$\equiv Si - OH + HO - Si\equiv \quad \rightleftharpoons \quad \equiv Si - O - Si\equiv + H_2O$$

In the above reactions R represents an alkyl group. This reaction is usually carried out in the presence of a solvent to compatibilize the reactants i. e. water with the metal alkoxide. Solvents other than alcohols have also been used (51, 52, 53, 54). It should be noted that alcohols used in these reactions are not inert participants (52). As indicated in the reverse reactions of (1) and (2) it can participate in esterification and alcoholysis. Non alcohol solvents also have a significant effect on the reaction and structure of the glasses formed in a sol gel reaction (53). These solvents are typically labelled DCCA's (drying control chemical additives) and have been used to control pore size distributions and internal curing stresses during the formation of homogeneous gels (54, 55).

Solvents may be classifed as polar or non-polar and as protic or aprotic (52). Important characteristics of solvents with regard to affecting the final properties of sol gels are polarity, dipole moment and the availability of labile protons. Highly polar solvents can be used to solvate polar tetrafunctional silicate species used in sol gel processing. Less polar solvents such as dioxane and tetrahydrofuran (THF) may be used in alkyl substituted or incompletely hydrolysed systems. Since hydrolysis is catalysed by either

hydroxyl (OH^-) (pH>7) or hydronium ions (H_3O^+) (pH<7), solvent molecules that hydrogen bond to hydoxyl or hydronium ions reduce the catalytic activity under acidic or basic conditions. Therefore aprotic solvents that do not hydrogen bond to hydroxyl ions have the effect of making hydroxyl ions more nucleophilic where as protic solvents make hydronium ions more electrophillic (56). Hydrogen bonding of the solvent with the reactants can also a bimolecular, nucleophilic reaction amongst weak leaving groups (57).

Solvent effects on the condensation reactions are not well documented and those that are, are few and far between. Depending on the pH, either protonated or deprotonated solvents are involved in the condensation mechanism (52). Because protic solvents hydrogen bond to nucleophilic deprotonated silanols and aprotic solvents hydrogen bond to electrophilic protonated silanols, protic solvents retard base catalyzed condensation and promote acid catalyzed condensation. Aprotic solvents have the reverse effect. Highly polar protic solvents can also decelerate the condensation rate, by deactivating the nucleophile through hydrogen bonding interactions (58). Due to a strong dipole moment, these solvents can stabilize the negative charge localized on the reactants, forming a shield around them and this causes a decrease in the rate of condensation as stated above. Dipolar aprotic solvents do not possess the hydrogen atoms capable of hydrogen bonding and hence do not deactivate the nucleophile. They can, however, stabilize the reactants with respect to the activated complex and as a result slow down the reaction to some extent. The condensation reaction is most efficient in non polar

aprotic solvents which lack the ability to interact both electrostatically and through hydrogen bonding to either the reactants or the activated complex (53).

Formamide has been found to be a suitable agent for the control of structures formed during a sol gel process. Artaki et al (55) conducted ^{29}Si NMR and Raman spectroscopy to gain an improved molecular understanding of the role of formamide on the hydrolysis and condensation mechanisms. They found that the addition of formamide to silicon alkoxide sols resulted in a drastic reductions of the rate of hydrolysis and led to extensively branched gel networks of increased porosity and reduced density. A tentative explanation given by the authors (59) is the formation of a strong hydrogen bonding between formamide and silicon species which slows hydrolysis due to steric hindrances. An increase in viscosity was attributed to this hydrogen bonding. Since hydrolysis proceeds by a nucleophilic attack on a silicon atom by a negatively charged hydroxyl group, the ability of silicon molecules to reorient will be adversely affected by the increase in viscosity caused by formamide. The decrease in the hydrolysis rate will result in a larger portion of bulkier dimers because of the existance of a greater population of partially hydrolyzed monomers. Spectroscopic results showed that hydrolysis of these dimers would then be decreased due to steric hindrances which result from these bulkier alkoxy groups. This tends to promote the formation of a very porous network. Boonstra et al (60) also conducted experiments to determine the effect fo formamide on hydrolysis and condensation at 50°C, both in the acid

and basic step of a two step sol gel process on TEOS, ethanol and water using ^{29}Si NMR. The results on the acid catalyzed TEOS are similar to Artaki et al. The effect of formamide on the base catalyzed system was found to negligable. However, Rosenberger et al (61) show more extensive condensation in the formamide system. This apparent contradiction may be explained by the partial hydrolysis of formamide to produce ammonia and formic acid. Because base catalyzed silanol condensation is generally known to be first order; ammonia should increase the condensation rate. The authors Artaki et al (59) also conducted experiments using TMOS and methanol as solvent. Here the hydrolysis was found to be faster than with the formamide.

Adachi and Sakka (62) perfromed experiments using DMF as a DCCA. They reported that crack free glasses could be produced using DMF. These glasses were found to have a high porosity and a bulk density around 0.62 g/cm^3 Nogami and Moriya (63) showed that a very high porosity and a density lower than 1.0 is typically obtained with base catalyzed samples. Artaki et al also used DMF as a DCCA and concluded that the unshielded oxygen atom can strongly hydrogen bond with other polar species forming a cage around other reactive species, thereby reducing the condensation rate and giving rise to high porosity.

Various techniques have been used to characterize the structure of gels formed using the sol gel technique. Some of these are small angle xray scattering (SAXS), Small angle neutron scattering (SANS), light scattering,

scanning electron microscopy, transmission electron microscopy, nitrogen adsorption, infra-red and NMR analysis. This section will deal exclusively with small angle xray scattering and consequent results obtained from Porod and Guinier analysis on crosslinking gels as well as nitrogen adsorption since these techniques have been used in the course of this research.

Solution small angle xray scattering has been used extensively by Brinker et al (64) in their investigation of HCl catalyzed TEOS. The second step consisted of the addition of excess water along with acid and base. The acid catalyzed gels showed a Porod slope greater than -2, which indicates that these molecules are so slightly branched that the distance between branches is approximately 20Å. Slopes more negative than -2 indicate that the molecules are more highly branched so that more dense structures are obtained. These more highly branched structures are typical of base catalyzed systems where ^{1}H NMR spectroscopy and GC analyses showed the molecules to be more highly condensed and discrete as compared with the acid system. The gel point does not appear as a special point in the Porod region, because gelation depends upon the critical connectivity on length scales that are very large compared to the 1-10 nm length scale probed by SAXS. Work done by Schaefer and Keefer (65) indicate that during the conversion of sol to gel polymerization proceeds mainly by the growth of a fixed number of solution species. An investigation of scattering behavior in the Guinier region to determine the radius of gyration $<R_g>$ showed overlapping at high concentrations for the acid catalyzed system. This leads to an over estimation of the measured

$<R_g>$. The base catalyzed system being highly condensed does not reveal such overlapping even at high concentrations.

Strawbridge et al (66) performed SAXS experiments with acid catalyzed TEOS where $H_2O/TEOS$ ratios were varied from 2 to 50. All these systems displayed microporosity in the region of 30Å or less. For $H_2O/TEOS$ = 25 and 50 the matrix density was found to be uniform, but the Porod analysis from SAXS showed density variations for the ratios 2, 4 and 10. The authors concluded that in the higher $H_2O/TEOS$ ratio systems small densified particles were produced, while in the lower ratio systems gelation resulted from the entanglement of linear chains, leaving free volume on a molecular between chains. Pope and Mackenzie (67) chose a theoretical approach to modelling gel structures. These models were based on viscosity measurements which an increase in viscosity with time. The models deal with chain growth in different contexts (a) linear and (b) fractal. These models predict molecular weight, fractal density, number of fractals and other parameters.

Nitrogen adsorption has been used extensively to characterize materials before and after sintering i. e. during the conversion from gel to glass. Surface area, pore volume and density have typically been obtained from these measurements. Strawbridge et al measured porosity at 77°K for the acid catalyzed systems with water ratios ranging from 2 to 50. Type I BET adsorption isotherms revealed a microporous solid with pore widths below 20Å The microporosity decreased with the increase in temperature. Upturns in

the porosity at p/p_0 = 0.97 indicate capillary condensation in macropores. However pore size was found to increase with increasing water content. Brinker and Scherer (68) also performed nitrogen adsorption on acid catalyzed TEOS. The isotherm obtained is of type IV according to Brunauer, Demming, Demming and Teller (BDDT). Hysteresis is observed for high pH samples indicating ink bottle type pores. This means that the pore cavities are larger in diameter than the openings (throats). the low pH amd low water content samples show no hysteresis. This is indicative of uniform diameter microporosity (69). Pore size analysis determined from the desorption and adsorption branches show a narrow distribution of small diameter pores around 30Å and a broader distribution of larger diameter pores around 40Å corresponding to the throat and interstitial cavities respectively. Neither pore size distribution showed any bimodality.

1.9 AGING OF GELS

Gelation is typically accompanied by a sharp increase in viscosity and the structure can often be "frozen" at this point. This frozen-in structure may change appreciably with time depending upon solvent, pH and temperature. It may also depend upon the rate of removal of solvent. Change in gel structure were described by Zarzycki et al (70) during the process of aging and

dessication. They described the structure of gels according to Iler's model or aqueous silicates and thus made no distinction between colloidal and polymeric gels. However there is now evidence that most gels are polymeric in nature and this may change the mechanism of aging significantly (71). As aging occurs the gel shrinks and this gives rise to cracks and voids. In order to obtain monolithic gels the processing has to be carried slowly at low temperatures. The principal reasons for cracking of gels is due to strains caused by large capillary forces generated in the 3 - 10 nm. pores. It is difficult to dry gels thicker than 1 cm or films thicker than 1 μm. Several techniques ar currently used to circumvent the problem of cracking in gels, prominent among them being supercritical drying, in which the gel is heated above some critical temperature T_c and the critical pressure of the liquid phase under which conditions no interface exists between liquid and gas (71). The liquid is intended to produce a high partial pressure of the solvent to prevent premature drying of the gel. When the system has exceeded the critical conditions the pressure is released while keeping the temperature above T_c. The drying process is accelerated significantly. The other method of drying gels without cracking is through the use of DCCA's, which as mentioned above tend to produce larger pores thereby reducing the internal capillary stresses.

G. W. Scherer (72-78) analyzed the forces responsible for shrinkage in gels. The transport of liquid in the gel is analyzed according to Darcy's law, which relates the rate of flow to the pressure gradient in the liquid. The contraction of a gel is termed "syneresis" since contraction occurs even when there is no

evaporation. The syneresis of a gel can be explained by several forces acting on the gel. The surface between the solid and liquid in a gel has an associated surface energy which causes it to shrink. Therefore the gel will expel and densify as explained by Partlow and Yoldas (79). As the liquid evaporates, the surface of the exposed solid will be in contact with vapor and the corresponding surface energy γ_{sv} is much greater than γ_{sl} This promotes a much greater tendency to shrink. The difference between the two surface energies give rise to a hydrostatic tensile stress, P, which causes the remaining liquid to spread itself across as much area as possible, giving rise to a redistribution pressure. Other factors which force a contraction in these gels are the changing chemical potential on the surface of a gel due to reactivity, osmotic pressure etc.

1.10 CERAMERS: SOME GENERAL STRUCTURAL FEATURES OF PTMO CONTAINING HYBRIDS

Ceramers containing isocyanatopropyltriethoxysilane endcapped polytetramethylene oxide oligomers were first prepared by Huang et al (80). The method of preparation consisted of reacting an triethoxysilane endcapped PTMO with TEOS in the presence of an acid catalyst. Solvents such as isopropanol and tetrahydrofuran were used in order to compatibilize the

reactants and obtain a homogenous reaction mixture (81, 82). The sol was then poured into a regular petri dish and allowed to gel. Films were removed after five to seven days and subjected to physical testing. The films were usually transparent indicating no microphase separation. However small angle xray scattering revealed microphase separation on a very localized scale i.e. ca 10nm. The scattering intensity was found to increase with the increase in the inorganic content in the composite. This trend continued upto 70wt% incorporation when there is a decrease in the intensity which was interpreted to be due to a phase inversion in the system. For a fixed composition the "Bragg spacing" of the scattering peak was found to shift to smaller angles with the increase in the molecular weight of the oligomer. As the molecular weight increased from 650gm/mole to 2900gm/mole the interdomain spacing, which is inversely related to the scattering angle, increased from 70Å to around 130Å. This would seem to indicate that the peak in the scattering profiles, is of the interparticle interference variety.

Dynamic mechanical analysis revealed an increase in the rubbery modulus with the increase in the TEOS content which is to be expected. This is due to the reinforcing action of the inorganic component. The storage modulus increases with temperature indicating that there is some uncured inorganic which reacts upon furthur heating thereby increasing the crosslink density which in return promotes greater stiffness. The Tan δ behavior which is a measure of the materials ability to dissipate energy revealed a bimodal loss system. This was attributed to the existance of the PTMO in two phases. The

lower temperature peak which occurs at around -20°C for a 60wt% filled system was attributed to the cooperative segmental motion of PTMO in a rich PTMO environment while the higher temperature peak was postulated to be due to the motion of PTMO chains trapped in an inorganic rich environment. The T_g of the material was also found to increase with the increase in the inorganic content.

Stress-strain analysis revealed an increase in the elastic modulus with the increase in the alkoxide content. This was accompanied by a decrease in the ultimate strength and final elongation of the hybrid. The samples also revealed an increase in the modulus with time. This was believed to be due to chemical aging or an increase in the extent of reaction in the glass phase which caused further densification of the inorganic phase with consequent entrapment of the polymer chains which increased the T_g of the material.

Huang (84) used the data obtained from SAXS, DMA and stress-strain analysis to propose a general morphological model for these TEOS/PTMO ceramers. A schematic of the model is depicted in the Fig 1.16. In this model the inorganic component (which is indicated by crosses) is shown to be phase separated from the oligomeric component. Some segments of the inorganic component are however mixed with the PTMO as shown in the figure. The average distance between the inorganic domains is indicated by d between the arrows. This value of d represents the interdomain spacing as measured from SAXS. This morphological model has been tested by changing some of the molecular

parameters in the ceramers and the results have been studied using small angle xray scattering. It has proved quite successful at explaining several features of these ceramer systems.

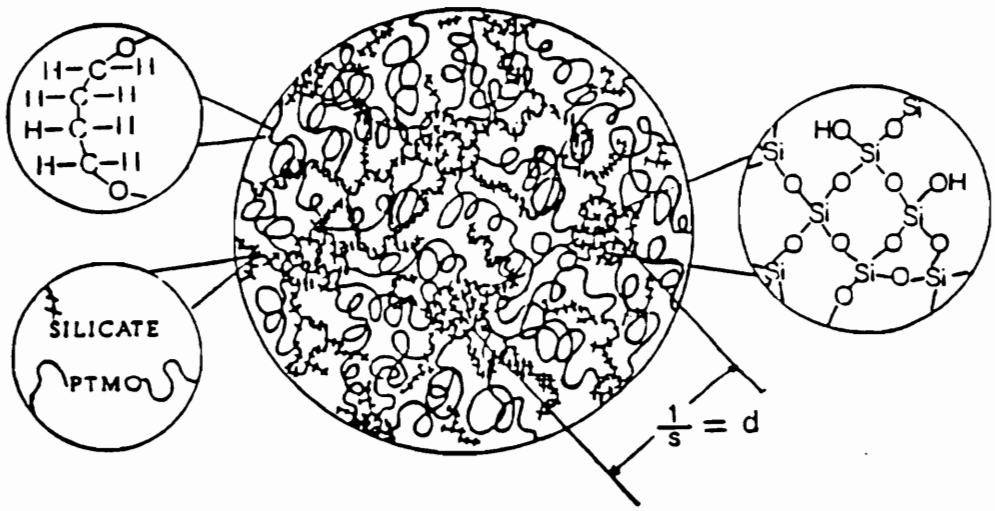


Figure 1.16. Schematic of the generalized morphological model

CHAPTER 2

EXPERIMENTAL

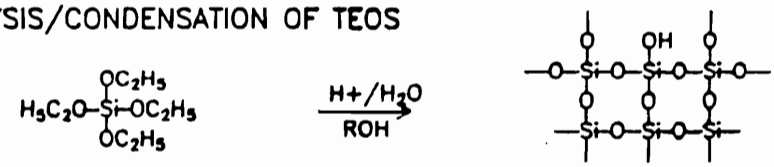
2.1 MATERIALS

Ceramers are typically prepared by the reaction of a metal alkoxide e. g. tetraethylorthosilicate (TEOS) with an endcapped oligomer e. g. polytetramethylene oxide endcapped with isocyanatopropyltriethoxysilane

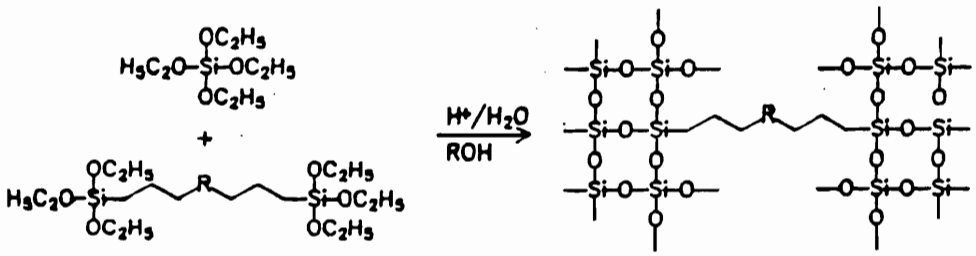
(PTMO) as shown in Fig 2.1. This reaction is usually carried out in the presence of a cosolvent system such as tetrahydrofuran (THF) and isopropanol (IPA) or N, N Dimethylformamide (DMF) and IPA. Solvents are used to compatibilize the reactants, since TEOS is not compatible with water or PTMO. Materials used in these reactions were typically purchased from vendors and used as received, except for the polytetramethylene oxide which had to be endcapped with isocyanatopropyltriethoxysilane (84) in a separate process as shown in Fig 2.2. All the ceramer films studied and documented in this dissertation were prepared from endcapped PTMO of M_n = 2000 gm/mole. The PTMO was purchased from Polysciences. TEOS was purchased from Petrarch Systems Inc. and was always of the highest purity grade (99% + distilled over quartz). Reagent grade titanium (IV) isopropoxide and zirconium isopropoxide (97% +) were used as shipped and these were obtained from Aldrich Chemical Company Inc. Isocyanatopropyltriethoxysilane (95%) was obtained from Petrarch Systems. THF, IPA and DMF were purchased from Fisher Chemical Co.. The individual reaction conditions will be detailed at the beginning of each chapter since these vary significantly depending upon the metal alkoxide used.

A REACTION SCHEME FOR THE PREPARATION OF "CERAMER" HYBRIDS

HYDROLYSIS/CONDENSATION OF TEOS



INCORPORATION OF FUNCTIONALIZED OLIGOMERS



R = VARIOUS FUNCTIONALIZED OLIGOMERS

Figure 2.1. Reaction between TEOS and PTMO to produce a hybrid ceramer.

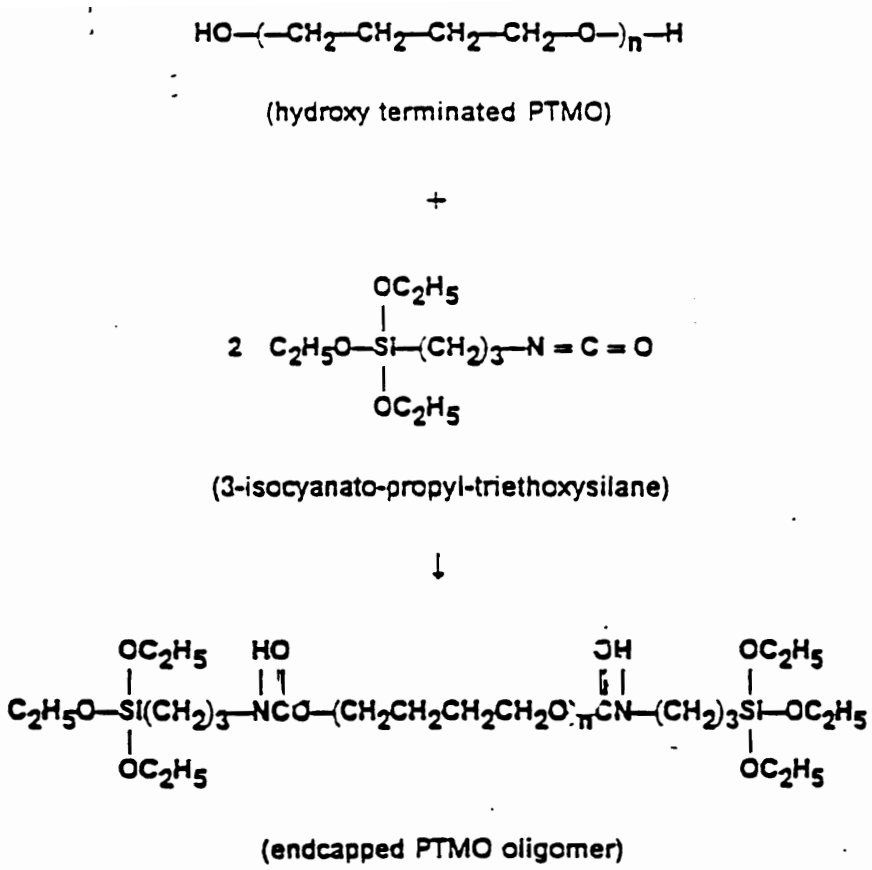


Figure 2.2. Endcapping reaction of PTMO with isocyanatopropyltriethoxysilane

2.2 MICROWAVE EQUIPMENT

The microwave equipment utilized for these reactions consisted of a continuous source generator with a maximum power of 85 watts. The frequency of the generator is 2.45 GHz and was purchased from Raytheon. The generator was connected to the waveguide through a system of coaxial cables as shown in the Fig 2.3. The power meters are connected to the generator through a circulator. The circulator allows for a power flow in one direction while diverting the power flowing in the opposite direction to another port and not to the generator thus saving the generator magnetron from overheating. The power meters are set up so as to be able to record the input power, reflected power and the transmitted power. The two systems that were used were the rectangular waveguide system and the cylinderical waveguide system. These will be discussed with respect to their use in particular experiments.

2.2.1 CYLINDERICAL CAVITY

The cylinderical microwave cavity was designed by Asmussen et al (87). This system was specifically designed with a view to subjecting the sample to a uniform horizontal field during microwaving. The special feature of this cavity

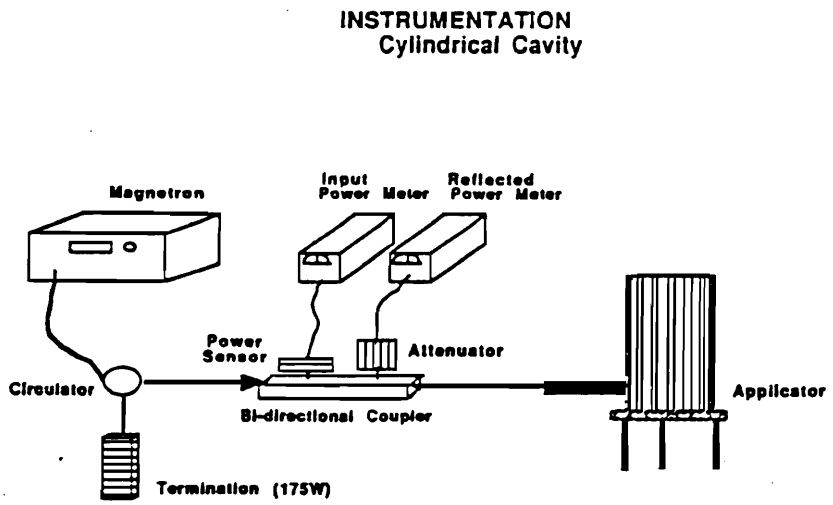
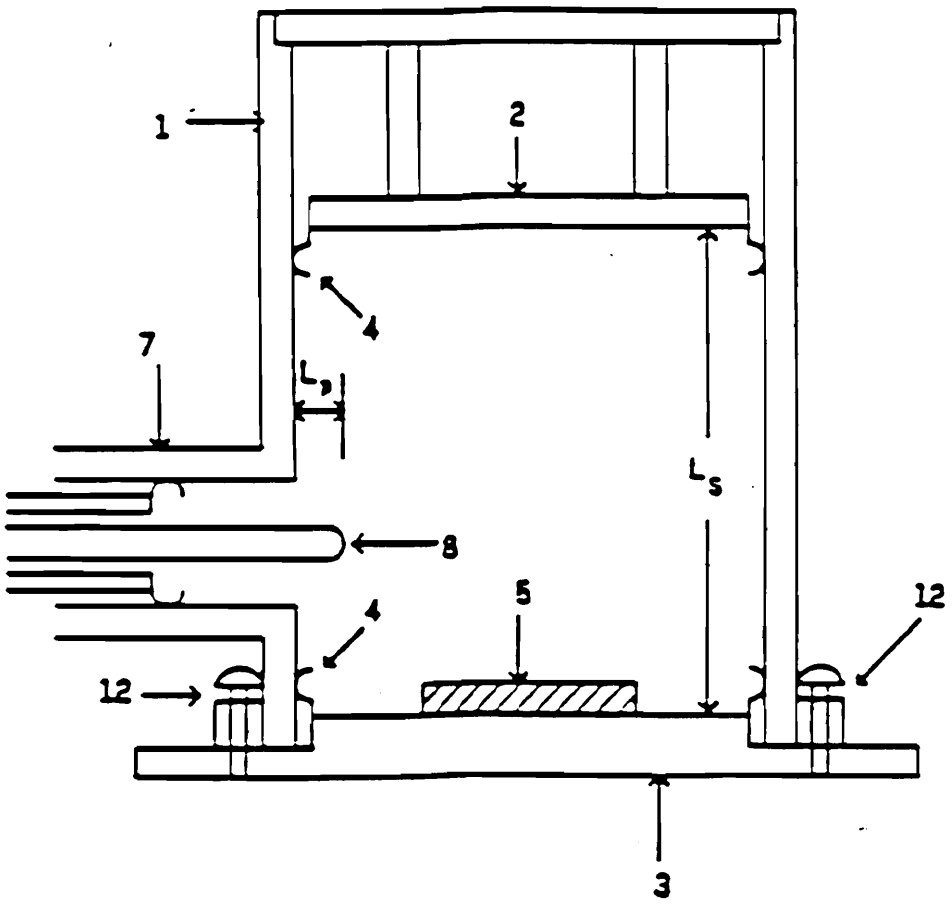


Figure 2.3. Schematic displaying the microwave setup utilized for curing ceramers (45).

is that it is tunable i. e. its physical dimensions can be changed to create a standing wave in the cavity and to alter the field strength in the vicinity of the samples and therefore control the temperature. The cavity dimensions are chosen so that the modes possible when the cavity is empty are TE_{111}, TM_{012}, TE_{211}, TE_{011}, and TM_{111} (degenerate modes) and TE_{311}. Loading of the cavity, however, causes a disruption of the above mentioned modes and the cavity then operates in a hybrid mode (88). Also, depending upon the material properties and placement, new cavity modes may be introduced. This multimode coupling reduces the sensitivity to the material geometry and other characteristics discussed in chapter 2. During heating, material properties change and as this occurs it is possible that new modes may take place in the heating.

A schematic of the cavity is shown in Fig 2.4 and 2.5. The resonant cavity is cylinderical in shape and made of brass. The inner diameter is 17.8 cm. The cavity length can be adjusted from 6 to 16 cms by means of an adjustable shorting plate. The other end of the cylinderical cavity is closed shut by another shorting plate which is fixed. The fixed shorting plate is on the bottom of the cylinder and hence its circumference is lined with silver plated finger stock to prevent radiation leakage. The periphery of the adjustable shorting plate is also lined with finger stock to ensure good electrical contact. The adjustable coupling probe penetrates into the cavity at about a height of 3 centimeter from the fixed shorting plate as can be seen in the photograph in Fig 2.5. Both adjustable pieces i.e. the probe and the sliding short are

provided with micrometers for fine tuning of the cavity. The plane of the TE_{111} mode is shown in the Fig 2.6. The lowest cavity length of 6 cms has the TE_{111} as the dominant mode (87). Knowledge of the power distribution in a cavity is vital before a material is subjected to microwaving. The dominant mode determines the power distribution in an empty cavity which has an important effect on the geometry of the sample chosen for microwaving. Power distributions for the TE_{111} mode have been calculated for an empty cavity by Jabbari. These are shown in the Figs 2.7 and 2.8. The recommendations made by the author based on these curves are that the ideal sample diameter should be less than approximately one inch and that the height of the sample should be less than one centimeter. In the case of this research the sample holder used was a petri dish of diameter approximately 2.5 inches, while the sample thickness was 5-10 mils in each case. This would cause a lower temperature to be developed on the periphery of the sample for the power distribution shown in Fig 2.7. This should not be cause for undue worry since an error here would be on the side of caution and not cause any significant temperature gradients above 70°C. or 120°C. The chosen temperatures for study as will be stated in later chapters.



1) brass cavity 2) sliding short 3) base plate 4) teeth 5) sample 7) guide 9) E probe

Figure 2.4. Schematic displaying the various parts of the cylinderical cavity (87, 88).

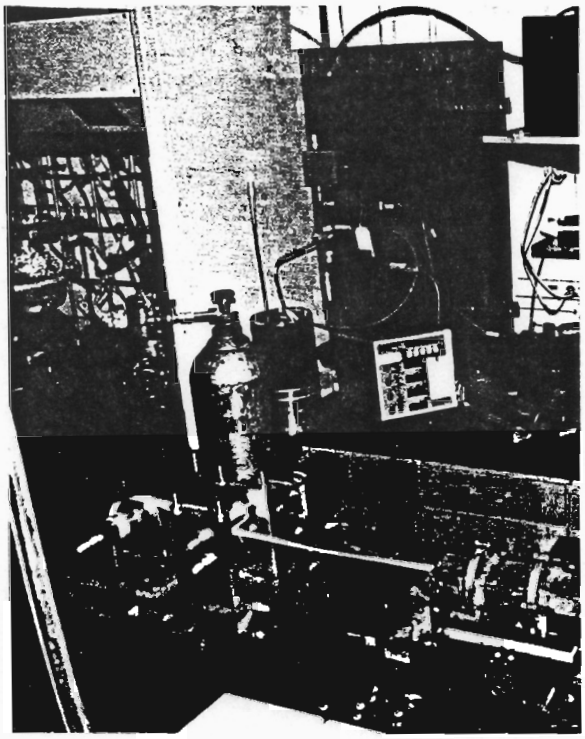


Figure 2.5. Photograph of the cylinderical cavity.

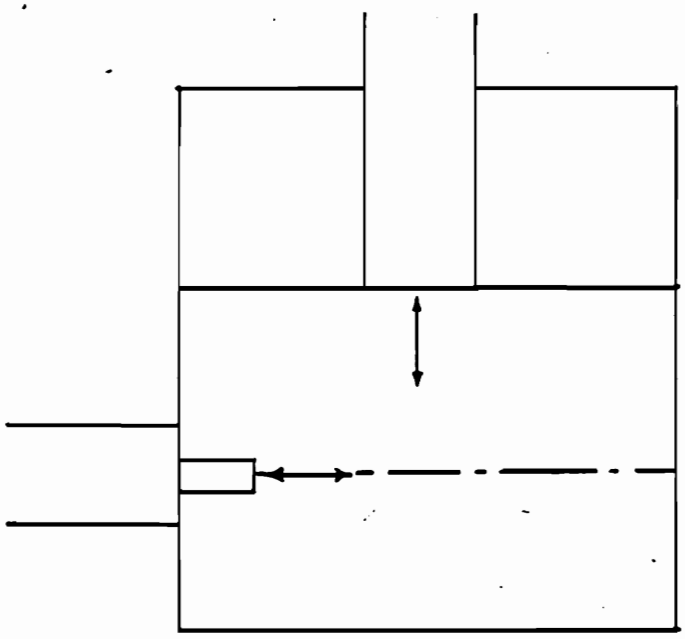


Figure 2.6. Plane of the TE_{111} mode in the cylinderical cavity (87, 88).

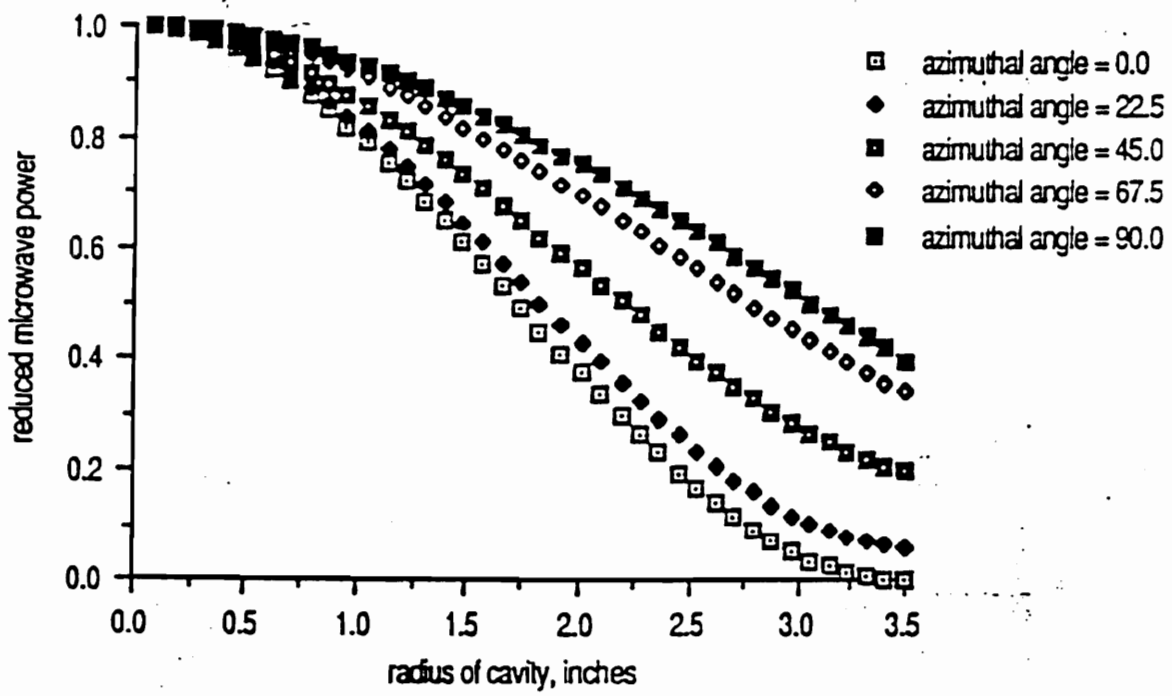


Figure 2.7. Power distribution in radial direction in the cylinderical cavity for the TE_{111} mode (45).

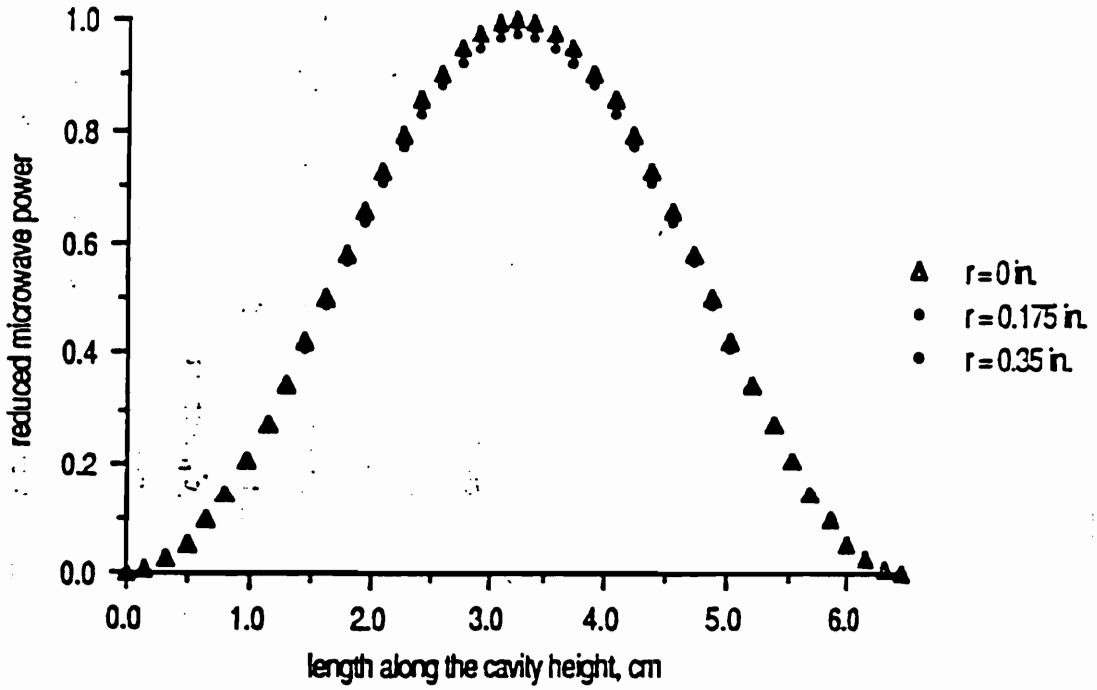
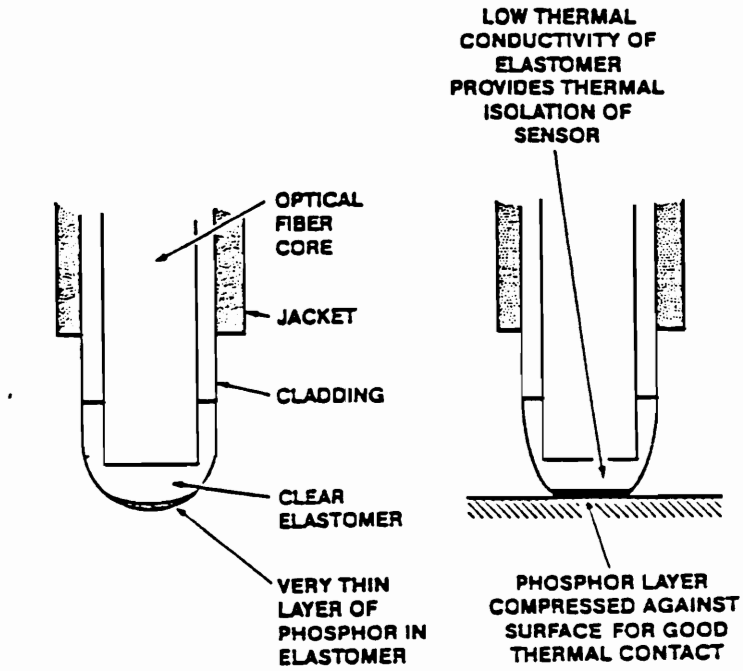


Figure 2.8. Power distribution in axial direction in the cylinderical cavity for the TE_{111} mode (45).

2.2.2 LUXTRON FIBRE OPTIC TEMPERATURE PROBE

The temperature in the microwave cavity is monitored by means of a fluoro-optic probe supplied by Luxtron. The probe is made of an optical fibre and is electrically non conducting and hence does not perturb the field. A thin layer of phosphor material is coated onto a surface of interest as shown in Fig 2.9. The characteristics of the phosphor are independent of excitation intensity. The phosphor used is magnesium fluorogermanate activated with tetravalent manganese. This phosphor apart from being thermally stable is also quite chemically inert and is not damaged by most chemicals. It can be excited by either ultraviolet or blue radiation and a Xenon flash lamp is used for the purpose. The fluoroscent emission is in the deep red and the fluoroscent decay is essentially exponential. The temperature measurement is made by measuring the rate of decay of the fluoroscence and comparing it with the calibration curve (89, 90, 91). Measurements can be made to within 2°C of any temperature within the working range of the sensor without any calibration. This limit can be decreased to within 0.2°C with calibration. The Luxtron Model 750 used has four channels which can measure simultaneously at any given time. The system was automated using an IBM PC so that the measuring was triggered from the computer and the measurements were recorded on the computer.



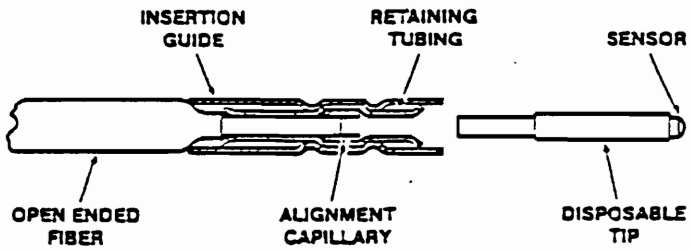


FIGURE 5. Low-cost disposable sensor to be bonded into a molded part. Phosphor sensor is in disposable tip. Fiber can be extracted and reused with a new tip.

Figure 2.9. Figure illustrates a) phosphor coated tip of a fibre optic probe b) assembly of one of these probes.

2.2.3 RECTANGULAR CAVITY

The rectangular cavity used was constructed from a WR284 waveguide. The wide dimension 'a' of this waveguide is 2.84 inches while the narrow dimension 'b' is 1.42 inches. The length of the cavity is adjustable by means of a sliding short while the adjustable probe of the cylinderical cavity can be replaced by means of an adjustable stub tuner both of which will be described shortly. The microwave power is coupled into the cavity by means of an E probe placed at a distance of $\lambda/4$ from the end of the cavity. The waveguide has a 3 mm slot cut in the upper face of the wide dimension as shown in the photograph in Fig 2.10. This slot does not perturb the fields significantly since the electric fields can short across it. This prevents any leakage from the field. The slot also facilitates the introduction of the Luxtron fibre optic temperature probe into the sample. The rectangular cavity in its present construction has the added advantage that it can also be used in the transmission mode and not only as a cavity.

2.2.4 STUB TUNER AND SLIDING SHORT

Stub tuners (posts and screws) consists of a cylinderical post which is adjustable and protrudes into the wall of the guide's wide dimension as shown

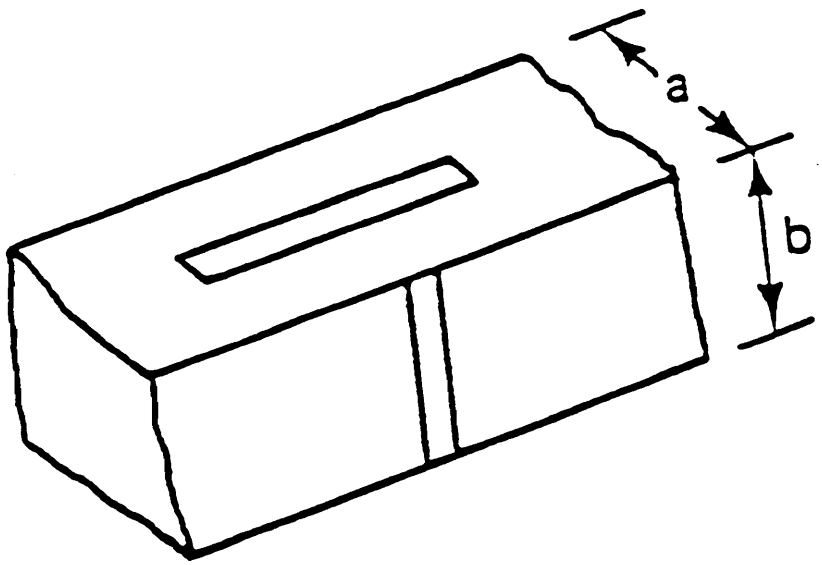


Figure 2.10. Figure illustrating a rectangular cavity along with the slit in the upper wide face (1).

in the Fig 2.11. The depth of penetration into the waveguide determines whether the post introduces a capacitive or inductive susceptance into the waveguide. A combination of two screws, $\lambda_g/4$, apart can be used to match a waveguide to its load (1). When carrying out the matching procedure, all the screws are fully retracted. One screw is then advanced, until the reflected power decreases to its lowest value possible, following which another post is lowered into the waveguide. This procedure is repeated until the reflected power is reduced to zero. The stub tuner used for the research documented in this thesis has five posts. The sliding short was purchased from Mauri Electronics. This is operated very simply by a knob shown in the photograph in Fig 2.12. The knob operates a rack and pinion mechanism which in turn moves the piston back and forward. This enables one to adjust the length and thus create a cavity (standing wave). It also facilitates easy tuning of the rectangular cavity thereby permitting a variation in the strength of the electric field around the sample.

The wavelength of a microwave of frequency 2.45 GHz is 12.24 cms. The cut-off wavelength in a WR284 waveguide is given by λ_c = 2a ('a' is the wide dimension in cms) = 14.42 cms and the corresponding cut-off frequency is 2.08 GHz. The guide wavelength is 23.15 cms. For most experiments carried out in the rectangular cavity the reflected power was retained at zero and hence the Voltage Standing Wave Ratio (VSWR) = 1.

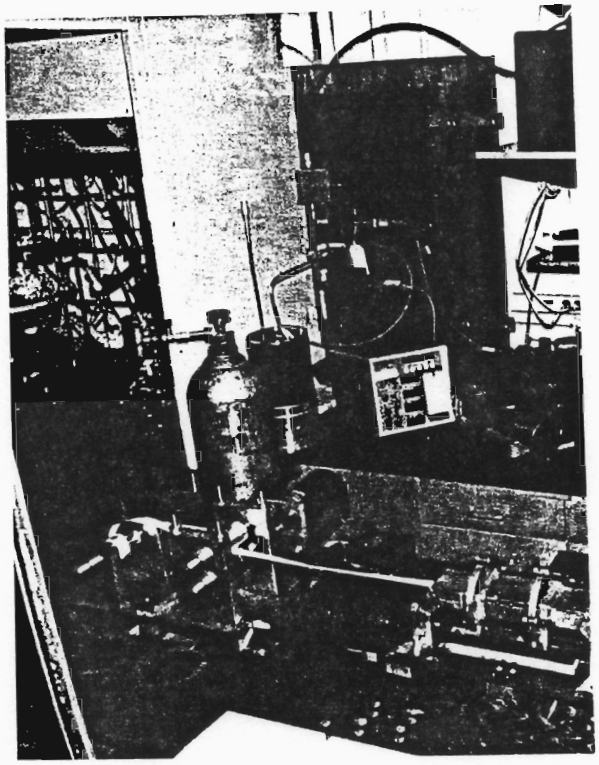


Figure 2.11. Figure illustrates the cross section of a rectangular stub tuner (1).

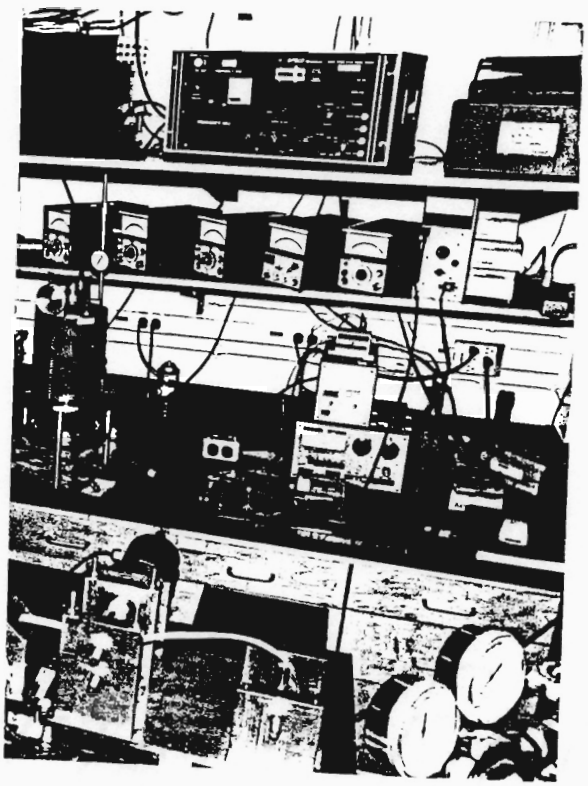


Figure 2.12. Photograph of the sliding short used with the rectangular cavity.

2.3 CHARACTERIZATION METHODS

2.3.1 SMALL ANGLE XRAY SCATTERING

Small angle xray scattering (SAXS) was carried out using a Siemens Kratky camera system in conjunction with an M. Braun position sensitive dectector system from Innovative Technology Inc. The generator used was a Philips tabletop generator PW 1729 operating at 40KV and 20mA. CuKα radiation having a wavelength of 1.54Å was used. A Nickel filter was used to remove low energy radiation. The sample to detector distance was 30.5 cm in all cases. The purge gas used was P-10, a mixture of 10% methane and 90% argon. The gas pressure was set at 10.8 bar. A voltage bias of 3.6 KV was used on the detector and the energy window set between 1 and 3 KV.

The angular measurements on the SAXS system were caliberated using lead stearate with a small angle spacing of 49.5Å Absolute intensity measurements were made using Lupolen as described by Kratky and Pilz (92). The total scattering of a sample was the result of subtracting the parasitic scattering from the sample scattering. Another fortran program written by Vonk (93) was utilized for desmearing as well as correlation function calculations. The theory behind the calculations of Bragg spacing, invariant, mean square electron

density, desmearing, correlation function calculations have been detailed extensively in (94, 95).

2.3.2 DYNAMIC MECHANICAL ANALYSIS

Dynamic mechanical analysis was carried out in the temperature range from -100°C to 170°C. Three frequencies were used - 1.1 Hz, 11 Hz and 110 Hz. The frequency chosen for display was 11 Hz because of its reproducibility. In some cases all three frequencies have been shown. The analysis was carried out using an automated (IMAS) DDV-IIC Rheovibron Dynamic Viscoelastometer which operates in the tensile mode. All samples were subjected to a tension of 15 grams and the rate of temperature increase was limited to 2°C/min. All samples were run under an atmosphere of pure pre-purified nitrogen and liquid nitrogen was used to cool the instrument down to -100°C.

2.3.3 DIELECTRIC ANALYSIS

The dielectric analysis was performed on a dielectric network analyser (DETA) manufactured by Polymer Labs Inc. The temperature range for the analysis was from -150°C to 120°C. In some cases the samples were tested to 200°C.

The rate of temperature rise was 1°C/min. All samples were tested at a five frequencies i. e. 1, 5, 10, 50, 100 KHz throughout the temperature range. Nitrogen was used as the purge gas, in order to prevent thermo-oxidative degredation. All samples were gold coated upto 150Å in order to provide better electrical contact between the electrodes and the sample. Surface impedance due to this coating was found to be negligable. The sample diameter in all cases was 20 mm and the thickness varied from 5 mils to 20 mils.

2.3.4 THERMAL ANALYSIS

Differential calorimetry (DSC) analysis was performed on a Seiko DSC 210. Most samples were about 25 mg in weight and were run under pre purified nitrogen. The Thermogravimetric analysis (TGA) was performed on a Seiko TG/DTA also under nitrogen, and samples weighing around 5 mg were utilized. The heating rate for both analyses was 10°C/min.

2.3.5 STRESS STRAIN ANALYSIS

Stress-strain analysis was performed on an Instron model 1122 at ambient conditions. The testing was always carried out at an initial rate of 2 mm/min. Ten millimeter dog bone samples were always used as per ASTM D 638. The width of the samples was 2.6 mm. The data was recorded on a chart and elastic modulus values were computed as the strain tended to zero (at approximately 2 - 5% strain). In almost all cases readings were taken for a minimum of five samples or more. The stress at break represents the load at failure divided by the original cross sectional area. The elongation at break is the percent strain at which the sample is observed to break.

2.3.6 SCANNING AND TRANSMISSION ELECTRON MICROSCOPY

A Cambridge Instruments Stereoscan 200 scanning electron microscope with a secondary electron detector was used to image the fracture surfaces of ceramers. The ceramers were fractured under liquid nitrogen (-170°C), which is well below the T_g of the PTMO phase.

Tranmission Electron Microscopy was performed on microtomed samples. The TEM used was a Philips 420 Scanning Transmission Electron Microscope. The samples were cryomicrotomed to a thickness of 400-600Å using a Reichert

microtome. Samples were examined under an accelerating voltage of 100 KV. The photomicrographs were then enlarged by a factor of four during developing to enhance the observed features.

2.3.7 SWELLING EXPERIMENTS

Swelling experiments on the ceramers were carried out in THF at room temperature. Samples were first evacuated to remove any residual solvent. Sample weights between 0.5 gm to 0.7 gm were usually immersed in a beaker containing THF for upto 72 hours, until the weight stabilized. The sample was then removed from the beakers and then immediately blotted dry and weighed. Results were reported as percent weight uptake of THF.

2.3.8 DIELECTRIC NETWORK ANALYSIS

This work performed on a HP 8510 network analyzer was done at room temperature. A cylinderical sample was placed in a resonant cavity and the change in the resonant frequency of the cavity as well as the Q factor was measured. This change in the resonant frequency was then mathematically broken down into the respective dielectric loss and storage factors for the

tested material as stated earlier in chapter 2. An empty NMR tube is first placed in the cavity and the analyzer caliberated with air as the dielectric.. The tube is then filled with the solution or the reacting medium to be measured and the storage and loss recorded as a function of either time or temperature. This technique is sensitive to changes in chemistry and has been used to monitor the build up of dielectric loss during the sol gel reactions. This technique is limited to materials possessing relatively low dielectric constants. For materials with high dielectric stroage and loss factors the cavity begins to operate in the distortion regime rather than in the perturbation regime.

CHAPTER 3

STRUCTURE PROPERTY BEHAVIOR OF TEOS/PTMO CERAMERS CURED IN SOLVENT MEDIA OF N, N DIMETHYLFORMAMIDE AND ISOPROPANOL

3.1 BRIEF HISTORY OF THE USE OF N, N DIMETHYLFORMAMIDE IN SOL GEL CHEMISTRY

The use of DCCA's (drying chemical control additives) as compatibilizing solvent media in sol gel reactions involving only TEOS as a reactant was pioneered by Hench and coworkers (53, 54). Since then several DCCA's have been studied, prominent among them being 1, 4 dioxane, N, N-dimethylformamide (DMF) and acetonitrile (55). DMF has, in particular, been reviewed extensively because gels produced from only TEOS or TMOS in this media yield monoliths. This has been found to occur because the pore distribution in the resulting silicate gels is shifted to a larger mean diameter (as compared with silicates produced in other solvents such as isopropanol or ethanol) which, in turn, reduces the magnitude of the capillary forces. This reduction in the capillary forces lessens the internal stresses in the gel and helps produce monolithic materials. It has also been shown, that apart from the larger pore sizes, the low surface tension of the liquid remaining in the pores during drying, is favourable for the formation of monoliths without cracks or fracture. DMF is known to hydrogen bond with the silanol moities in the reaction mixture thereby forming a shield around these reactive sites and slowing down condensation by reducing the diffusion of reactive species. This can result in the formation of ring (silicate) structures which then give rise to porous gels upon undergoing dessication.

3.1. INTRODUCTION AND OBJECTIVES

In our own laboratories Huang (84) discovered that the use of a 1:1 mixture of DMF and isopropanol (IPA) as compatibilizing solvents in the acid catalyzed reaction between TEOS (tetraethylorthosilicate) and endcapped PTMO (polytetramethylene oxide) resulted in ceramer systems which displayed unique properties. This ceramer film was shown to be more sharply phase separated as seen from DMA and SAXS data and possessed a much higher modulus than corresponding TEOS/PTMO ceramers prepared in THF (tetrahydrofuran) and IPA. Very few detailed studies were however conducted on the TEOS/PTMO ceramers reacted in DMF/IPA with regards to their structure property relationships and their aging characteristics.

The sharper phase separation between the oligomeric component and the inorganic component seen in these TEOS/PTMO materials reacted in DMF/IPA provides a unique opportunity to enhance the reaction between reactive dipoles using microwave processing. Further hydrogen bonding which also occurs between the DMF and the hydrolysed TEOS in these systems (59) has been found to play an important role in the absorption of microwave radiation.

Based on these observations an attempt was made to study the action of DMF/IPA cosolvent system on the structure property relationships of TEOS/PTMO ceramers when the reaction was carried out at elevated temperatures. As stated earlier in chapter 1 this was brought about by using conventional heating (convection oven) as well as microwave radiation. The reactants were heated to 70°C by both the above mentioned means. Room temperature cured TEOS/PTMO ceramers were also studied in order to contrast their properties with those obtained for the ceramer films cured at 70°C. This chapter will therefore essentially detail the effects of microwave radiation on the reaction between TEOS endcapped PTMO and the consequent structure property relationships of these microwaved films. Properties of TEOS/PTMO films produced by conventional means at 70°C or at room temperature will be compared with the properties of the microwaved films. Thus the structure property relationships of these ceramers i. e. microwaved, oven cured and RT cured films will be studied using stress strain, DMA, SAXS, FTIR and some DSC analysis. Aging studies were also conducted on these materials after a period of one month to determine the long term effects of elevated temperature processing.

3.2 EXPERIMENTAL METHODS AND SAMPLE PREPARATION

Sample formulation for these materials consisted initially of 60wt% of TEOS with the remainder (i. e. 40 wt%) constituted by triethoxysilane endcapped polytetramethylene oxide (Mn=2000). Water was added in an amount equivalent of 100wt%, the theoretical stoichiometric amount necessary to hydrolyse all alkoxy functionalities present in the reaction mixture. Hydrochloric acid (10N) was added to catalyse the reaction and the molar ratio of HCl to TEOS was 0.048. DMF and IPA were used as cosolvents to promote miscibility between the polymer, water and TEOS. They were added in a volume ratio of 1:1 to the reacting mixture. The nomenclature for this material is shown in Fig 3.1.

The procedure chosen for sample preparation is shown in Fig 3.2. The reactants TEOS and PTMO were initially added to a cosolvent system of IPA and DMF. This mixture was stirred for a period of twenty minutes to enhance miscibility between the reactants and also to produce a homogenous reaction mixture. Water and acid catalyst were then added to the reaction mixture which was stirred for an additional period of two minutes. The samples were then poured into petri dishes, following which they were subjected to their respective curing processes which will be detailed shortly.

NOMENCLATURE FOR SOL GEL HYBRIDS
TEOS(60)-PTMO(2K)-100-0.048

ITEM	DESCRIPTION
TEOS	Tetraethylorthosilicate
(60)	Wt% Of TEOS To Oligomer
PTMO(2K)	Functionalized Oligomer (MW)
100	Ratio Water To Alkoxide (Mol%)
0.048	Ratio Acid To Alkoxide (Mol%)
(THF/IPA) (DMF/IPA)	Solvents For Compatibility

Figure 3.1. Nomenclature for the ceramers described in this chapter.

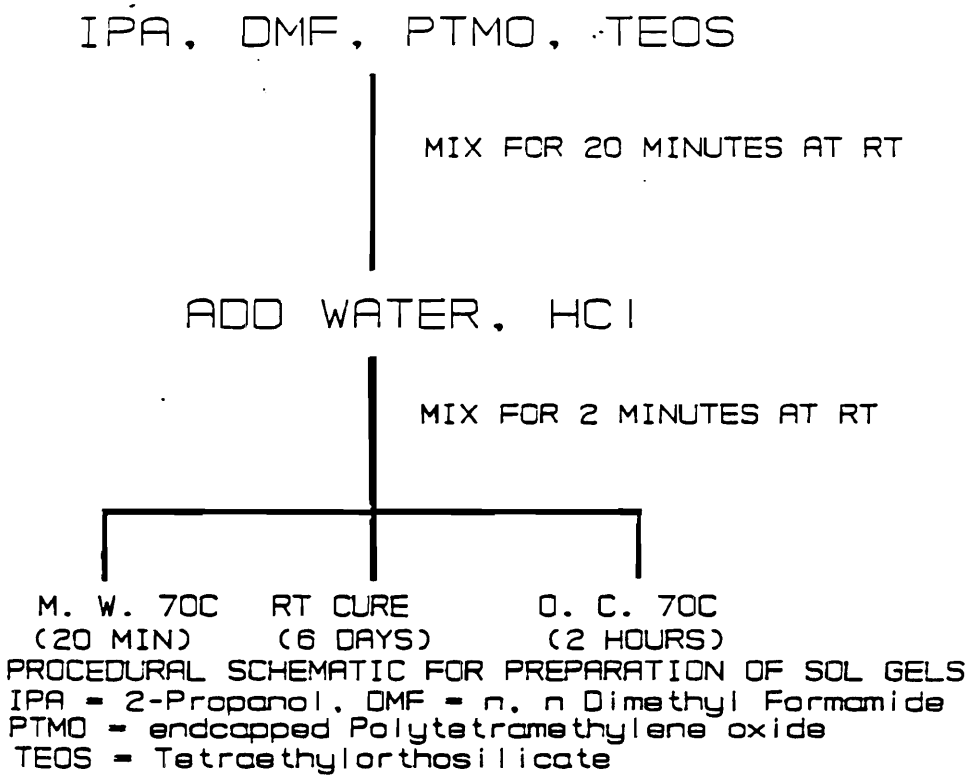


Figure 3.2. **Procedure used for the preparation of ceramers in solvent media consisting of IPA and DMF.**

As stated earlier, the elevated temperature chosen for the structure-property study was 70°C. The oven cured ceramers were heated for two hours in a convection oven after which they were removed and subjected to physical testing. These samples were denoted as "O. C. 70C". Microwaved samples were prepared in a manner identical with that of their oven cured counterparts; the chief exception being that they were placed in the cylinderical microwave cavity and heated due to the coupling between polar groups in the reacting mixture and microwave radiation as described in chapter 2. A glance at the microwave heating profile shown in Fig 3.3 indicates a steeper initial heating rate as compared with the oven curing. The sample placed in the microwave cavity began to heat almost as soon as the power was turned on. Samples heated to 70°C in the microwave cavity are denoted by "M. W. 70C". The temperature was raised to 70°C in approximately 6 minutes. The rate of heating decreased as the temperature reached 70°C. The temperature was then held at 70°C for an additional 13 minutes making the total 'heating' time in the cavity equal to 20 minutes. The temperature was continuously monitored using a fiber optic probe placed directly into the center of the reacting mixture and three others placed on the periphery to check for thermal gradients. Fluctuations in temperature of the sample (M. W. 70C) at 70°C were not permitted to exceed 1°C. This is usually achieved by constantly tuning the microwave cavity. The heating profiles for oven as well as microwave cured films in in Fig 3.3 shows that the rate of temperature increase in a conventional convection oven is much slower than for the microwave process. The

temperature of the reactive solution in the oven reaches 70°C after 25 minutes, while in the microwave cured material the temperature of the reactants is raised to 70°C in approximately 6 minutes. Room temperature (RT) cured samples were also placed in petri dishes and stored under ambient conditions for six days before they can be handled and physically tested.

The input power used initially in the microwave curing process was 10 watts and is shown in Fig 3.4. This level of power was sustained until the sample temperature reached 70°C. At this point in the curing process the input power level to the sample was reduced in order to maintain the temperature at 70°C. The cylinderical cavity is tunable which means that its physical dimensions can be adjusted so as to create a standing wave of high intensity thereby improving the Q-factor of the cavity. By tuning the cavity the input power is still maintained at 10 watts but the reflected power which was initially zero is now increased to 3 watts. The dipoles in the sample therefore experience an electric field strength equivalent of only 7 watts of power. This reduces the rate of heating to zero and the sample temperature is maintained at 70°C.

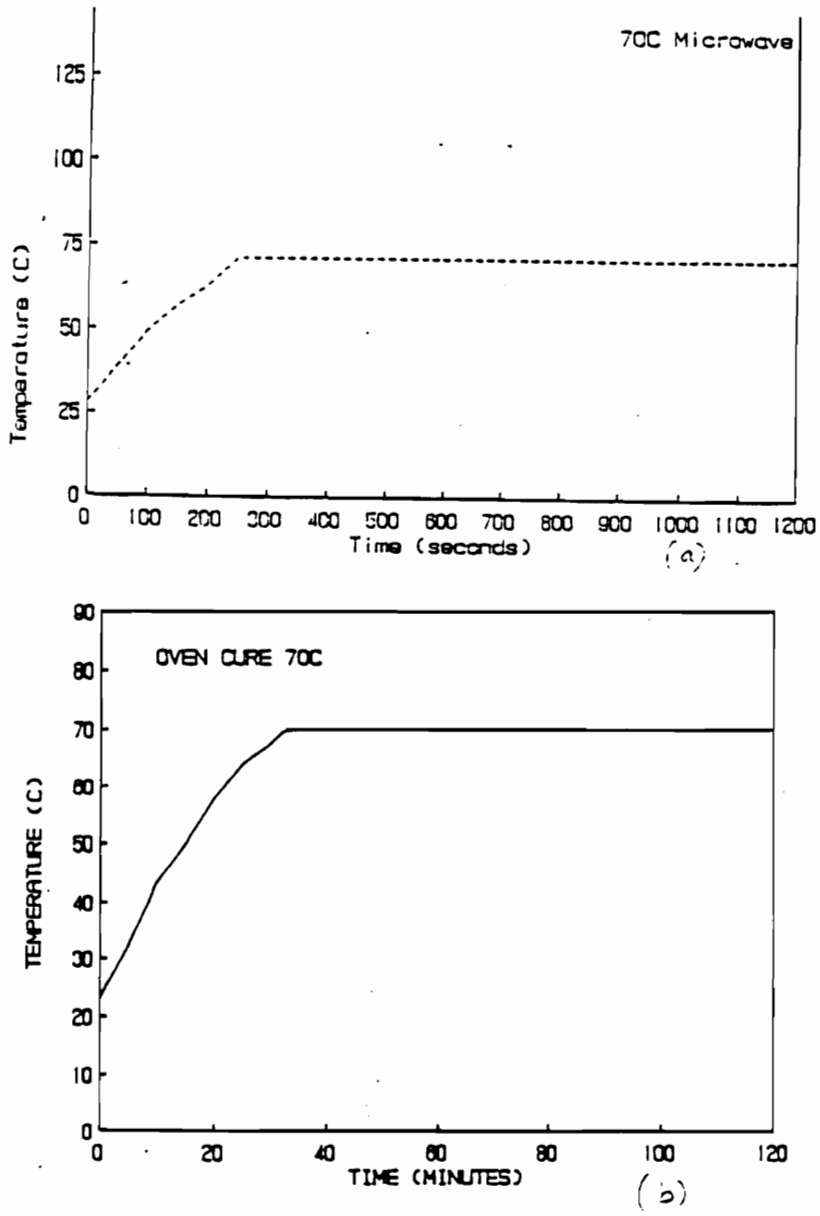


Figure 3.3. Heating profiles utilized for the microwave curing and oven curing process.

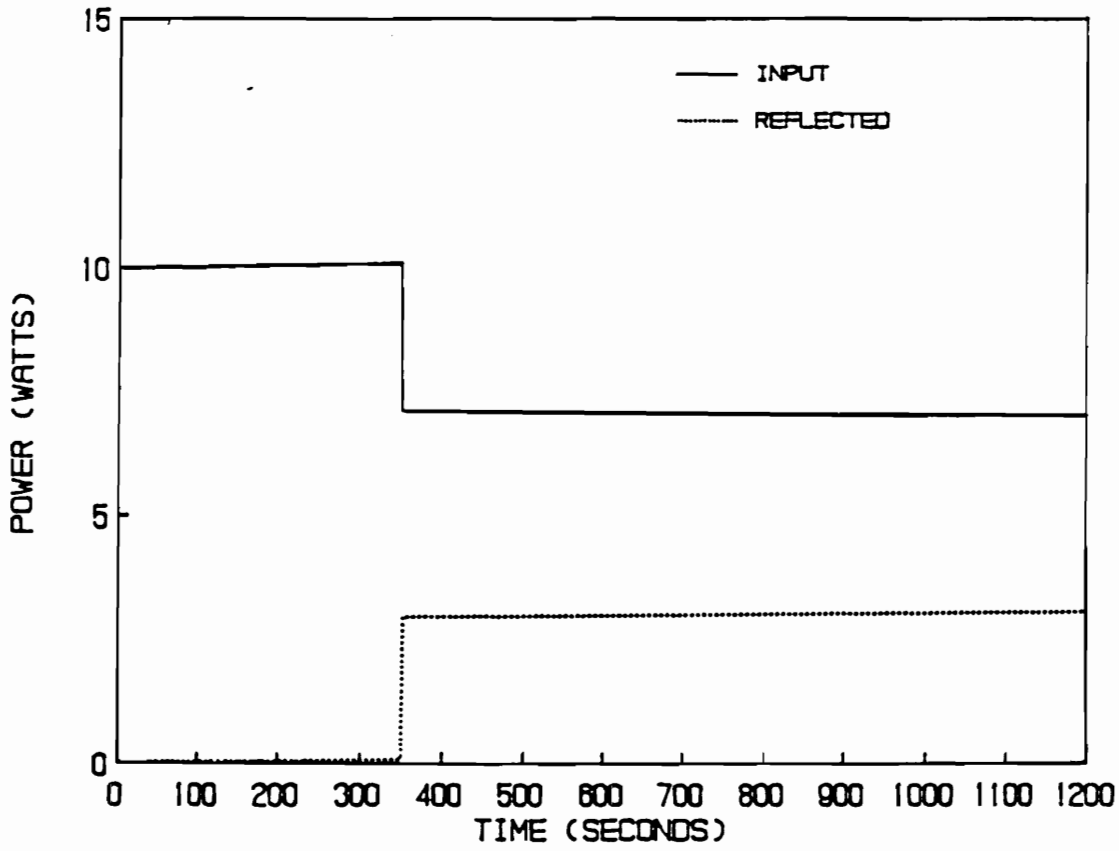


Figure 3.4. **The power profile used to heat the sample to 70°C in the microwave cavity.**

3.3 RESULTS AND DISCUSSION

3.3.1 STRESS STRAIN ANALYSIS

Samples were subjected to stress strain analysis almost immediately after microwave processing or removal from the oven (within two hours). The results for the stress-strain analysis are shown in Table 3.1. The microwave cured samples show a high elastic modulus of 250 MPa which is approaching the value of a polymeric glass. The stress at break is approximately 40 MPa and the elongation at break is 21%. A glance at the stress strain curve for the M. W. 70C film in Fig 3.5 shows a material exhibiting somewhat brittle behavior. The materials cured in a conventional oven at 70°C show an elastic modulus of only 4 MPa and are extremely tacky. The reason for this difference is because the microwave cured samples undergo a higher extent of reaction and this can be explained in terms of the coupling that occurs between microwave radiation and the polar reactants. The coupling between microwaves and molecules is dependent upon the dielectric loss of the dipolar relaxation of individual molecules. However, induced dipoles and molecules which hydrogen bond can respond very rapidly to electromagnetic fields. The silanol groups are known to be strongly dipolar and can absorb microwave radiation more efficiently because of the presence of the hydroxyl moiety.

These groups are stronger than the other dipoles in the reacting solution and this feature will be further discussed in chapter 7. Artaki et al (59) have also pointed out to the ability of the unshielded oxygen atom of DMF to hydrogen bond with the silanol. It is possible that such hydrogen bonding can cause a greater coupling between the microwave radiation and the reactants which can give rise to localized regions with higher temperatures than those measured in the bulk of the reactive solution. Evidence from other studies indicates that such coupling can greatly enhance the rate of reaction (41, 43).

Room temperature cured samples take almost six days to become sufficiently strong so that they can be subjected to testing. They display elastic modulus and stress at break values which are much higher than those cured in the oven, but lower than those cured in the microwave process. The superior mechanical properties of the RT cured film as compared with the O. C. 70C film may indicate that a slow reaction rate in the oven curing process as well as the evaporation of some solvent during the curing in the oven causes the gel to be relatively unreacted and hence very tacky. It is known that IPA boils at 82°C while DMF evaporates at 153°C. Since the oven temperature is 70°C and the rate of heating in the oven is slow as seen earlier in section 4.2, IPA will be prone to evaporate more easily from the reaction mixture. The evaporation of isopropanol leaves the remaining reactants in a relatively greater concentration of DMF before any significant extent of reaction has taken place. The excess concentration of DMF slows down the condensation reaction significantly as pointed out by Artaki and co-workers (in their work with TEOS)

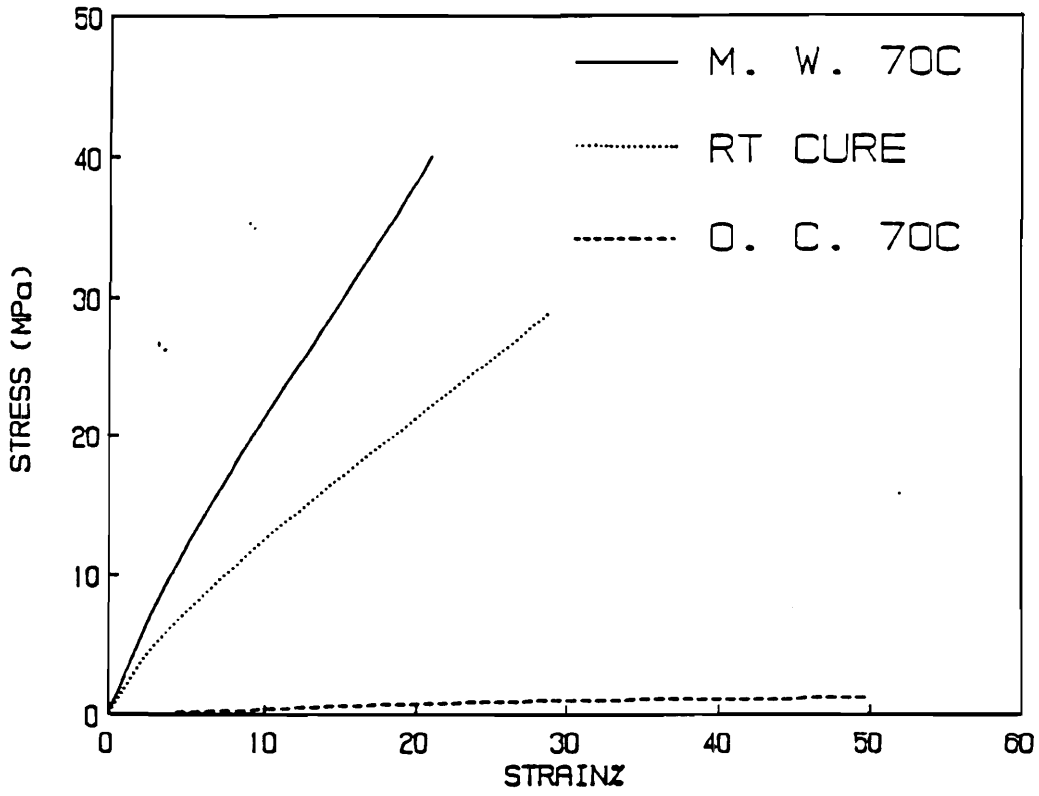


Figure 3.5. The stress strain response of the three cured (M.W.70C, O.C.70C AND RT CURED) materials under ambient conditions.

Table 3.1. Stress strain properties for the differently cured materials as labelled in figure.

	Young's Modulus(MPa)	Stress at Break (MPa)	Elongation%
M. W. 70C (20 min)	250	40	21
RT cure (6 days)	153	29	29
O. C. 70C 2 hours	4	1	50

and as will be seen in the next paragraph also hinders the incorporation of PTMO into the network. Extraction studies conducted on the M. W. 70C and the O. C. 70C film (using THF as the extraction media) show that while the extractables from the former is less than 2 wt%, it is almost 22 wt% for the latter. This indicates that there is a lack of incorporation of the PTMO into the reaction mixture.

A separate experiment was conducted expressly for the purpose of determining the effect of a greater DMF concentration on the properties of the film. This experiment consisted in reacting the same materials in an environment of IPA/DMF, only this time the amount of DMF was three times that of IPA. It was found that macrophase separation takes place almost at the instant that catalyst is added to the reaction. This macrophase separation can be observed visually. In the case of the O. C. 70C material (initial IPA/DMF

ratio = 1/1) the excess DMF remaining behind does not cause any visible macrophase separation, in part, because, some incorporation of the oligomer into the ceramer network will already have taken place during the early stages of heating in the oven, i. e. before the IPA evaporates in significant amounts. Nevetheless, this lack of incorporation of PTMO results in a film with lower mechanical properties than the microwave cured and RT cured films.

3.3.2 DYNAMIC MECHANICAL ANALYSIS OF THE DIFFERENTLY CURED CERAMERS

The DMA spectra provide useful information about the phase separation characteristics between the inorganic and the PTMO and also contains additional structural and morphological information about these ceramers. As can be seen in the Fig 3.6, the storage modulus at -100°C (the glassy state) for all three materials is of the order of 10^9 Pa. However, as the temperature is raised above -80°C there is a drop in the storage modulus of all three differently cured ceramers because of the onset of cooperative segmental motion in the PTMO oligomers. All three materials display a two step decrease in the storage modulus between -100°C and 0°C. These reductions in the storage factor are believed to be due to the dissipative abilities of the PTMO trapped in different environments as will be explained shortly.

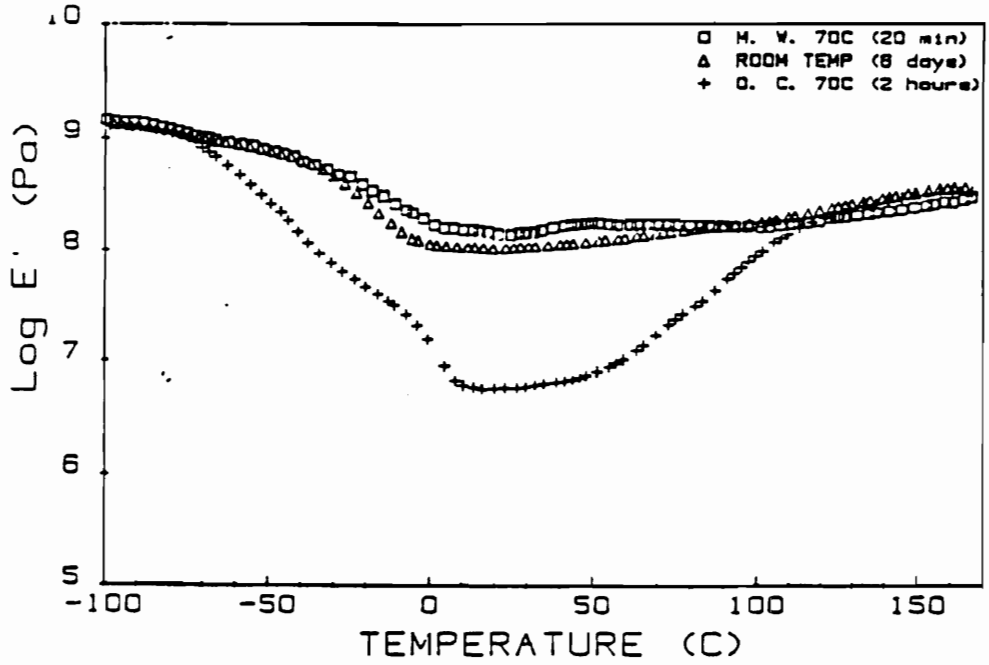


Figure 3.6. Dynamic storage modulus of the three differently cured materials (as labelled) at a frequency of 11Hz.

The two step drops in the DMA storage behavior for either the M.W. 70C and RT cured materials are small when compared with those observed for the oven cured material which is very pronounced and rather steep. In all of these three films, the first drop in the storage modulus occurs between -90°C and -50°C and is believed to be due to cooperative segmental motion of the oligomer chains present in relatively rich PTMO regions. In the case of the oven cured materials some of this response is certainly due to cooperative segmental motion of the PTMO which, as we have seen earlier, is not fully incorporated into the ceramer network. This results in a steeper drop in the storage modulus for the O. C. 70C material, than the M. W. 70C or the RT cured film. The second steep drop which occurs in the O. C. 70C film at temperatures between -40°C and 0°C is due to the melting of crystallites of PTMO as well as the relaxation of PTMO chains trapped in relatively richer inorganic phases. The drop in the storage modulus in this temperature regime i. e. -40°C to 0°C for the M. W. 70C and the RT cured films is small and is believed to be solely due to the relaxation of PTMO trapped in richer inorganic phases.

With respect to the oligomers trapped in the richer inorganic phases, it is to be pointed out that this author believes that there are possibly two general situations arising out of such interactions in all the highly phase separated ceramer systems. The highly phase separated systems being referred to here are - the TEOS/PTMO material (cured in DMF/IPA) as well as the titania/PTMO and the zirconia/PTMO ceramers which have been documented earlier by Brennan (96). One type of interaction arises from the adsorption of the

oligomer chains onto the surface of the inorganic domains. This kind of interaction usually causes some loss of mobility of the oligomer chains due to a reduction in the degrees of freedom of the PTMO molecule in contact with the inorganic. Similar behavior has been reported by Ko and Wightman (97) for polysulfone bonded to Aluminum substrates. In their work, the authors found that the glass transition of the polysulfone film in contact with the substrate was higher by about 20°C than that of the bulk polysulfone. This concept may be considered as a possibility in these ceramer systems as well. In all the ceramer systems which display a higher degree of phase separation such interactions due to adsorption cause a broadening of the lower temperature loss dispersion as can be seen in the Tan δ plot in Fig 3.7. This broadening takes place in the temperature region between -50°C to -10°C. The higher temperature broadening indicates that a greater amount of thermal energy is required to cause mobility in segments subjected to this kind of restriction versus those which are relatively unrestricted by virtue of their existance in a PTMO rich phase. Since these interactions with the inorganic are not as restrictive as those which are yet to be described i. e. encapsulations, the magnitude of the shift (in terms of the temperature at which the relaxation occurs) is relatively small and is ca. 40°C.

The second kind of interaction which occurs in some of these highly phase segregated systems is likely actual encapsulation of the oligomers by the inorganic domains. This feature is further addressed in chapter 9 and these interactions create a highly restrictive environment for the oligomer chains.

The chains, constricted thus, would require a much larger amount of energy to undergo cooperative segmental motion and typically the PTMO chains encumbered thus display relaxations above 20°C which is almost 100°C above the T_g of endcapped crosslinked PTMO (not containing any TEOS).

While the drop in storage modulus between -100°C and 0°C for the M. W. 70C and the RT cured materials is approximately one decade, the corresponding drop in for the O. C. 70C film is around 2.5 decades, reinforcing the notion that this system has undergone a lesser extent of reaction. At around 0°C the storage modulus for all three materials plateaus out. At this temperature, all three differently cured materials are in the rubbery regime of the viscoelastic spectrum. The storage modulus values at room temperature are similar to those seen in the stress strain tests. The microwave cured material displays the highest value of storage modulus while the O. C. 70 C material displays the lowest. The storage modulus for all three materials now begins to increase with temperature above 20°C. It can seen that there is a small increase (about a factor of five) in the storage modulus of the microwaved and six day RT cured samples as the temperature is raised above 50°C. This behavior has been previously observed by Huang (84) and Brennan (96) for acid catalyzed TEOS/PTMO ceramers reacted in THF/IPA. Both authors attributed this behavior to an increased extent of reaction within the system. Hence the upturn in the storage modulus seen in these TEOS/PTMO samples cured in DMF/IPA can also been attributed to further reaction brought on by the heating in the DMA.

The increase in the storage modulus with temperature above 50°C is considerable in the case of the O.C.70C material which substantiates the earlier postulation of a lower extent of reaction. This dramatic increase in the storage modulus could also result partly from evaporation of water and solvent (earlier by products of the reaction) in all these systems. The fact that the storage modulus values at 170°C are identical for all three samples indicates that reactants such as TEOS are not lost due to evaporation during the elevated temperature curing processes. Hence the evaporation of reactants can be ruled out as a possible reason for the low elastic and storage modulii of the oven cured materials.

The microwave cured sample displays a slight hump in the storage modulus between 20°C and 70°C. This behavior is a source of controversy, but is believed to be due to a variety of effects ranging from motion in the inorganic phase as has been documented by Glaser (85) and Stevels (98, 99, 100) to evaporation of solvents and additional reaction as documented by Brennan (96). Glaser has shown that relaxation behavior in the same temperature regime is seen for MTMOS (methyltrimethoxysilane) as well as MTEOS (methyl triethoxysilane) reacted into gels using HCl catalyst. Both materials had storage modulii of 10^9 Pa. at the temperature where these relaxations took place. No reasons was given for this relaxation.

Stevels (98, 99, 100) has documented that the perfect three dimensional silicate glass network is composed of Si^{4+} and O^{2-} ions which cohere in space.

In this perfect glass network, all the oxygen ions are bridging oxygens i. e. they are bonded to two silicon ions. However, in most cases, the glass network is not perfect and consists of both bridging and non-bridging oxygen ions. The non-bridging oxygens are not bonded to two silicon ions and are known to serve as interstitial sites at which other ions present in the glass such as Na^+ can bond temporarily. These non-bridging oxygen sites thus serve as points where other ions can pass from one interstice to another. Mauritz et al (101) have further documented that proton (H^+) migration can occur via the non-bridging oxygen ions present in the silicate phase in such glasses. Stevels (98) has also pointed out that the smaller the migrating ion the larger will be the extent of migration in such silicate glasses. It is indeed possible that the mobility of these protons or other ions (present in the ceramer system as impurity) can cause some relaxation in the inorganic phase which may be seen in the DMA Tan δ curves. Further, as will be seen in chapter 8 dielectric analysis on all the highly phase separated ceramers show a tremendous loss in the same temperature range due to Maxwell Wagner Sillars interactions which are brought on by charge trapping at the interfaces.

Relaxation of the encapsulated PTMO chains is another factor which needs to be considered in this temperature regime. This will be detailed in the section on Tan δ behavior for these materials. Brennan (96) has documented that this relaxation (above 20°C in the titanium/PTMO and zirconium/PTMO ceramers) may be associated with increased condensation reactions in the system. All the various types of relaxations discussed above should effectively produce a

decrease in the storage modulus above 20°C, since, typically, there occurs a decrease in the storage modulus whenever a relaxation takes place. However, in the same temperature range additional curing takes place in the ceramer which is known to enhance the extent of reaction thereby increasing the storage modulus. It may then be construed that the increase in storage modulus caused by additional condensation reactions competes with a decrease in storage modulus brought on by relaxations (in the inorganic phase and in the PTMO) within the ceramer. It is therefore speculated that these opposing effects may be responsible for the hump which is caused by a greater magnitude of the effect due to the former (increasing stiffness due to additional reaction) over the latter (decreasing stiffness due to relaxation) within the temperature range 20°C to 70°C.

The Tan δ (Fig 3.7) behavior provides some useful information about the morphology of these systems. In general the Tan δ response for all systems displays bimodal loss behavior with one region of loss occuring between -90°C and 0°C and a second region starting at around 20°C and continuing to 150°C. The lower temperature loss dispersion for these films is due to the PTMO cooperative segmental which begins at -90°C. The onset of relaxation behavior at -90°C reflects a greater degree of phase separation between oligomer and inorganic when compared with TEOS/PTMO ceramers reacted in THF/IPA, which, typically show the onset of cooperative segmental motion (due to the PTMO) at around -75°C. This delayed onset of cooperative segmental motion in these ceramers was attributed to more extensive mixing between segments.

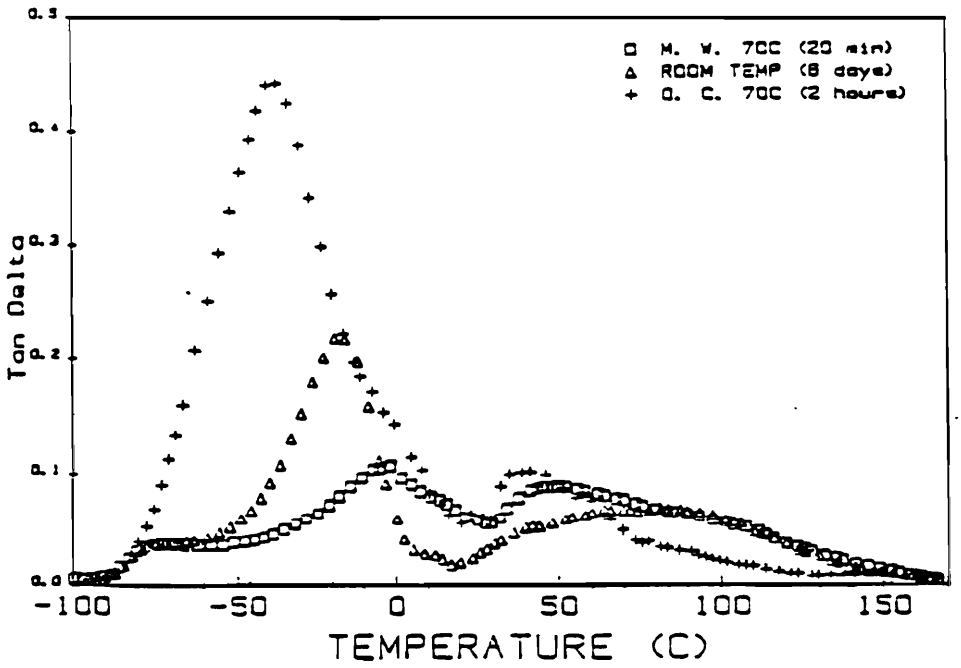


Figure 3.7. The Tan δ spectra for these three differently cured materials (as labelled) at a frequency of 11 Hz.

In the case of the TEOS/PTMO ceramers reacted in DMF/IPA, the onset of cooperative segmental motion at -90°C as seen in Fig 3.7 points out to the existance of some pure or rich PTMO phases in all of these systems. In the case of the oven cured sample, the Tan δ intensity increases steeply to 0.45 around -35°C. This loss behavior is much greater than that seen for the M. W. 70C and RT cured samples and this is a manifestation of the lower extent of reaction in this O. C. 70C ceramer system. Above -35°C there is a drop in the Tan δ intensity and at 15°C. the intensity of the Tan δ function is almost zero.

The Tan δ spectra for the RT cured and the M. W. 70C samples displays a response which plateaus out between -80°C and -60°C. Both of these materials subsequently display increases in the Tan δ intensity. The peak for the RT cured ceramer is located at -20°C and has an intensity of 0.2, while the M. W. 70C ceramer has a peak at -5°C with an intensity of 0.1. This shift in the lower temperature peak position from -35°C for the O. C. 70C material to -5°C for the M. W. 70C as well as the decrease in the Tan δ intensity (for the microwaved material) indicates once again the increase in the extent of reaction for these systems as compared with the O. C. 70C system.

All these (DMF/IPA) ceramer materials show another loss peak at higher temperatures i. e. between 20°C and 150°C. This behavior is believed to be due one or all of the following factors: a) cooperative segmental motions of PTMO chains encapsulated by the inorganic phase b) a relaxation response from the inorganic phase as postulated by Glaser (85) and as described earlier

using observations made by Stevels (98). c) additional reaction within the system and possible evaporation of solvents and earlier by-products of the reaction as documented by Brennan (96). It is extremely difficult to determine the magnitude of contribution of each of the above effects to this upper temperature relaxation. However, it will be stated without proof here, that its presence in the Tan δ spectra is dependent upon the type of metal alkoxide as well as upon the metal alkoxide content in these TEOS/PTMO ceramers reacted in DMF/IPA.

3.3.3 SMALL ANGLE XRAY SCATTERING

SAXS has typically been used extensively (84, 85, 96) to gain an understanding of the microstructure of the ceramers. The SAXS spectra (Fig 3.8) for all these differently cured TEOS/PTMO ceramers shows a single scattering peak which indicates the existance of microphase separation in these materials. This peak is due to interparticle interference as has already been documented by Huang (84) and Brennan (96). The scattering profiles obtained for these TEOS/PTMO ceramers reacted in DMF/IPA is much sharper than those obtained for any of the other ceramers studied by Huang (84), Brennan (96) or Glaser (85). This sharpness indicates a narrower distribution in the interdomain spacings or domain sizes or both. The tail regions for all these SAXS curves in Fig 3.8 are further flattened which also suggests a sharper boundary between PTMO rich

and the inorganic rich regions as compared with the scattering behavior of the TEOS/PTMO films prepared in THF/IPA. However, the breadth of the profiles obtained for the oven cured sample is greater than that for the other two films. The tail region for the oven cured sample also displays a higher scattering intensity which may reflect a greater extent of mixing between the inorganic and the PTMO component in the O. C. 70C film.

As can be seen, the scattering intensity at the peak position for the M. W. 70C ceramer is highest while that for the O. C. 70C ceramer is lowest. The intensity of small angle xray scattering is dependent upon the electron density difference between the two phases in the system (94, 95) i. e. the greater the electron density difference between two phases the greater will be the scattering intensity. In these TEOS/PTMO ceramers reacted in DMF/IPA the difference in scattering intensity can therefore be related to the extent of densification and consequently to the extent of reaction within the inorganic phase of the material. Thus the M. W. 70C ceramer which displays the highest scattering intensity would be the most reacted while the O. C. 70C film which shows the lowest scattering intensity would be the least reacted. Hence these results correlate very well with those obtained from mechanical property measurements where the microwaved film showed the highest elastic modulus and the oven cured film the least.

The peak position for M. W. 70C and the RT cured films is around $0.07 nm^{-1}$ which corresponds to an interdomain spacing of 140Å The O. C. 70C material

has an interdomain spacing of 110Å The interdomain spacings obtained from the peak positions are only approximate values because of the slit smearing effect. In order to obtain a more accurate estimate of the peak position desmearing was performed on these materials. These results show a shift in the maxima of the microwave cured sample from 142Å to 120Å while on the oven cured sample the maxima shifted from 110Å to 87Å. Table 3.2 compares the values obtained of interdomain spacings obtained from smeared curves with those obtained from desmeared curves as well with those obtained from the first maxima in the correlation function. The values obtained from the first maxima in the correlation function are quite similar to those obtained from the desmeared spectra.

3.4 AGING BEHAVIOR OF THESE TEOS/PTMO CERAMERS

These TEOS/PTMO ceramers investigated by Huang (84) and Brennan (96) showed a change in mechanical properties with time and these changes were attributed to additional extent of reaction in the system. There is also the evaporation of solvent (IPA, THF) as well as previously released reaction by-products such as water and ethanol from the film. These small molecules (THF, DMF, IPA) act as plasticizers and a decrease in their concentration due to evaporation cause considerable changes in the mechanical properties. The

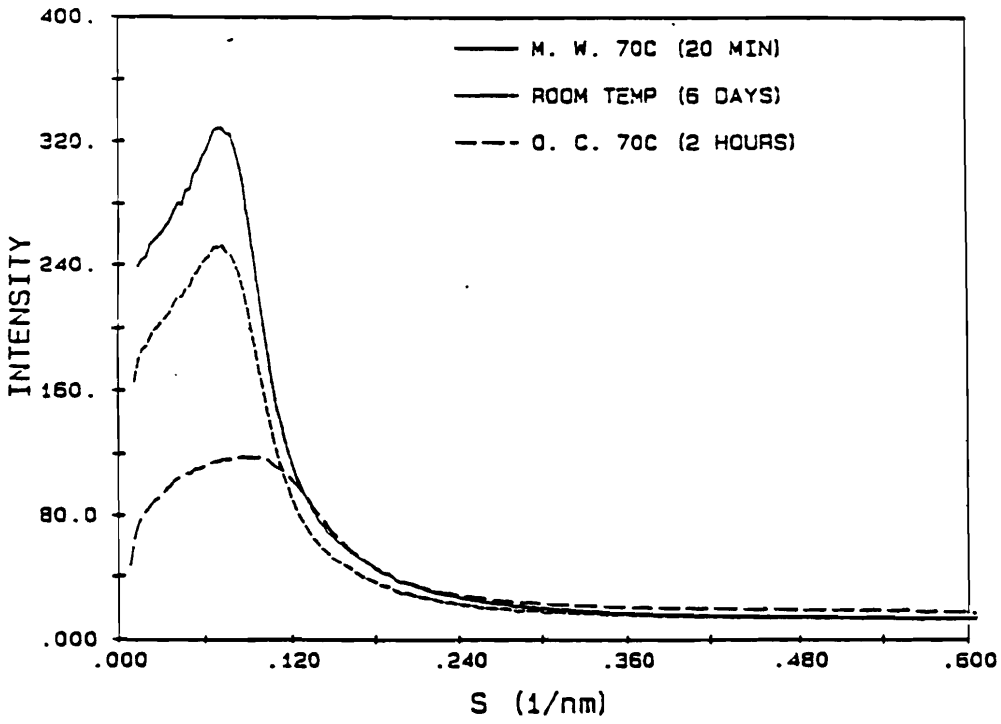


Figure 3.8. SAXS spectra for these three differently cured materials (as labelled in figure).

Table 3.2. Interdomain spacings as obtained from smeared, desmeared and correlation function data.

	Smeared Data(Å)	Desmeared Data(Å)	Correlation Function Data(Å)
M. W. 70C (20 min)	140	120	117
RT cure (6 days)	140	120	117
O. C. 70C 2 hours	110	90	86

TEOS/PTMO ceramers being described in this chapter also show a change in the mechanical properties with time. These changes, as will be seen, reflect the initial curing processes to which the reactants were subjected. The aging of these ceramers was therefore studied after a period of one month using stress strain analysis, dynamic mechanical analysis and small angle xray scattering. The next sections will document the aging behavior of these materials and some of the reasons for this phenomenon.

3.4.1 STRESS STRAIN ANALYSIS ON AGED TEOS/PTMO CERAMERS

Stress strain tests conducted after an ageing period of one month show an increase in the elastic modulus of all these three ceramer materials after a

period of one month. These results are documented in Table 3.3. The microwave cured materials show an approximate increase of 50% in the elastic modulus. It increases from 250 MPa to 380 MPa after one month. However, there is virtually no change in the stress at break which remains at 40 MPa and the elongation at break which remains constant at 21%. The room temperature cured sample shows an increase in modulus from 150 to 380 MPa, almost two and a half times its original value. After a period of one month the mechanical properties of the room temperature cured samples are identical with those subjected to microwave curing. This similarity in the results after aging underscore the necessity of the presence of an adequate amount of solvent, especially IPA, during the reaction and curing process. In the case of the O. C. 70C materials the evaporation of a significant amount of IPA during the reaction in the oven leads to different short term as well as long term mechanical properties when compared with the RT and the M. W. 70C films. The modulus after one month is 150 MPa. while the elongation at break (7%) and stress at break (7 MPa) are significantly reduced when compared with the other materials. The low stress at break of 7 MPa and the low elongation are believed to be related to defects within the material as shown in the SEM photomicrographs in the Fig 3.9. The photomicrographs shown in the Fig 3.9 represent fracture surfaces of a microwave cured film and a oven cured film. Both films were aged for slightly over a period of one month before these photomicrographs were taken. These films were fractured under liquid nitrogen and subsequently examined in a scanning electron microscope. The

magnification of the fracture surfaces as seen in both the photomicrographs is approximately 1200 times. As can be seen in Fig 3.9(a) the surface of the microwave cured sample appears relatively smooth as compared with that seen in Fig 3.9(b) which represents the O. C. 70C. In photomicrograph 9 (a) only small striations across the fractured surface can be seen. The O. C. 70C film fractured surface is very cratered and rough. These defects which do not display any particular characteristic size can give rise to the low stress at break and the low elongation at break as seen in the aged O. C. 70C material.

3.4.2 SMALL ANGLE XRAY SCATTERING OF AGED MATERIALS

Small angle xray scattering has also been used by Huang (84) and Brennan (96) to monitor the aging behavior of ceramer materials. Huang obtained SAXS data on acid catalyzed TEOS/PTMO ceramers reacted in THF/IPA while Brennan's data was based on the same reactants catalyzed using polystyrene sulfonic acid (PSS). Both their results indicated that with age there was an increase in the scattering intensity, but no significant shift occured in the peak position. This increase in the scattering intensity gives some indirect information about the additional reaction and consequent densification within the inorganic phase. The three ceramer materials being described in this chapter also display an increase in the scattering intensity with time. The increase in the scattering intensity as seen in Fig 3.10 is smallest for the M.

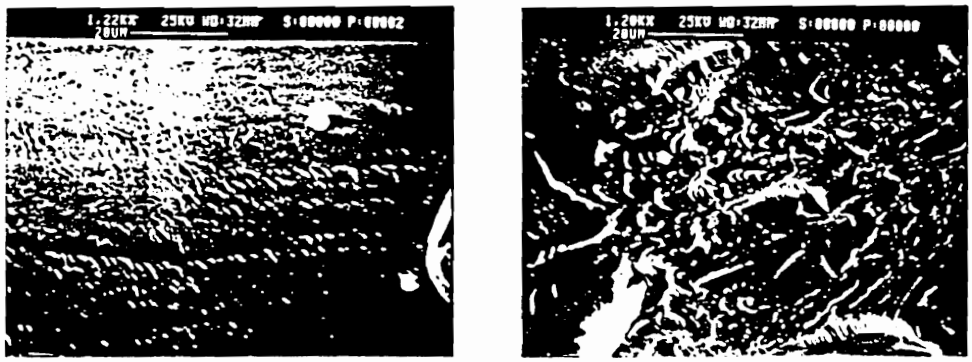


Figure 3.9. Photomicrograph of fracture surface a) microwave cured material b) oven cured material

Table 3.3. Stress strain properties for the differently cured materials after a period of one month.

Aged One Month	Young's Modulus(MPa)	Stress at Break (MPa)	Elongation%
M. W. 70C (20 min)	380	38	21
RT cure (6 days)	380	40	21
O. C. 70C (2 hours)	150	7	7

W. 70C material while there is a significantly larger increase in the scattering intensity for the O. C. 70C material. This indicates that in the O. C. 70C film, densification in the inorganic phases is brought on by a significant amount of additional reaction. This is expected since in section 3.4.2, it was shown that the elastic modulus for this film increases almost forty times over a period of one month. The breadth of the scattering peak is still greater than those of the M. W. 70C and the RT cured materials and the intensity in the tail region is also slightly higher. Further, the smeared spacing between the domains in this system is still around 100Å which is much smaller than the spacing for the M.W. 70C and RT cured systems (around 140Å). The smaller interdomain spacing as well as the broader scattering profile seen in these oven cured systems indicate the permanent nature of the initial curing process on the structure of this ceramer system.

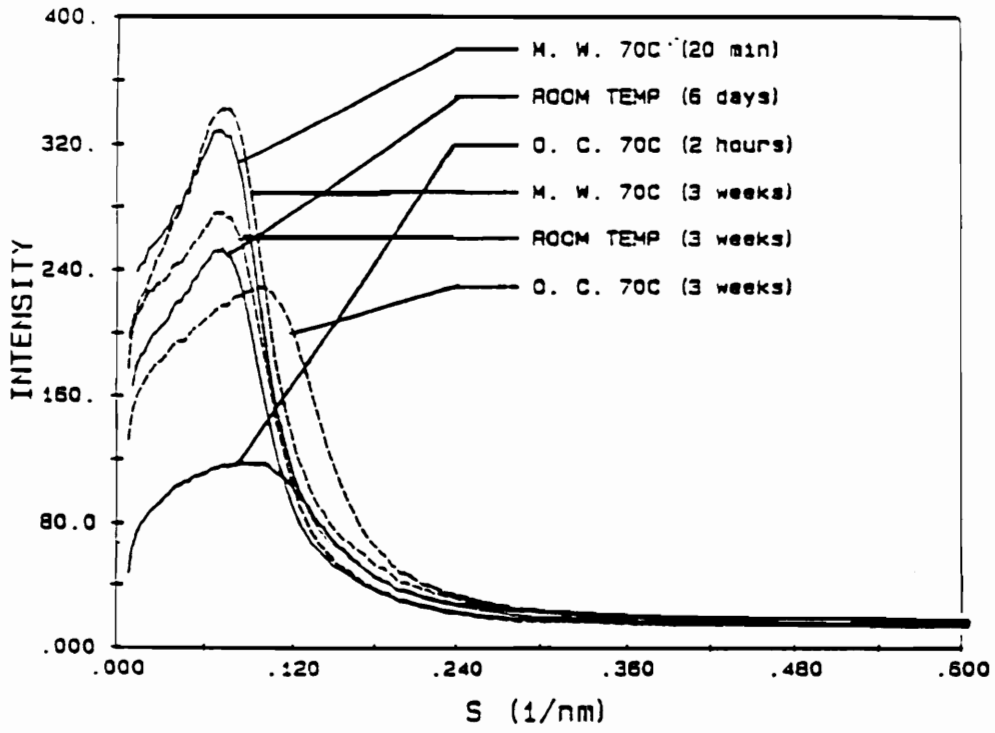


Figure 3.10. SAXS profiles for the differently cured ceramers after a period of one month.

3.4.3 DYNAMIC MECHANICAL ANALYSIS OF THE AGED CERAMERS

Dynamic mechanical analysis conducted on the three cured samples after a period of one month of ambient ageing reveal some interesting features which only serve to reinforce some of the arguments already proposed above. Nevertheless it is worth documenting some of these characteristics in the interests of consistency. As shown in the Fig 3.11 the storage modulus (taken at one month) at 11Hz indicates a glassy storage modulus of approximately 2 x 10^9 Pa. The storage modulus for the aged RT cured and M.W.70C materials again shows an early drop in stiffness at -70°C due to the presence of pure PTMO. The two step drop is still visible for room temperature cured material while for the microwave cured material it has almost vanished due to a tightening of the network. Both these materials i. e. RT cured and M. W. 70C cured systems display a decrease of approximately half a decade in the storage modulus as the temperature is increased from -100°C to 0°C. The O.C. 70C material shows a drop of ca. one decade in the storage modulus in the same temperature range indicating that this material is still relatively unreacted when compared with the M. W. 70C and the RT cured material. The storage modulus between 0°C and 100°C for the RT and M. W. 70C materials are identical. Both these materials show a hump in the storage modulus between 30°C and 80°C (whose origins have been speculated upon earlier) and both also display a very slight increase in the storage factor above 100°C. The oven cured material on the other hand displays a significant increase in

the stiffness with increasing temperature above 30°C. These increases in the storage modulus are believed to be due to additional curing taking place in the ceramer system with a consequent tightening of the network.

The Tan δ (Fig 3.11) response for these aged RT cured and M. W. 70C films shows the onset of cooperative segmental motion in the purer oligomer phases at -90°C. The oven cured film on the other hand shows the onset of loss behavior at -80°C. The loss response between -90°C and -40°C in the oven cured films is much lower than the other two materials. This indicates a greater degree of mixing between the inorganic phase and the oligomer phase in the O. C. 70C material. Indeed, this speculation correlates well with the observed higher scattering intensity in the tail region of the SAXS profiles for these oven cured ceramer systems as described in the earlier section. The loss behavior for the O. C. 70C material then increases upto an intensity of approximately of 0.2 at 10°C. The RT cured film as well as the M. W. 70C film both also display an increase in the loss behavior with increasing temperature upto around 40°C following which the intensity of loss for all systems decreases.

The bimodal behavior displayed by these three differently cured ceramers in the Tan δ spectra (seen one month earlier in Fig 3.7) has disappeared completely. In the temperature range -30°C to 20°C the Tan δ intensity for the oven cured material is higher than that for the microwave cured and room temperature cured materials. The disappearance of the bimodal loss behavior

seen earlier in all these films is reflective of further encapsulation and tightening of the network and the breadth of the peaks is reflective of the large variety of environments in which the PTMO chains are trapped. Again it must be reiterated that some of the relaxation behavior seen in the temperature range above 30°C for all systems may also have a contribution from the inorganic phase.

3.5 EXPERIMENT TO OBTAIN AN ACTUAL IMAGE OF THE MICROWAVE CURED TEOS/PTMO CERAMERS

In order to obtain an actual image of these ceramers, transmission electron microscopy (TEM) was carried out on a series of these ceramer materials prepared in DMF/IPA media. Since the intensity of scattering as seen from SAXS is highest for the microwave cured materials it was decided to attempt TEM (on the microwaved samples) to be able to visually observe the microstructures in these materials and to correlate these observations with those seen from the SAXS spectra. The weight percent of the TEOS was varied from 40 to 80 so as to be able to observe changes in the microstructure with an increase in the inorganic weight fraction. These changes in composition were also undertaken in order to determine that the visual observations as seen in TEM micrographs were due to the microstructure within the ceramer

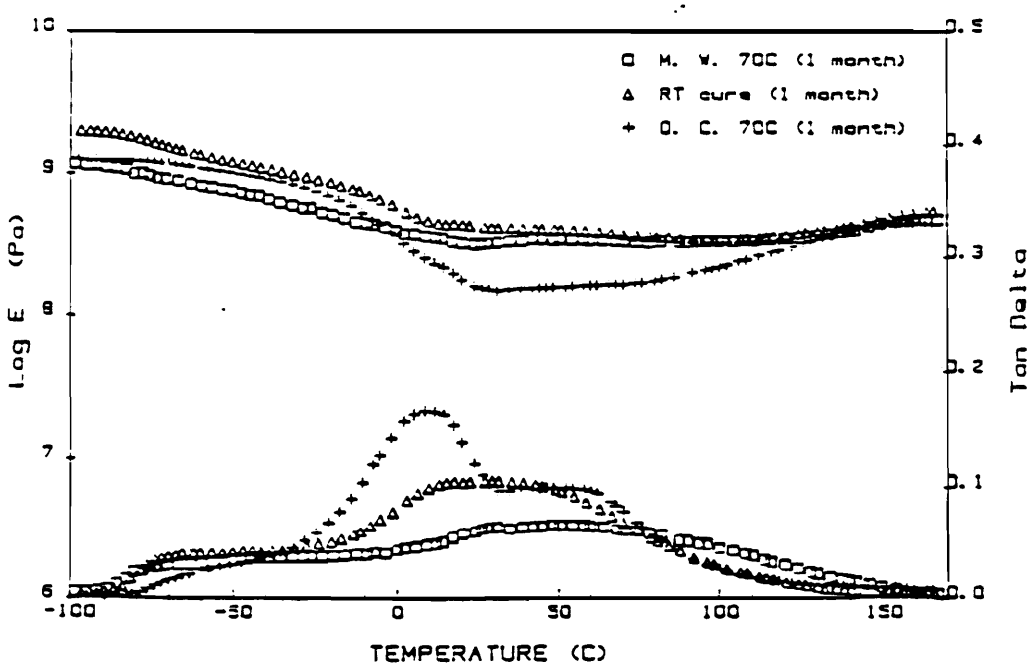


Figure 3.11. Dynamic storage and loss behavior for these materials after a period of one month.

film and not due to artifacts arising from the transmission electron microscopy methodology as has been clearly documented by York (102) in his dissertation.

The materials containing 40wt% TEOS and 80wt% TEOS were prepared in a manner identical with the procedure used for the TEOS(60)-PTMO(2K)-100-0.048 ceramers described earlier in section 3.2 in this chapter. These three ceramers i. e. those containing 40wt%, 60wt% and 80wt% TEOS, used for TEM analysis were all microwave cured. RT cured systems and O. C. 70C systems were not tested and will not be alluded to any further in this section. The microwave curing for all three systems was carried out at 70°C exactly for a period of twenty minutes using the profile described earlier in Fig 3.3. As stated earlier, only SAXS and TEM were used to study the structure of these materials.

3.5.1 SMALL ANGLE XRAY SCATTERING OF THE TEOS/PTMO CERAMERS AS A FUNCTION OF METAL ALKOXIDE CONTENT

The small angle xray scattering profiles as seen in Fig 3.12 show that as the metal alkoxide content is increased in these TEOS/PTMO ceramers reacted in DMF/IPA, the interdomain spacings increase. The interdomain spacing for the 40 wt% TEOS/PTMO film is around 120Å, for the 60 wt% TEOS/PTMO film is 140Å while for the 80wt% TEOS/PTMO films it is around 270Å Further, the

scattering intensity at the peak position increases with the amount of metal alkoxide in these ceramers. This increase in the scattering intensity is related to an increased phase separation between the inorganic and PTMO components and this characteristic has been further dealt with in the last chapter of this thesis.

3.5.2 TRANSMISSION ELECTRON MICROSCOPY STUDIES OF THESE TEOS/PTMO CERAMERS AS A FUNCTION OF METAL ALKOXIDE CONTENT

The transmission electron micrographs are shown in the Fig 3.13. The structure as seen from these micrographs appears to be random with no particular ordering. The approximate values of interdomain spacing as measured from these micrographs are approximately equal to the values measured from SAXS and documented in the earlier section. In these micrographs the white phase represents the PTMO, while the dark represents the inorganic silicate component. This is because the silicate phase is more electron dense. In the micrograph of the 40 wt% TEOS ceramer there appears a large number of small black specks which are believed to be inorganic particles; there is a small percentage of white regions (PTMO), while large areas of the photomicrograph are grey. The grey regions in the

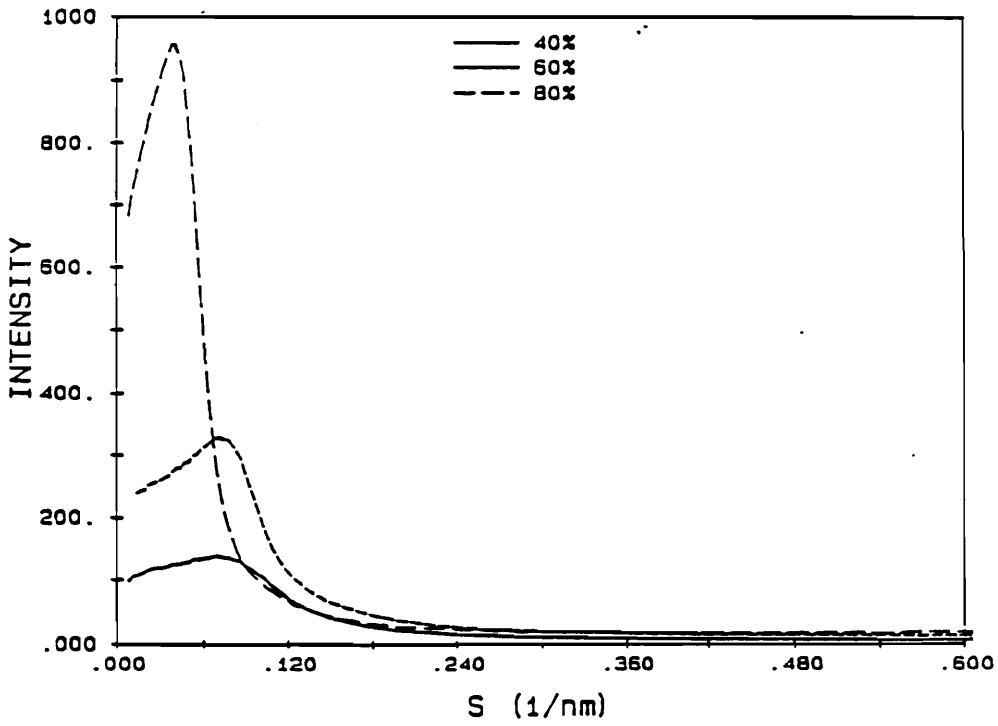


Figure 3.12. SAXS profiles for the ceramers as the TEOS content is varied from 40wt% to 80wt%.

photomicrograph represent the regions of mixing between the PTMO and the inorganic domains.

As the TEOS content is increased, there appears to be an increase in the particle size as seen from the micrograph. This was earlier proposed in his model for the ceramers documented in the literature review section of this dissertation. In the micrograph it can be seen that for the TEOS(60)-PTMO(2K)-100-0.048 ceramer, the blacker regions are better defined than in the 40 wt% TEOS materials. This indicates a higher degree of phase separation, while in the 80 wt% TEOS/PTMO ceramers there is even more distinct contrast between the black and white regions indicating further phase separation between the inorganic and the PTMO components. In this micrograph (for the 80 wt% TEOS/PTMO) there is greater connectivity between the inorganic regions than in the 40 and 60 wt% TEOS/PTMO ceramers. This may indicate that the inorganic domains are beginning to impinge upon each other in the higher metal alkoxide ceramers.

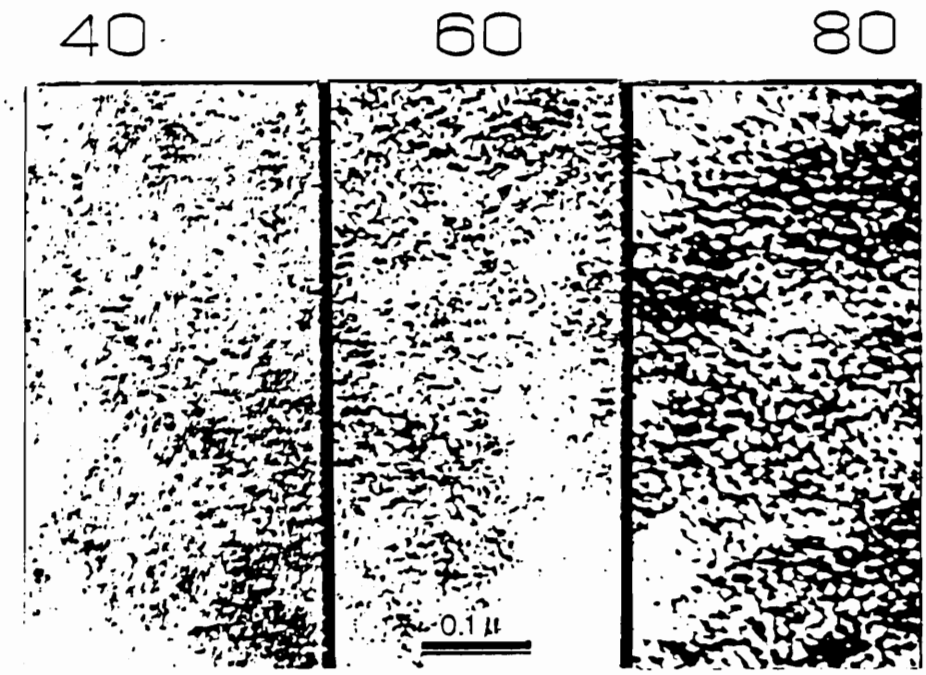


Figure 3.13. TEM micrographs of the ceramer as the TEOS content is varied from 40wt% to 80wt%.

3.6 CONCLUSIONS

The TEOS/PTMO reactants (in DMF/IPA = 1/1 solvent media) lend themselves to microwave processing in a fashion that is unmatched by some of their other TEOS/PTMO ceramer sytems as will be seen in the following chapters in this dissertation. That these ceramers show unique properties is in no small part due to the phase separation between the inorganic and PTMO components brought on by the use of DMF. This phase separation is believed to help bring more of the reactive dipoles together, which then enables a more rapid curing rate when microwaves are used to heat the reactants.

On the other hand the oven cured samples heat more slowly, and the IPA solvent thus has more time to evaporate before much reaction occurs. This evaporation leaves the reactants in a greater concentration of DMF which slows down the condensation reaction significantly. The excess of DMF also fosters a lack of incorporation of PTMO into the network since DMF tends to drive the phase separation of the reactants. This points to another advantageous effect of microwave processing i. e. the direct energy transfer to the polar molecules in the reacting solution permits the use of different initial heating rates which can effect the nature of the reaction.

The additional extent of reaction brought on by microwave processing in these systems produces better mechanical properties as seen from the stress strain

data and the dynamic mechanical data. The higher scattering intensity as seen from the SAXS curves permits one to conclude that the additional extent of reaction contributes to a greater densification of the inorganic phase in these systems. Hence the M. W. 70C sample displays the highest scattering intensity and the O. C. 70C material the lowest.

The long term effects of the respective curing processes on these ceramers have also been studied. From these it is seen that the evaporation of IPA during the oven curing process leaves the film with a greater amount of mixing between the inorganic phase and the oligomer. It has also been shown that the oven curing process leaves the film with a large number of defects which affect the mechanical properties well after the processing in the oven is completed.

CHAPTER 4

STRUCTURE PROPERTY RELATIONSHIPS IN TEOS/PTMO CERAMERS CURED IN SOLVENT MEDIA OF TETRAHYDROFURAN AND ISOPROPANOL

4.1 INTRODUCTION AND OBJECTIVES

In the previous chapter it was shown that the reaction rate between TEOS (tetraethylorthosilicate) and triethoxysilane endcapped PTMO (polytetramethyleneoxide) was significantly enhanced when the reactants were cured using microwave radiation. This was in contrast to the oven curing process where it was seen that the slower rate of heating to 70°C was an impediment to the reaction rate and hence to the development of good mechanical properties. The enhancement in the rate of reaction using microwave radiation was attributed to the ability of the reactive hydroxyl groups to efficiently absorb this electromagnetic radiation. The positive results obtained when curing these specific ceramers in a microwave field spurred an effort to try and achieve similar results with similar TEOS/PTMO compositions cured in another cosolvent system i. e. tetrahydrofuran (THF) and isopropanol (IPA).

Huang (84), previously evaluated the effects of several solvents such as tetrahydrofuran (THF), isopropanol (IPA) and formamide on the structure property relationships of TEOS/PTMO ceramers. Of all the various solvents used to compatibilize the TEOS/PTMO reactants, a cosolvent combination of THF and IPA in a 1:4 volume ratio was used extensively and the effects of this particular solvent combination on the structure property relationships of TEOS/PTMO ceramers were studied and documented in detail. Some of the

results obtained by Huang on these TEOS/PTMO ceramers reacted in THF/IPA have been detailed in the literature review in chapter 1. However two prominent features of this particular hybrid material system will be described, so as to give the reader an idea why this material was chosen as the next candidate for microwave curing.

From DMA results Huang showed that TEOS/PTMO ceramers reacted in THF/IPA displayed a significant amount of mixing between the inorganic phase and the oligomer phase. This is in contrast to other ceramers where the same reactants cured in DMF/IPA showed a more phase separated system. The reason for the extensive mixing between the inorganic and PTMO phases in the ceramer reacted in THF/IPA was attributed to the more linear chain growth of the silicate phase. This significant difference in the morphology of the two ceramer systems (i. e. the TEOS/PTMO system reacted in THF/IPA versus that reacted in DMF/IPA), especially the difference in the nature of growth of the inorganic phase provided a good reason for investigating the effect of microwave curing on these ceramer systems reacted in THF/IPA. In other words it was decided to determine whether the absorption of microwave energy by the reactive hydroxyl groups varied with the nature of growth of the inorganic phase.

It has been documented by Gedye (49) that the extent of reaction in a microwave field is dependent upon the dipolar strength of the solvating media. This provided another reason to investigate the effect of microwave curing on

TEOS/PTMO ceramers cured in THF/IPA. The replacement of DMF (dipole moment = 3.8 Debye) with THF (dipole moment = 1.7 Debye) presented the opportunity to investigate the effect of dipole strength on these materials. In view of these objectives it was therefore decided to cure these TEOS/PTMO ceramers in THF/IPA in a microwave cavity and in a conventional oven to compare structure and properties with those measured for the ceramers described in chapter 4. Room temperature cured films were also studied in order to compare and contrast their properties with those cured at elevated temperatures. As in the previous chapter stress strain behavior, DMA and SAXS were used to evaluate material characteristics.

4.2 SAMPLE PREPARATION PROCEDURES

The reactants for this set of experiments were the same as in the previous chapter. Endcapped PTMO (M_n = 2000 g/mole) initially constituted 40 weight percent of the reactants while TEOS constituted the remaining 60 percent. Water, which is required for the hydrolysis of the alkoxy functionality, was added upto 100 wt% by stoichiometry to allow functionalization of all alkoxy moities present in the reacting mixture. 10N HCl was added to catalyse the reaction. The ratio of 10N HCl to TEOS in the reaction mixture was 0.048. The

nomenclature for the TEOS/PTMO materials described in the previous chapter holds good for the ceramers described in this chapter as well.

The procedure employed to enhance miscibility between the reactants was to add the PTMO and TEOS to the cosolvent mixture of THF/IPA and stir the mixture for 20 minutes. Following this the water and HCl were added and the reaction mixture was stirred for an extra two minutes as shown in Fig 4.1. The initial pH of the solution was between 3.5 and 4.0, while it decreased to between 1.5 and 2.0 after the addition of HCl. This measurement was made using litmus paper as detailed in chapter 3. The mixture was then cast in petri dishes and subjected to heating in a microwave cavity or a conventional convection oven. Some samples were cured at room temperature.

The samples cured in the microwave cavity were either heated to 70°C or 120°C respectively for twenty minutes. The heating profiles for ceramers microwaved to 70°C and 120°C are both shown in Fig 4.2. The temperature vs time profile for the reactants microwaved to 70°C was chosen to be almost similar to that for the reactants in the previous chapter. The profile for the material microwaved to 120°C was chosen somewhat arbitarily since there was no previous data which could be used as a benchmark. A brief glance at the profiles shows that in both cases (materials microwaved to 70°C as well as 120°C) the reactants began to heat almost as soon as the power was turned on. The rate of heating decreases with the increase in temperature for both materials. For the material heated to 120°C there appears a steep drop in the

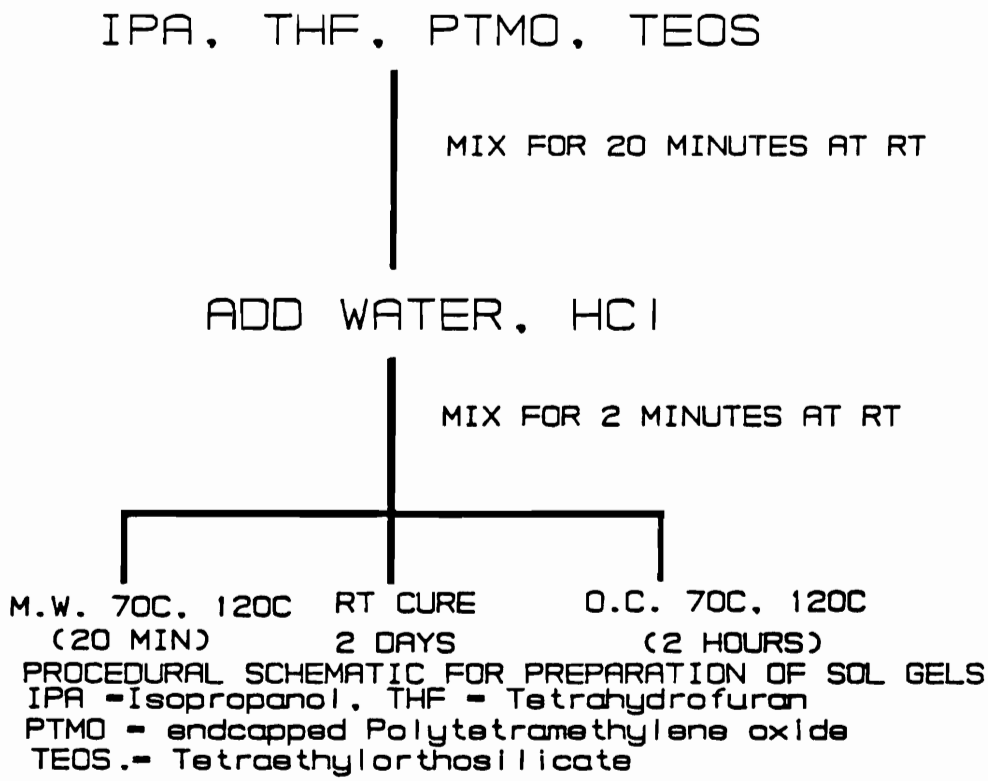


Figure 4.1. Schematic showing the preparation of TEOS-PTMO ceramers in a cosolvent system of THF/IPA

heating rate at approximately 80°C. This is to accomodate for the heat of vaporization of isopropanol which boils at 82°C and which initially constitutes one-sixth of the reactant mixture. THF boils at 66°C but constitutes less than 1/12 the initial reaction mixture and hence the reduction in the heating rate caused by its evaporation from the mixture is less noticeable as compared with that of IPA. When the desired temperature was reached i. e. 70°C or 120°C, the cavity was detuned as described previously in chapters 2 and 3 to maintain the temperature at the desired values. The total time of microwave curing in both cases was 20 minutes. The input power initially used to heat the reactants to 70°C was 15 watts as can be seen in Fig 4.3. These samples will be denoted as M. W. 70C. At 70°C the cavity had to be detuned in order to maintain the temperature within the sample at a steady state. The input power was reduced to 5 watts while the reflected power was increased from zero watts to 10 watts. As stated in the last chapter the process of detuning involves changing the physical dimensions of the cavity and this results in the reflection of some of the energy out of the cavity, thus causing the polar molecules to see a lower electric field strength and consequently a lower amount of energy. While the lower field strength reduces the rate of heating to zero, its entire effect on the reaction is not possible to detail without the utilization of in-situ spectroscopic techniques such as NMR. For the reactant solution heated to 120°C in the microwave cavity the initial power used was 20 watts. In order for the reactants to reach 120°C the power had to be raised to 70 watts in steps as can be seen in Fig 4.4. These samples will be denoted as M. W. 120C. The

cavity was not detuned in this case and hence no power was reflected throughout the microwaving process.

The oven cured samples were placed in a regular convection oven preheated to either 70°C or 120°C. Each sample was kept in the oven for a period of two hours. The samples made this way will be denoted as O. C.70C and O. C. 120C respectively. The time temperature heating profiles for both these materials are shown in the Fig 4.5. In both cases the rate of heating was seen to decrease as the temperature increased. Both materials cured in the oven (70°C and 120°C samples) heated slower than their microwave cured counterparts. The samples heated to 70°C took almost 32 minutes to reach this temperature while samples heated to 120°C took approximately 40 minutes to reach this temperature after placement in the convection oven.

Room temperature (RT) cured samples were stored under ambient conditions (ca. 23°C and 50+/-10 % relative humidity) for two days before they gained sufficient strength to warrant handling and physical testing. All samples whether microwave cured, oven cured or room temperature cured were in the form of a film with thickness ranging between 5 mils - 10 mils. The films were all transparent and flexible.

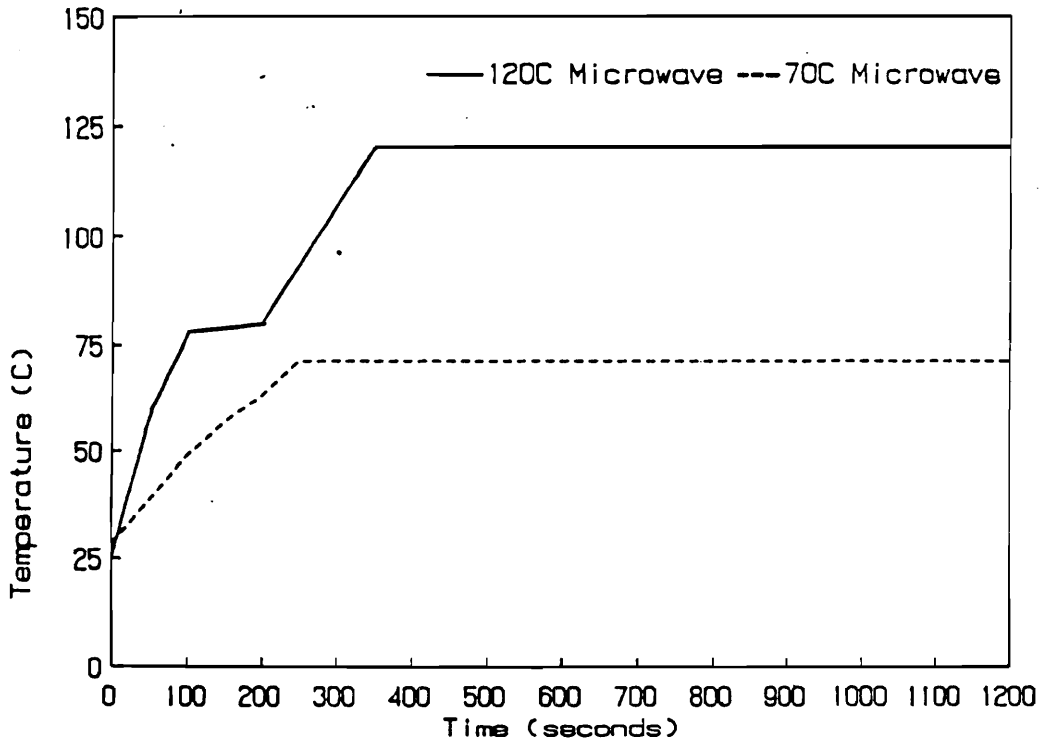


Figure 4.2. The heating curves for the microwaved samples cured to 70°C and 120°C.

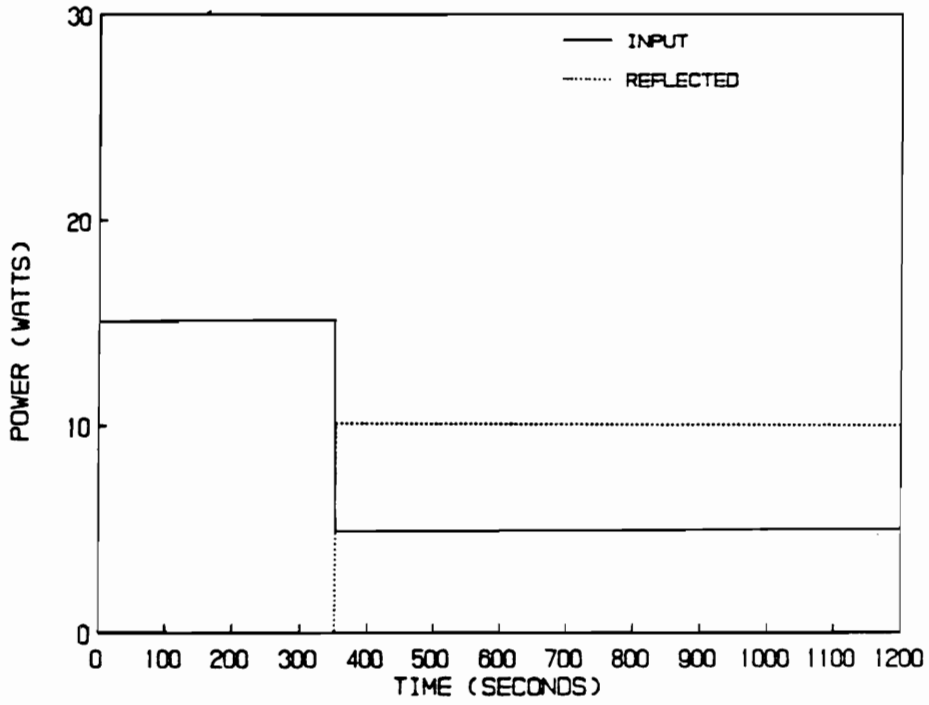


Figure 4.3. Figure depicts the variation in power with time required to cure a sample to 70°C.

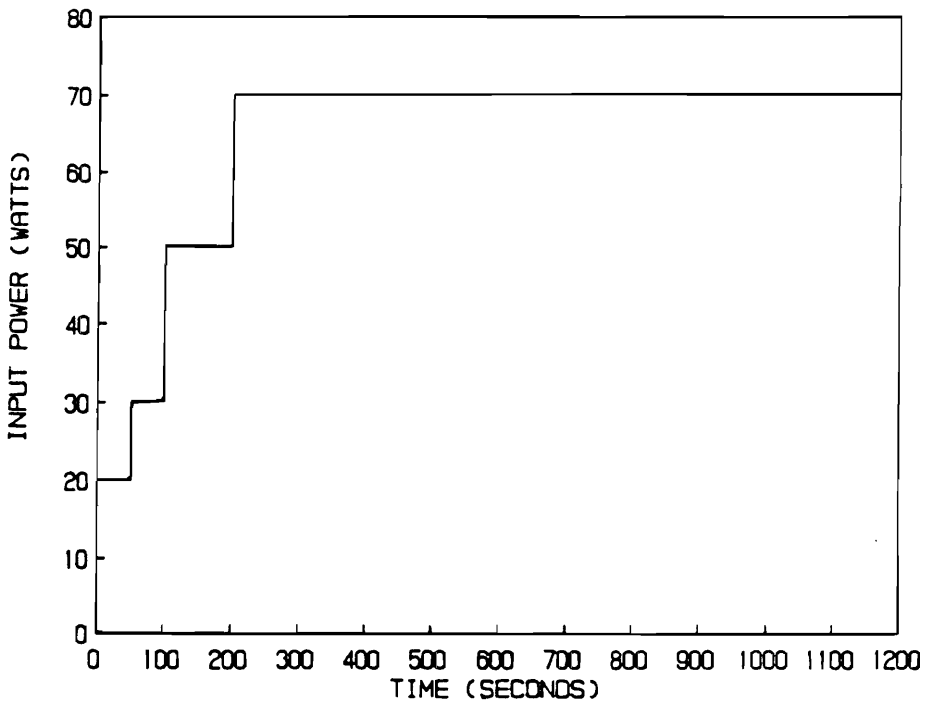


Figure 4.4. Increase in the power levels required to cure a sample at 120°C

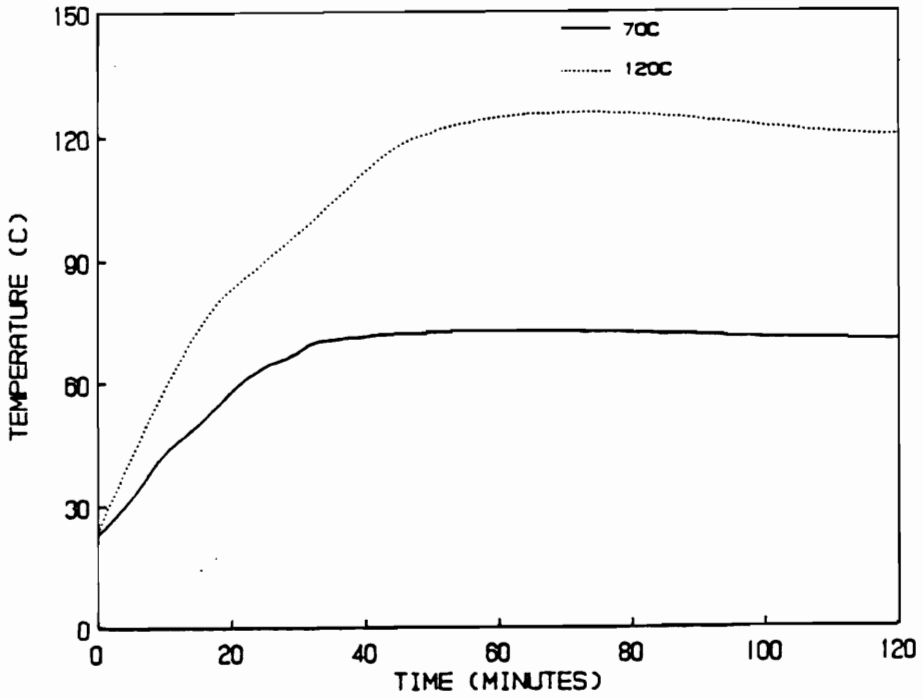


Figure 4.5. Heating profiles for the O. C. 70C and O. C. 120C films.

4.3 RESULTS AND DISCUSSION

4.3.1 DYNAMIC MECHANICAL ANALYSIS

Dynamic mechanical analysis (DMA) has been used extensively by Huang (84), Glaser (85) and Brennan (96) in their characterization of various ceramer systems and the data obtained provided some important ideas about the morphology of ceramers. In the case of these TEOS/PTMO films reacted in THF/IPA the DMA at 11 Hz shows some very interesting trends. As can be seen in Fig 4.6 all the samples display a storage modulus of approximately 10^9 Pa. at -100°C. All five materials then begin to display a decrease in the storage modulus as the temperature is increased above -70°C. This decrease in the stiffness of all films is attributed to the onset of cooperative segmental motion in the oligomeric component of the ceramer. Above -50°C all these ceramer films show a sharp decline in the storage modulus. For the O. C. 70C and the M. W. 70C film the decline is sharper than the other films and is approximately two orders of magnitude. This decrease progresses upto 40°C for both films and the magnitude of the decrease in the storage modulus indicates lightly crosslinked ceramer films. The decrease in the storage modulus above -70°C as seen for the RT cured and the O. C. 120C films is of the order of one and a half decades in magnitude and this indicates a greater extent of reaction in

these films as compared with the O. C. 70C and the M. W. 70C materials. The M.W. 120C film shows the lowest reduction in the storage modulus between -100°C and 50°C of approximately one order of magnitude, thus suggesting that the extent of reaction was the highest.

Between 50°C and 80°C the storage modulus for all these ceramers remains fairly constant and this indicates that all the materials are now in the rubbery regime of the viscoelastic spectrum. Above 80°C the storage modulus for all materials begins to increase with temperature and this behavior is attributed to an additional extent of reaction within the ceramer film. The additional reaction increases the crosslink density of the material and this in turn increases the stiffness of the film. The increase in the extent or reaction also results in further densification within the inorganic phase. As would be expected this increase in the storage modulus (above 50°C) is greatest for the O.C. 70C and the M. W. 70C materials since they have undergone the lowest extent of reaction and is the least for the M.W. 120C film which has undergone the highest extent of reaction.

The Tan δ spectra for all these ceramer films provides information about the morphology of the films and gives some indication about the phase separation behavior in these materials. The Tan δ behavior as seen in Fig 4.7 shows that cooperative segmental motion in all these films begins at -65°C. This behavior when contrasted with that seen in the previous chapter (where cooperative segmental motion in the PTMO component began at -90°C) indicates that these

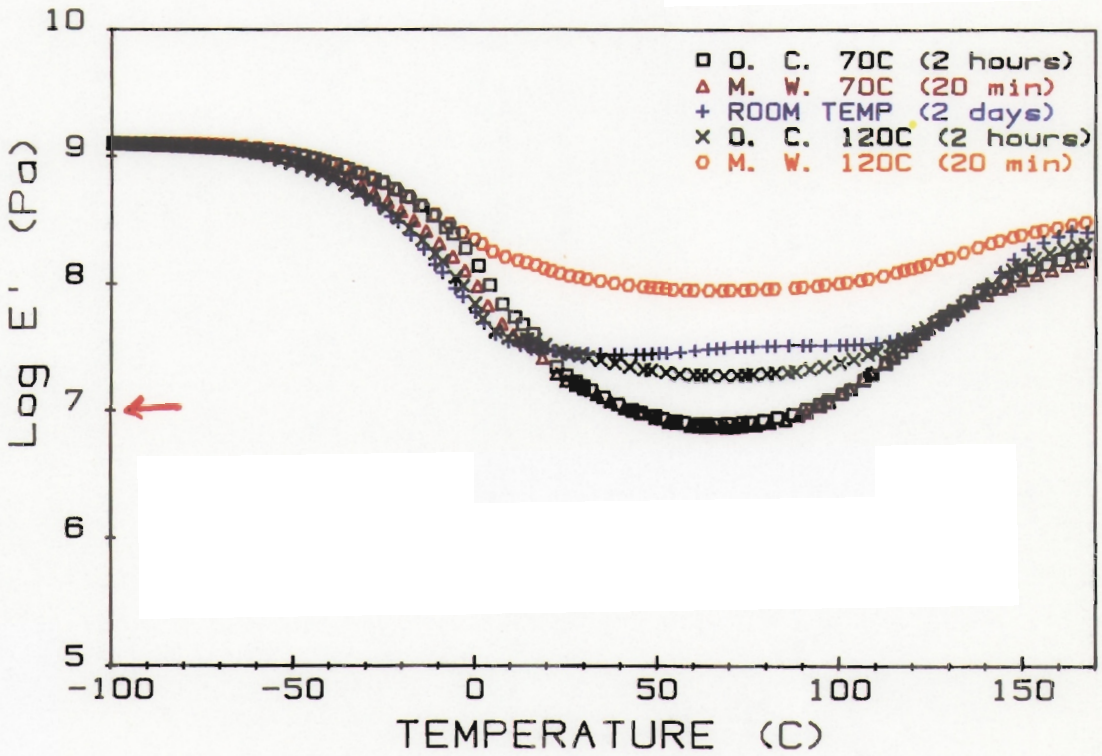


Figure 4.6. The storage modulus behavior for the differently cured materials (as labelled) at a frequency of 11 Hz.

TEOS/PTMO ceramers reacted in THF/IPA possess a greater degree of mixing between the inorganic and the oligomer. In other words the amount of mixing between the inorganic and the oligomeric phase is significant enough to cause an upward shift of 25°C in the onset of cooperative segmental motion behavior.

The intensity of Tan δ behavior for the O. C. 70C film and the M.W. 70C film increased between -65°C and 10°C. Both these films were lightly crosslinked as seen from the storage modulus curves and hence display significant dissipation behavior. The peak position in the Tan δ curves is taken as the T_g for these materials. The Tan δ curve for the O.C. 70C material has a peak at 10°C. and the intensity at the peak position is approximately 0.8. The M.W. 70C film also displays a peak at 10°C with a slightly lower intensity. In contrast the T_g for the O.C. 120C film occurs at 0°C while the T_g for the RT cured film is located at -5°C. Both the RT and the O. C. 120C cured films display a Tan δ peak intensity of 0.4. The M.W. 120C film which displays the highest extent of reaction as indirectly evinced from the storage modulus spectra also shows the lowest intensity of loss behavior at around 0.1. The Tan δ peak for the film microwaved to 120°C is around -5°C. All the materials show a steady decrease in the loss intensity above the peak positions. It can be seen that the Tan δ curves for all these materials are not symmetrical but are skewed at the higher temperatures i. e. above the T_g of the respective films. This points out to a difference in the nature of the environment in which the oligomer is trapped as described below.

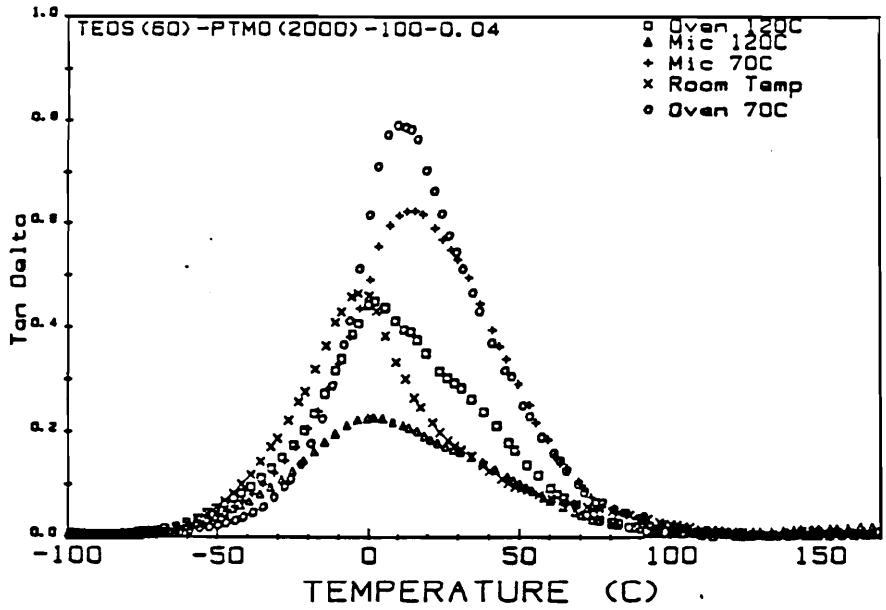


Figure 4.7. The Tan δ behavior for the differently cured materials (as labelled) at a frequency of 11 Hz.

The Tan δ curves for all these materials are very broad extending from -65°C to approximately 90°C which indicates a large range of inorganic environments within which the oligomer chains are trapped. The loss behavior at the lower temperatures i. e. around -65°C is believed to be due to cooperative segmental motion of the PTMO chains in a relatively rich PTMO environment while the loss behavior at 90°C is believed to be more representative of PTMO trapped in an inorganic rich environment. Between these two extremeties of oligomer concentration in the inorganic phase it is speculated that there exist all possible concentrations of one component in the other which therefore give rise to the broad Tan δ spectrum.

From the above description of the dynamic mechanical behavior it can be seen that Tan δ peak position shifts to lower temperatures with additional curing. In other words (the TEOS/PTMO reacted in THF/IPA) ceramer samples which display higher modulii have lower glass transition temperatures, which is unusual since the T_g for networks typically increases with the extent of reaction. One plausible explanation for this behavior is that because of the densification of the inorganic network with temperature and the consequent constriction of the PTMO chains there is a greater decrease in the loss response of the oligomer in the temperature range of 50°C - 100°C than there is in the temperature range of 65°C - 0°C. This causes the skewness in the Tan δ curves at temperatures above 50°C and also shifts the peak position towards lower temperatures with increasing extent of reaction in these ceramer films.

4.3.2 MECHANICAL PROPERTIES

All samples were subjected to stress strain analysis after removal from the microwave cavity or oven. The tests were performed within two to ten hours of having undergone their respective curing processes. As stated earlier, the room temperature cured materials were tested after two days after casting. The stress strain properties of all these materials are documented in Table 4.1. The actual stress strain curves are displayed in Fig 4.8. Both the ceramers cured at 70°C i.e. M.W. 70C and O.C. 70C have elastic modulii of around 4 MPa. The stress at break for these two films is approximately 8 MPa while the average elongations at break is around 125%.

The reason for the equivalence in the mechanical properties for both the M. W. 70C films and the O. C. 70C films is attributable to the extended time period for which the samples were retained in the oven at 70°C i. e. 2 hours as compared with twenty minutes in the microwave cavity. After twenty minutes in the convection oven the sample temperature was around 58°C as can be seen from Fig 4.5 and the O. C. 70C films were still quite tacky and could not be removed for physical testing. Microwaves, on the other hand, are known to couple directly with the polar molecules in the solution. The greater the dipole moment the more effective the coupling (2, 4, 5). The silanol moities are known to be highly polar and are efficient absorbers of microwave energy as will be discussed in chapter 5. This may result in higher localised

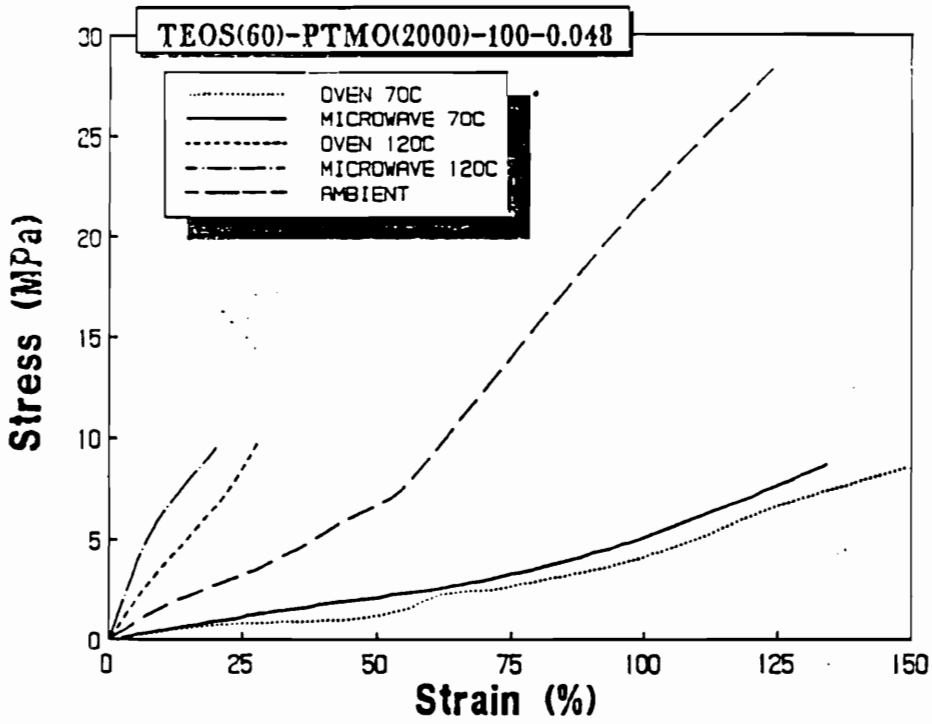


Figure 4.8. Figure shows the stress strain curves for the variously cured samples (as labelled in figure).

Table 4.1. Stress strain properties for the differently cured materials.

	Young's Modulus(MPa)	Stress at Break (MPa)	Elongation%
M. W. 70C (20 min)	4	8	130
O. C. 70C 2 hours	4	9	125
RT cure (6 days)	25	29	120
M. W.120C (20 min)	70	9	8
O. C. 70C (2 hours)	30	8	8

temperatures at reactive sites (hydroxyl groups) than in the bulk of the material (41, 42, 43) which, could possibly facilitate the condensation reaction in which Si-O-Si linkages are formed as documented in chapter 1. As a result of this effect of microwave radiation on the polar moities in the reaction mixture a larger number of condensation reactions can take place at lower temperatures before 70°C is reached.

The elastomeric behavior at room temperature (low modulii and high elongations) of the M. W. 70C and O.C. 70C samples can be related in some part to a relatively low extent of reaction within the inorganic phase as well as

the relatively large amount of mixing between inorganic and PTMO phases as seen from DMA data. Brinker et al (64) have documented that when TEOS is reacted under acidic conditions, linear silicate species are formed which have small branches (2 - 3 repeat units) spaced 20Å apart along the chain backbone. The formation of such linear silicate species in this acid catalyzed TEOS/PTMO ceramer system is believed responsible for the large extent of mixing between the oligomeric and the inorganic components.

Room temperature cured samples have elastic modulus when compared with their 70°C cured counterparts. The average elastic modulus was around 25 MPa, stress at break appproximately 25 MPa, with an elongation at break around 125%. A cursory glance at the stress strain curves seen in Fig 4.8 indicates that the RT cured film undergoes strain hardening at around 50% elongation. The presence of solvent in the reaction mixture for a longer time period during RT curing as compared with curing at 70°C in the oven and microwave cavity appears to facilitate an increased extent of reaction. This increased extent of reaction results in a the development of better mechanical properties for this RT cured film. The better mechanical properties of the room temperature cured materials seem to suggest that rapid evaporation of the solvent during the heating processes puts a limitation on the extent of reaction. This would help explain the low mechanical properties for the O. C. 70c and the M. W. 70C ceramers. This limitation can be overcome by conducting the reactions at higher temperatures.

Materials heated to 120°C in both the oven and microwave cavity display an increased elastic modulus but much lower elongation at break than the room temperature cured films. The increase in temperature (from 70°C to 120°C) helps provide more thermal energy to the reactive molecules thereby causing additional mobility to overcome some of the limitations placed on the reaction by the evaporation of solvent. This additional energy helps increase the extent of reaction. There is a significant difference in the elastic moduli of oven cured material and microwaved material at 120°C. The modulus of the oven cured material is approximately 30 MPa while the microwaved film has an elastic modulus of approximately 70 MPa. The stress at break for both materials is 10 MPa, while the elongation at break is 10%. The most likely explanation for the higher modulus of the microwaved materials is that at 120°C most of the solvent (which are polar) will have evaporated as would all the free water. The only remaining polar molecules are the silanol groups which are strong absorbers of microwave energy. Absorption of microwaves by these silanol groups may result in higher localized temperatures at the reactive sites which could give rise to an additional extent of reaction. This results in a densification of the inorganic phase as will be seen later from the SAXS data. This densification and the subsequent encapsulation of the oligomer molecules results in a very low elongations for both the M.W. 70C and O.C. 70C films.

4.3.3 SMALL ANGLE XRAY SCATTERING (SAXS) ANALYSIS

As stated above, the films of these ceramers are all optically clear which indicates that there does not exist any macrophase separation. SAXS was therefore performed on all these ceramer materials in order to ascertain whether there exists any possible microphase separation of the inorganic from the oligomer. SAXS also helps determine the possible existance of any periodicity or "correlated structure" within the material. The SAXS profiles shown in the Fig 4.9 for these ceramers are plots of the smeared scattered intensity I(s) versus the scattering vector s. The angular factor s is defined as follows:

$$s = \frac{2}{\lambda} \sin \theta$$

where θ is one half of the scattering angle and λ is the wavelength of the incident beam. In the case of an interference peak or shoulder, the reciprocal of s at the peak or shoulder position is taken as an approximate measure of the interdomain spacing. Since the SAXS profiles presented in the figure are slit smeared, more precise values of the interdomain spacing would be obtained from desmearing. However this operation has not been performed on the profiles presented in this chapter.

All the SAXS profiles seen in Fig 4.9 have a maxima around s = $0.1nm^{-1}$ (d = 100Å). These profiles are much broader when compared with the SAXS profiles seen in the previous chapter for a similar ceramer composition prepared in a cosolvent system of DMF and IPA. The greater breadth of the scattering profiles for these TEOS/PTMO films prepared in THF/IPA would indicate a large distribution in either the interdomain spacings or the domain sizes or both.

The SAXS analysis also help provide some understanding of the extent of curing and densification in the films. It can be seen that the intensity of the SAXS scattering peak increases with the extent of cure. The sample heated to 120°C in the microwave cavity which has the highest elastic modulus also shows the highest intensity of scattering, indicating the greatest degree of densification in the inorganic phase. The increased densification is produced as a result of increased reaction in the inorganic phase. Thus the trend in the scattering intensity at the peak position matches the trend in the elastic modulus values for the various samples. This again indicates that the amount of reinforcement provided by the inorganic phase is dependent upon the degree of reaction within the system and hence the correspondence between structure and properties of the ceramer.

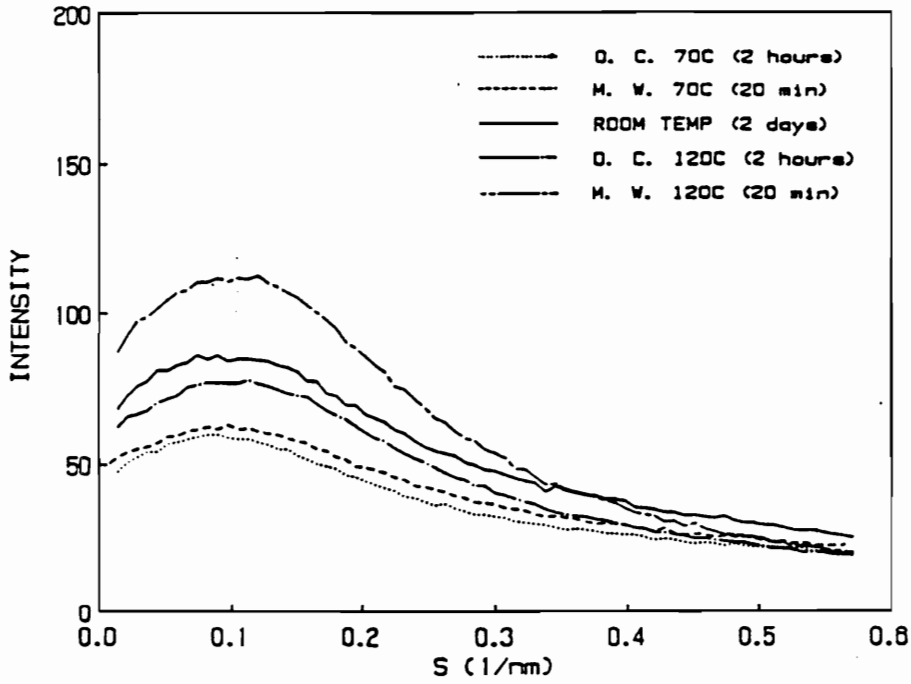


Figure 4.9. SAXS scattering profiles for the variously cured samples as labelled in the figure.

4.5 CONCLUSIONS

In conclusion it can be stated that the difference in properties between these microwave and oven cured TEOS/PTMO materials are not as significant as the differences seen for the same ceramers documented in the last chapter. This is believed to be primarily because of the difference in morphologies between the ceramers cured in THF/IPA as compared with those cured in DMF/IPA. It is also related to the difference in reaction environments i. e. THF is less dipolar than DMF and hence does not absorb microwaves very efficiently. This difference in absorption capabilities may also be responsible for the lack of a significant difference in mechanical properties between the O. C. 70C and the M. W. 7OC ceramer films. The inorganic phase of these ceramers cured in THF/IPA is less condensed than that witnessed in the preceeding chapter. The linear growth of the silicate chains observed for the systems cured in THF/IPA causes a greater degree of mixing between the inorganic phase and the oligomer phase and this reduces the ability of the electromagnetic radiation to induce any significant reaction rate in these materials when compared with oven curing.

In general the microwave radiation appears to cause a slightly greater extent of curing than conventional convection oven curing at equivalent temperatures. This has been attributed to localized heating at the strongly dipolar reactive sites as well as the different initial heating rates in the two

processes. The heating of the reactants to 70°C either by microwave radiation or conventional oven appears to put a limitation on the extent of reaction because of the rapid evaporation of solvent. This causes the M. W. 70C and the O. C. 70C films to undergo a lower extent of reaction than those cured at room temperature. This limitation on the extent of reaction can be overcome by heating to 120°C either in the oven or by microwaves.

CHAPTER 5

EFFECT OF SOLVENT ON THE TEOS/PTMO REACTION

5.1 INTRODUCTION AND OBJECTIVES

In chapter 4 it was shown that microwave processing had a significant influence on the properties of the TEOS/PTMO ceramers cured in DMF/IPA as

compared with conventional oven curing, both being conducted at 70°C. This was attributed to the ability of microwaves to couple effectively with the dipolar reactive species and thus influence the rate of reaction. On the other hand the slow rate of heating of these ceramer samples in the oven curing process permitted the IPA to evaporate from the reaction mixture leaving behind the reactants in a greater relative concentration of DMF which from previous studies is known to hinder the condensation reaction (59).

However, when a cosolvent system of THF/IPA was used as the compatibilizing media for the TEOS/PTMO reaction, the differences between the properties of microwave and oven cured materials were negligable as shown previously in chapter 4. In order to determine the reason for the differences between microwave and oven curing seen with the DMF/IPA cosolvent system and, the lack of any significant differences in the THF/IPA system it was decided to conduct an investigation on the effects of these solvents on the reaction between TEOS and functionalized PTMO. To achieve this objective TEOS and PTMO were reacted in a THF/IPA cosolvent system in a 1:4 volume ratio (henceforth denoted as THF/IPA::1/4) as well as in DMF/IPA having volume ratios of 1:1 (denoted as DMF/IPA::1/1), 1:3 (DMF/IPA::1/3), and 3:1 (DMF/IPA::3:1). Pure IPA and pure DMF were also used to compatibilize the reactants and their effects on the properties of the film were studied.

To determine the effects of these solvent systems upon the microwaveability of TEOS/PTMO ceramers and consequently upon the structure property

realtionships, a different investigative approach from that pursued in the previous two chapters was required. This approach consisted of researching the three stages shown in Fig 5.1. (stage A, B and C) involved in the process of producing ceramer films. The three stages are documented in the flow chart in Fig 5.1. Stage A or the precursor stage consisted primarily of making measurements on the reaction precursors and comprised a) measuring the dielectric loss factors of each of the reactants individually at 2.45 GHz and room temperature to determine their microwave absorption capabilities and b) conducting temperature time heating experiments on the individual reactants in a microwave field at 2.45 GHz to correlate the microwave absorption capabilities with the measured dielectric loss factor. Stage B or the processing stage consisted of making measurements on the reactants after they were combined together in a mixture i. e. measuring the dielectric loss properties at 2.45 GHz and room temperature and the temperature-time heating profiles of the reactant mixtures before and after the addition of the acid catalyst. This was to determine if the dielectric loss properties of the reactant solutions after the addition of the acid catalyst influenced microwave absorption capabilities of the solution and if this ability to absorb EM radiation had any significant effect on the mechanical properties of the resultant films cured to 70°C as compared with films cured in an oven. SAXS was also performed on the reactants before and after the addition of acid catalyst to the system to determine the existance of any correlated structure in the solution state. The existance of any correlated structure in the solution state, before or

immediately after the addition of acid to the reactants would indicate that possibly the morphology of these ceramer films is already preset before the processing step (heating in the oven or microwave cavity) and hence the nature of processing cannot significantly alter the microstructure of these materials. Stage C represents an investigation of the finished product i. e. microwaved and oven cured films and consisted of performing stress strain tests as well as SAXS experiments on the films (prepared in the different solvents) in an attempt to establish a linkage between the dielectric properties in the solution state with the structure and properties seen in the films.

5.2 EXPERIMENTAL

The reactants used for the investigations documented above were essentially the same as those used in the previous chapters i. e. the TEOS/PTMO weight ratio was maintained at 60/40. The PTMO molecular weight was retained at 2000 g/mole and the oligomer was endcapped with isocyanatopropyltriethoxysilane. In all cases the water added was 100% of the theoretical amount necessary to hydrolyze all alkoxy functionalities in the

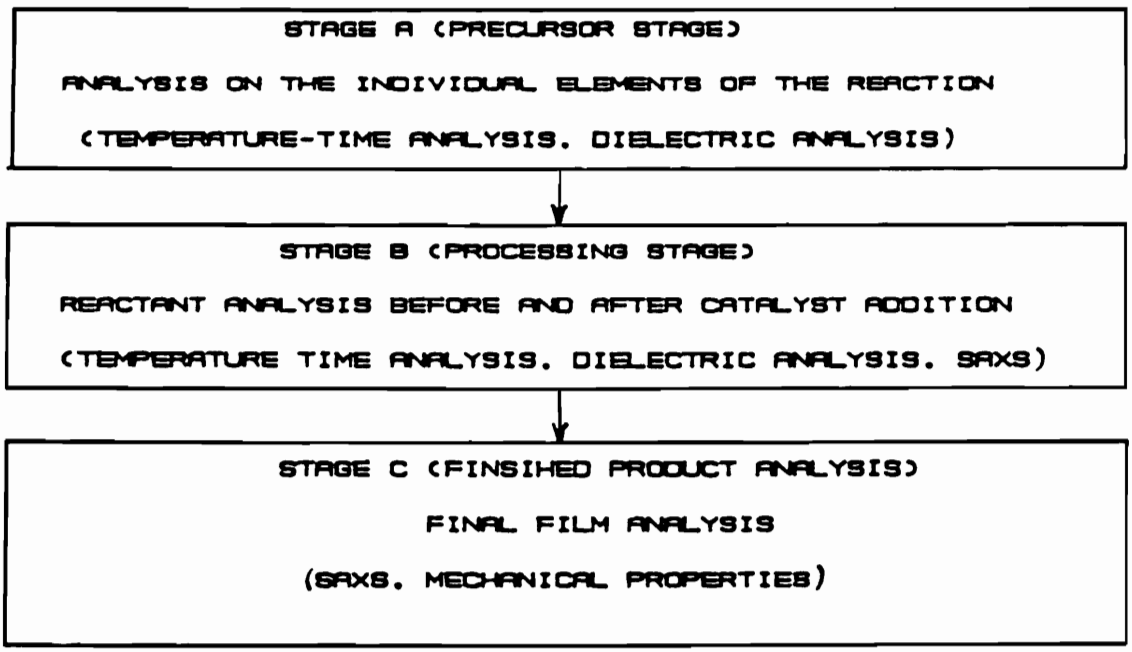


Figure 5.1. Flow chart for the research conducted and detailed in this chapter.

reaction mixture and HCl acid catalyst was always added in a 0.048 (mol/mol) ratio. As stated earlier the only variable was the solvent composition which was varied from pure IPA to pure DMF. Intermediate volume composition ratios of IPA/DMF of 1:3, 1:1 and 3:1 were also used as compatibilizing media for this reaction. The cosolvent system THF/IPA::1/4 was also used to compatibilize the reaction media.

The dielectric properties of the individual reactants as well as the compatibilizing media were measured using a dielectric network analyzer. This analyser measures the dielectric properties of materials using the principle of cavity perturbation and this has been previously documented in chapter 1. The temperature vs time heating investigations were conducted in a WR284 rectangular cavity. A schematic of the cavity with its dimensions and other characteristics has already been detailed in chapter 2. The microwave set-up for the temperature time heating measurements is shown in Fig 5.2. This schematic shows a coaxial cable connecting the microwave generators to the rectangular cavity via power meters which monitor the input and reflected power to the cavity. The cavity is tuned by means of a stub tuner and sliding short which have both been previously described in chapters 1 and 2. Tuning of the cavity helps create a standing wave in the cavity which increases the Q-factor. All heating experiments to be described in this chapter utilized an input power of approximately 5 watts. The reflected power was kept at zero in all cases which means that the cavity was always tuned.

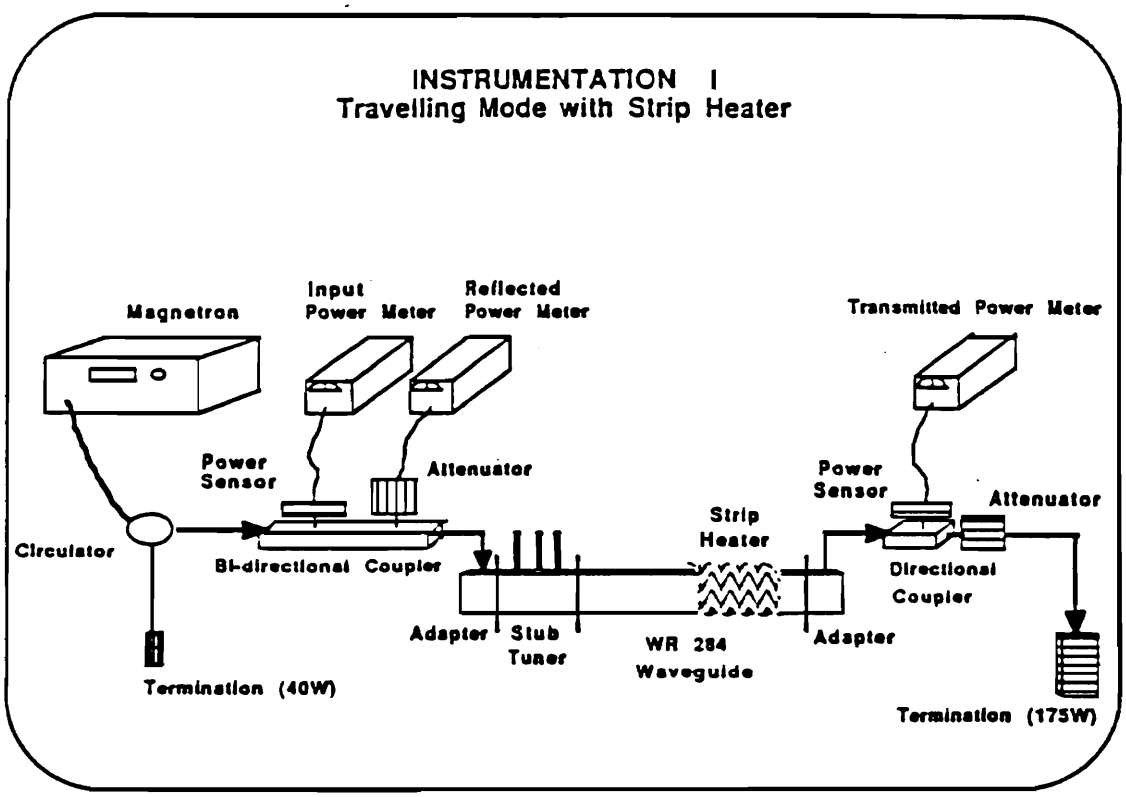


Figure 5.2. Schematic of the microwave setup used for the temperature-time studies

The sample holder used for the purpose of holding the reactants during the temperature-time microwave heating study was made of teflon and is shown in Fig 5.3. The use of teflon ensures that a minimal amount of power is absorbed by the sample holder. Further, the walls of the sample holder are very thin (0.2 mm) so that virtually no distortion of the electromagnetic field is caused by its presence in the cavity during heating experiments. The holder was cylinderical in shape which is the preferred geometry for the TE_{10} mode and was one inch in diameter and one inch in height. The sample holder was filled with approximately 6 ml of reactants for each heating experiment. The sample volume was kept constant at 6 ml primarily because the heating volume plays a critical role in the rate of temperature increase in a microwave cavity. The sample holder had three small holes drilled in the cap through which three fiber optic temperature measuring probes were inserted to check for any possible temperature gradients in the heating volume.

The teflon sample holder for the temperature time solution heating experiments was always placed at the same position in the rectangular cavity i.e. the position of maximum power intensity. This ensures that almost all power stored within the cavity is absorbed by the sample except for power which is dissipated by the cavity walls. The temperature increase in all the microwaved materials was recorded for 240 seconds from the instant the power was turned on. From the temperature increase in the first 50 seconds as seen in the heating profiles, the differential of temperature with respect to time $(\frac{dT}{dt})$ was calculated and these values will be compared with the

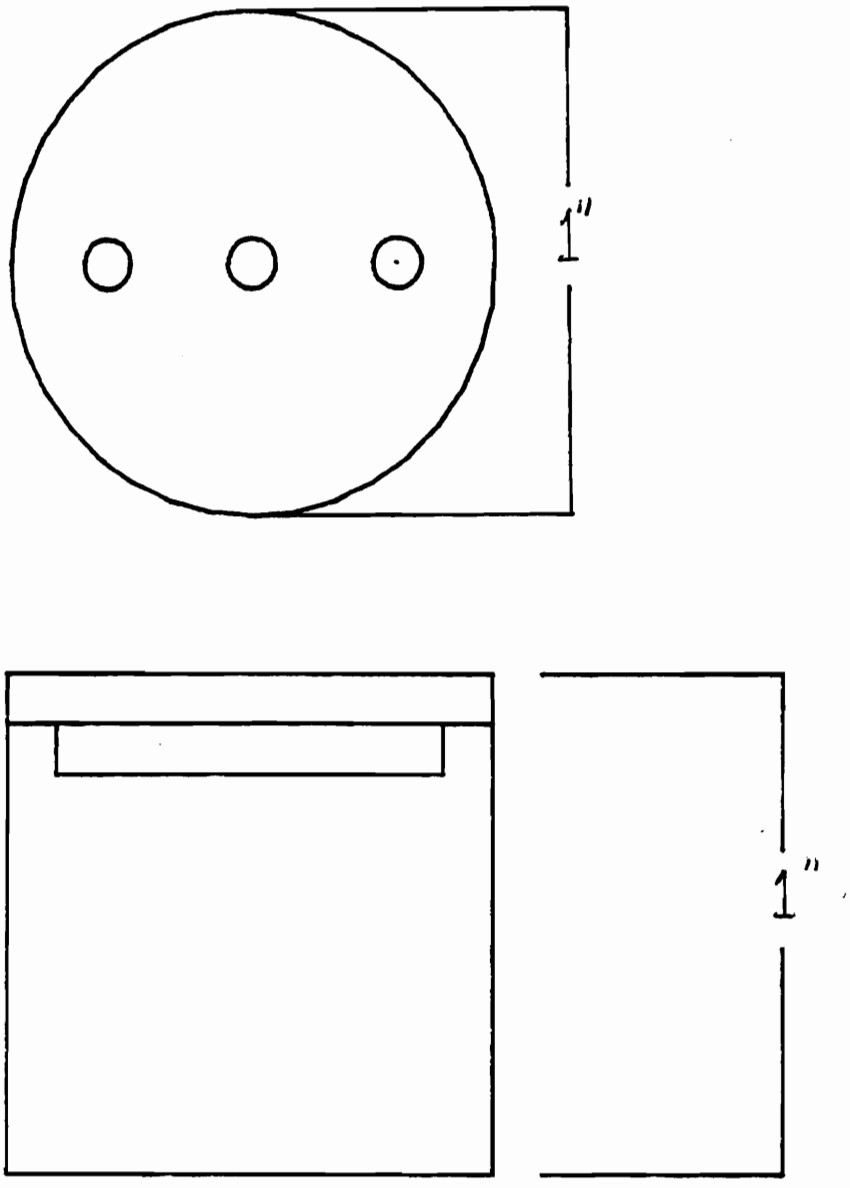


Figure 5.3. Schematic of the Teflon sample holder used in the temperature time heating experiments.

dielectric loss factor obtained from the network analyser where ever possible, so as to establish a correlation between the dielectric loss and microwave absorption.

Microwave cured and oven cured films were also investigated for their mechanical properties using an Instron. SAXS was used to probe the structures of only the microwave cured films in an attempt to correlate the effect of solvent on the structures produced with their stress strain properties. The method of preparation of these microwave cured and oven cured TEOS/PTMO films has already been discussed in detail in chapters 4 and 5 and this aspect will not be discussed any further in this chapter.

5.3 RESULTS AND DISCUSSION

STAGE A

5.3.1 MEASUREMENTS MADE ON INDIVIDUAL REACTANTS

Heating profiles were first obtained on all the individual reaction components to determine which of these were efficient absorbers of microwave energy. The

temperature vs time heating profiles for all these materials are shown in Fig 5.4a and Fig 5.4b. Fig 5.4a displays profiles for the actual reactants i. e. those materials which actually take part in the reaction (TEOS, PTMO and water) while Fig 5.4b shows microwave heating curves for the compatibilizing solvents. In Fig 5.4a it can be seen that water heats faster than PTMO which heats faster than TEOS. Water is known to be very strongly hydrogen bonded and has a dipole moment of 1.8 Debye. The dipole moment for TEOS is 1.72 (18) while that for PTMO has been calculated at 1.13 Debye (103). Thus it can be seen that the rate of heating as seen in the microwave cavity is not directly proportional to the dipolar strength of the molecules. This is because the heating rate is, however, related to the dielectric loss of the dipole moment of the molecules at any particular temperature or frequency. The equation relating the heating rate to the the dielectric loss factor is:

$$\frac{dT}{dt} = 0.556x10^{-10}\frac{\varepsilon'' f E_{rms}^2}{\rho} C_p \qquad (5.1)$$

where dT represents the change in temperature in time dt, ε'' is the loss factor of the dielectric, f is the microwave frequency which is equal to 2.45 GHz for these heating experiments, E_{rms}^2 is the average electric field strength in the cavity for a given input power, ρ is the density and C_p is the heat capacity of the material being heated. Hence, while TEOS has a higher dipole moment than PTMO, its dielectric loss factor at 2.45 GHz and room temperature is much lower than that of PTMO and hence it does not heat well in the cavity.

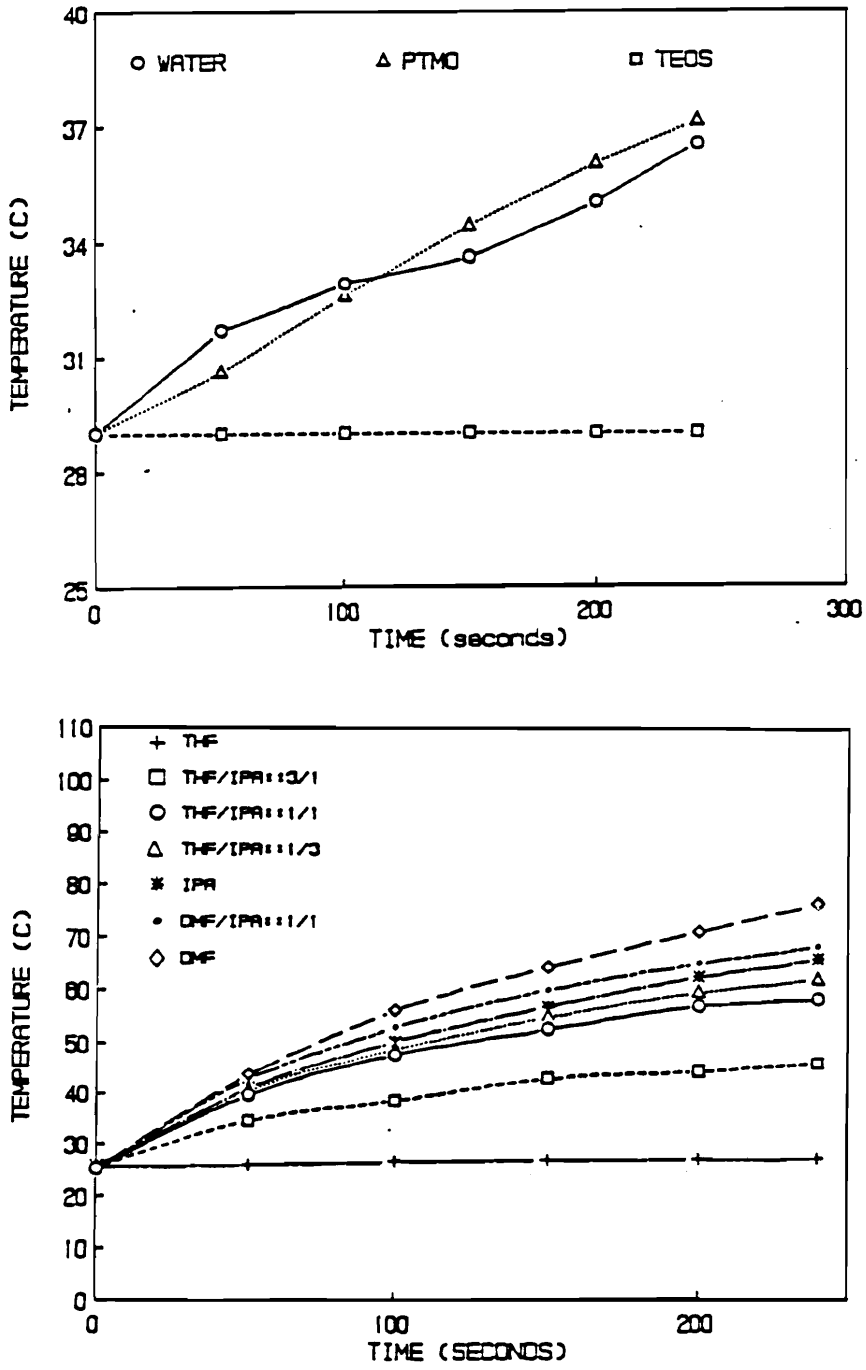


Figure 5.4. a) Temperature-time microwave heating studies for the reactants b) for the compatibilizing solvents.

Another manifestation of this relationship between the heating rate and the dielectric loss factor can be seen in the Fig 5.4b in which the time temperature heating profiles for pure THF, THF/IPA::1/4, THF/IPA::1/1, THF/IPA::4/1, pure IPA, DMF/IPA::1/1 and pure DMF are plotted. In this figure it can be seen that pure THF increases in temperature from 25°C to 31°C in 240 seconds while DMF reaches 80°C in the same time period. IPA has a heating rate intermediate between THF and DMF and its temperature increases to 65°C after 240 seconds of heating in the microwave cavity. Both IPA and DMF possess dipole moments of 1.7 Debye. However, the dielectric loss factor of THF at 2.45 GHz is 0.36 while for IPA it is approximately 5.1. Hence IPA heats much faster that THF at an input power of 5 watts.

Figure 5.5 represents the heating rate ($\frac{dT}{dt}$) calculated for the various composition ratios of THF/IPA shown in Fig 5.4b. In this figure it can be seen that as IPA concentration in THF is increased, the initial heating is also increased. This would indicate that the dielectric loss factor at 2.45 GHz of the mixture increases with IPA concentration. A verification of this can be seen in Fig 5.6 where the dielectric loss factor is plotted versus percentage THF. This figure shows that the dielectric loss factor increases linearly with IPA concentration in THF. Similarly, Fig 5.7 shows how the heating rate increases with the addition of DMF to IPA. The increase in the heating rate, however, does not vary lineary with the increasing composition ratio of DMF to IPA. DMF has a loss factor of 8 and thus its addition to IPA (loss factor = 5) causes

an increase in the loss factor of the mixture and consequently to the initial heating rate.

.STAGE B

5.3.2 MEASUREMENTS MADE ON THE REACTION MIXTURE BEFORE THE ADDITION OF ACID

5.3.2.1 DIELECTRIC AND TEMPERATURE-TIME HEATING MEASUREMENTS

As stated earlier TEOS/PTMO materials cured in DMF/IPA solvent media showed a much better response to microwaving than those cured in THF/IPA in terms of their mechanical properties. Further the difference between the

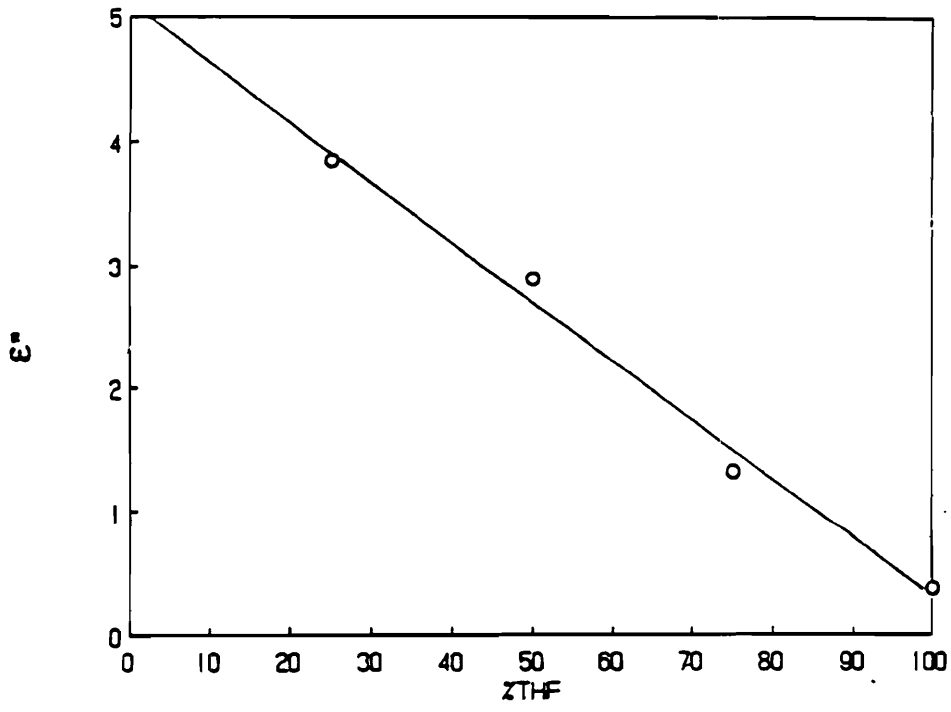


Figure 5.5. Increase in the dielectric loss factor for a THF/IPA solution with increasing IPA concentration.

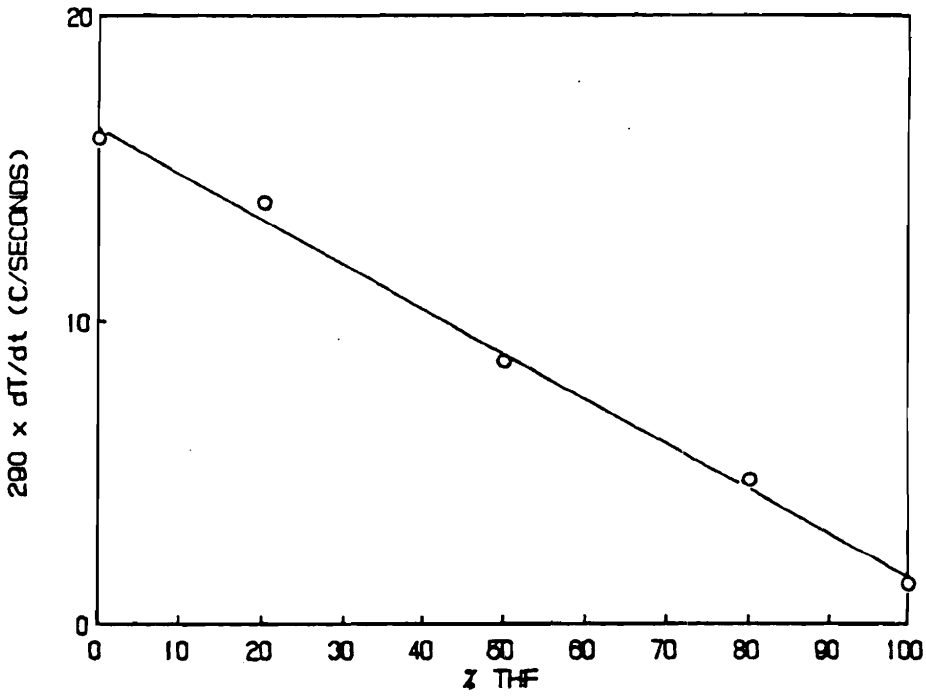


Figure 5.6. Increase in the heating rate for a THF/IPA solution with increasing IPA concentration.

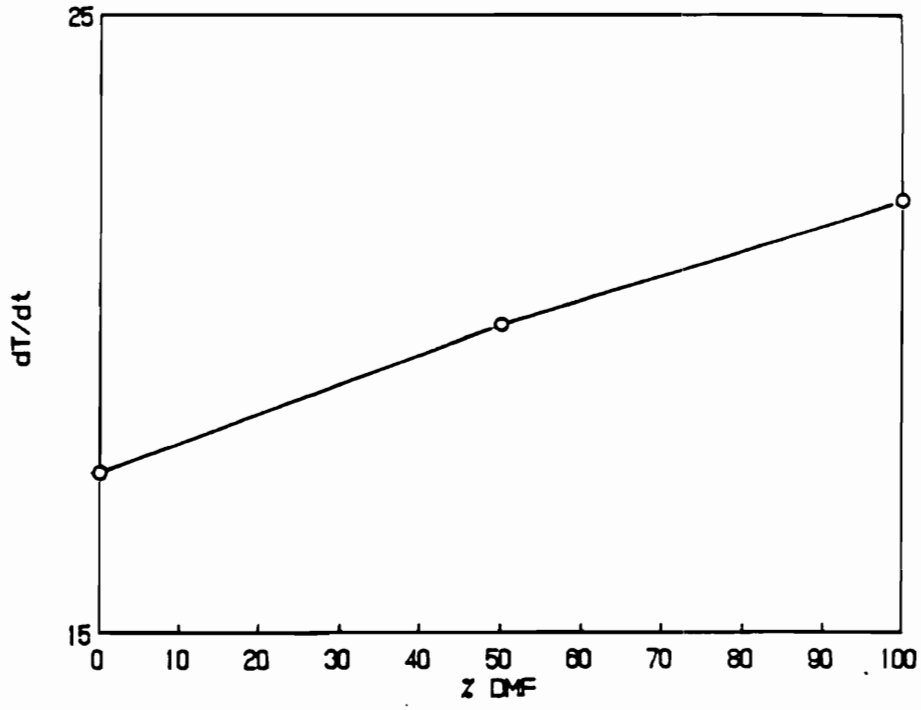


Figure 5.7. Increase in the heating rate for a DMF/IPA solution with increasing DMF concentration.

mechanical properties of the microwave cured materials and oven cured materials was greater in the case of the TEOS/PTMO samples reacted in DMF/IPA versus those reacted in THF/IPA. In view of these observations it was decided to investigate some of the solution state properties of the reactants and determine the reason for the effectiveness of the microwaves in the case of the ceramers cured in DMF/IPA. This was done in two ways. One method consisted of measuring the dielectric loss of the reactants in a network analyzer at room temperature before and after the addition of the acid catalyst. Dielectric measurements were made on the TEOS/PTMO reactants (compatibilized in either THF/IPA::1/4, DMF/IPA::1/1 or DMF/IPA::1/3) without the acid catalyst. The reactant mixture was contained in a small glass tube and analyzed for 150 seconds. After 150 seconds the acid catalyst was added to the reactants in the glass tube and the change in the dilectric properties was monitored as a function of time.

Temperature-time heating measurements were also made on the TEOS/PTMO reactants in the same compatibilizing solvents (THF/IPA::1/4, DMF/IPA::1/1, DMF/IPA::1/3) before and after the addition of acid to correlate these results with the observed dielectric properties as determined from the network analyser measurements. The input power used for all the temperature-time measurements was 5 watts. The sample volume was retained at 6 ml for all these heating experiments. Reactants cured in DMF/IPA::3/1 macrophase separated almost instantaneously upon the addition of the HCl catalyst and

hence were not examined using dielectric spectroscopy or temperature-time measurements.

5.3.2.2 DIELECTRIC MEASUREMENTS

The dielectric property measurements made on the reactants without the acid catalyst for the first 150 seconds are shown in Fig 5.8. For the reactant mixture in THF/IPA::1/4, the dielectric loss is approximately 1.8, while the reactant mixture in DMF/IPA::1/3 displays a dielectric loss of approximately 4.0. The reactant mixture in DMF/IPA::1:1 shows the highest dielectric loss of approximately 4.8. In all cases the dielectric loss factor during the 150 second time period remained relatively constant and this is an indication that there is no reaction taking place in the mixture before the addition of the acid catalyst. This figure indicates that there is an increase in the dielectric loss of the reactants with the addition of DMF. This increase (before the addition of acid) is primarily because of the high dielectric loss factor of the DMF component at 2.45 GHz which is approximately 8.0 as compared with 0.36 for THF or 3.1 for IPA. The increase in DMF concentration causes the loss factor of the reaction mxiture to increase.

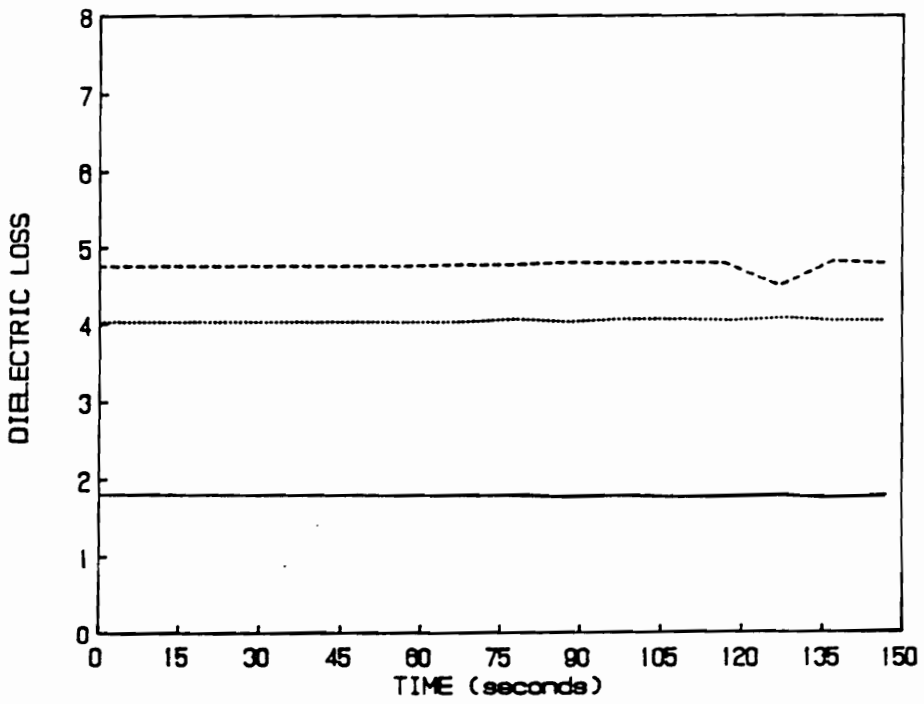


Figure 5.8. Dielectric measurements made on the TEOS/PTMO reactants in various cosolvent systems before the addition of acid

5.3.2.3 TIME-TEMPERATURE HEATING EXPERIMENTS

These experiments were carried out to compare the rate of heating of the TEOS/PTMO reactants compatibilized in either THF/IPA::1/4, DMF/IPA::1/3 or DMF/IPA::1/1 with the results obtained from dielectric loss factor measurements. Figure 5.9 shows the temperature-time profiles for these mixtures before the addition of acid to the reactants. As can be seen the initial heating rates for the reactants in the three different solvents are almost identical. After 50 seconds, differences in the rate of heating between the three mixtures begin to manifest themselves. The mixture containing DMF/IPA::1/1 which possessed the highest dielectric loss factor of 4.8 before the addition of acid shows the highest rate of temperature increase. The system compatibilized in DMF/IPA::1/3 which had a dielectric loss factor of 4.0 showed a slightly lower rate of temperature increase than the system containing DMF/IPA::1/1. Finally, the system compatibilized by THF/IPA::1/4, which had the lowest dielectric loss factor of approximately 1.8 before the addition of acid, also showed the lowest heating rate in these temperature-time measurements. Thus we see that the microwave absorption capabilities of the

TEOS/PTMO reaction mixtures (without the acid catalyst) are dependent upon the dielectric loss factors of the mixtures which are in turn dependent mainly upon the loss factors of each of the compatibilizing solvents and the ratio in which these solvents are added to the solution.

5.3.3 MEASUREMENTS MADE AFTER THE ADDITION OF ACID CATALYST

5.3.3.1 DIELECTRIC MEASUREMENTS

After the addition of the HCl catalyst to the reactant mixture at 150 seconds, there is a dramatic increase in the dielectric loss factor of all the reactants as seen in Fig 5.10. This increase is almost instantaneous and very steep. In the case of the reactants compatibilized with THF/IPA::1/4 the dielectric loss factor increases from 1.8 before the addition of acid to approximately 7.3, 100 seconds after the addition of the catalyst. The dielectric loss factor then gradually increases to approximately 10 in 800 seconds. This increase is

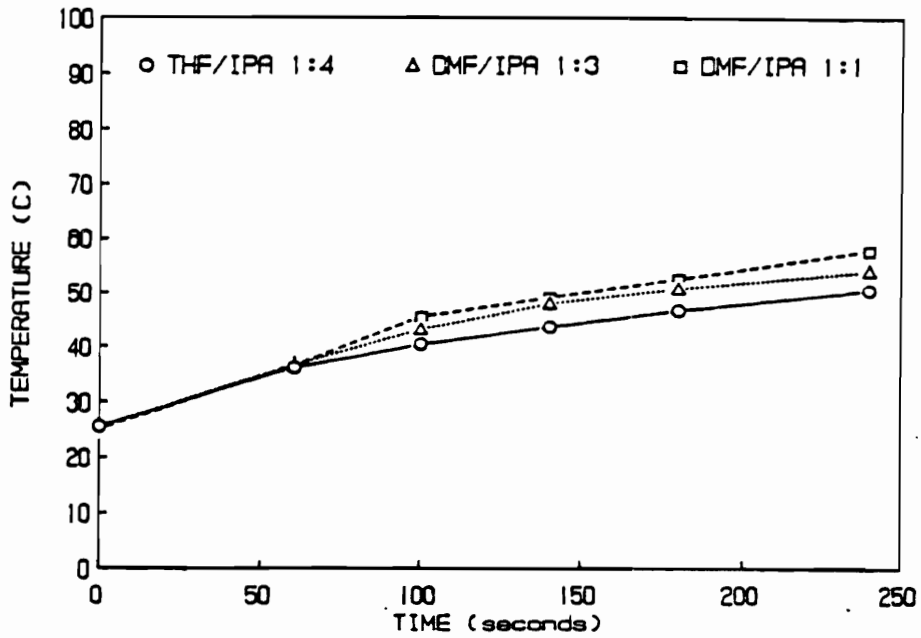


Figure 5.9. Temperature time measurements made on the TEOS/PTMO reactants in various cosolvent systems before the addition of acid

believed to be due to the hydrolysis of TEOS leading to the formation of silanol groups. These groups are highly dipolar because of the hydroxyl moities and this can contribute to the increased dielectric loss. After 800 seconds there is a gradual decrease in the dielectric loss factor from 10 to ca. 6.5. This decrease in the dielectric loss factor is most probably due to the condensation reaction in which the silanol groups react to form Si-O-Si linkages. These Si-O-Si species are known to have very low dipole moments (0.47 Debye) and further since these Si-O-Si linkages are part of the inorganic network their mobility would be significantly reduced as the condensation reaction progresses. This would therefore contribute to a reduction in the dielectric loss.

In the case of the reaction conducted in DMF/IPA::1/3, the loss factor increases from 4.0 before the addition of acid to a value of approximately 9, ten seconds after the addition of the catalyst. The loss factor gradually increases to 13.2 in about 150 seconds. The increase seen in the dielectric loss factor for the reactants is again attributed to the development of SiOH functionalities in the system. Artaki et al have pointed out that DMF hydrogen bonds to the polar molecules in the reactive solution and this interaction may also be responsible for the increase in the dielectric loss factor seen in these systems. The dielectric loss factor then drops off to approximately 7.5 and this decrease is again attributed to the condensation of SiOH groups to form Si-O-Si linkages.

believed to be due to the hydrolysis of TEOS leading to the formation of silanol groups. These groups are highly dipolar because of the hydroxyl moities and this can contribute to the increased dielectric loss. After 800 seconds there is a gradual decrease in the dielectric loss factor from 10 to ca. 6.5. This decrease in the dielectric loss factor is most probably due to the condensation reaction in which the silanol groups react to form Si-O-Si linkages. These Si-O-Si species are known to have very low dipole moments (0.47 Debye) and further since these Si-O-Si linkages are part of the inorganic network their mobility would be significantly reduced as the condensation reaction progresses. This would therefore contribute to a reduction in the dielectric loss.

In the case of the reaction conducted in DMF/IPA::1/3, the loss factor increases from 4.0 before the addition of acid to a value of approximately 9, ten seconds after the addition of the catalyst. The loss factor gradually increases to 13.2 in about 150 seconds. The increase seen in the dielectric loss factor for the reactants is again attributed to the development of SiOH functionalities in the system. Artaki et al have pointed out that DMF hydrogen bonds to the polar molecules in the reactive solution and this interaction may also be responsible for the increase in the dielectric loss factor seen in these systems. The dielectric loss factor then drops off to approximately 7.5 and this decrease is again attributed to the condensation of SiOH groups to form Si-O-Si linkages.

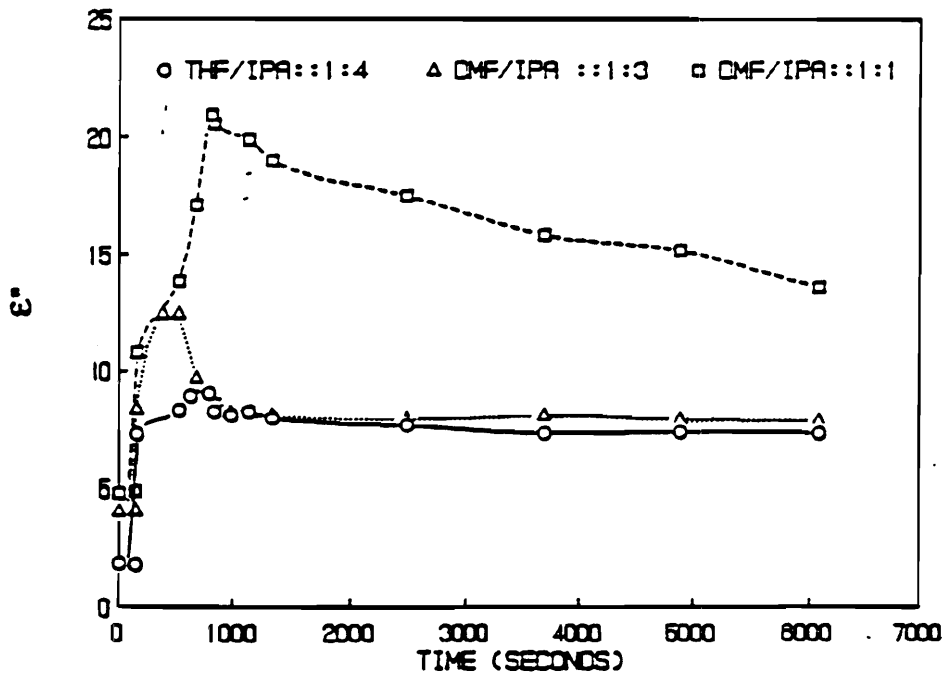


Figure 5.10. Dielectric measurements made on the TEOS/PTMO reactants in various cosolvent systems after the addition of acid

The reaction conducted in DMF/IPA::1/1 shows the largest increase in the loss factor from 4.8 to approximately 22 in about 600 seconds after the addition of acid. This dramatic increase indicates either a more rapid build up of silanol in the system or increased hydrogen bonding between DMF and the silanol moities or both. In this system the decrease in the dielectric loss factor, after reaching a maximum, is very gradual compared with the two systems described previously. The loss factor decreases from 22 to approximately 15 over the next 5400 seconds. Artaki et al have documented that when DMF is utilized as a solvent for the reaction of TEOS the condensation reaction is significantly retarded because of the tendency of the DMF to hydrogen bond with the reactive polar species thus hindering them from diffusing to the reactive sites. Thus a slower condensation reaction rate may help explain the gradual decrease in the loss factor seen for this system as compared with the THF/IPA::1/4 and DMF/IPA::1/3.

5.3.3.2 TEMPERATURE TIME HEATING MEASUREMENTS AFTER THE ADDITION OF ACID

Temperature-time heating profiles for these TEOS/PTMO reactants subjected

to microwaving after the addition of acid are shown in Fig 5.11. The time taken between the addition of acid to the reactants and switching on the microwave power was one minute. All these materials were heated in the microwave cavity for approximately 240 seconds. For the reactants compatibilized in DMF/IPA::1/1 and DMF/IPA::1/3, the initial temperatures were 42°C and 45°C respectively before the microwave energy was turned on. This initial increase in temperature from room temperature for these two reactive solutions immediately after the addition of the acid catalyst is due to the exothermic condensation reaction (66). In the case of the reactants compatibilized in THF/IPA, the solution temperature did not increase before the microwave energy was turned on. This difference in the starting temperatures of the three solutions at the point of turning on the microwave energy indicates that the zero point in the reactions for these microwave heating processes was not the same. This, however, is a feature over which the author had no control during the experiment. It should be noted, however, that the temperature for acid catalyzed TEOS/PTMO reactants in the THF/IPA solution eventually increases to around 40°C when retained at room temperature due to the exotherm of the condensation reaction, but takes slightly longer than one minute. This measurement was made in a separate experiment and will not be dealt with any further in this chapter.

As seen in Fig 5.11 the initial increase in temperature is greatest for the reactant solution containing THF/IPA. This steep increase in temperature is due to the onset of the reaction exotherm as well as the heating caused by the

interaction of the polar molecules in solution with the electromagnetic field. The solutions containing DMF/IPA in the ratios of 1/1 and 1/3 show a much lower initial rate of heating as compared with the solution containing THF/IPA probably because the thermal (heat) contribution from the exothermic reaction is somewhat reduced having already heated the reactant mixtures to around 40°C before the microwave power is switched on. At approximately 70 seconds after the microwave power was turned on, the temperature of all solutions is almost equal at 55 - 60°C. After 70 seconds, the temperature of the solution containing DMF/IPA::1/1 shows the highest rate of temperature increase. This matches the results obtained from the dielectric loss measurements which show an increase from 4.8 to approximately 22 after the addition of acid. Thus the higher rate of temperature increase seen for this reactive solution indicates that its capability to absorb microwave energy is much greater than for the other solutions seen in the figure. From the figure it can also be seen that the solution containing DMF/IPA::1/3 heats to a temperature of approximately 75°C in 240 seconds while the solution containing THF/IPA does not increase much in temperature above 65°C in the same time indicating that its ability to absorb microwave energy is lower than both the solutions containing DMF/IPA. Thus the trends seen in these results match the trends seen for the dielectric loss factor after the addition of acid catalyst.

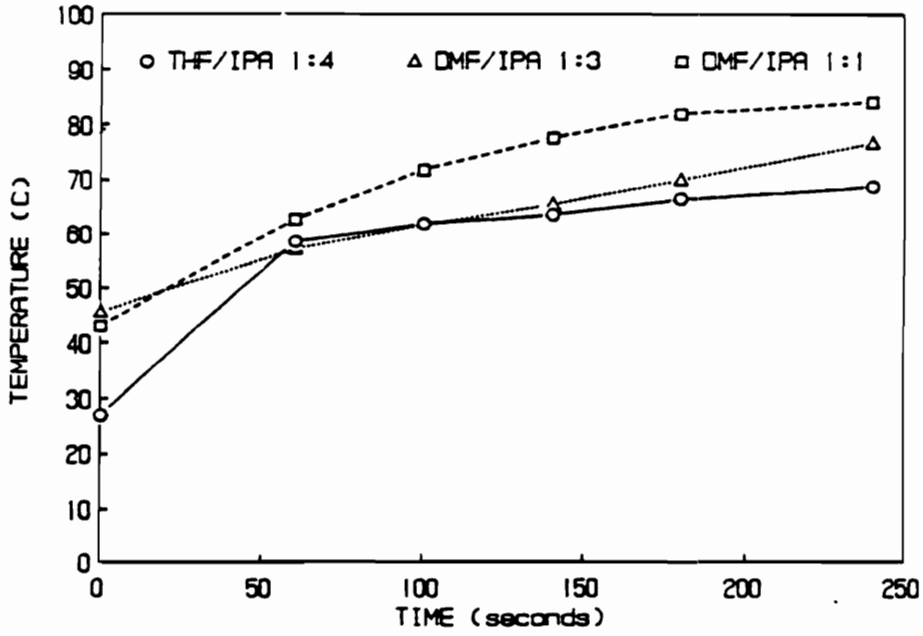


Figure 5.11. Temperature time measurements made on the TEOS/PTMO reactants in various cosolvent systems after the addition of acid

5.4 SOLUTION SMALL ANGLE XRAY SCATTERING RESULTS

In the above sections it was seen that solutions which show the maximum increase in the dielectric loss after the addition of catalyst also display a tendency to absorb microwave energy more efficiently. However, in the earlier chapters it was seen that even though microwave curing produced better properties in the TEOS/PTMO ceramers reacted in DMF/IPA than those reacted in an oven, the morphological structure as seen from small angle xray scattering essentially remained the same. This was also found to be true of the ceramer systems cured in THF/IPA, even though the differences in the mechanical properties between the microwave cured and oven cured materials were not significantly different. This reflects the inability of the microwave curing process or the oven curing process to affect the phase separation kinetics of these ceramer systems. In other words it is possible that the phase separation between the inorganic component and the oligomeric component begins almost at the instant the acid is added to the TEOS/PTMO reaction mixture and the kinetics of growth of the inorganic phase and its consequent segregation from the oligomer phase are influenced to only a very small degree by either of these thermal curing processes. In order to investigate this possibility it was decided to determine whether there existed

any correlated structure in the reactant mixtures before or immediately after the addition of acid to the reactants. The TEOS/PTMO reactant mixtures were therefore subjected to small angle xray scattering before and after the addition of acid in the solution state.

The solution scattering was performed on only the TEOS/PTMO solutions containing DMF/IPA::1/1 and THF/IPA::1/4. The solutions were injected into a stainless steel sample holder of 0.3 mm path length containing Kapton windows of 0.1 mil thickness. The Kapton film does not scatter significantly in the small angle region. The scattering profiles for the TEOS/PTMO solutions before the addition of the acid catalyst are shown in the Fig 5.12. Both profiles show a very low scattering intensity compared with those profiles seen for the respective films in the preceeding two chapters. The scattering profiles show a gradual increase in the scattering intensity as s increases and such behavior is typical of homogenous liquids (liquid scattering). Since there are no interparticle interference peaks (as seen in the ceramer films) or shoulders in the scattering profiles, no correlated structure is assumed to exist in the solution state before the addition of the acid catalyst.

Immediately after the addition of the acid catalyst to the reaction mixture the solutions were then cast into polystyrene (PS) petri dishes and allowed to gel at ambient conditions. At ten minutes the solutions (in the PS dishes) began to gel and were subjected to SAXS along with the PS substrate. The scattering due to the PS substrate was later subtracted from the scattering profile. In

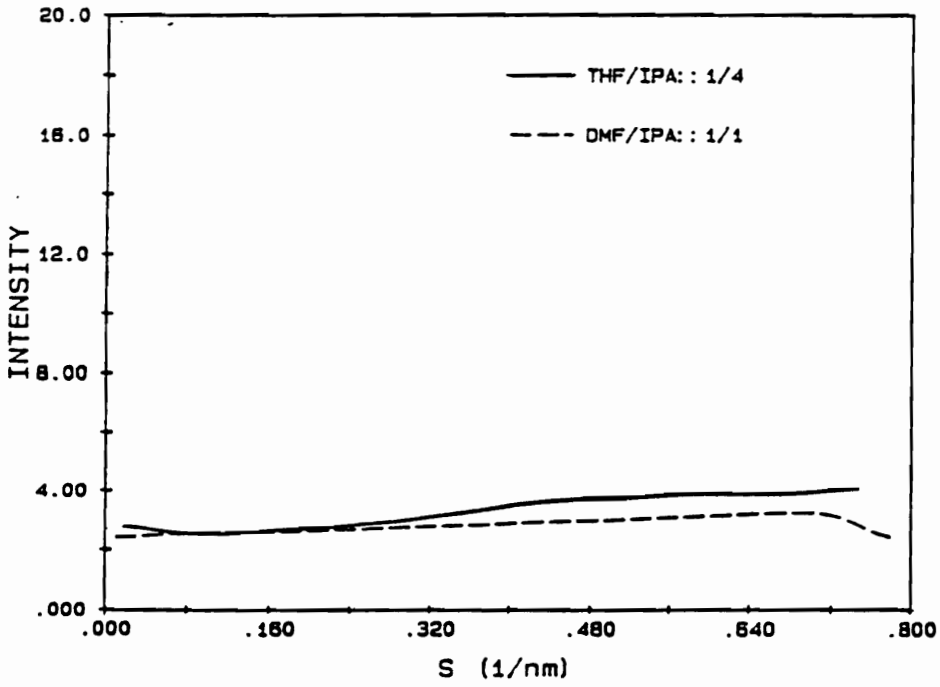


Figure 5.12. SAXS scattering profiles for the TEOS/PTMO reactants in various cosolvent systems before the addition of acid

order to obtain a scattering profile as quickly as possible, the scans were conducted for only 300 seconds. Fig 5.13 shows the scattering profiles obtained after the addition of acid to the respective reactant mixtures. For the TEOS/PTMO film reacted in DMF/IPA there occurs an interference peak at around 193Å. For the TEOS/PTMO ceramers reacted in THF/IPA scans could only be taken six hours after casting because these films do not gel as quickly as their counterparts reacted in DMF/IPA. These TEOS/PTMO gels reacted in THF/IPA do not show any distinct interference peak. However, this may be due to the fact that the ceramer reacted in THF/IPA does not show as strong an interference peak as the material reacted in DMF/IPA even after ageing for extended periods of time. Thus the presence of an interference peak in the TEOS/PTMO ceramer reacted in DMF/IPA almost immediately after casting as well as the fact that there is virtually no difference in the scattering profiles between the microwave cured film and the room temperature cured material (as seen earlier in chapter 3) suggests that the microstructure is already determined shortly after casting and hence unaffected by the microwave curing process.

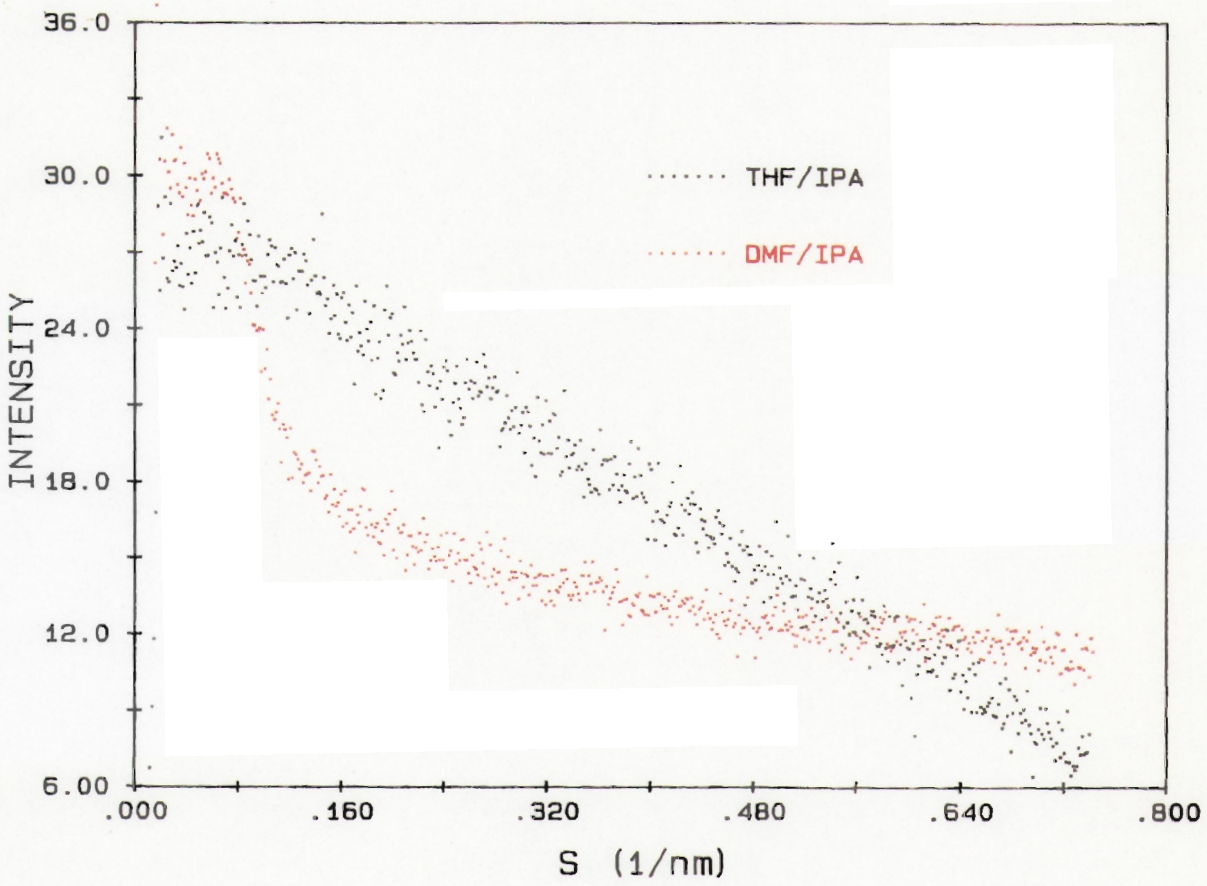


Figure 5.13. SAXS scattering profiles for the TEOS/PTMO reactants in various cosolvent systems after the addition of acid

5.5 STRESS STRAIN PROPERTIES OF TEOS/PTMO CERAMER MATERIALS

Stress strain properties of these TEOS/PTMO ceramers microwaved to 70°C were studied for the purpose of establishing a link between the dielectric properties of the TEOS/PTMO solutions and the mechanical properties of the corresponding films. Stress strain properties of the oven cured samples, heated to 70°C, were also studied in order to make comparisons with their microwave cured counterparts. As stated earlier these stress strain measurements were made on an Instron under ambient conditions at an initial crosshead speed of 2 mm/min. The tests were made within two hours of completion of the respective 70°C curing processes i. e. oven or microwave curing for each film. The stress strain properties of these ceramers are documented in Table 5.1. This table also shows the highest value of the dielectric loss factor for each of the reactive solutions obtained after the addition of acid to the reactant solutions. From the table it can be seen that 8 the higher the value of the dielectric loss factor for a particular TEOS/PTMO/solvent combination (after the addition of acid) the greater the difference between the elastic modulii of the microwave cured and oven cured film. The reason for these differences in the elastic modulus of the microwave cured and oven cured films for a particular compatibilizing solution is

therefore relatable to the build up of the dielectric loss factor in that solution after the addition of acid. In other words, phase separation characteristics aside, the greater the dielectric loss factor (after the addition of acid) for a particular TEOS/PTMO/solvent combination, the better the mechanical properties of the films microwaved from the solution. However phase separation characteristics in these films also play an important role in the mechanical properties of the final film as will be described shortly.

The elastic modulii of the microwave cured and oven cured films are plotted versus the volume fraction of DMF with respect to IPA in Fig 5.14. As can be seen in this figure the modulii for the microwave cured materials increases with the increasing DMF concentration upto 50% volume fraction with regard to IPA. At higher DMF concentrations the elastic modulii of the microwave cured materials decreases. This decrease in the elastic modulus is because of the macrophase separation of the inorganic from the PTMO caused by the greater DMF concentration in the reaction mixture. This macrophase separation is visible before the insertion into the microwave cavity TEOS/PTMO compatibilized in DMF/IPA::3/1, while in the case of samples reacted in only DMF solvent the macrophase separation is instantaneous and the crosslinked PTMO drops out of solution almost completely.

For the oven cured films the highest modulus occurs for the samples compatibilized in DMF/IPA::1/3. This is because, as stated earlier in chapter 4, the samples cured in the oven heat very slowly, (they take almost 30 minutes to reach 70°C) which permits more time for the IPA to evaporate. The

Table 5.1. Elastic modulus values for the microwave and oven cured materials are shown along with the dielectric loss factor.

	M. W. 70C (MPa)	O. C. 70C (MPa)	Dielectric Loss
THF/IPA::1/4	4	4	10
DMF/IPA::1/3	96	16	13
DMF/IPA::1/1	250	4	22
DMF/IPA::3/1	46	4	--

excess DMF left behind because of this evaporation of IPA slows down the condensation reaction and also drives the phase separation of the reactants i. e. the inorganic from the oligomer. The lower extent of reaction as well as the lack of incorporation of PTMO into the network gives rise to a reduced elastic modulii when compared with equivalent microwave cured materials. In the case of the ceramer films cured in DMF/IPA::1/3 the larger IPA content present in the reaction mixture as compared with the solution containing DMF/IPA::1/1 permits a greater extent of reaction in the TEOS/PTMO system before it evaporates. Thus the ceramer films prepared in a cosolvent system containing volume concentrations of DMF greater than 33% with regard to IPA display lower values of elastic modulus when cured in a conventional oven at 70°C.

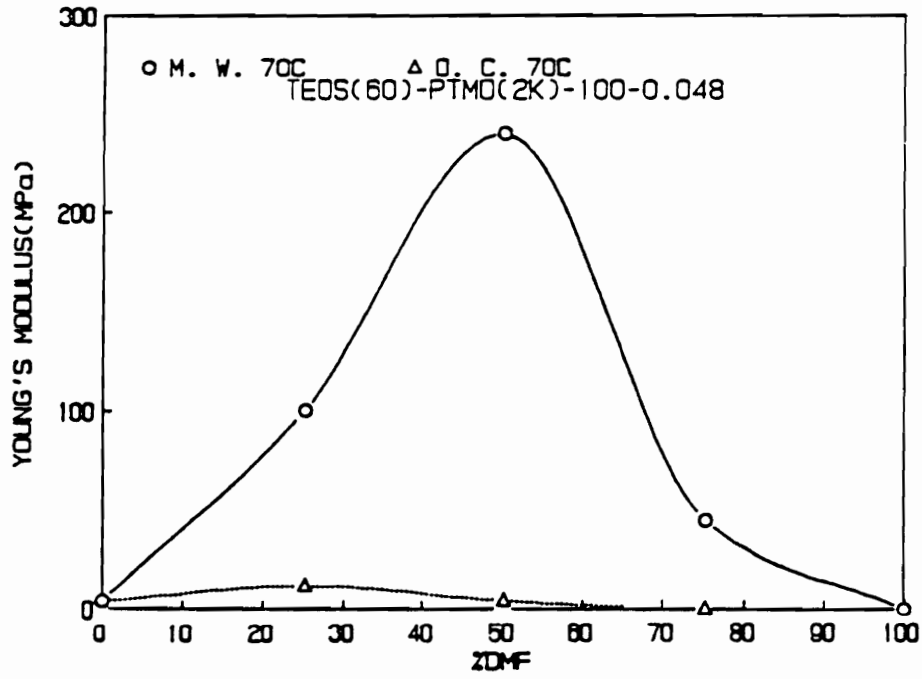


Figure 5.14. Plot the elastic modulus of microwave cured and oven cured films versus DMF concentration in the TEOS/PTMO ceramers

5.6 SMALL ANGLE XRAY SCATTERING ON FILMS

As stated above the phase separation characteristics of the TEOS/PTMO ceramers begin almost at the instant the acid catalyst is added to the reactant solution. The nature of growth of the inorganic phase determines the extent of phase separation and also plays an important role in the observed mechanical properties of the films. A more detailed study of the growth of the inorganic phase in these ceramer systems is detailed in chapter 8. In other words it is not only the dielectric properties of the solutions which determine the extent of reaction in a microwave field but also the phase separation characteristics (nature of growth of the inorganic phase).

Small angle xray scattering experiments were therefore performed on all the microwaved cured TEOS/PTMO films to study the effects of solvent on the structure of the films. The scattering profiles for the TEOS/PTMO ceramers microwave cured to 70°C in THF/IPA::1/4, DMF/IPA::1/3 and DMF/IPA::1/1 are displayed in Fig 5.15. From this figure it can be seen that scattering profile for the ceramer cured in THF/IPA::1/4 is broader than those cured in either of the DMF/IPA cosolvent ratios. The intensity of scattering is lowest and the interdomain spacing as seen from the peak position is around 106Å The system cured in DMF/IPA::1/3 shows a scattering profile which is has a higher intensity of scattering than that seen for the THF/IPA::1/4 system. The breadth

of the peak is narrower (indicating a narrower distribution of interdomain spacings or domain sizes or both) and the tail region is also more flattened (possibly suggesting lesser mixing between the inorganic and the oligomer phase) than for the ceramer cured in THF/IPA::1/4. The interdomain spacing as measured from the peak position is located at 140Å The film prepared in DMF/IPA::1/1 has the highest scattering intensity and the breadth of the peak is narrowest of all these three ceramer films. The scattering profile is furthur flattened in the tail region and the interdomain spacing is 148Å. At composition ratios of DMF/IPA::3/1 macrophase separation takes place in these materials and hence SAXS was not performed on these materials.

The reduction in breadth of the scattering profiles, the increasing intensity at the peak position, the flattening of the tail region with increasing DMF concentration in the reaction mixture indicates that DMF may well drive the phase separation in these ceramer systems. From the stress strain properties displayed in the microwave cured films it was seen that the elastic modulus increased with increasing DMF concentration with respect to IPA upto vol% DMF with regard to IPA. These results indicate that elastic modulus also increases with the increased degree of phase separation upto 50 vol% DMF concentration in the cosolvent system. It can therefore be concluded that, in as much as the increase in the dielectric loss factor of a particular reactant solution determines the extent to which these systems lend themselves to microwave curing, the phase separation characteristics (or the nature of growth of the inorganic phase) determines the degree to which the reactive

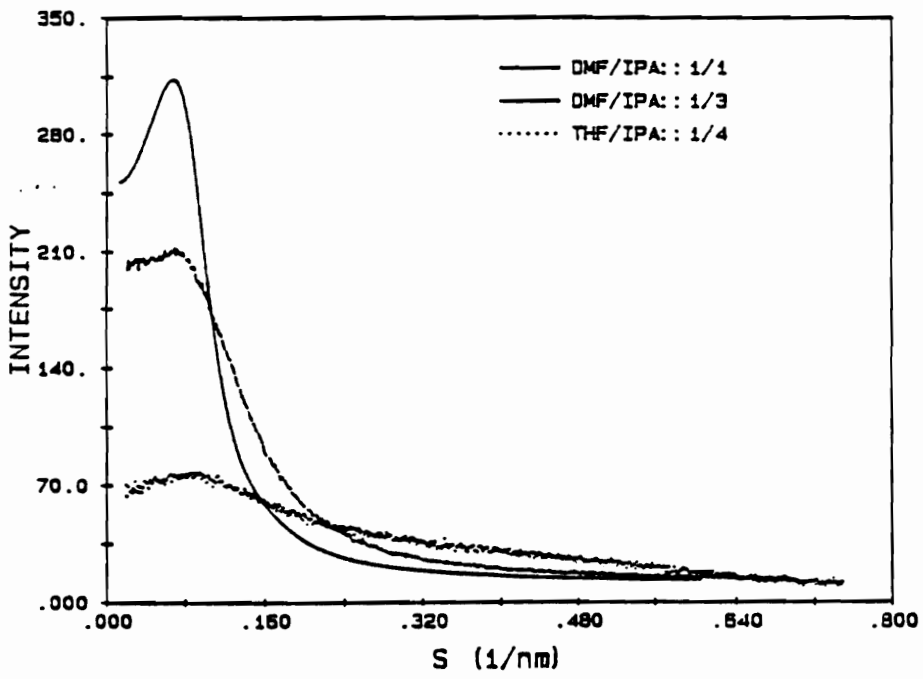


Figure 5.15. SAXS profiles from the TEOS/PTMO ceramers reacted in DMF/IPA::1/1, DMF/IPA::1/3 and THF/IPA::1/4.

components can actually interact and this single factor, more than any other, establishes in a very decisive manner, the short as well as the long term mechanical properties of these TEOS/PTMO ceramer films.

5.7 CONCLUSIONS

It has been clearly shown that the dielectric loss properties of the solutions before the addition of the acid catalyst are dependent upon the dielectric loss properties of its components. These loss properties determine the abilities of the solutions to absorb microwaves as witnessed from the temperature time heating profiles. The systems containing the greatest amount of DMF had the highest dielectric loss factors and these solutions exhibited the greatest ability to absorb electromagnetic radiation.

Results obtained from the dielectric network analyser showed that the solutions containing DMF tended to develop a higher dielectric loss factor after the addition of acid as compared with those containing THF. In particular the TEOS/PTMO solution compatibilized with DMF/IPA::1/1 showed the maximum increase in the loss factor after the addition of the catalyst. This

increase in the loss factor promotes the absorption of microwave energy and causes the mechanical properties of the microwaved samples to be significantly greater than their oven cured counterparts.

It was also shown that the reason for the lack of any significant difference in the morphology of these TEOS/PTMO ceramers cured either in a microwave cavity or in an oven in any particular cosolvent system is due to the fact that phase separation characteristics are set almost at the instant the reaction begins and cannot be significantly altered by the method of curing. These phase separation characteristics also play an important role in the mechanical properties of the ceramer films irrespective of the dielectric properties.

CHAPTER 6

STRUCTURE PROPERTY RELATIONSHIPS IN MICROWAVE CURED TIOPR/PTMO AND ZROPR/PTMO CERAMERS

6.1 INTRODUCTION

The use of only titanium isopropoxide (TiOPr) or zirconium isopropoxide (ZrOPr) as metal alkoxides in ceramer systems containing endcapped polytetramethyleneoxide (PTMO) was first undertaken by Wang (104). Though TiOPr and ZrOPr are much faster reacting than TEOS, Parkhurst et al (105)

have previously reported that TiOPr can be prehydrolysed to form a very stable sol. A similar procedure was adopted by Wang in which TiOPr or ZrOPr were first diluted in isopropanol (IPA) and then prehydrolysed to form a stable sol. Endcapped PTMO was then added to this sol and the solution was cast into petri dishes and allowed to remain at ambient conditions until a thin, transparent ceramer film was formed. These films were first characterized by Brennan (96). Some of the general structure property features of these ceramer systems have already been documented in chapter 1 of this dissertation and hence the author will not elaborate upon these features any further.

6.2 RESEARCH AND OBJECTIVES

In the previous chapters it was observed that microwave curing enhanced the extent of reaction in TEOS/PTMO ceramers when DMF/IPA was used as a cosolvent system for the reaction. This increased rate of reaction seen with microwave curing was attributed to the increased dielectric loss factor of the reactants after the addition of acid which allows for efficient absorption of microwave energy. Another factor that allows for efficient curing of these ceramers in a microwave field is the degree of phase separation (nature of growth of the inorganic phase) in some of the ceramer systems. This phase

separation allows for the agglomeration of reactive sites in close proximity to each other in the inorganic domains and thus an increased extent of reaction is possible when microwave heating is used. Ceramers produced in DMF/IPA display sharp phase separation between the inorganic and the oligomer phases. As stated above, microwave curing can enhance the extent of reaction when there is a greater amount of such phase separation between the inorganic and the PTMO components. Since a higher degree of phase separation was also shown to exist in the TiOPr/PTMO and ZrOPr/PTMO ceramers by Brennan it was decided to attempt curing these materials in a microwave cavity to try and reproduce the successful results obtained with TEOS/PTMO materials cured in DMF/IPA.

As stated earlier TiOPr and ZrOPr are known to be faster reacting metal alkoxides than TEOS. Hence it was decided to react TiOPr or ZrOPr with endcapped PTMO at 70°C in a microwave cavity as well as in a conventional convection oven and examine the differences in the resulting films. Room temperature cured films were also investigated for their structures and properties.

6.3 EXPERIMENTAL

The method developed by Wang for the incorporation of PTMO into the ceramer network containing TiOPr or ZrOPr has been documented elsewhere (104) and consisted primarily of mixing the water of hydration, HCl and the TiOPr with a large excess of IPA (56 mol/mol with regard to TiOPr). To this mixture was added PTMO which was also diluted in IPA. The reactants were then cast into petri dishes and allowed to react under ambient conditions. The films could be removed for testing five days after casting. The use of Wang's formulation without modification resulted in some difficulties when curing was attempted in the microwave cavity primarily because of the large amount of solvent present in the reactants. As the solvent evaporated it gave rise to tremendous variations in the electromagnetic field within the cavity and caused power fluctuations which rendered the microwave cavity uncontrollable. These fluctuations arise mainly from the displacement of solvent vapor in the cavity as well as its condensation on the walls of the cavity. The distortion of the electromagnetic field causes non uniform heating in the samples which gives rise to thermal gradients within the sample. Such gradients can promote gross sample distortion which results in films with a foam like appearance.

It became obvious that in order to microwave cure these ceramers a new method of formulation was required in which the amount of solvent was

drastically reduced and which still yielded optically tranparent, homogenous films. This new method of formulation is shown in Fig 6.1 and consisted of first mixing 5 ml of IPA with 5 gm of TiOPr. To this was added a mixture of 5 ml IPA, 0.35 ml water and 0.2 ml of 10N HCl. This addition was carried out in ten minutes while continuously stirring at high speed. Finally a mixture of 5 gms of PTMO and 7 ml of IPA were added to the flask and stirred for two minutes. The homogenous reactant mixture was then poured into petri dishes and then subjected to microwave curing or oven curing, 15 minutes after casting. This new method of formulation reduces the amount of solvent by 85% from that used in Wang's formulation and the time for preparation of the reaction mixture before casting is reduced by 20 minutes. The nomenclature for these titania based ceramers is TiOPr(50)-PTMO(2K)-25-0.06.

The method of formulation for the zirconia ceramers was modified in a similar manner with the sole aim of reducing the amount of solvent used for sample preparation. This method is shown in Fig 6.2. Water was not added to the reaction mixture and the only water (for hydration) came from the acid catayst. The nomenclature for this material is ZrOPr(50)-PTMO(2K)-0-0.02.

The materials in the petri dishes were then subjected to their respective curing processes i. e. one set of samples was cured in a microwave oven to 70°C while another set of samples was placed in an oven preset at 70°C. Some samples were cured at room temperature for 1 day before being subjected to testing. The microwaved samples are denoted as M. W. 70C and were heated

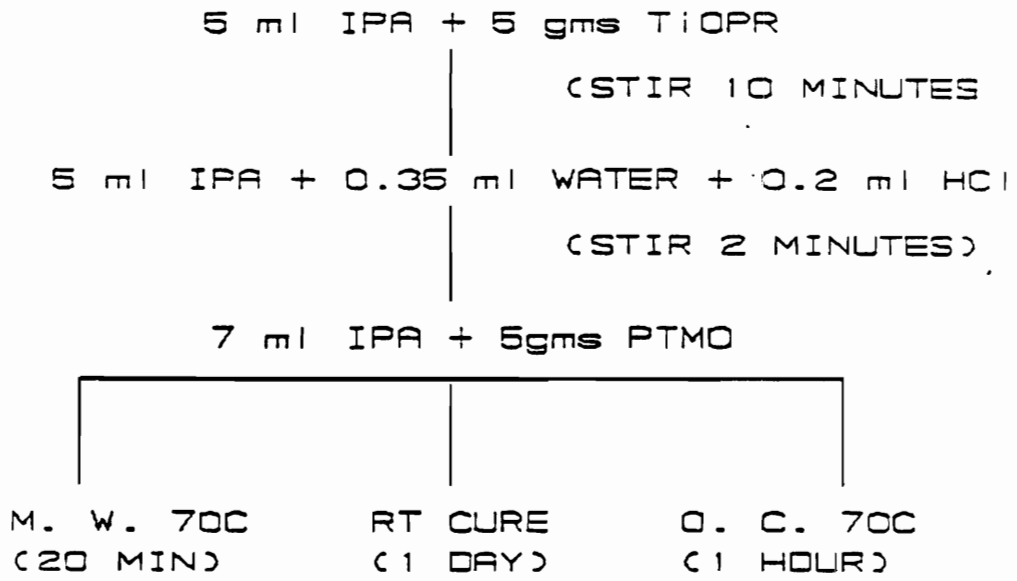


Figure 6.1. Schematic for the preparation of TiOPr(50)-PTMO(2K)-25-0.06.

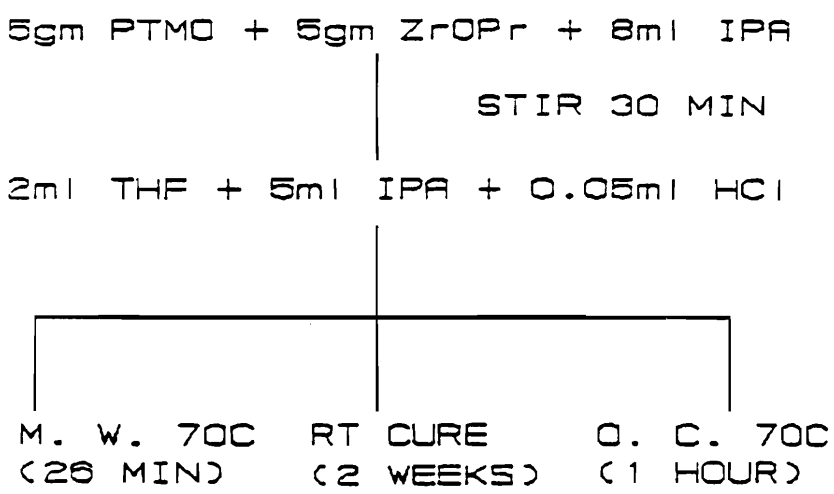


Figure 6.2. Schematic for the preparation of ZrOPr(50)-PTMO(2K)-25-0.06.

for a period of twenty minutes. The heating profile for the microwaved films is shown in Fig 6.3. The initial rate of heating for the TiOPr/PTMO system is much slower when compared with the materials containing TEOS as described in the earlier two chapters. This is primarily to effect a slow evaporation of the IPA from the reaction mixture so as not to permit the formation of voids and consequent distortion in the film. A glance at the temperature versus time profile shows a higher rate of heating initially, and this rate decreases as the temperature approaches 70°C. The temperature of the TiOPr/PTMO reactants was raised to 70°C in 1000 seconds. The reactants were held at 70°C for a period of approximately 3 minutes.

The input power used for the microwaving curing was increased in steps as can be seen in Fig 6.4. The initial input power was 10 W. The cavity was fully tuned and all the power was conserved within the cavity throughout the course of heating. In other words no power was reflected out of the cavity. The final power used was 23 W. These ceramers are known to cure very fast because of the high reactivity rates of TiOPr. The conversion of TiOH to Ti-O-Ti and Ti-O-Si would cause a decrease in the dielectric loss factor and thus necessitate an increase in the input power required to maintain the temperature at 70°C. Further, with the evaporation of isopropanol, the majority of dipoles left in solution are those of the C-O-C bonds since the PTMO volume fraction increases from approximately 50% initially to 67% with curing (84, 96). These PTMO molecules have a low dielectric loss factor of approximately 0.36

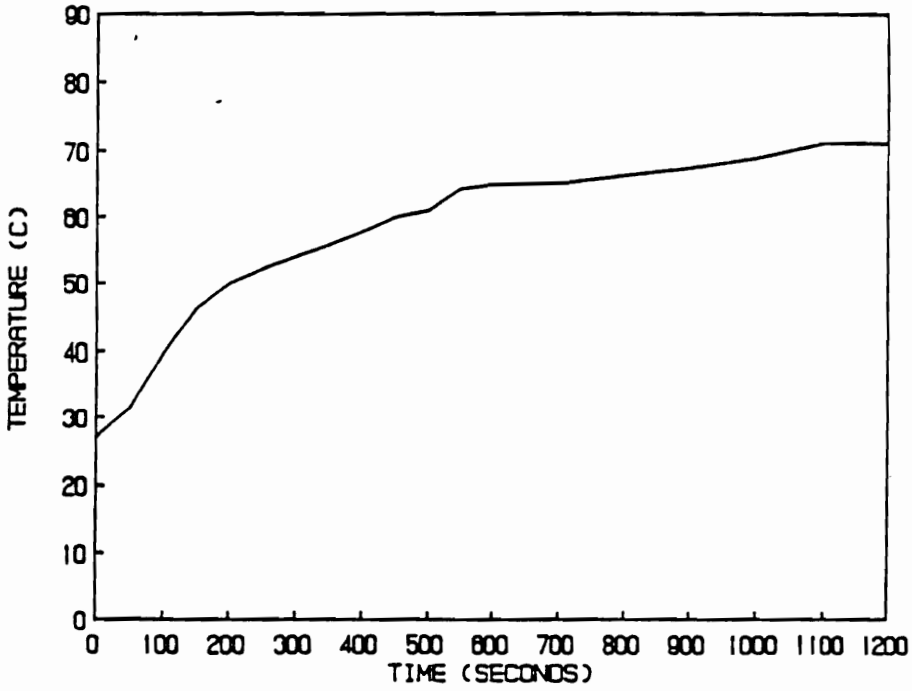


Figure 6.3. Temperature time heating profile for the TiOPr/PTMO film cured to 70°C.

and this would also contribute to the requirement for additional power in order to maintain the temperature at 70°C.

TiOPr/PTMO samples cured in the conventional convection oven (denoted by O. C. 70C) were cured for one hour and then subjected to physical testing. The samples cured at room temperature were stored under ambient conditions for one day before being tested and these were denoted as RT (room temperature) cured materials.

The ceramers containing ZrOPr/PTMO were prepared in a somewhat identical manner as their TiOPr/PTMO counterparts. After being poured into petri dishes the materials were then subjected to their individual curing processes i. e. either microwave curing, oven curing or RT curing as in the cases of the titania ceramers. The notations for the materials are the same as above i. e. the microwave cured material is designated as M. W. 70C etc. The temperature vs time profile for the microwave cured zirconia ceramer is shown in Fig 6.5. As can be seen the temperature is increased to 70°C very slowly. The rate of heating is reduced with the increase in temperature. The total time of heating in the microwave cavity for the ZrOPr/PTMO ceramers is 1800 seconds as compared to 1200 seconds for the TiOPr/PTMO or the TEOS/PTMO ceramers discussed in chapters 3 and 4. ZrOPr/PTMO samples taken out of the microwave cavity after 1200 seconds and were found to be ungelled. Hence it was decided to increase the time of curing in the microwave cavity. At 1800 seconds the samples were found to be cured sufficiently to be physically

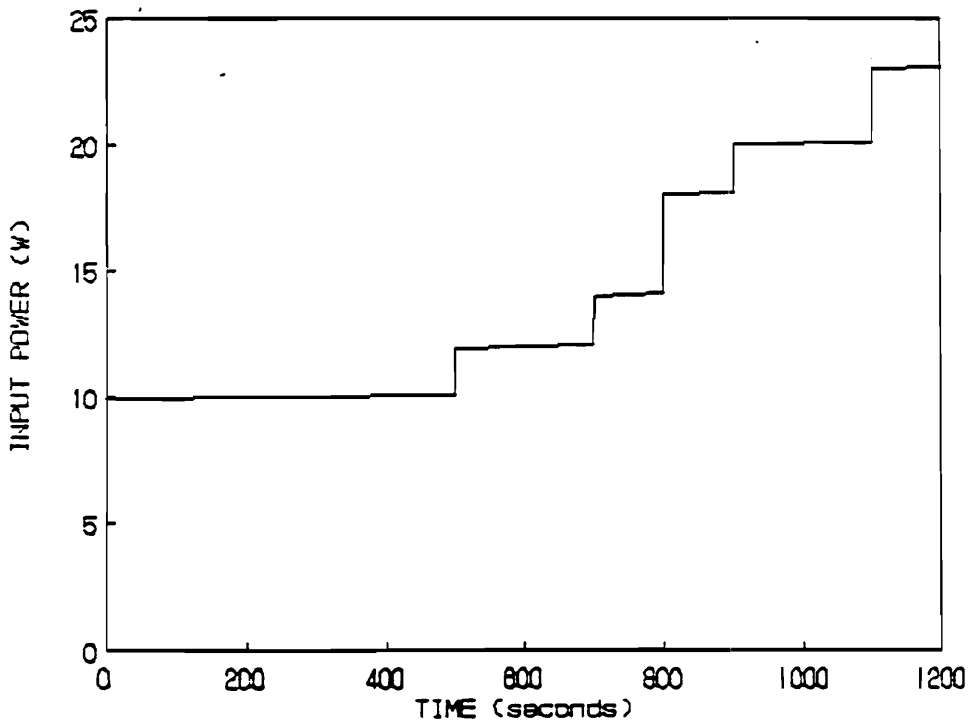


Figure 6.4. Power versus time profile for the TiOPr/PTMO film cured to 70°C.

tested. The reason for the extended time period for curing the ZrOPr/PTMO ceramers as compared with the other ceramer materials discussed previously in this dissertation is believed to be related to the low water content present in the initial formulation for the ZrOPr/PTMO materials. Since the initial water content in the reaction mixture is almost negligable it is expected that the small amount of ZrOH does not facilitate a rapid rate of conversion to Zr-O-Zr and Zr-O-Si in these ceramers.

The power vs time curves for the ZrOPr/PTMO ceramers cured in the microwave cavity are shown in Fig 6.6. The power was stepped up during the curing process to raise the temperature to 70°C. The initial power used was 5 watts while the final power was 16 watts. From the figure it can be seen that 2 watts of power was reflected out of the cavity. This was done to stabilize the temperature of the curing material at 70°C. The reason for the use of a lower amount of power in the case of the zirconia ceramers as compared with the titania ceramers is probably due to the lower extent of reaction in these systems. This lower extent of reaction stems primarily from the use of low amounts of water and the lower extent of reaction allows for a looser network which permits a greater amount of dipole mobility in the samples thereby permitting more absorption in these materials. Samples placed in a convection oven at 70°C and were also found to be cured sufficiently at approximately 1800 seconds. The RT cured material was tested two weeks after casting. Despite the delay in time, the results obtained from the RT cured ZrOPr/PTMO ceramers will nevertheless be documented for the sake of consistency.

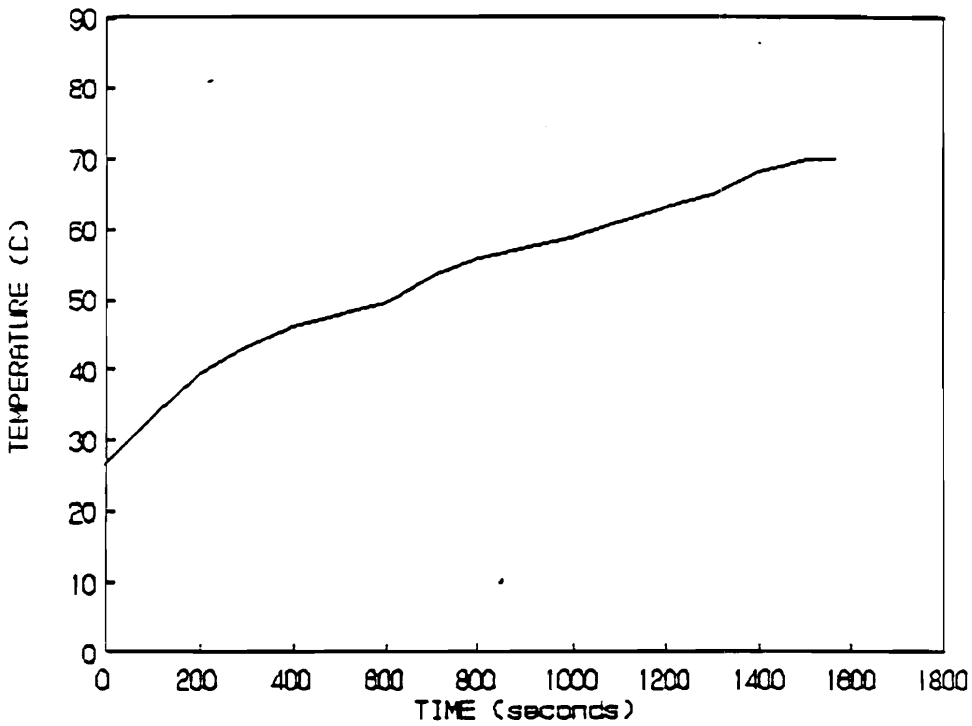


Figure 6.5. Temperature time heating profile for the ZrOPr/PTMO film cured to 70°C.

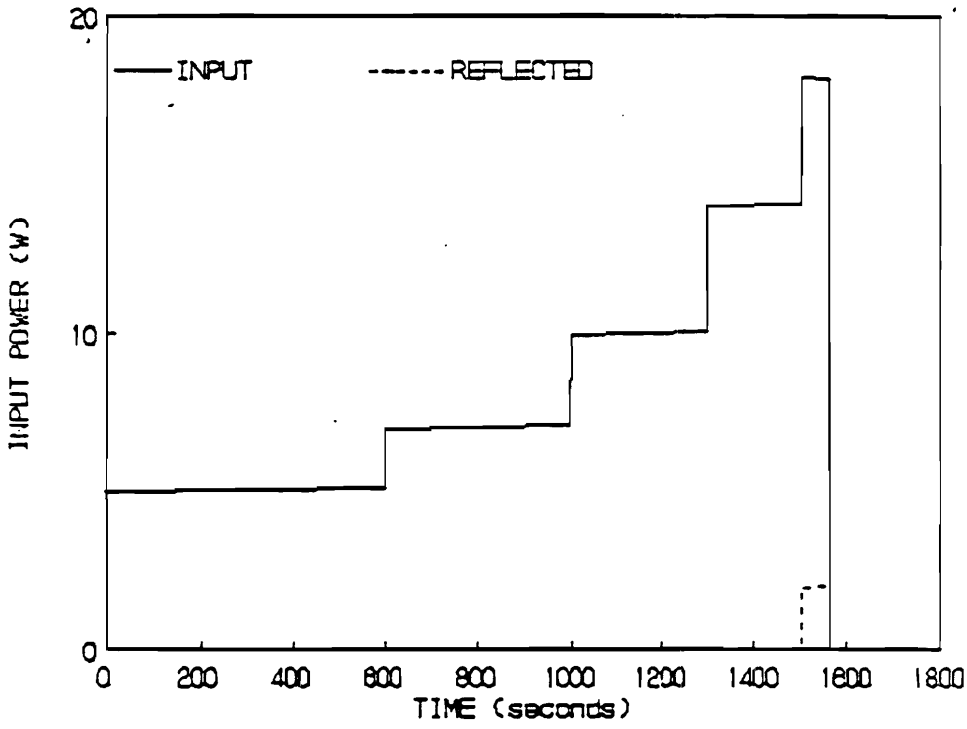


Figure 6.6. Power versus time profile for the TiOPr/PTMO film cured to 70°C.

6.4 RESULTS AND DISCUSSION

6.4.1 MECHANICAL PROPERTIES OF THE TiOPr/PTMO CERAMERS

Stress strain analysis conducted at ambient conditions on an Instron reveal a higher average value of the elastic modulus for the M.W. 70C TiOPr/PTMO samples than for the O. C. 70C or RT materials. These values are shown in Table 6.1. The stress strain curves are shown in Fig 6.7. The M. W. 70C material which has a modulus of 180 MPa, displays a linear stress strain response upto a stress of approximately 9 MPa, while there occurs some plastic yielding of the material above this stress value. The elongation at break for the M. W. 70C material is 70%. The RT cured material shows an elastic modulus of 120 MPa and an elongation at break of about 110%. The O. C. 70C material shows the lowest elastic modulus of 50 MPa and an elongation at break of 70%. The linear stress strain response in the O. C. 70C material occurs upto a stress value of 5 MPa. The lower elastic modulus seen for the oven cured materials as compared with the RT cured materials indicates again that the evaporation of solvent during the oven curing process puts limitations on the extent of reaction. On the other hand the microwave curing process produces improved mechanical properties because of the ability of microwaves to efficiently couple with the reactive dipoles in solution. This ability is further enhanced by the high degree of phase separation between the

inorganic and the oligomeric phase seen for these TiOPr/PTMO ceramers and this permits a high extent of reaction in the M. W. 70 C system.

While neither of the stress strain curves for the three films shown in Fig 6.7 display a distinct yield point, Brennan has shown that TiOPr/PTMO ceramers containing 55 - 58% TiOPr clearly display a yield point during tensile tests (96). No explanation was given for this yield behavior. Such yield behavior has not been seen in the ceramers discussed previously in chapters 4 and 5 in this dissertation. Yield has, however, been observed in ceramer materials containing mixed metal alkoxides TEOS and TiOPr with PTMO (85) as well as the ceramers containing multifunctional PTMO (84) containing 6 pendent groups.

The stress strain data documented in Table 6.1 shows clearly that the elongation at break for the room temperature cured material is much higher than both the M. W. 70C or O. C. 70C materials. This may be due to defects in the material due to the evaporation of large amounts of solvent which can possibly lead to the formation of voids and defects as seen earlier in the oven cured TEOS/PTMO films cured in DMF/IPA as seen in chapter 4.

Table 7.1. Stress strain properties for the differently cured TiOPr/PTMO ceramers

	Young's Modulus(MPa)	Stress at Break (MPa)	Elongation%
M. W. 70C (20 min)	180	12	70
RT cure (1 day)	120	15	110
O. C. 70C (1 hour)	50	10	65

6.4.2 MECHANICAL PROPERTIES OF THE ZrOPr/PTMO CERAMERS

The stress strain analysis for the zirconia containing samples shows no significant difference between the M. W. 70C samples and the O. C. 70C samples. Inspection of Fig 6.8 shows nearly the same stress strain behavior for the M. W. 70C and the O. C. 70C ZrOPr/PTMO ceramer materials upto a stress of approximately 8 MPa. The reactant composition for this ceramer contains virtually no free water and it is therefore presumed that there would be very few ZrOH groups in the reactant system during the microwave curing process. Thus with very few such reactive dipolar groups in the system to absorb electromagnetic radiation, the effect of the microwaves on the material is negligable. The data for these materials is shown in Table 6.2. As can be seen the elastic modulus for these materials is much lower than that for the titania

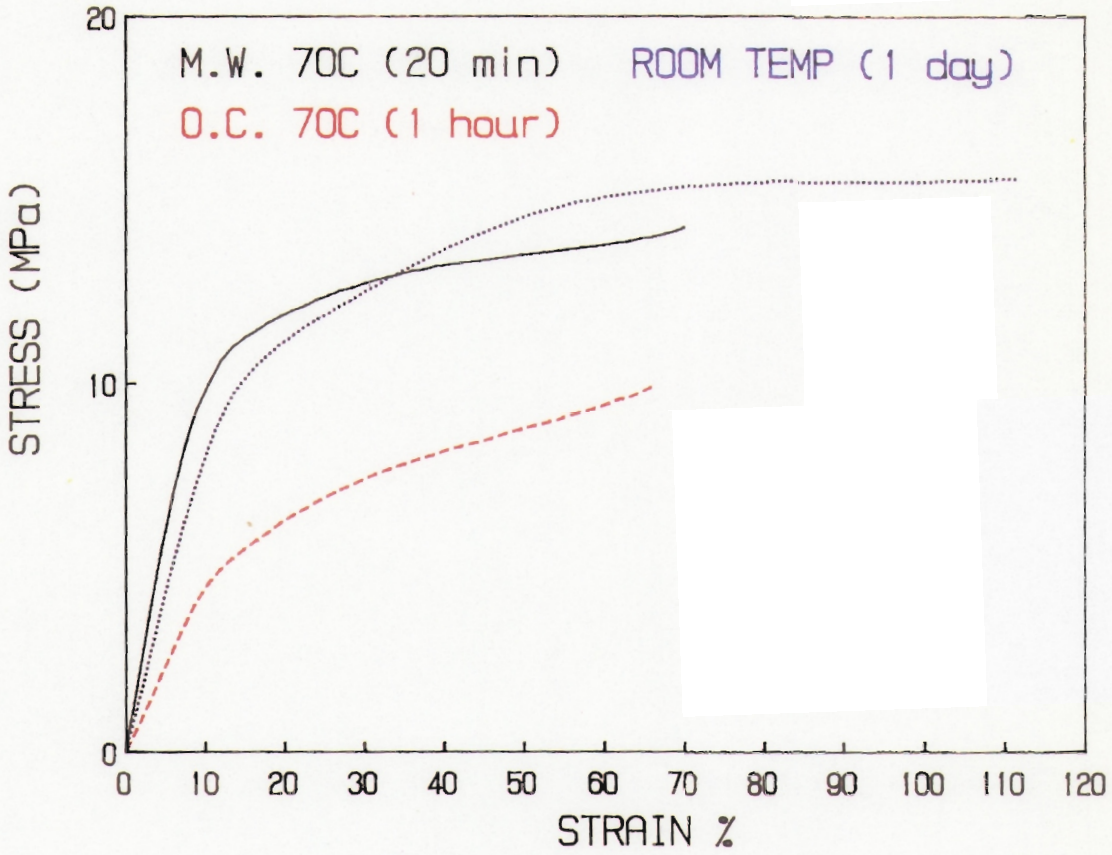


Figure 6.7. **Stress strain curves for the three differently cured TiOPr/PTMO ceramerfilms.**

containing ceramers. This can be related to the fact that these systems contain very little water for hydration. The RT cured material shows an elastic modulus of approximately 80 MPa; however as stated earlier these measurements were made two weeks after casting. Above a stress value of 8 MPa all the three stress strain curves in Fig 6.8 show the beginnings of yield behavior. Again Brennan has shown that systems containing similar amounts of the metal alkoxide show similar yield behavior when strained under the same conditions.

6.4.3 DYNAMIC MECHANICAL SPECTROSCOPY FOR THE TiOPr/PTMO CERAMERS

The storage modulii for the TiOPr/PTMO ceramers are displayed in Fig 6.9. All three samples (M. W. 70C, O. C. 70C and the RT cured films) display a glassy modulus of approximately 10^9 Pa at -100°C. As the temperature is increased above -100°C, the three films show a decrease in the storage modulus. The reduction in the storage modulii for all three TiOPr/PTMO films is attributed to the onset of cooperative segmental motion of the PTMO oligomers. As with the TEOS/PTMO films cured in DMF/IPA, (described in chapter 4) here too, there is a two step drop in the storage modulus. For the M. W. 70C and the RT cured materials the first drop occurs at around -80°C

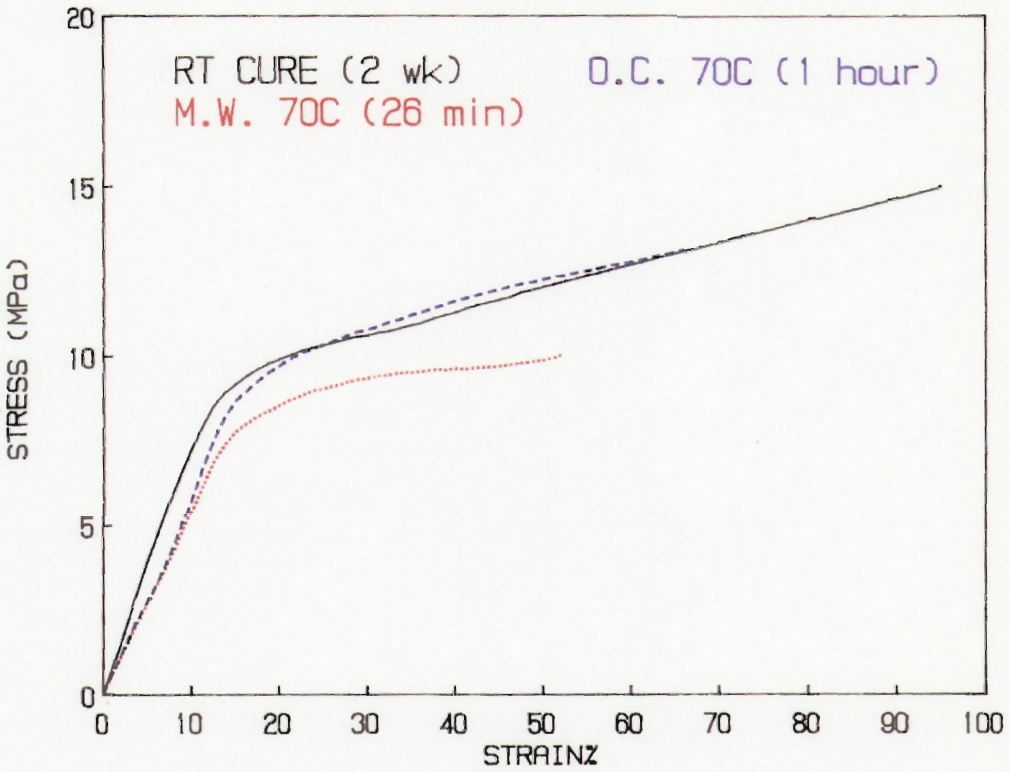


Figure 6.8. **Stress strain curves for the three differently cured ZrOPr/PTMO ceramer films (as labelled).**

Table 7.2. Stress strain properties for the differently cured ZrOPr/PTMO ceramers

	Young's Modulus(MPa)	Stress at Break (MPa)	Elongation%
M. W. 70C (20 min)	57	10	48
RT cure (2 weeks)	75	14	60
O. C. 70C (1 hour)	58	12	60

while the second occurs at around -20°C. The M. W. 70C and the RT cured materials both display a drop of approximately half a decade in the storage modulus between -100°C and 0°C. The decrease which occurs at around -80°C is attributed to the dissipative motion of PTMO in a PTMO rich environment, while the decrease which occurs around -20°C is possibly due to the cooperative segmental motion of PTMO chains present in an inorganic rich environment. These drops in the storage modulus are more pronounced in the O. C. 70C material (than in the M. W. 70C and RT cured films) and the decrease in the storage modulus between -100°C and 0°C is around 2 decades. This indirectly indicates that the O. C. 70C film is less reacted than the M. W. 70C and the RT cured films. The steep drop which occurs at around -20°C in this material is believed to be partly due to crystalline melting of the PTMO. However no DSC studies were conducted to prove this point.

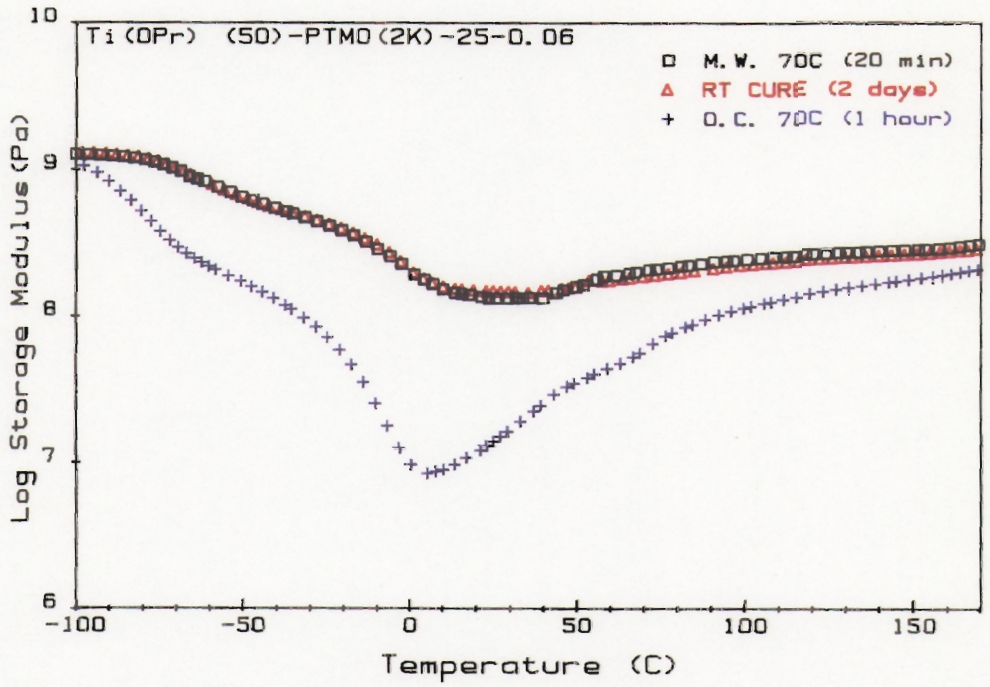


Figure 6.9. Storage modulus behavior for the differently cured TiOPr/PTMO ceramer films as labelled.

Above 0°C the storage modulus of all three materials in Fig 6.9 can be seen to increase and this is believed to be due to the additional extent of reaction within the system. The increase in the storage modulus is greatest for the O. C. 70C film, which is expected since this material shows the lowest extent of reaction. The storage modulus for the M. W. 70C and RT cured films above 0°C also increases, but only very slightly, and can be seen to be identical throughout the entire temperature range. This is because the RT cured material was tested two days after casting (one day after the stress strain studies were conducted) while the M. W. 70C material was tested within one day of curing.

The Tan δ spectra seen in Fig 6.10 for these TiOPr/PTMO materials display bimodal behavior with one relaxation dispersion occuring betweem -80°C and 0°C (lower temperature dispersion) and another starting at around 40°C and continuing up to 170°C (higher temperature dispersion). The low temperature dispersion as indicated above is due to the cooperative segmental motion of the PTMO chains. The distinct onset of cooperative segmental motion at -80°C indicates that the inorganic component is quite highly phase separated from the oligomer. The breadth of the Tan δ dispersions seen in these TiOPr/PTMO systems are similar to those seen initially in the TEOS/PTMO ceramers cured in DMF/IPA which are also highly phase separated. The SAXS profiles for the TiOPr/PTMO materials (as will be seen later) are, however, broad and more like those seen the TEOS/PTMO materials cured in THF/IPA which display a greater degree of mixing between phases and are discussed in chapter 5. The

Tan δ spectra for the M. W. 70C and the RT cured films are almost identical while the O. C. 70C film which is cured to a lower degree than the other two films has the highest Tan δ intensity of 0.25 for the lower temperature dispersion.

The higher temperature dispersion seen in these TiOPr/PTMO ceramers is speculated to be due to relaxations in the inorganic phase similar to those described in chapter 4; this aspect will not be discussed any further. Brennan (96) has previously shown that this higher temperature dispersion does not bear any relationship to the TiOPr/PTMO composition ratio. One interesting fact to be noted is that this higher temperature peak is seen only in the more sharply phase separated materials such as the TiOPr/PTMO and ZrOPr/PTMO ceramers as well as the TEOS/PTMO ceramers which were cured in DMF/IPA. This behavior is not seen in the TEOS/PTMO ceramers seen in THF/IPA which show extensive mixing between the inorganic phase and the oligomeric phase.

6.4.4 DYNAMIC MECHANICAL BEHAVIOR OF ZrOPr/PTMO CERAMERS

The dynamic mechanical storage modulus behavior for the three differently cured ZrOPr/PTMO materials shown in Fig 6.11 and displays only one steep drop occuring in the proximity of -80°C as the temperature is raised above -100°C. This is in comparison with the TiOPr/PTMO ceramers shown in Fig 6.9

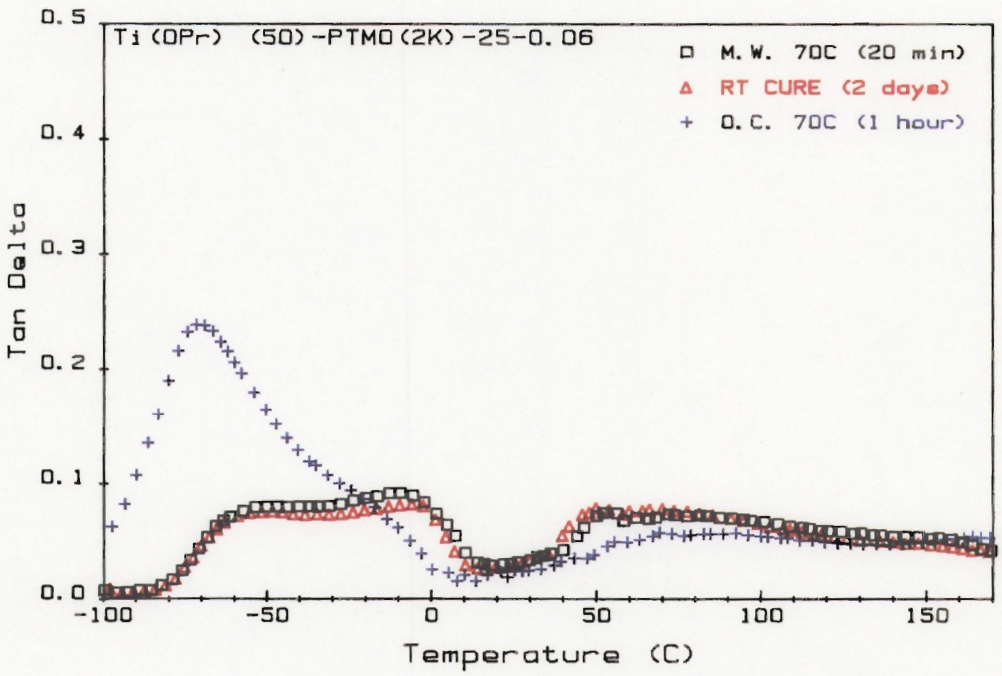


Figure 6.10. Tan δ behavior for the differently cured TiOPr/PTMO ceramer films as labelled.

where the storage modulus showed two drrops in the stiffness value between -100°C and 0°C. The M. W. 70C, O. C. 70C and the RT cured materials in Fig 6.11 show similar storage behavior which is as expected since the mechanical properties show virtually no difference. The stiffness for all these three materials increases with temperature above 50°C. Here again this is attributed to the increase in the extent of reaction as the temperature increases.

The Tan δ spectra for all the differently cured ZrOPr/PTMO materials are shown in Fig 6.12 and each displays bimodal behavior as was also seen in their titania based counterparts. The lower temperature dispersion occurs between -80°C and 0°C and is very symmetrical but is narrower than that seen for the films containing TiOPr given in Fig 6.10. The shape of this peak may also point out to the fact that there is a fundamental difference in the response of the PTMO chains in the zirconia based ceramer system versus the titania ceramer system. In other words the interaction of the oligomer with the inorganic phases may be different. The higher temperature dispersion for the three films in the ZrOPr/PTMO system seen in Fig 6.12 begins at around 20°C and also has a slightly different shape from that seen for the titania based ceramer shown earlier. This might indicate that these upper temperature dispersions are peculiar to the metal alkoxide used in the ceramer, a fact that manifests itself significantly in the dielectric behavior as will be seen later in chapter 8.

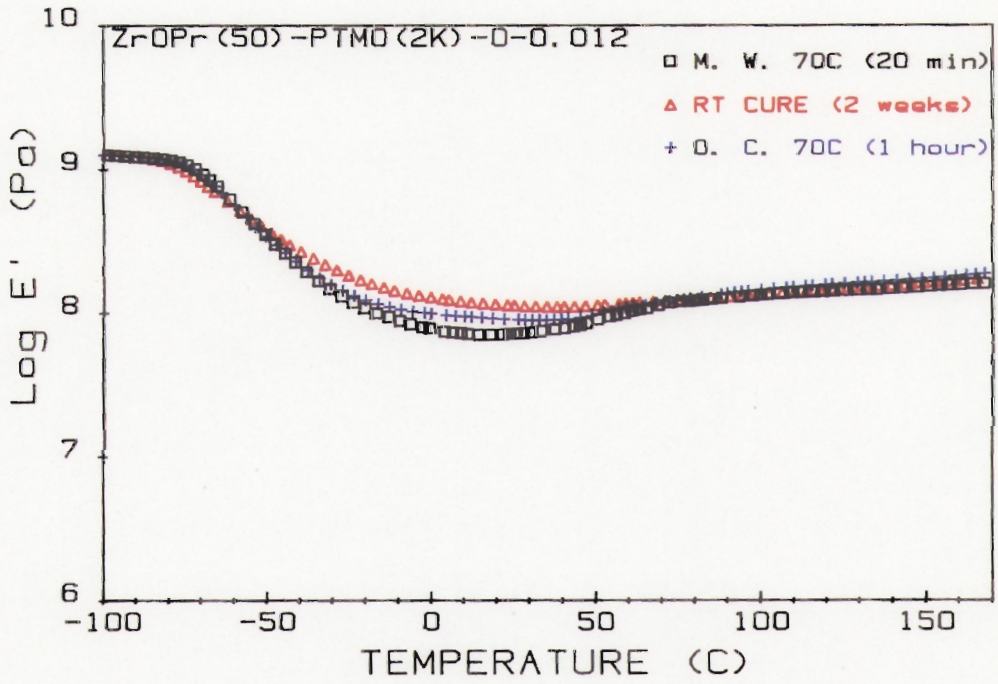


Figure 6.11. Storage modulus behavior for the ZrOPr/PTMO ceramer films as labelled.

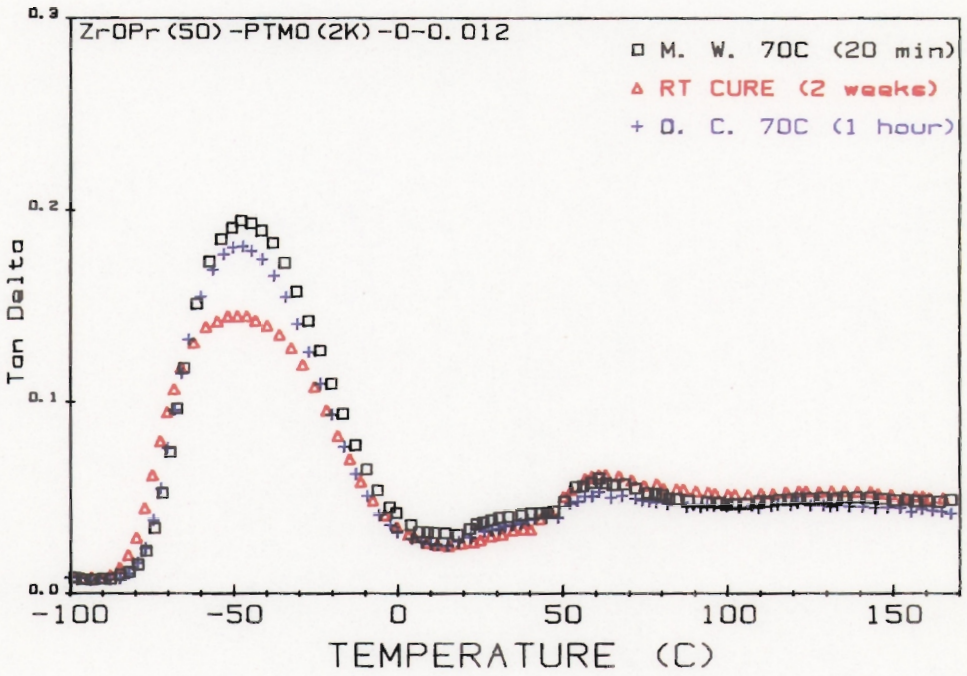


Figure 6.12. **Tan δ behavior for the differently cured ZrOPr/PTMO ceramer films as labelled.**

6.4.5 SMALL ANGLE XRAY SCATTERING OF THE TiOPr/PTMO CERAMERS

The small angle scattering data for the TiOPr/PTMO ceramer is displayed in Fig 6.13. The data for the room temperature cured material was taken after four days due to a machine problem. This additional period of time permitted the sample to undergo further curing and hence shows the highest intensity of scattering. The M. W. 70C and the O. C. 70C films were examined within a few hours of their respective elevated temperature curing processes. Both these films cured at 70°C show a slightly higher value of interdomain spacing which is around 200Å while the RT cured material has and spacing around 150Å. Similar interdomain spacing for the RT cured material has also been observed by Brennan (96). The reason for the larger interdomain spacing seen in the M. W. 70C and the O. C. 70C material is not known but may be related to differences in film thickness as will be addressed in chapter 8. The intensity at the peak position for the microwave cured material is almost twice as high as the oven cured material and this is reflective of the higher extent of reaction in the microwave cured film. The scattering curves for these TiOPr/PTMO materials are all broad and are similar to those displayed by the TEOS-PTMO ceramers reacted in an environment of THF and IPA. The breadth of the scattering profiles for the TiOPr/PTMO films is believed to be due to a large distribution in the interdomain spacings or the domain sizes or both. This has yet to be verified by an independent technique such as TEM.

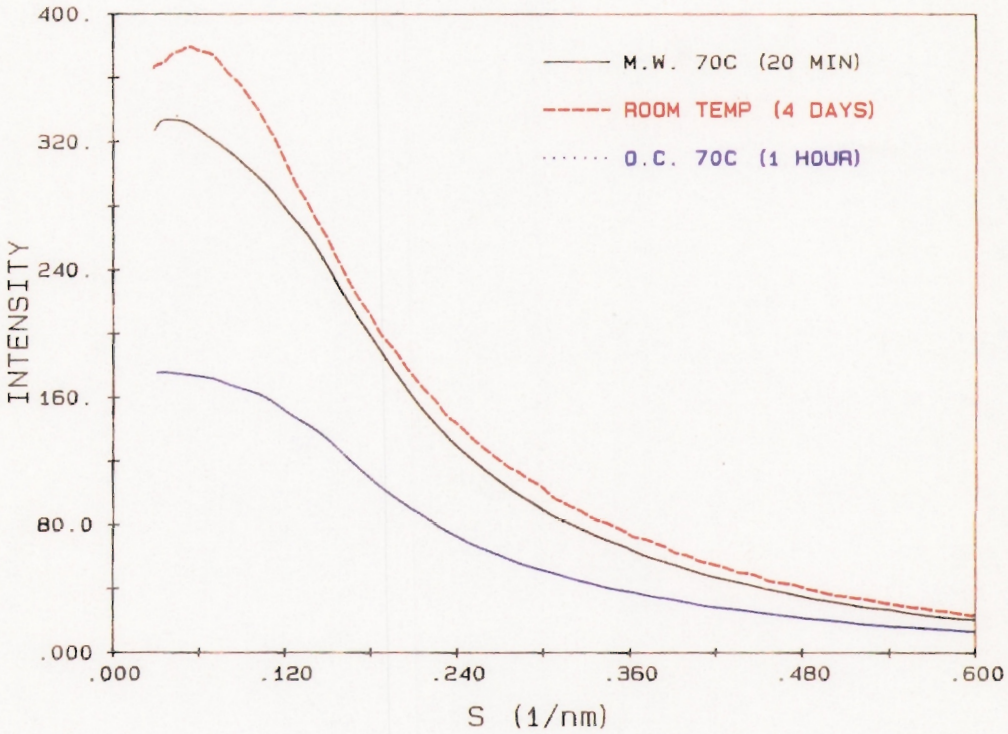


Figure 6.13. SAXS profiles for the differently cured TiOPr/PTMO ceramer films as labelled.

6.4.6 SAXS PROFILES FOR THE ZrOPr/PTMO CERAMERS

The scattering profiles for the three ZrOPr/PTMO ceramers shown in Fig 6.14 are broad and again this suggests that there may be a large distribution in the interdomain spacings or domain sizes or both. The scattering intensity for these zirconia ceramers is typically higher than that for the titania ceramers and this difference in intensity can be related to the higher electron density of zirconium as compared with the titanium systems. The scattering profiles for the O. C. 70C and the RT cured ZrOPr/PTMO materials all display a maxima corresponding to an interdomain spacing of approximately 150Å The microwave cured material displays a higher scattering intensity at the peak position than the O. C. 70C and the RT cured materials and the interdomain spacing is approximately 200Å. The higher scattering intensity indirectly indicates a higher extent of reaction within the zirconia phase. However, this is not reflected in the mechanical properties of the M. W. 70C film. The reason for this larger interdomain spacing and higher scattering intensity for the M. W. 70C material was not investigated further and hence no reason for the behavior can be given at the current time.

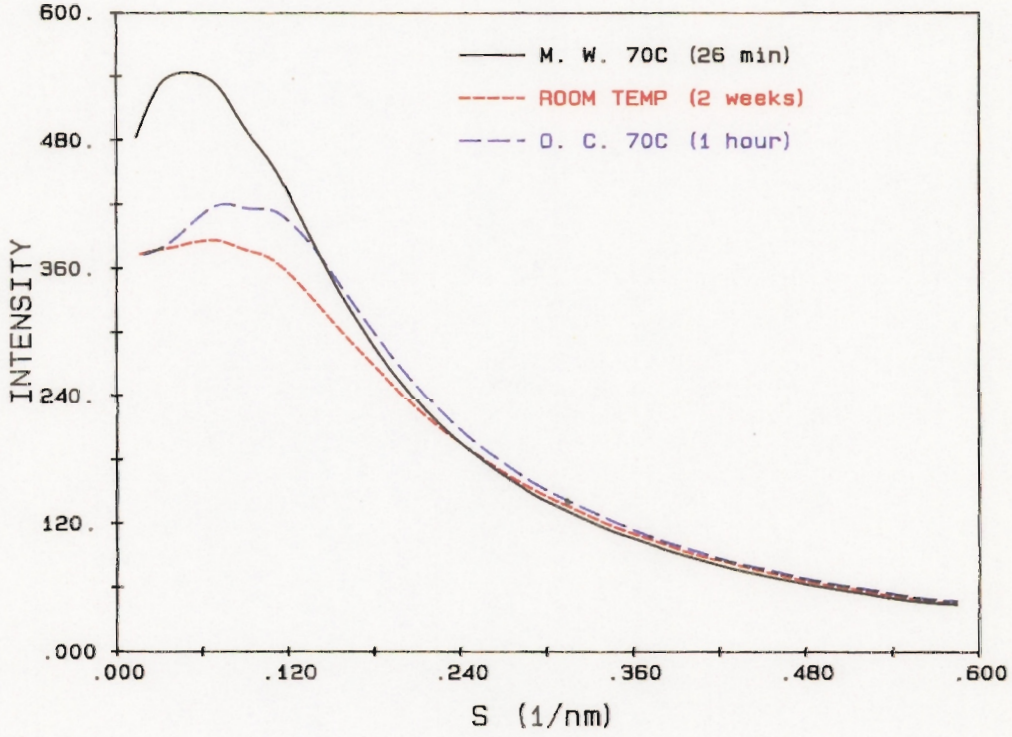


Figure 6.14. SAXS profiles for the differently cured ZrOPr/PTMO ceramer films as labelled.

6.5 CONCLUSIONS

From the results seen in this chapter it can be concluded that microwave curing displays a positive effect on the TiOPr/PTMO ceramers cured to 70°C. It was clearly established in the last chapter that microwaves were able to influence the rate of reaction when a ceramer system displayed a high degree of separation between the inorganic phase and the ceramer phase. This conclusion was found to hold good for the TiOPr/PTMO ceramers, which from the DMA data show a high degree of phase separation. The difference between microwave cured and the oven cured TiOPr/PTMO materials is not as great as that seen for the TEOS/PTMO materials cured in DMF/IPA. This is attributed to the faster reaction rate of TiOPr as compared with TEOS. Finally the effect of different curing temperatures on the TiOPr/PTMO ceramers in the microwave cavity indicates that curing at 70°C almost brings these materials to their final state of cure with an elastic modulus of approximately 180 MPa.

The ZrOPr/PTMO ceramer system on the other hand shows virtually no difference between oven and microwave curing. This is attributed to the low amount of water used for hydration in these materials. This points out to the necessity for water in these ceramer reactants so that the metal alkoxides can be hydrated. The hydrated groups of the respective metal alkoxides have a higher dielectric loss factor than the alkoxy functionality and microwave

energy can couple efficiently with these hydrated groups such as SiOH, TiOH and ZrOH, thereby increasing the reaction rate.

CHAPTER 7

INVESTIGATIONS INTO THE DIELECTRIC PROPERTIES OF CERAMERS

7.1 INTRODUCTION

This chapter marks a deviation from the previous four chapters in that it does not deal with the microwaving of ceramers or the structure property relationships of films produced thereof. The dielectric spectroscopy of these ceramer films was undertaken in an attempt to better understand some of the

structural features of these materials which could not be explained using other techniques as previously explained such as DMA, DSC etc. From the dynamic mechanical data in previous chapters, it was seen that for the more phase separated ceramer systems such as the TEOS/PTMO ceramers cured in DMF/IPA, the TiOPr/PTMO ceramers or the ZrOPr/PTMO ceramers, there existed a relaxation dispersion in the Tan δ spectra at temperatures between 20°C to 150°C. This relaxation has, in the past, been attributed to a variety of factors and effects such as the encapsulation of PTMO (84, 85, 96) by the inorganic, additional extent of reaction, evaporation of solvent from the ceramer etc. In order to gain a better understanding of the origin of this higher temperature relaxation behavior it was decided to conduct dielectric spectroscopy on these materials. Another significant reason for performing these dielectric tests was because of the potential use of ceramers as coatings for electronic materials. Such an application would necessitate the use of a material with a low dielectric constant. The dissipative qualities of any such coating materials would also have to be low so as not to produce any unwanted dielectric losses in electronic equipment which could lead to unnecessary heating.

7.2 EXPERIMENTAL

All experimental measurements were made on a dielectric network analyser (DETA) manufactured by Polymer Labs. Films used were 5 - 10 mils in thickness and were gold coated before testing in order to improve contact between the electrodes and the film. Coating with gold also helps reduce the surface impedance in these films. The thickness of the gold coating was approximately 150Å. The electrodes were 20mm in diameter and the samples used had a diameter greater than 20mm. This larger sample diameter was used in order to prevent any arcing fields around the sample circumference which can give rise to erroneous readings during measurements. All films were tested at five frequencies 1, 5, 10, 50, 100 kHz in the temperature range -150°C to 100°C. In some cases the upper temperature limit was extended to 150°C in order to investigate certain additional features of the ceramer systems and in such cases this author will make special mention of the experimental parameters. The temperature rate on the DETA was maintained at 1°C/min throughout the experiment. Films of TiOPr/PTMO ceramers with TiOPr contents of 0, 14, 25, 33, 50 and 58 wt% were used for dielectric analysis. Similarly, ZrOPr/PTMO ceramer films containing 35, 40 and 50 wt% were studied. In the case of TEOS/PTMO ceramers dielectric studies were conducted on TEOS(60)-PTMO(2K)-100-0.048 films prepared in THF/IPA::1/4, IPA, and DMF/IPA::1/1. The various dielectric spectra obtained from these

TEOS/PTMO ceramer materials will be discussed further in the course of this chapter.

As stated above, the main purpose behind making these dielectric measurements was to determine the origin of the higher temperature dispersion (20°C - 150°C) seen in the dynamic mechanical Tan δ spectra of these films. However, as will be seen, these dielectric measurements may also be used to provide a rough estimate of the PTMO chain dimensions in these systems. This will be detailed furthur in the later sections of this chapter. Some of the dielectric spectra shown in the preceeding figures will contain storage and loss curves obtained at all the five aforementioned frequencies. The main reason behind displaying all five frequencies in some cases is that certain trends in the material response to the alternating field can only be studied this way. Secondly, certain behavior can only be seen at certain frequencies and not at others. In order to present a balanced view of the behavior of these systems, this author has decided to print all the dielectric curves in some cases such as for the TiOPr/PTMO ceramer systems described in section 7.3.1.1. In some cases only dielectric behavior at the lowest frequency is plotted because the author deemed this single spectra sufficient enough to make material responses to the applied alternating field obvious.

7.3 RESULTS AND DISCUSSION

7.3.1 DIELECTRIC SPECTROSCOPY OF TiOPr/PTMO CERAMERS

7.3.1.1 EFFECT OF METAL ALKOXIDE CONTENT

The method of preparation of these TiOPr/PTMO ceramers has been detailed elsewhere (96) and will not be described again. The dielectric storage and loss for the TiOPr/PTMO ceramer films containing 0, 14, 25, 33, 50 and 58 wt% TiOPr were studied and all of these except the 25 and 50 wt% TiOPr will be described here. Figure 7.1a displays the dielectric storage for the film containing 0 wt% TiOPr (pure isocyanatopropyltriethoxysilane endcapped crosslinked PTMO without any metal alkoxide). As can be seen in this figure the film containing 0% TiOPr has a dielectric constant (dielectric storage) of around 2.88 at -150°C at 100kHz which is close to the value of 2.65 reported by Read et al (106) at frequencies of 10^7 Hz at room temperature. In other words the semicrystalline dielectric constant for these two PTMO films i.e. that tested by Read et al as well as the film containing 0% TiOPr (tested in our laboratories) are almost identical. The dielectric storage at any given

temperature increases with decreasing frequency for all these ceramer materials. As can be seen in Fig 7.1a the dielectric constant at all frequencies then begins to increase gradually with temperature as the temperature is increased above - 150°C. This increase in the dielectric storage is expected, since dipolar mobility increases with temperature, thereby permitting a larger amount of reorientation polarization in the PTMO molecules and allowing the network to store more energy. At around -75°C there occurs a small step in the dielectric storage curves at all frequencies. This step in the storage is due to the glass transition of pure PTMO which typically occurs at -80°C (106). The glass transition temperature (T_g) for all these ceramer systems is typically taken as the temperature at which the Tan δ peaks for the α relaxation.

The origins of the glass transition or α relaxation for PTMO in dielectric spectroscopy are not known, but are speculated to arise from the rotational motion of the ether linkage in the backbone of the PTMO chains (107). At T > T_g the dielectric storage (100 kHz) for the 0 wt% TiOPr/PTMO plateaus out at a value of 4.0 up to around -30°C. This upturn in the dielectric storage at T > -30°C is due to the melting of crystallites in the PTMO network. Read et al (106) were amongst the first to work on the dielectric spectroscopy of PTMO and they claimed that PTMO molecules in a crystalline phase cannot undergo dipolar rotation and hence did not contribute to the dielectric processes in the system. Thus the melting of crystallites allows for a larger amorphous content in the material which in turn permits a higher amount of reorientation polarization which increases the dielectric storage.

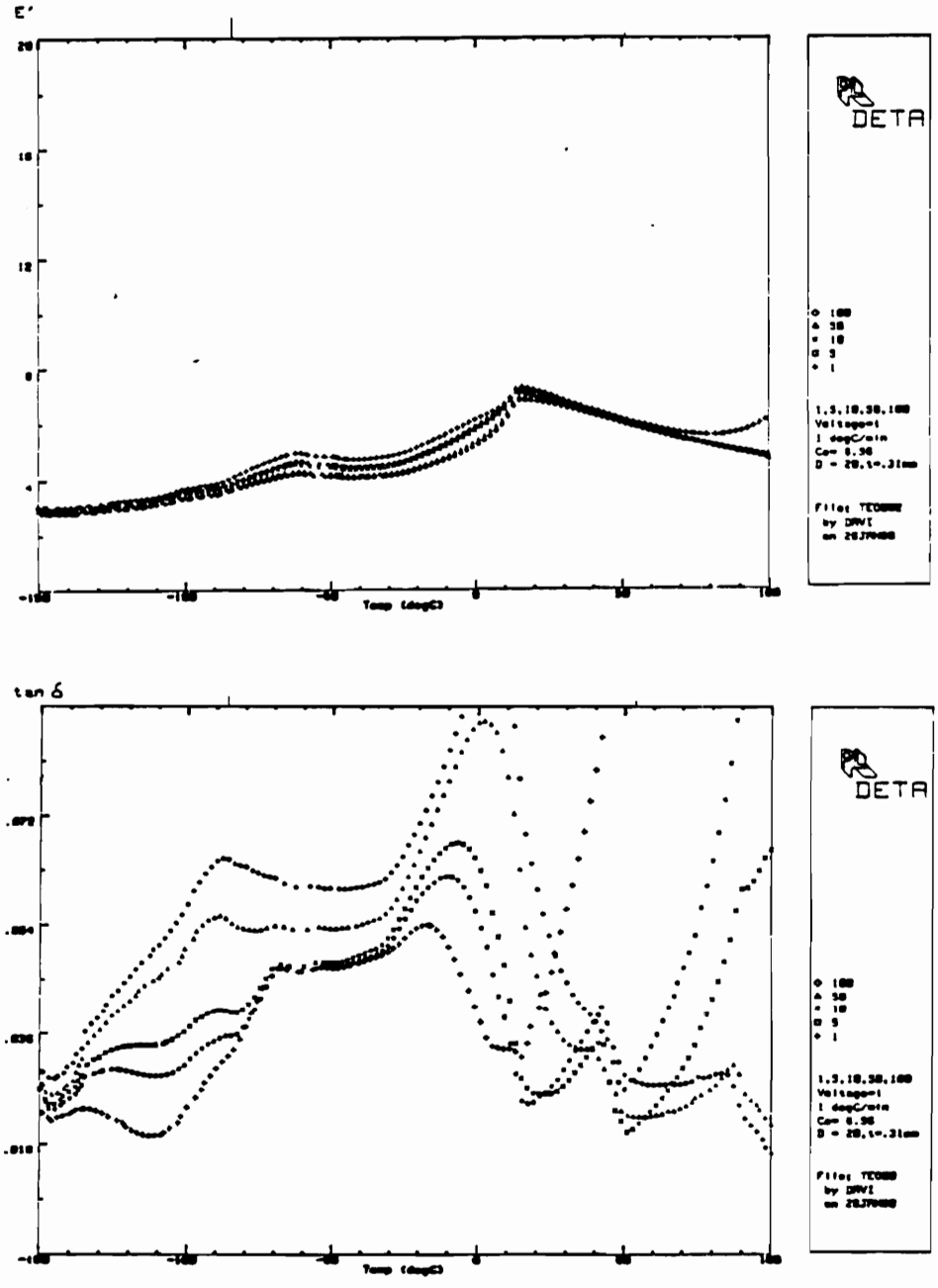


Figure 7.1. a) Dielectric storage and b) Tan δ spectra for the TiOPr(0)-PTMO(2K)-100-0.048 ceramer at 1, 5, 10, 50 and 100 kHz.

The dielectric storage curve in the Fig 7.1a peaks at around 10°C for all frequencies which is the T_m of the crosslinked PTMO as seen from the DSC trace in chapter 4. Above 10°C the dielectric storage begins to decrease with temperature because the dipolar mobility increases to a stage where the reorientation polarisation fails to follow the applied field and thus contributes less to the ability of the system to store energy. The dielectric storage at 1 kHz however begins to increase above 50°C and this is due to ionic conductivity in the system. These ionic charges typically arise from the presence of impurities in the film and they are known to be responsive to lower frequencies at certain temperatures. Hence this behavior is visible at 1 kHz and not at frequencies of 5 kHz or above. However, if the temperature range of the experiment is raised to above 100°C then ionic conductivity would be seen to manifest itself at the higher frequencies as well.

The dielectric loss spectra for the 0 wt% TiOPr/PTMO ceramer is shown in Fig 7.1b. The loss value for the 1 kHz scan at -150°C is 0.024 while for the 100 kHz scan it is around 0.030. The β transition for this film typically arises from dipolar mobility of the ether linkage due to crankshaft motion in the PTMO backbone and occurs between -150°C and -100°C. It peaks at -135°C for the lowest frequency i.e. 1 kHz. The β transition shifts to higher temperatures with increasing frequencies indicating Arrhenius type behavior. The activation energy for these systems is obtained from the plot on Fig 7.2 and is tabulated in Table 7.1. The activation energy is obtained using three frequencies (1, 5 and 10 kHz) is around 9 kcal/mole which is good agreement with that

computed by Wetton and Read (106, 107). Since the activation energy for the β transition is typically lower than that for the α transition (the glass transition) the relaxations for the higher frequency (50 and 100 kHz) β transitions merge with those of the α transitions of the corresponding frequencies. Thus the β transitions are not clearly visible at 50 and 100 kHz.

The α or the glass transition manifests itself in the temperature range of -90°C to -40°C in all the dielectric spectra for TiOPr/PTMO systems. In the TiOPr(0)-PTMO(2K)-100-0.048 film the α peak position increases to higher temperatures with increasing frequency. The activation energy calculated for this α transition from the plot in Fig 7.2. is 56 kcal/mole. The intensity of the α transition in the TiOPr(0)-PTMO(2K)-100-0.048 ceramer is lower than that seen for the films containing higher amounts of TiOPr as will be shown shortly. This is because the extent of crystallinity varies inversely with the amount of metal alkoxide in these systems. Since this 0 wt% TiOPr/PTMO has very no titania it has a larger amount of crystallinity than those systems containing larger TiOPr contents and consequently has a lower intensity of relaxation for the α transition.

The melting of these PTMO crystallites causes another transition to be observed between -30°C and 30°C in the Tan δ spectra. It can be seen that the breadth of this (melting) dispersion is narrow for the lowest frequencies and broadest for the highest frequencies. Futher the intensity of the dispersion increases with increasing frequency. The activation energy for this transition

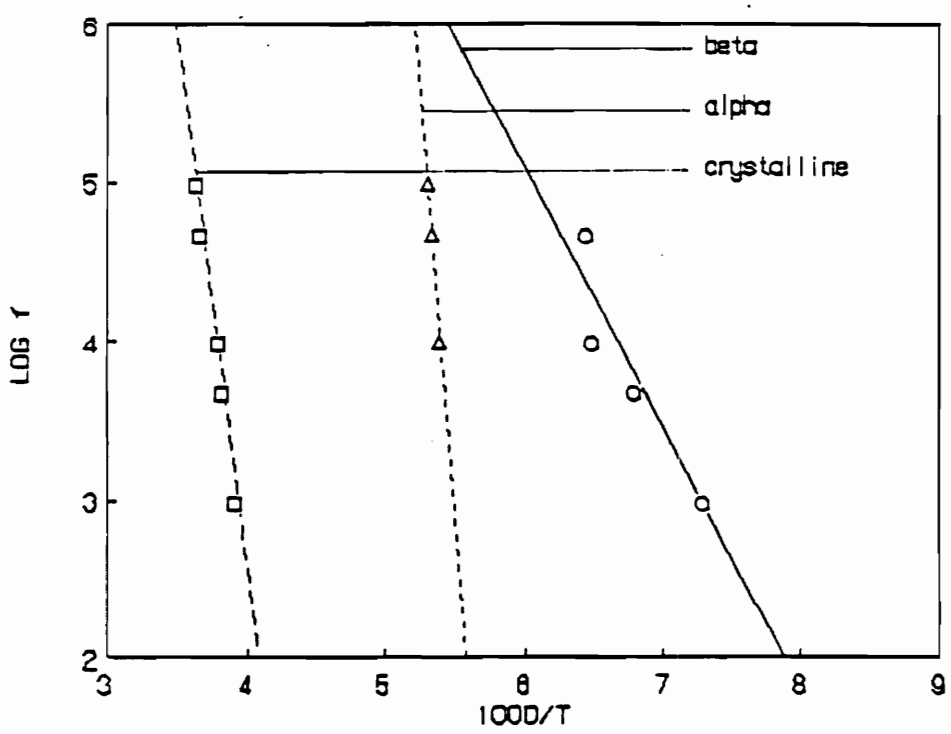


Figure 7.2. Plot of log f (f = frequency) vs 1/T (T = temperature) for the 0 wt% TiOPr/PTMO ceramer.

Table 7.1. Activation energy for transitions in the TiOPr/PTMO ceramers.

wt. fraction TiOPr	β kcal/mole	α kcal/mole	crystalline kcal/mole
0	9	54	32
14	8	50	33
25	--	60	56
33	--	78	77
50		56	
58		64	

is lower than the α transition and is approximately 32 kcal/mole. No such transition for PTMO has been previously documented but similar transitions have been seen for polyethylene at the melting point and this behavior has been attributed to relaxation of PE chains at the interface of the crystalline and the amorphous regions (108). Still another sharp peak but of low intensity occurs at 40°C and another at 80°C in the dielectric Tan δ spectra for PTMO. However, the origin of these peaks is not known and may be due to the presence of the urea linkages utilized to facilitate the endcapping process. The lower frequency spectra (1, 5, 10 kHz) show a large increase in the Tan δ curves at higher temperatures. This increase in the Tan δ is due to the presence of ionic conductivity and manifests itself strongly at the lowest

frequency (1 kHz) around 10°C while the increase in such conductivity occurs at higher temperatures for the higher frequencies.

The dielectric storage profile for the material containing 14% TiOPr is shown in Fig 7.3a. and shows a value of around 3.4 at -150°C and 100 kHz. This increase in the dielectric storage from 2.9 (for the material containing 0 wt% TiOPr) to 3.4 (for this sample containing 14 wt% TiOPr) indicates some contribution from the titania phase (assuming that most of the TiOPr is converted to titania). As in the case of the film containing 0% TiOPr, here too, the dielectric storage at all frequencies increases gradually with temperature upto -100°C at which there is a steep increase upto a storage value of ca. 5. This is due to the onset of cooperative segmental motion in the PTMO phase which increases the amount of dipolar reorientation. At around -70°C the dielectric storage value for all frequencies decreases slightly due to crystallization occuring in the PTMO. This behavior i. e. decrease in the dielectric storage was not seen in the film containing 0 wt% TiOPr and the reason for its occurence in the TiOPr(14)-PTMO(2K)-25-0.06 film may be due to the presence of some additional crosslinks in the system which make it difficult for all the PTMO to crystallize as it is cooled down to -150°C. Hence some of the PTMO which cannot crystallize during the cooling process in the DETA does so as the material is raised above its T_g during the scan. Since the development of such crystallites reduce the ability of the system to undergo reorientation polarization, the dielectric storage value decreases. The dielectric storage subsequently begins to increase again with temperature

above -60°C. This occurs since some of the crystallites begin to melt thereby permitting greater reorientation polarization to occur in the network. The dielectric storage curves for the TiOPr(14)-PTMO(2K)-25-0.06 peak at 10°C. Above this temperature there is a decrease in the dielectric storage value, the origins of which have already been described above. The dielectric storage value at 100°C is approximately 4.2.

The Tan δ spectra for the TiOPr(14)-PTMO(2K)-25-0.06 ceramer is shown in Fig 7.3b. Here too, it can be seen that the value of the dielectric loss is 0.024 at -150°C for the 1 kHz frequency and increases with increasing frequency at the same temperature. The β transition occurs in the temperature range -150°C to - 100°C. This β transition is broader than the same transition seen for the TiOPr(0)-PTMO(2K)-100-0.048 sample and peaks at a temperature of around -120°C for the 1 kHz frequency. Again the β transition merges with the α transition at higher frequencies of 10, 50 and 100 kHz and therefore is not very visible. The α transition at all frequencies for the 14 wt% TiOPr/PTMO ceramer starts at ca. -100°C and extends upto - 70°C. The α transition is much more pronounced in the 14 wt% TiOPr/PTMO ceramer sample than the 0 wt% TiOPr/PTMO ceramer material and has a much higher intensity at all frequencies. This is because the lower amount of crystallinity present in the 14 wt% TiOPr/PTMO ceramer permits greater dipolar orientation of the PTMO oligomer as compared with the 0 wt% TiOPr/PTMO ceramer. The intensity of the α transition increases with increasing frequency and the peak position shifts to higher temperatures with increasing frequencies. The activation

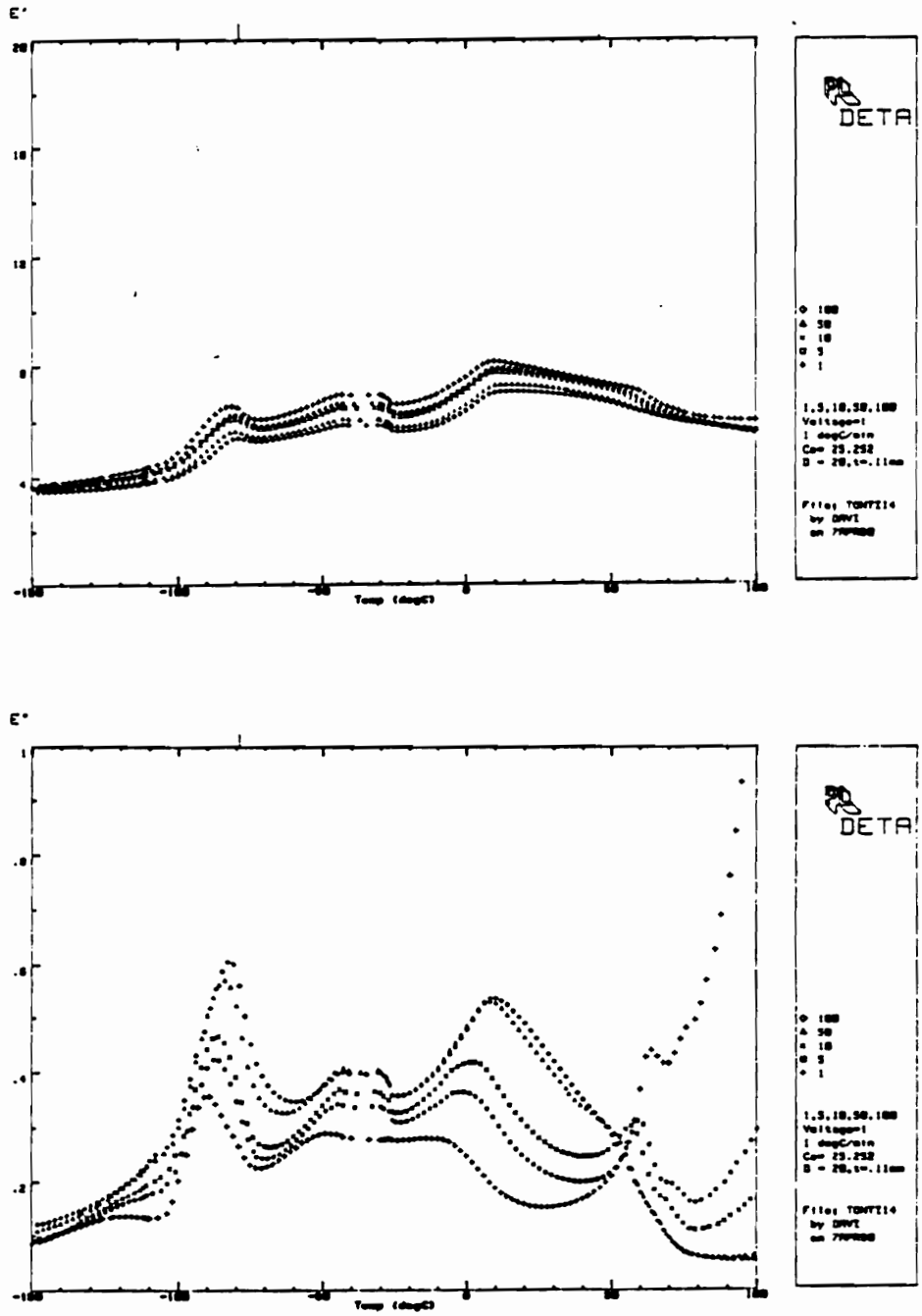


Figure 7.3. a) Dielectric storage and b) Tan δ curves for the TiOPr(14)-PTMO(2K)-100-0.048 ceramers.

energy associated with the α transition for the 14 wt% TiOPr/PTMO ceramer is calculated from the plot in Fig 7.4 and is 50 kcal/mole which is slightly lower than that for the system containing no TiOPr. As the temperature is increased above -70°C there is an increase in the Tan δ value for the TiOPr(14)-PTMO(2K)-25-0.06. This is because of the development of crystals in the oligomeric phase as the temperature is raised above the T_g of the PTMO component of the ceramer. At around -30°C there occurs another loss dispersion due to the melting of these crystallites. The breadth of this dispersion associated with the melting of crystallites increases with increasing frequency and the peak position shifts to higher temperature with increasing frequency. The intensity of this transition at any given frequency is, however, lower than that observed in the 0wt% TiOPr/PTMO ceramer which is also an indication of the lower extent of crystallinity in this ceramer system. The activation energy for this crystalline melting transition is 32 kcal/mole. At temperatures above 50°C the dielectric loss value increases significantly due to presence of ionic conductivity in the ceramer. The loss behavior due to ionic conductivity manifests itself at the lower frequencies rather than at the higher frequencies as is apparent in the figure.

The ceramer system containing 33wt% TiOPr displays dielectric behavior below 0°C which is similar to the film containing 14wt% of the metal alkoxide as can be seen in Fig 7.5a. The dielectric storage value is around 3.6 at -150°C for the 100 kHz and as in the 0 and 14 wt% TiOPr/PTMO systems described previously, increases with decreasing frequency at any given temperature. The

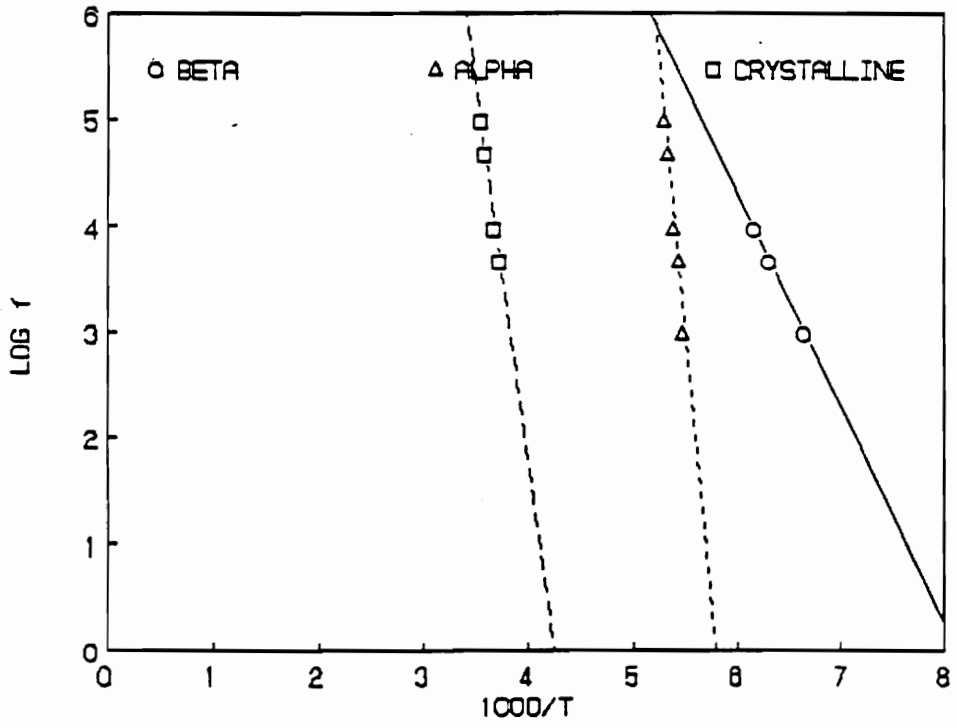


Figure 7.4. Plot of log f (f = frequency) vs 1/T (T = temperature) for the 14 wt% TiOPr/PTMO ceramer.

dielectric storage value of 3.6 for the 33 wt% TiOPr/PTMO ceramer indicates once again that the dielectric storage at -150°C is dependent upon the metal alkoxide content in the ceramer. The dielectric loss at all five frequencies also increases gradually with temperature up to -100°C where it increases steeply due to the onset cooperative segmental motion of the oligomeric component. Following this somewhat steep increase to around ca. 5.5, the dielectric storage at all frequencies peaks at -80°C and then decreases due to crystallization of the PTMO component. The dielectric storage at all five frequencies then gradually increases upto 0°C to a value of ca. 6, at which temperature there is a steep increase in the dielectric storage of only the 1 kHz frequency. This steep increase is believed to be due to Maxwell Wagner Sillars (MWS) type interfacial relaxations which have been documented extensively for a variety of two phase systems. The MWS relaxation displays sharp bimodal behavior with one peak occuring at 30°C and another at 50°C. These dipolar relaxations typically occur because of charge build-up and relaxation at an interface between two phases in a two phase system. This MWS behavior typically manifests itself at lower frequencies and this will be clearly visible in these TiOPr/PTMO ceramer systems as the TiOPr content is increased above 33 wt%. At 5 kHz, the MWS relaxation bimodal is still visible though very much reduced in intensity and it is virtually non existant at the higher frequencies in the dielectric storage spectra.

The presence of a bimodal in the MWS behavior in these systems indicates the possible existance of two interfaces or two different kinds of ionic dipolar

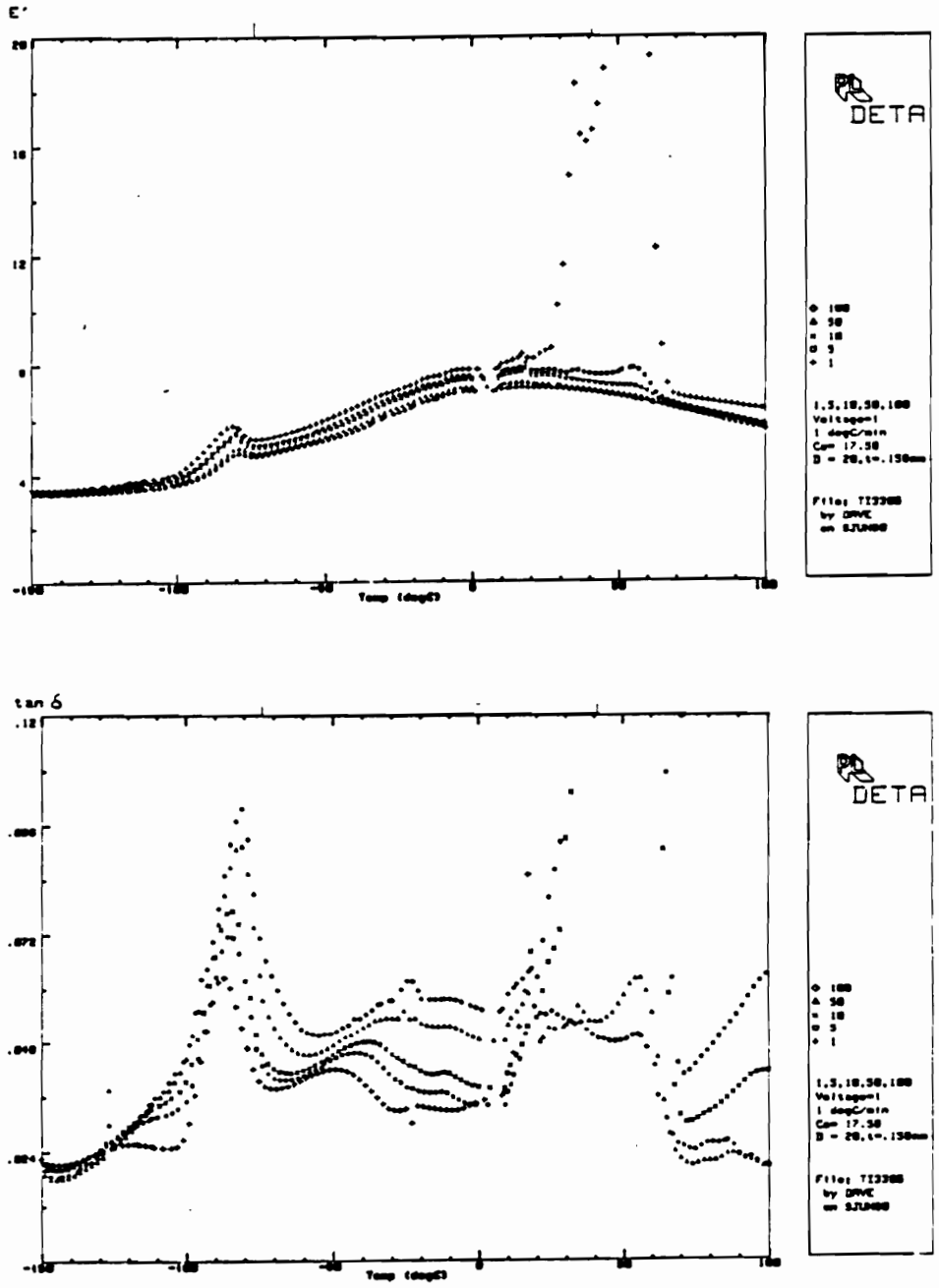


Figure 7.5. a) Dielectric storage and b) Tan δ spectra for the 33 wt% TiOPr/PTMO ceramer system.

interactions at any one interface. However, the possibility of two different kinds of ionic interactions at a single interface can be discounted, because, as will be seen, the TEOS/PTMO ceramer system can be made to display a single MWS relaxation or a bimodal depending upon the nature of the inorganic phase and the amount of mixing of the inorganic with the PTMO. Thus it seems indeed plausible that this MWS interfacial interaction may arise from the presence of two interfaces or three phases in these ceramer systems. The three phases which have now been confirmed to exist (as will be demonstrated in the chapter 8) in a ceramer (via SAXS) are the inorganic, the oligomeric and the air phase. The air phase is present in the inorganic due to porosity. The bimodal peak due to the MWS relaxation in the dielectric storage and loss spectra then results from an agglomeration of charges either at the inorganic-organic interface and the inorganic-air interface. The lower temperature peak (which for the TiOPr/PTMO ceramers is typically of a lower intensity compared with the higher temperature peak) of the bimodal is speculated to be due to the interfacial polarization at the inorganic polymer interface while the higher temperature peak is probably due to polarization at the inorganic-air interface. Sillars (109) has demonstrated that elliptical particles dispersed in a matrix give a higher value of the MWS relaxation as compared with spherical particles. Thus polarization i.e at the inorganic-air interface would typically be of a higher intensity because the porosity within the inorganic phase can be viewed as elliptical with the 'a' dimension (major axis) of the ellipse being much larger than the 'b' dimension (minor axis). In

other words the porosity within the inorganic phase may be capillary like in shape. The existance of capillaries in pure silicates has already been studied by Brinker and Scherer (65). Bergna and Simpko (110) have also shown that a continuous pore network continues to exist in pure silicates even at very high densities approaching theoretical values.

As stated earlier, the MWS relaxation is due to charge trapping of ionic species and their consequent relaxation at the interface. Stevels (98, 99) has shown that the presence of non-bridging oxygens in silicates gives rise to the possibility of charge migration (H^+). As a result of this behavior glasses behave as conductors. Stevels has also shown that the resistivity of glasses decreases with temperature. Thus the MWS effect as seen in dielectric spectroscopy as well as the relaxation seen in the DMA above 20°C is either caused by or influenced by the charge migration within the inorganic phases in these ceramers. Sillars (109) has also documented that the presence of moisture can significantly increase the intensity of the MWS relaxations in any given system. Thus the MWS interfacial polarizations seen in these ceramers may be the result of a combination of charge migration and polarization at the interface as well as due to the presence of water at the interface.

The Tan δ spectra for the TiOPr(33)-PTMO(2K)-25-0.06 ceramer is shown in the Fig 7.5b. It also displays similar trends to that displayed by its 14wt% TiOPr/PTMO counterpart. The β transition for the PTMO occurs between -150°C and -100°C and is clearly visible at the 1 kHz frequency. The peak position at

this frequency for the β transition occurs at -120°C. The α or glass transition occurs between -100°C and -60°C and is of a much lower intensity (at all frequencies) than that seen for the same transition in the TiOPr(14)-PTMO(2K)-25-0.06 ceramer. The activation energy for the α transition in the TiOPr(33)-PTMO(2K)-25-0.06 ceramer is obtained from the plot in Fig 7.6. This value of the activation energy is 78 kcal/mole and is higher than that seen for the 0 and 14 wt% TiOPr/PTMO ceramers.

The activation energy for the β, α and the crystalline melting transitions for the TiOPr/PTMO ceramers are shown in Table 7.1. This table shows that the activation energy for the α transition and the crystalline transition increases with metal alkoxide content upto 33 wt% suggesting that a greater energy is required to undergo cooperative segmental motion with an increase in the crosslink density of these ceramers. At metal alkoxide contents above 33 wt% the crystalline transition does not exist anymore and the activation energy for the α transition decreases as TiOPr content is increased. This can be seen for the 50 wt% TiOPr/PTMO ceramer where the activation energy is 46 kcal/mole. When the metal alkoxide content is increased to 58 wt% the activation energy for the α transition once again increases and is 66 kcal/mole.

Above -60°C all the frequencies in the 33wt% TiOPr/PTMO ceramer show another relaxation believed to be associated with crystallite melting as explained earlier. From Table 7.1 it can be seen that there is an increase in the activation energy for this crystalline transition with increasing metal alkoxide

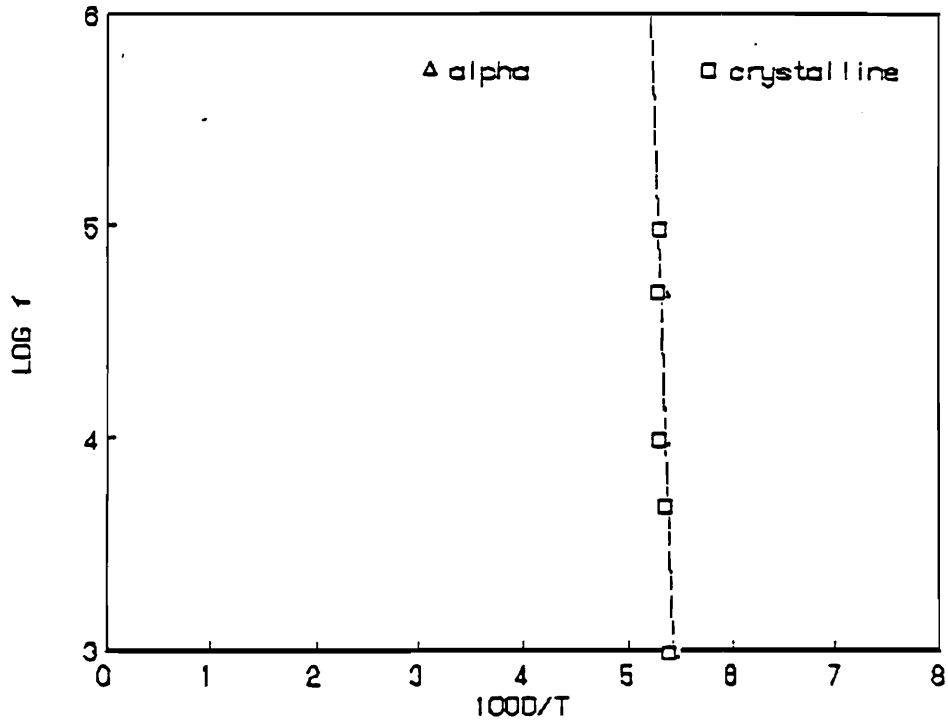


Figure 7.6. Plot of log f (f = frequency) vs 1/T (T = temperature) for the 33 wt% TiOPr/PTMO ceramers.

content. The reason for this increase is not known however, and needs to be further investigated. The MWS interfacial relaxation behavior manifests itself above 0°C and the bimodal is clearly visible at all frequencies in the loss spectrum as against the dielectric storage spectra which show such behavior at only the 1 and 5 kHz frequencies.

The sample containing 58 wt% TiOPr was tested twice, at one month intervals apart, and both these spectra will be described since they bring forth some essential features of the system with regard to the effect of ageing on the MWS relaxation seen in these ceramer systems. The storage spectra for the sample tested earlier (denoted as (58)-PTMO(2K)-25-0.06-EARLY) is shown in Fig 7.7a and 7.7b. Fig 7.7a contains the dielectric storage spectra plotted on an expanded scale in order to display spectral features at low temperatures since the Maxwell Wagner Sillars behavior which typically manifests itself at temperatures above 0°C is of a very large magnitude and obliterates the low temperature features of the spectra. Figure 7.7b contains the entire dielectric storage spectra plotted from - 150°c to 100°C. In Fig 7.7a the dielectric storage at -150°C is around 4.5 reinforcing the earlier observation that with increasing metal alkoxide content in the TiOPr/PTMO ceramers, the value of the dielectric storage in the glassy state is increased. The dielectric storage at all frequencies increases with temperature upto -60°C at which temperature there occurs a step in the spectra due to the T_g of the oligomeric component. Above -30°C the onset of the MWS effect causes a steep increase in the dielectric storage behavior. The bimodal due to the MWS interfacial polarization is now

distinct at all frequencies in the dielectric storage spectra, with the lower temperature peak (which is typically lower in intensity for the TiOPr/PTMO ceramers) located at 10°C and the higher temperature peak (which is typically higher in intensity) located at 80°C. These MWS peaks always remain at the same position (temperature) irrespective of frequency and as seen in both the 33 wt% and 58 wt% TiOPr/PTMO ceramers typically decrease in intensity with increasing frequency.

The Tan δ plot for this Ti(58)-PTMO(2K)-25-0.06-EARLY ceramer shows some similar features as the other TiOPr filled ceramers and is depicted in Fig 7.8a and 7.8b. Fig 7.8a represents a expanded Tan δ spectra while Fig 7.8b is shows the full range of data obtained on this ceramer. The β transition occurs between -150°C and -100°C as seen in Fig 7.8a (which is expanded) and clearly produces a visible peak at 1, 5 and 10 kHz while at the higher frequencies of 50 and 100 kHz it appears as a shoulder on the α transition. The α transition begins at - 100°C and the peak intensity at the 100 kHz frequency is 0.054 which is lower than the intensity value seen for the Ti(33)- PTMO(2K)-25-0.06 ceramer at the same frequency for the same transition. This reduction in the intensity of the α transition reflects the reduced value of the PTMO content in the 58 wt% TiOPr/PTMO ceramer as well as the additional crosslinking produced by a larger amount of TiOPr initially used in this ceramer system. The α transition peaks again shift to higher temperatures with increasing frequency.

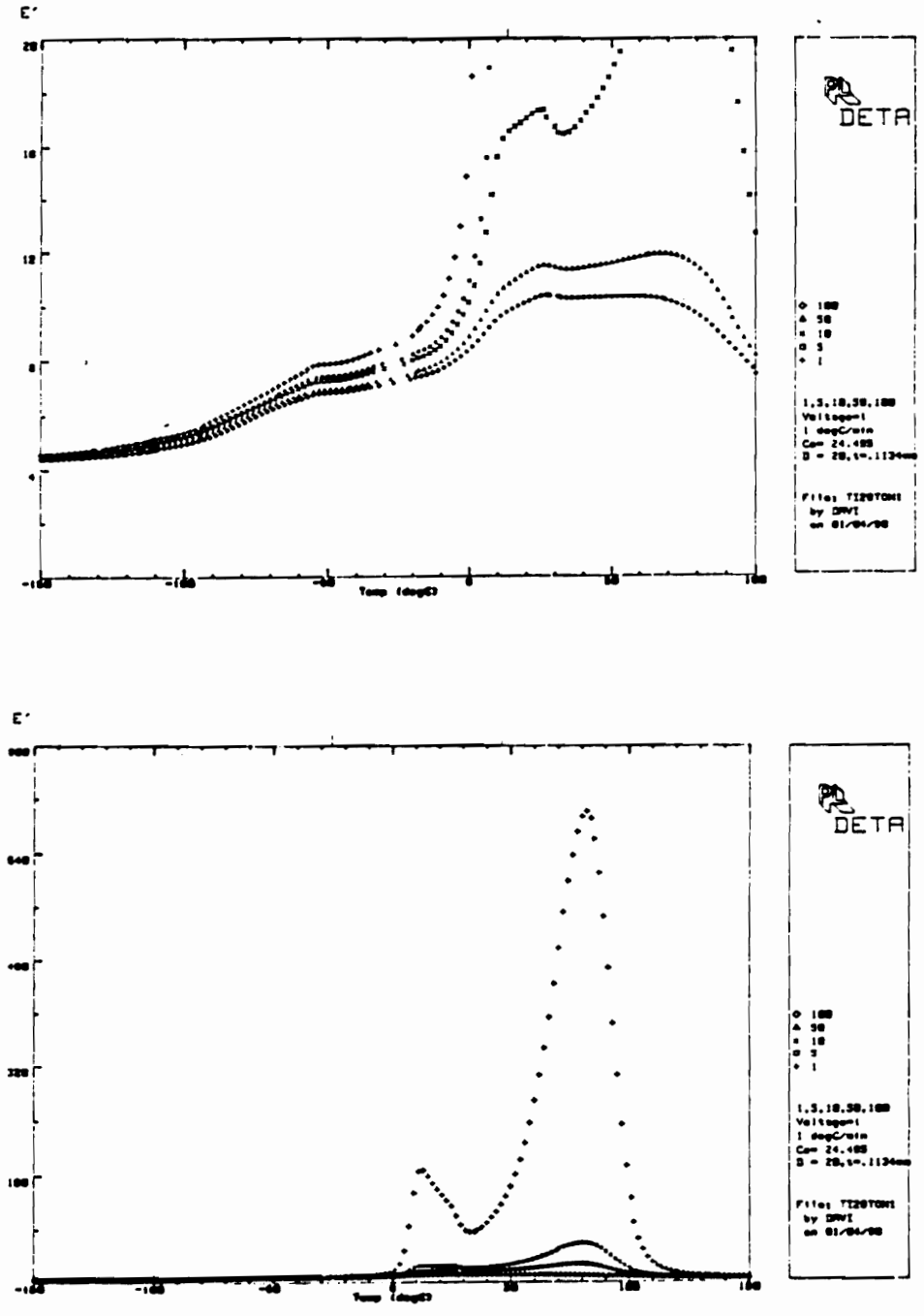


Figure 7.7. Dielectric storage for 58 wt% TiOPr/PTMO-EARLY ceramer on a) enlarged plot b) complete spectra.

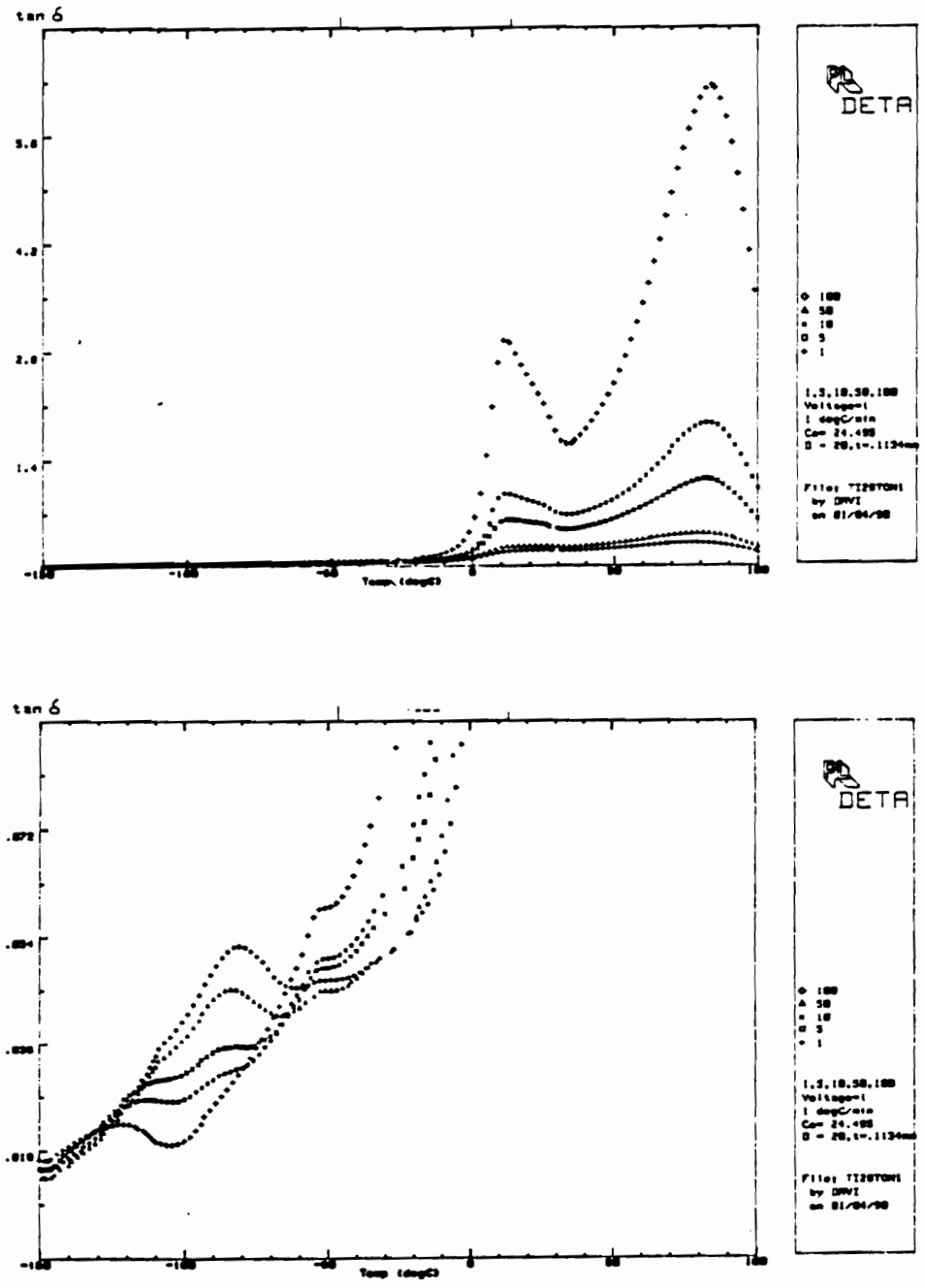


Figure 7.8. Tan δ for the TiOPr(58)-PTMO(2K)-25-0.06 ceramer a) -150°C to 0°C. b) -150°C to 100°C.

For the frequency of 1 kHz, (in the Tan δ spectra) however, the α transition is not visible because of a manifestation of the MWS behavior at almost -90°C. This interfacial polarization behavior is also seen to begin for the 5 kHz at ca. -70°C and occurs for the other frequencies in the same temperature range. Above -50°C the loss factor for all frequencies increases rapidly due to the MWS interfacial polarization contribution. It can be seen that the intensity of the MWS relaxation in the Tan δ spectra for the TiOPr(58)-PTMO(2K)-25-0.06-EARLY is very high when compared with the 33wt% TiOPr/PTMO sample or the 58 wt% TiOPr/PTMO ceramer tested one month later which will be described shortly. This indicates that the Ti(58)-PTMO(2K)-25-0.06-EARLY system may contain more moisture and non-bridging oxygens i. e. TiOH species, which then possibly give rise to a larger amount of interfacial polarization. The existance of solvent and other reaction by-products also may help contribute to the intensity of the MWS relaxation. Thus, the magnitude of MWS behavior appears to be dependent upon the number of polarizable species present in the system. The Tan δ spectra as shown in Fig 7.8b is plotted on a larger scale and has an intensity of 2.8 for the lower temperature MWS peak and approximately 6.4 for the higher temperature peak.

The same sample containing 58 wt% TiOPr when run after a period of one month (denoted by TiOPr(58)-PTMO(2K)-25-0.06-LATE) showed somewhat similar characteristics to the TiOPr(58)-PTMO(2K)-25-0.06- EARLY except for the intensity of the MWS behavior. The spectra can be seen in the Fig 7.9a. The

dielectric storage at -150°C is around ca. 5. The upturn in the dielectric storage at the glass transition is now more pronounced and steep than in the sample examined a month earlier. The dielectric storage plateaus out above -60°C at around 7 and around 0°C begins to show an upturn due to the interfacial polarization. The bimodal for the MWS peaks is now less pronounced than that seen in the film studied one month earlier and the low temperature relaxation appears more as a shoulder to the higher temperature peak rather than as a separate peak. The position of the maxima in the shoulder as well as the maxima in the peak position lie at exactly the same temperatures as in the earlier run on the same film.

The dielectric loss factor for the TiOPr(58)-PTMO(2K)- 25-0.06-LATE shows a β transition between -150°C and -100°C and an α transition between -100°C and -70°C. The intensity of the β and α transitions are similar in intensity to those seen a month earlier on the same film. The only major difference between the two dielectric loss spectra occurs in the MWS behavior. As stated above the onset of MWS relaxation which is due to interfacial polarization occurs at a higher temperature in the TEOS(58)-PTMO(2K)-25-0.06-LATE sample (0°C in the 58 wt% TiOPr/PTMO material aged for one month as against -50°C for the same material run one month earlier). The activation energy for the TiOPr(58)-PTMO(2K)-25-0.06-LATE is calculated from the plot in Fig 7.10. and is 64 kcal/mole.

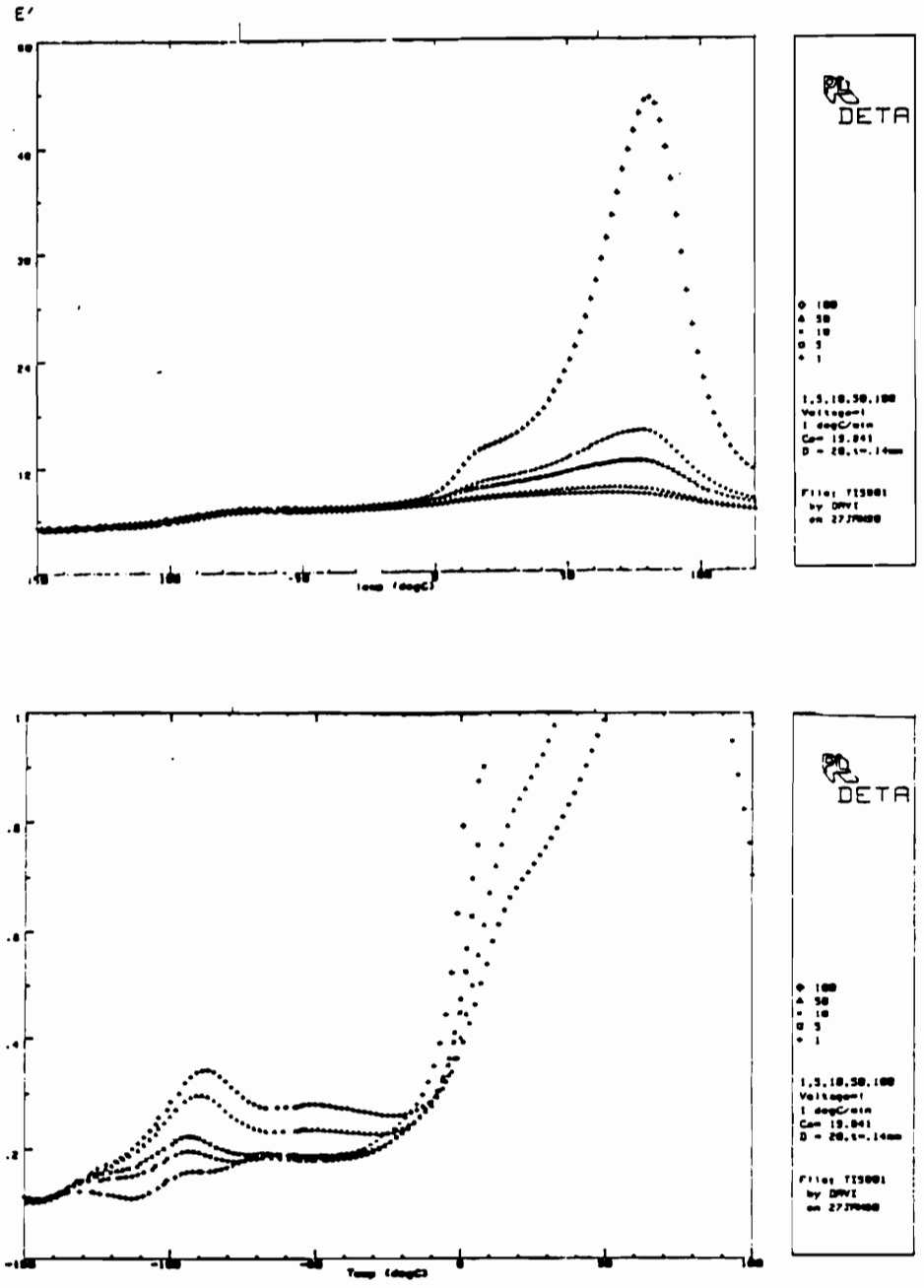


Figure 7.9. a) Dielectric storage and b) Tan δ for the TiOPr(58)-PTMO(2K)-25-0.06-LATE ceramer.

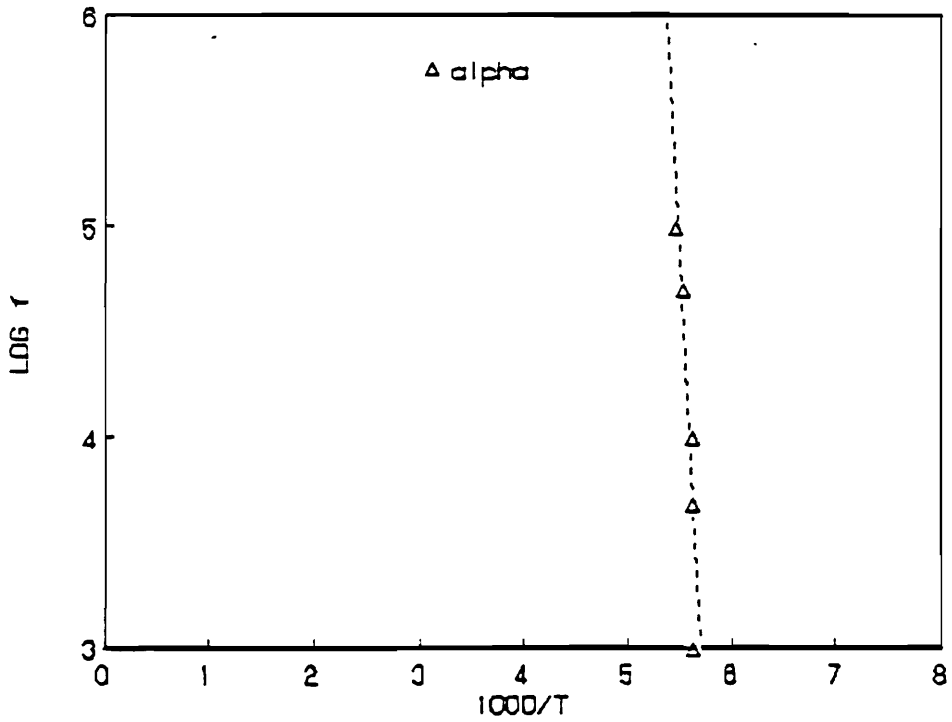


Figure 7.10. Plot of log f (f = frequency) vs 1/T (T = temperature) for the TiOPr(58)-PTMO(2K)-25-0.06-LATE ceramer.

7.3.1.2 EFFECT OF METAL ALKOXIDE TYPE

This section will discuss the effect of metal alkoxide type on the dielectric properties of the the ceramer films. The discussion will, however, be limited to more phase separated ceramer systems i. e. TiOPr/PTMO, ZrOPr/PTMO and TEOS/PTMO films reacted in DMF/IPA. As in the section on the TiOPr/PTMO ceramers above, the discussion on dielectric behavior will be restricted to the dielectric storage and Tan δ behavior for these three ceramer systems. The ceramer systems considered all contain only 50 wt% of the respective metal alkoxides. Only 1 kHz spectra will be utilized to demonstrate the effect of different metal alkoxides on the dielectric properties of these ceramers in the temperature range -150°C to 100°C.

All the three ceramer materials i. e. TiOPr(50)-PTMO(2K)-25-0.06, ZrOPr(25)-PTMO(2K)-0-0.06 and TEOS(50)-PTMO(2K)-100-0.048 in Fig 7.11a display a glassy dielectric storage of approximately 4.0 and the dielectric storage gradually increases with temperature upto around -80°C. All three materials show a glass transition between -80°C and - 70°C which as stated above is due to the occurrence of cooperative segmental motion in PTMO which permits greater rotational polarization in the ether linkages. The dielectric storage for all three ceramers i. e. TiOPr/PTMO, ZrOPr/PTMO and TEOS/PTMO reacted in DMF/IPA then plateaus out at a storage value of 6.5 and remains constant upto around 0°C at which temperature the MWS

relaxation begins to manifest itself. The MWS relaxation for the ZrOPr/PTMO ceramer results in a single peak at 20°C. The peak intensity for this ceramer is approximately 16 and the relaxation extends from 0°C to 110°C. The MWS relaxation for the ZrOPr/PTMO ceramer does not show a distinct bimodal as in the case of the TiOPr/PTMO and TEOS/PTMO ceramers (reacted in DMF/IPA) but does contain a slight shoulder at approximately 60°C. This shoulder is more visible in the dielectric loss spectra shown in Fig 7.11b for the ZrOPr/PTMO ceramer. The MWS relaxation for the TIOPr/PTMO ceramer as explained earlier contains a bimodal whose origins have been speculated upon in the last section. The intensity of the MWS relaxation in the TiOPr/PTMO ceramer is greater than that seen in the ZrOPr/PTMO ceramers at 1 kHz.

The TEOS/PTMO ceramer reacted in DMF/IPA is known to be highly phase separated (as described in chapter 4 from dynamic mechanical analysis) and also shows a MWS relaxation in the dielectric storage spectra above 0°C. There are two peaks for this material, one located at 20°C of a lower intensity (approximately 15) and the other located at approximately 100°C which is of a much higher intensity (approximately 140). Since the shape, intensity and position of these MWS relaxations vary with the metal alkoxide used in the ceramer it therefore appears that the MWS behavior is dependent upon the type of metal alkoxide. It may be speculated that the intensity of these MWS peaks seen in the dielectric storage/Tan δ spectra are related to the extent of reaction occuring in these systems. It is known that the reactivity rate of the

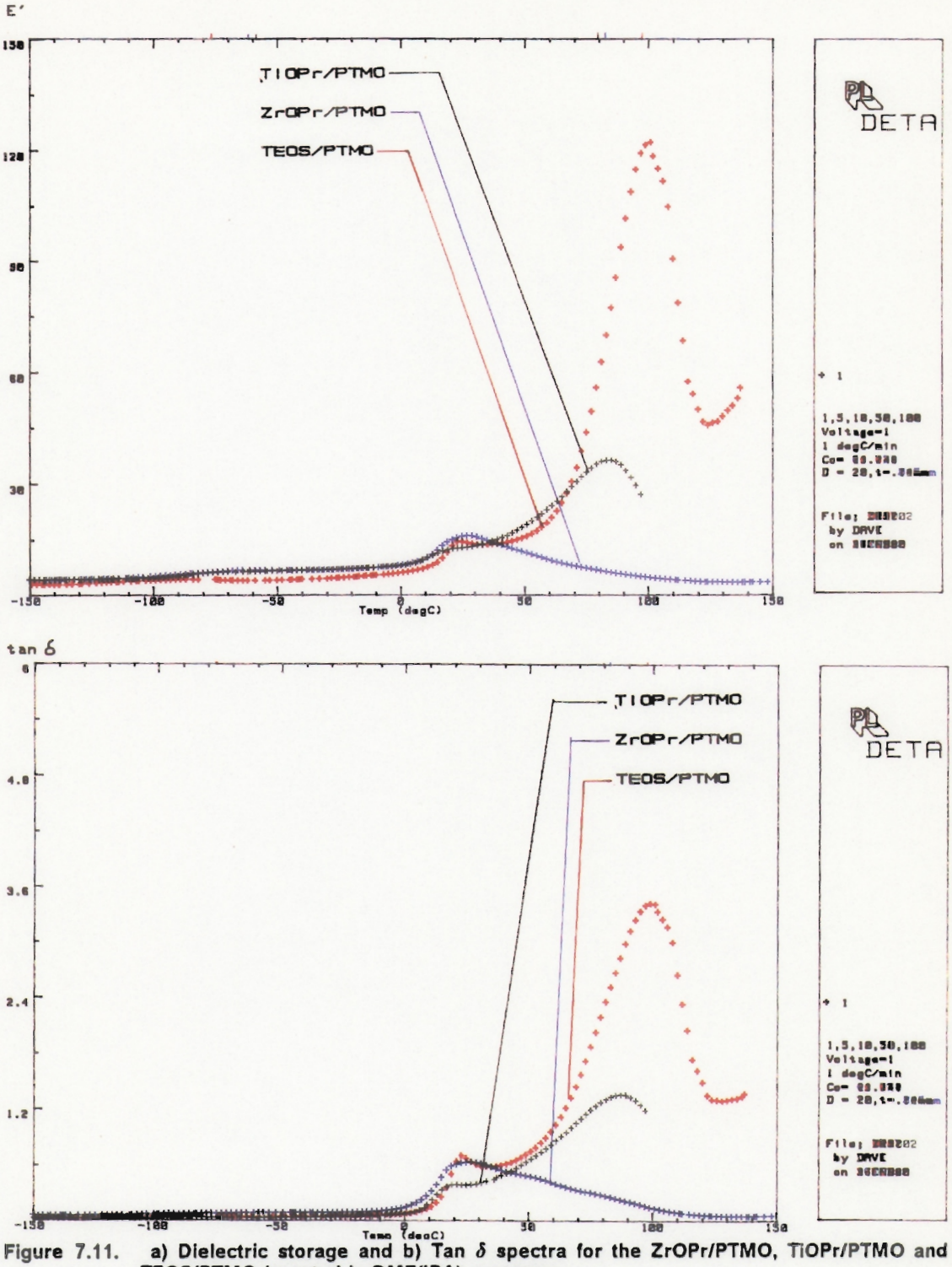


Figure 7.11. a) Dielectric storage and b) Tan δ spectra for the ZrOPr/PTMO, TiOPr/PTMO and TEOS/PTMO (reacted in DMF/IPA) ceramers.

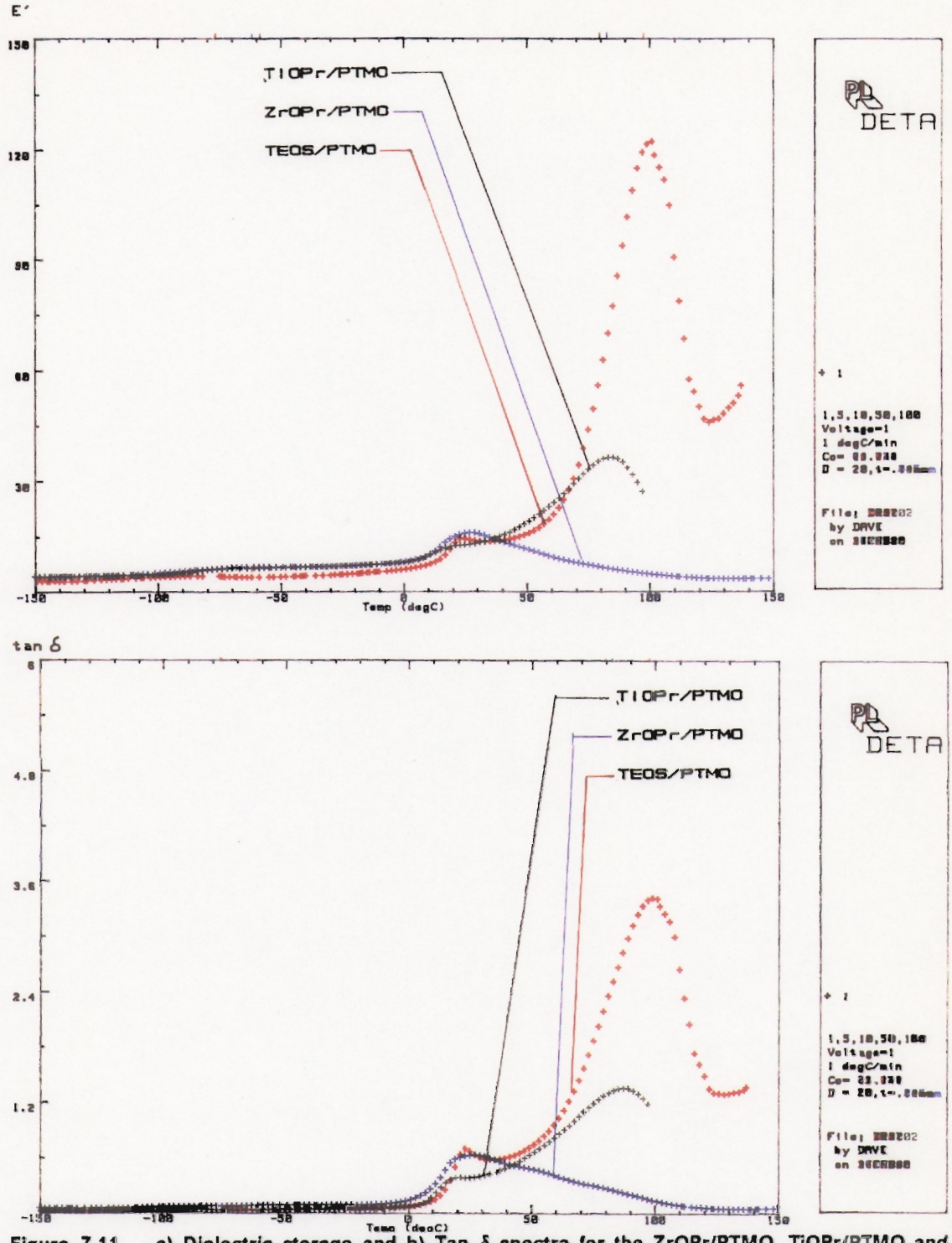


Figure 7.11. a) Dielectric storage and b) Tan δ spectra for the ZrOPr/PTMO, TiOPr/PTMO and TEOS/PTMO (reacted in DMF/IPA) ceramers.

ZrOPr > TiOPr > TEOS and therefore the number of mobile protons (H^+) resulting from non-bridging oxygen species would be highest in the TEOS/PTMO ceramers and lowest in the ZrOPr/PTMO ceramers. Thus the intensity of MWS activity would be least in the zirconia based ceramers and highest in the TEOS based ceramers cured in DMF/IPA. Conversely, it may also be reasoned that since for a given amount of metal alkoxide the amount of water added is greatest in the TEOS/PTMO ceramers and least for the ZrOPr/PTMO ceramers, then the contribution to the MWS relaxation made by mositure may result in a greater extent of interfacial activity in the TEOS/PTMO materials than in the TiOPr/PTMO or ZrOPr/PTMO materials.

7.3.1.3 EFFECT OF SOLVENT ON THE TEOS/PTMO CERAMERS

The aim of these experiments was to study the effect of solvent on the dielectric properties of the TEOS/PTMO ceramers. From previous experiments and studies detailed in chapter 7, we have seen that there is an effect of solvent on the inorganic phases formed in these ceramers. In the case of TEOS/PTMO ceramers reacted in THF/IPA::1/4 the inorganic phase has been determined to be more ramified (the growth of the silicate species is more linear as shown by Brinker) and the two components (the inorganic component and the PTMO component) are more mixed as shown by Brennan (96) and Huang (84) . In the case of the same reactants reacted in DMF/IPA::1/1 the

inorganic phase is more particulate like and hence there is a greater phase separation between the inorganic and the PTMO. Since the MWS relaxation displays behavior which was found to be dependent upon the nature of the metal alkoxide it was decided to attempt a study of the MWS spectra behavior as a function of the nature of the inorganic phase.

The solvents used for the preparation of the ceramer during this study were THF/IPA::1/4, IPA and DMF/IPA::1/1. All the materials tested in this experiment were run from -150°C to 100°C and all five frequencies will be shown in the spectra since the spectra for each ceramer show different behavior at different frequencies and this needs elaboration. The dielectric storage spectra for the TEOS(60)-PTMO(2K)-100-0.048 ceramer reacted in THF/IPA is shown in Fig 7.12a. The dielectric storage at -150°C is ca. 4 at a frequency of 100 kHz and increases with decreasing frequency at all temperatures. The dielectric storage for all frequencies increases gradually with temperature upto -65°C. The onset of cooperative segmental motion in the oligomeric phase at this temperature causes a maxima in the storage behavior. Above -65°C the dielectric storage increases more rapidly with temperature than below -65°C. There also occurs a divergence in the storage at the different frequencies i. e. the storage at the lowest frequency 1 kHz increases at a greater rate than the increase at 100 kHz. This may be attributed to the large variety of structural environments existing in the ceramer examined at these different frequencies. At lower frequencies there may be a response from the more loosely bound structures in the ceramer system while some of the PTMO segments

encapsulted tightly by the inorganic phase may respond better to higher frequencies. The maxima in the 1 kHz dielectric storage curve occurs at 50°C and is approximately 11 while that in the 100 kHz curve occurs at ca. 70°C. and is approximately 8.5. Because of the mixing between the inorganic and the organic components in these TEOS/PTMO ceramers reacted in THF/IPA the T_g of the oligomeric component is increased significantly as compared with the TiOPr/PTMO ceramers discussed earlier. At temperatures above the temperature of the peak position, all the storage curves show a steady decline in the value of the dielectric storage. This decline in the storage behavior with temperature above the T_g has been explained earlier for the 0 wt% TiOPr/PTMO ceramer which displays similar behavior above the T_m.

The Tan δ curves (shown in Fig 7.12b) for the TEOS(60)-PTMO(2K)-100-0.048 ceramer reacted in THF/IPA displays broader β and α transitions than their TiOPr/PTMO and ZrOPr/PTMO counterparts and this feature may be attributed to mixing between inorganic and PTMO components in the TEOS/PTMO ceramer. It may also be related to the looser networks typically produced in the TEOS/PTMO materials reacted in THF/IPA as previously demonstrated from elastic modulus measurements described in chapter 5. The Tan δ value at -150°C at a frequency of 100kHz is approximately 0.048 which is twice as high as the value obtained at the same temperature and frequency for the more phase separated TiOPr/PTMO and ZrOPr/PTMO materials. This would indicate a higher value of dielectric loss for these TEOS/PTMO networks which again reflects a looser network than their more phase separated counterparts.

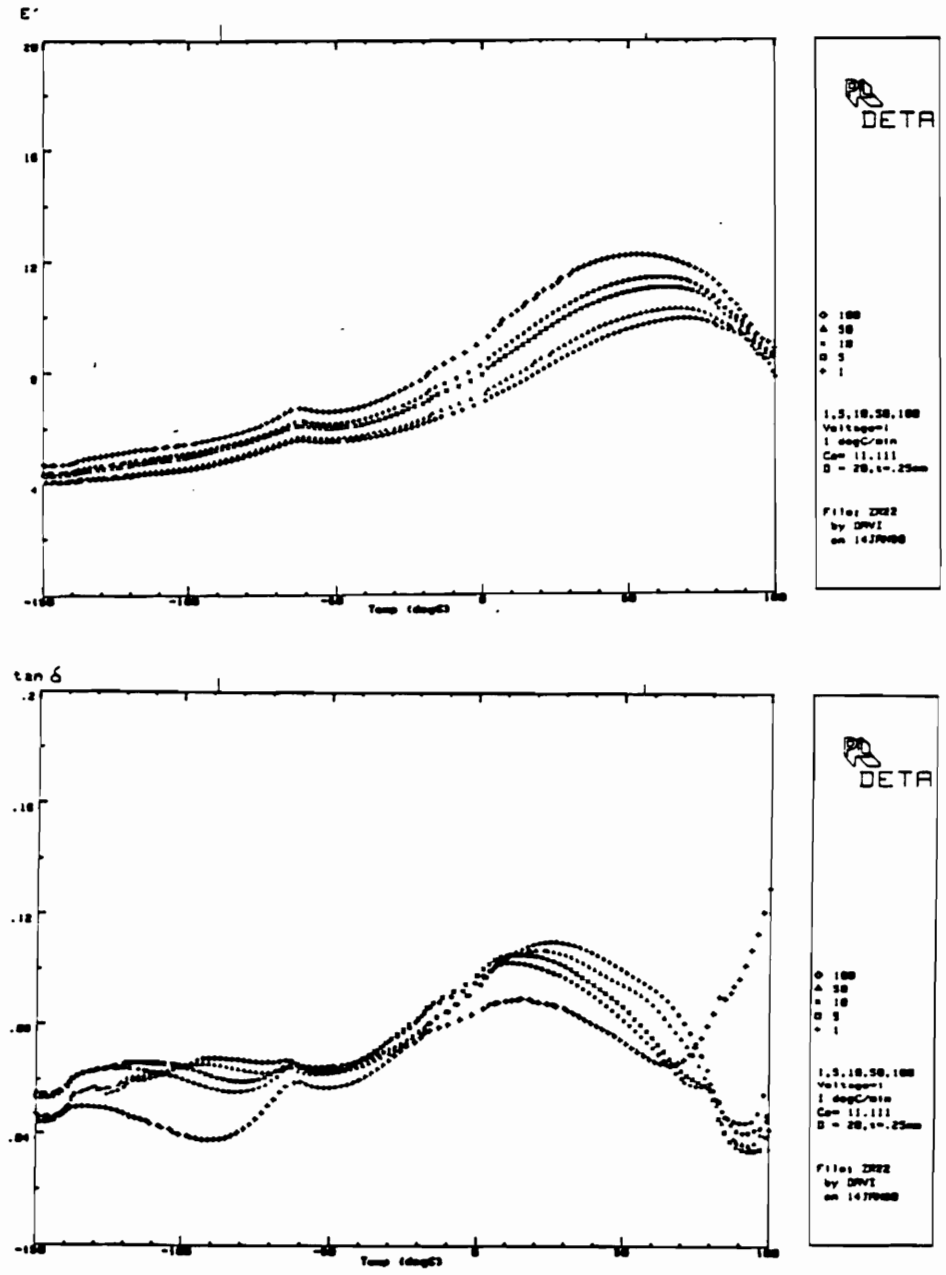


Figure 7.12. a) Dielectric storage and b) Tan δ spectra for the TEOS(60)-PTMO(2K)-100-0.048 ceramers reacted in THF/IPA.

All five frequencies display a β relaxation peak for the TEOS/PTMO ceramer film reacted in THF/IPA. The β relaxation is also much broader than that seen in the TiOPr/PTMO and ZrOPr/PTMO ceramers and occurs between -150°C and -65°C.

The α transition is very broad and occurs between -50°C and 90°C as has between previously shown in chapter 5. The breadth and intensity of the α transition reflect the extent of mixing between the two phases as well as the possible encapsulation of the PTMO chains by the inorganic phase. The α relaxation at the 1 kHz frequency shows two maxima one at -65°C and the other at 10°C. The maxima at -65°C may suggest the existance of some relaxation due to pure PTMO, but this needs to be further verified. The need for further verification arises especially since this behavior does not manifest itself in the DMA analysis discussed earlier in chapter 4. However, the author would conceed that because of the nature of dielectric testing, and the response of molecular dipoles to this probe, that small domains of pure PTMO may actually exist in these TEOS/PTMO ceramers reacted in THF/IPA and display a loss at around -65°C. At 1 kHz there occurs a maxima at 10°C while for the 100 kHz frequency it shows a peak at 35°C. This shift in the peak position with temperature indicates that the relaxation behavior is due to cooperative segmental motion behavior of oligomers and not due to MWS interfacial polarization where the peaks do not shift along the temperature axis with frequency. There is no MWS behavior seen in these systems, indicating the possible non-existance of a distinct interface between the PTMO and

inorganic components. The mixing between the two components also appears not to allow for the existance of an inorganic - air interface (due to porosity) which also produces MWS behavior. Above 60°C there is an upturn in the loss curves starting with the 1 kHz frequency and then followed at higher temperatures by the higher frequencies. This behavior, as stated earlier, is due to ionic conductivity in the systems.

The TEOS/PTMO ceramer material reacted in only IPA has a dielectric storage value of approximately 3.8 at -150°C at a frequency of 100 kHz as shown in Fig 7.13a. The dielectric storage value at all frequencies increases gradually with temperature up to the onset of the glass transition which occurs in these materials at -75°C. The shift of the T_g to -75°C for this TEOS/PTMO ceramer indicates that these materials are more phase separated than their counterparts reacted in THF/IPA (which display onset of cooperative segmental motion at -65°C). The dielectric storage for these materials increases rapidly with temperature above -75°C. The increase steeper for the lower frequencies as compared with the higher frequencies. This divergence in the storage spectra may again indicate that a variety of structures and environments are present in these materials. Different environments permit different mobilities and hence allow for a broad range of relaxations which manifest themselves in the Tan δ spectra. This dielectric storage for this TEOS/PTMO ceramer reacted in IPA peaks at approximately 20°C for the 5 kHz frequency while for the 100 kHz frequency it peaks at 30°C. The dielectric storage at the lowest frequency (1 kHz) displays a single relaxation peak

because of the Maxwell Wagner Sillars behavior. This MWS relaxation in this TEOS/PTMO materials has only a single peak as compared with the bimodal seen in the TiOPr/PTMO ceramers. The occurence of the MWS behavior in this TEOS/PTMO ceramer system cured in IPA (when compared with that cured in THF/IPA which does not display MWS behavior) has an interesting connotation i. e. only those systems which possess a certain amount of phase separation display Maxwell Wagner Sillars interfacial relaxation. In other words one of the requirements for MWS relaxation to occur in a two phase system is that a significant amount of phase separation between the two components must exist in order to produce an interface where charge trapping and interfacial polarization can occur. It is difficult, however, to define a minimum amount of phase separation necessary to observe this behavior.

The Tan δ spectra for these TEOS/PTMO reacted in IPA materials is shown in the Fig 7.13b. The Tan δ value at -150°C is 0.025 (which is slightly lower than 0.04 displayed the TEOS/PTMO system reacted in THF/IPA) and increases with increasing frequency at the same temperature. All the frequencies display a β transition between -150°C and -100°C. The β transition is more pronounced at the lower frequencies than at the higher frequencies. The α transition begins at around -90°C and its breadth increases with increasing frequency. The intensity of the α transition also increases with increasing frequency and the peak position shifts to higher temperatures with increasing frequency. The peak position for the α transition occurs at -50°C for the 1 kHz frequency as against 10°C (at 1 kHz) for the corresponding TEOS/PTMO ceramer reacted in

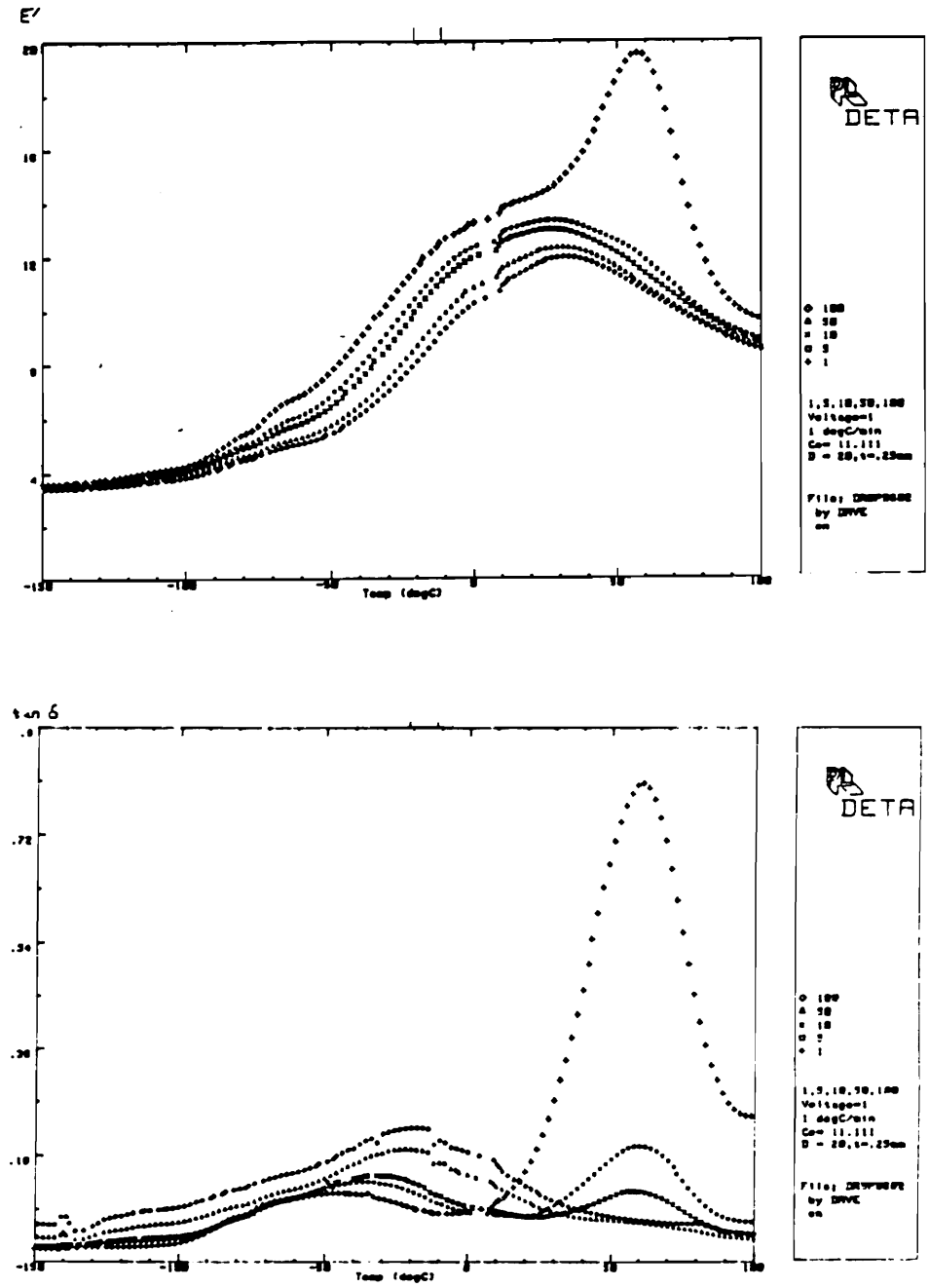


Figure 7.13. a) Dielectric storage and b) Tan δ spectra for the TEOS(60)-PTMO(2K)-100-0.048 ceramers reacted in IPA.

THF/IPA. This shift in the peak position to a lower temperature in the system reacted in IPA indicates the existance of a PTMO phase less mixed with the inorganic component than in the TEOS/PTMO ceramer reacted in THF/IPA. At temperatures above 0°C in this TEOS/PTMO system reacted in IPA, there occurs the onset of MWS behavior. This relaxation manifests itself at frequencies of 1, 5 and 10 kHz and shows a higher intensity at the lower frequencies (which is the typical signature of this relaxation process) but is not visible at 50 and 100 kHz. The peak of the MWS relaxation in this TEOS/PTMO system occurs at 70°C and does not shift to different temperatures with frequency. The breadth of this relaxation also increases with decreasing frequency.

The TEOS/PTMO system reacted in DMF/IPA is known to be highly phase separated from previous studies detailed in chapter 4. The dielectric properties of this ceramer have already been detailed above in the section above and hence only specific features of this system which pertain to this discussion will be addressed. The dielectric storage at -150°C for this TEOS/PTMO ceramer system reacted in DMF/IPA is around 3.6 as seen in Fig 7.14a. The upturn in the dielectric storage due to the glass transition is now shifted to a much lower temperature of -100°C. Above the T_g the dielectric storage plateaus out at around ca. 4 upto 30°C. At around 30°C the MWS relaxation begins to manifest itself. As described previously the MWS behavior in this TEOS/PTMO ceramer system shown in Fig 7.14a is bimodal. The MWS

relaxation extends to 130°C and the upper temperature peak has an intensity of 140 for the dielectric storage.

The Tan δ spectra for this TEOS/PTMO (shown in Fig 7.14b) ceramer reacted in DMF/IPA shows some further manifestations of the trend indicated by these ceramers as the solvent was changed from THF/IPA to IPA. This trend involved the development of a rather intense MWS relaxation as the phase separation between the inorganic and the PTMO increased. In this ceramer reacted in DMF/IPA the glass transition of the PTMO is shifted to lower temperatures i. e. -90°C and the MWS relaxation as seen in the Tan δ spectra extends form -50°C to 130°C. The α dispersion (due to cooperative segmental motion) also displays a bimodal, which was also previously seen in the DMA Tan δ spectra. The lower temperature part of this bimodal was attributed to the relaxation of PTMO chains trapped in pure PTMO surroundings, while the higher temperature part of the relaxation was attributed to the presence of PTMO adsorbed onto the inorganic. Thus, it can be seen that this ceramer reacted in DMF/IPA shows a greater amount of phase separation between the inorganic and the oligomeric components. This increased phase separation leads to the development of a rather intense MWS relaxation.

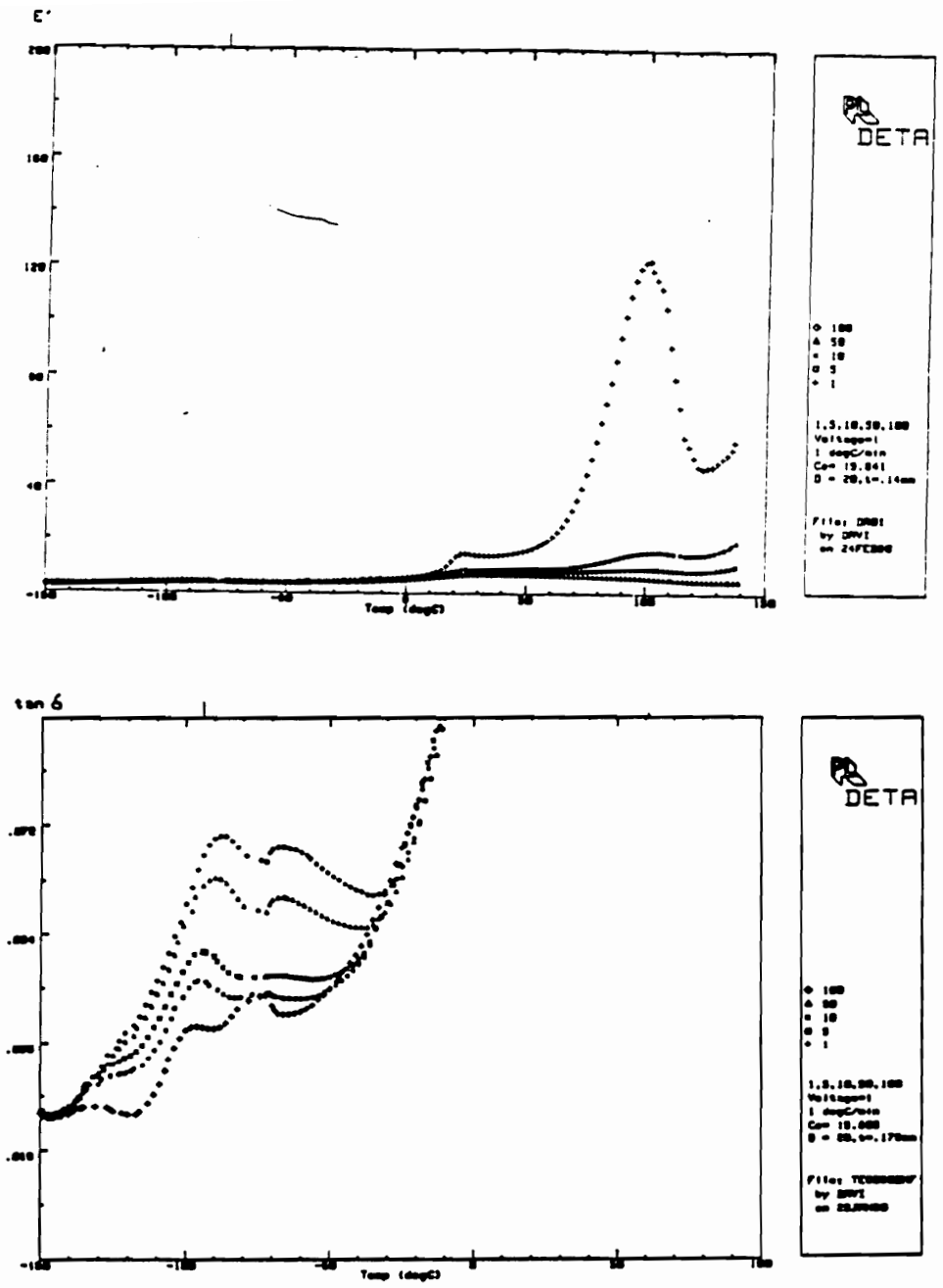


Figure 7.14. a) dielectric storage and b) Tan δ spectra for the TEOS(60)-PTMO(2K)-100-0.048 ceramers reacted in DMF/IPA.

7.3.1.4 EFFECT OF AGEING

All the ceramer systems studied previously have been known to display the effects of ageing on their mechanical properties and upon the SAXS scattering profiles. The extent of such changes in the structure and properties of a given ceramer with age, depend upon the metal alkoxide and oligomer chosen, as well as the temperature of cure and the solvent used to compatibilize the reactants. The main purpose of this short section is to demonstrate the effect of higher temperature (ageing) on the dielectric properties of these ceramer systems. The TEOS/PTMO material reacted in IPA will be chosen to illustrate the effect of temperature on these systems. Once again, only the dielectric storage and loss at a frequency of 1 kHz will be discussed, since this is the only frequency which shows clearly the effect of the β transition, the α transition and the MWS relaxation too. This TEOS/PTMO sample was heated from -150°C through to 100°C and the data recorded. The same film was subjected to this temperature cycle three times and thus three scans (dielectric storage and loss at 1kHZ) of the sample will be displayed, compared and contrasted.

The dielectric storage profiles for the three scans are shown in Fig 7.15a. The dielectric storage value at -150°C remains the same through all three scans at approximately 3.6. The dielectric storage spectra for the the first scan of this TEOS/PTMO ceramer system will not be described since this has already been

done. On heating the same TEOS/PTMO ceramer film a second time from -150°C, the upturn in the dielectric storage is more pronounced and occurs at a lower temperature than that seen in the first scan. Above 0°C the value of the dielectric storage for the second run decreases with temperature as compared with the first run. The MWS relaxation peak while remaining at the same temperature as in the first run, is significantly reduced in intensity and breadth on the second. This indicates that the interfacial polarization is significantly reduced on undergoing heating. This was the same effect noticed with the TiOPr(58)-PTMO(2K)-25-0.06 (EARLY AND LATE) system described earlier. This reduction in the intensity of interfacial polarization can be related to the increase in the extent of reaction in the system i. e. some of the hydroxyl groups attached to the metal alkoxide which contribute to the interfacial polarization (as described earlier) undergo further reaction to form Si-O-Si linkages. The reduction in the MWS intesity is also possibly related to the lack of solvent and reaction by products which would be reduced in quantity after two scans to 100°C. Thus, while phase separation and porosity can exist in a ceramer system the presence of charges which can migrate to an interface is necessary for the MWS relaxation to manifest itself. Hence, it is seen that as the network tightens the value of interfacial polarization is significantly reduced. The tightening of the network also serves to increase the elastic modulus at room temperature as seen from previous studies in chapters 4 and 5.

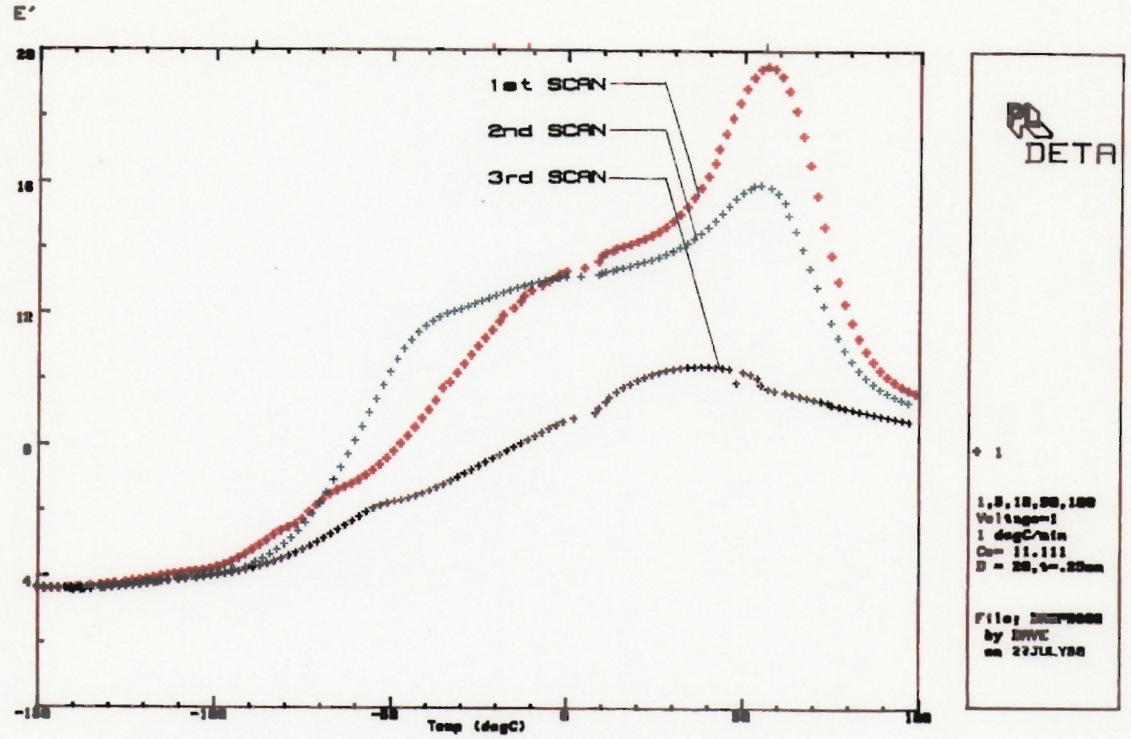
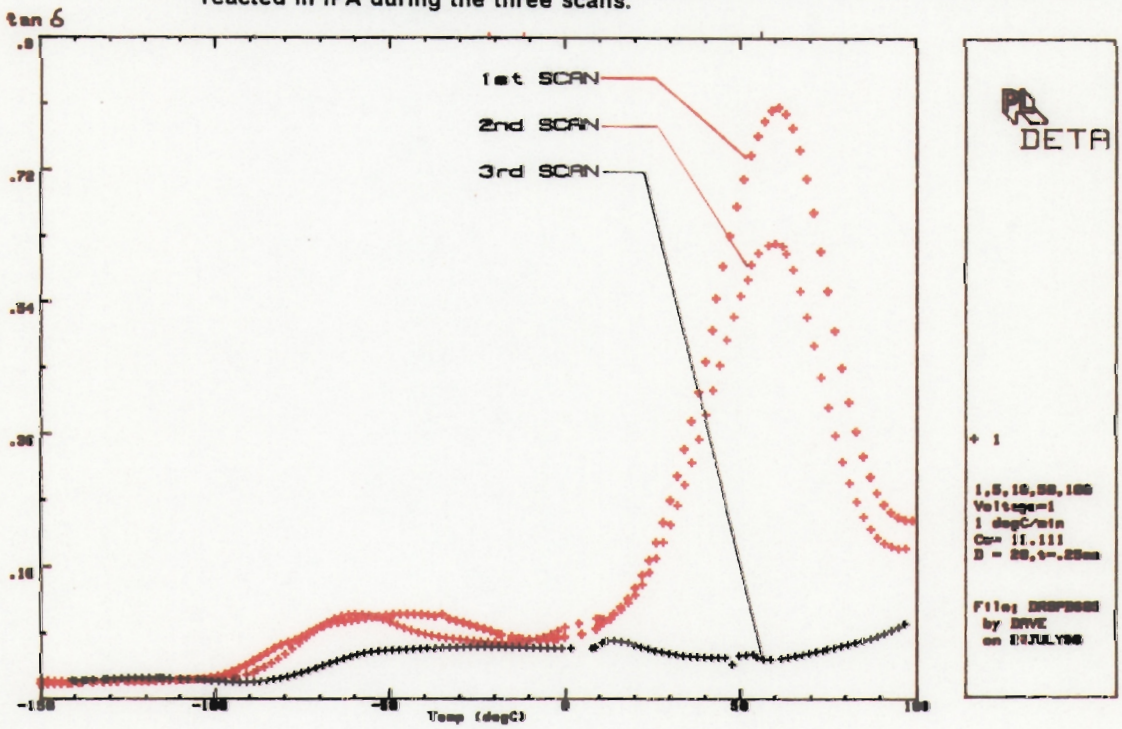


Figure 7.15. a) Dielectric storage and b) Tan δ spectra for the 60wt% TEOS/PTMO ceramer reacted in IPA during the three scans.



On heating the material a third time from -150°C the upturn in the dielectric storage is less steep than that seen for the second run. The MWS peak is barely vislble and its intensity is reduced from approximately 20 (on the first run) to approximately 8 (on the third run). The reasoning for this further reduction in the MWS relaxation behavior has already been given above.

The Tan δ spectra for these three materials is shown in Fig 7.15b. The β transition which occurs between -150°C and - 100°C increases in intensity with each run. The behavior of the α transitions with each scan show some important changes. The α transition begins at around -90°C in all cases. In the first run the α transition extends from -90°C to approximately 0°C at which temperature the MWS relaxation begins. The peak for this α transition occurs at -45°C and has an intensity of ca. 0.11. On the second run the α transition shows a peak which is sharper than that seen in the first run. The breadth of this transition is now reduced primarily because of a tightening of the inorganic network which causes the PTMO relaxations occuring at higher temperatures to be reduced in intensity. The relaxations which occur at higher temperatures are believed to be due to PTMO trapped in an inorganic rich environment. This feature has already been discussed earlier in chapter 5 on the TEOS/PTMO ceramers reacted in THF/IPA which also displays a considerable amount of mixing between the inorganic and the PTMO components. Thus as a result of this tightening of the network, which causes a reduction in the intensity of the α relaxation at higher temperatures (above

40°C) the peak position for this α relaxation is shifted to a lower temperature of -60°C.

On the third run there is a decrease in the intensity of the α relaxation at the lower temperatures as well i.e. below -50°C. This causes the intensity of the α relaxation to decrease significantly throughout the entire temperature range of its existance. The peak position for this relaxation is again shifted to a higher temperature ca. -30°C. One interesting feature of the system is that when the MWS relaxation is not visible any more (as is the case with the third run) then it can be seen that the dispersion due to cooperative segmental motion continues to above 100°C. This implies that in the TEOS/PTMO system reacted in IPA the MWS relaxation is superimposed upon the relaxation due to cooperative segmental motion. Above 50°C, there occurs an upturn in the Tan δ behavior which is attributed to ionic conductivity in these systems.

7.4 THE CASE FOR EXPANDED PTMO CHAINS

The dielectric storage spectra can be used to gain a very rough estimate of the radius of gyration of the PTMO chains. However, the author would like to emphasize that these dimensions are at best only rough estimates of the

actual dimensions and therefore the values obtained from the series of calculations to be presented below should be considered only for the trends they provide. The reasons for the inaccuracies in the chain dimensions are due to the use of certain assumptions made in the following computations and these will be alluded to and discussed as the pertinent equations are presented. Chain dimensions will be calculated for the TiOPr/PTMO ceramers containing 0, 25, 33, 50 and 58 wt% of metal alkoxide as well as for the TEOS(60)-PTMO(2K)-100-0.048 ceramers reacted in THF/IPA, and DMF/IPA.

As described in the literature review section of this dissertation, Frohlich related the dielectric parameters of any given material to the dipole moment of the molecules through the equation:

$$\varepsilon_r - \varepsilon_u = \frac{3\varepsilon_r}{(2\varepsilon_r + \varepsilon_u)} \frac{4\pi N}{3kT} \left[\frac{(\varepsilon_u + 2)}{3} \right]^2 \frac{P^2}{n} \phi \qquad (1)$$

where ε_u and ε_r are the values of the dielectric storage below and above the glass transition respectively as shown in the Fig 7.16. P represents the dipole moment of the molecules and n represents the number of repeat units in the chain, N is the number of molecules per unit volume. A special term ϕ has been inserted into the equation (1) above to account for the volume fraction of the metal alkoxide in the ceramer . This metal alkoxide fraction is assumed not to make any contribution to the dielectric spectra at the temperature at which ε_r is taken. The value of ϕ included in equation above was taken from Brennan's dissertation (96). These values of the metal alkoxide volume fraction

were obtained from the invariant (from SAXS data) and by utilizing a parallel model for the density of the ceramer. This parallel model will not be elaborated upon any further but it is important to state that this model does not accurately represent the ceramer system and the basis for its foundations are absolutely invalid. However, in view of the fact that there is no better manner by which the volume fractions of the ceramer components can be obtained, recourse will be taken to the use of this model. In view of the variations seen in the spectra with the metal alkoxide content as well as the nature of the inorganic phase, it becomes evident that a rather judicious choice has to be made in the selection of ε_r

In the case of the TiOPr/PTMO ceramers, the systems containing 0, 25 and 33 wt% metal alkoxide displayed crystallinity and hence the value of ε_r was chosen at 10°C which is the melting point of the PTMO component in these materials. It should be noted that the highest frequency i. e. 100 kHz was used to calculate the chain dimensions. The reason for using the highest frequency is two fold a) the value of ε_u at -150°C at 100 kHz is most representative of the glassy behavior of the system since the dielectric storage increases with decreasing frequency at all temperatures b) the MWS relaxation shows an inverse frequency dependence i. e. the higher the frequency the lower the intensity of the MWS relaxation. The systems containing 50 and 58 wt% TiOPr show significant MWS behavior at temperatures above 0°C. Therefore, to avoid any influence of this relaxation on the computations the dielectric storage data at the highest frequency was utilized. Therefore for the 50 and 58

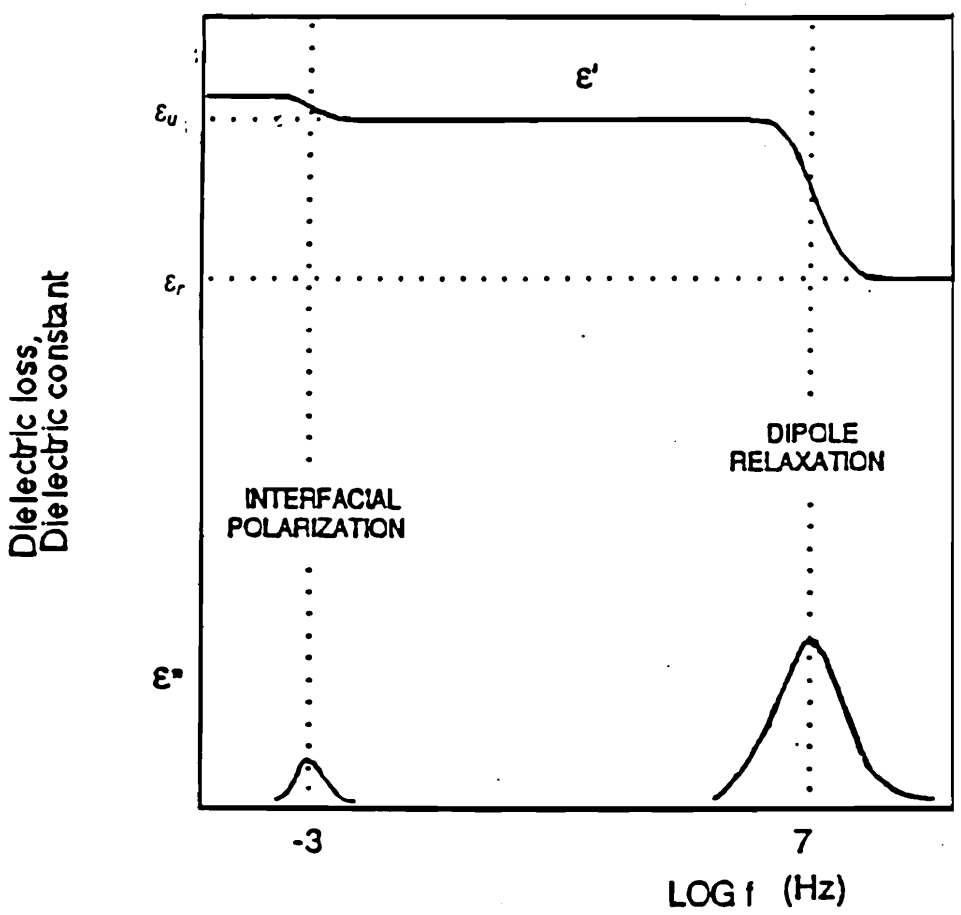


Figure 7.16. **Plot shows the positions at which ε_u and ε_r values are typically taken.**

wt% TiOPr/PTMO ceramers ε_r was chosen at -50°C at 100 kHz. In the case of the TEOS/PTMO ceramers the value of ε_r (from the dielectric storage data) was chosen at the first temperature at which the α relaxation was reduced to its minimum value in the Tan δ spectrum. Thus in the case of the more mixed TEOS/PTMO ceramer reacted in THF/IPA ε_r was chosen at 90°C while in the same ceramer reacted in DMF/IPA the storage value at -50°C and 100 kHz was chosen.

One of the implicit assumptions made by the author in these calculations (which is not accurate) is that the value of ε_u for all these systems does not reflect any contribution from the inorganic phase. However, this is not the case as has already been shown in the section 7.3.1.1. Here it was seen that the value of ε_u at -150°C at 100 kHz increased from 2.88 to 4.5 as the metal alkoxide content was changed from 0 wt% to 58 wt%. Further in the TEOS(60)-PTMO(2K)-100- 0.048 ceramers it was observed that the value of ε_u decreased with the amount of phase separation in these ceramers. In the case of the TiOPr/PTMO ceramers the values of ε_u for all metal alkoxide contents were reduced to 2.88 (these will be referred to as 'reduced' values) and the chain dimensions were computed and are contrasted with their unreduced values in Table 7.2. The values of the interdomain spacing d as calculated from the SAXS profiles are also shown in the same table.

The second equation used to compute the PTMO chain dimensions is shown below.

$$\frac{P^2}{2nk^2} = (1 - cos\alpha)(1 - \eta^2)(1 - \eta)\ X$$

$$\frac{[1 + \eta + \eta^2 - 3\eta cos^2\alpha - (1 - \eta)^2 \cos^4\alpha]}{[1 - \eta^5 - 5\eta^2(1 - \eta)cos\alpha - 5\eta(1 - \eta)^3 \cos^3\alpha - (1 - \eta)^5 \cos^5\alpha]} \qquad (2)$$

Equation (2) was derived by Read et al (107) and relates the rotational potential η of the PTMO chains to the dipole moment P. In this equation $\eta = <\cos \phi'>$ where ϕ' represents the angle of rotation of an atom or molecule around a bond (111). The value of the dipole moment for the C-O-C bond which is represented by k is taken to be 1.13 Debye by Read et al (106, 107).

The last equation used in this computation is

$$R^2 = nl^2 \frac{(1 + cos\theta)}{(1 - cos\theta)} \frac{(1 + \eta)}{(1 - \eta)} \qquad (3)$$

where n is the number of repeat units (taken as 153 for the endcapped PTMO chain of 2000 g/mole) and l is the length of the C-C bond (taken as 1.54Å). θ represents the bond valence angle which for the C-C bond of PTMO is 109° The valence angle for the C-O-C bond is assumed to be similar to the C-C-C bond as described by Read et al (106, 107).

The use of equation (3) to arrive at a measure of the chain dimensions represents a serious violation of one of the main assumptions behind the

derivation of this very equation i. e. the chain must be free at its ends. However, in this case, the PTMO chains are either endlinked to the inorganic domains or another PTMO chain. Nevertheless, despite these violations, the author will persist with these computations and the results as it turns out, sheds some new light on the structure of the ceramer systems cast onto surfaces to which they adhere. In order to verify or disprove the chain dimension results obtained from dielectric analysis neutron scattering should be performed on these systems.

7.4.1 EFFECT OF METAL ALKOXIDE CONTENT UPON THE CHAIN DIMENSIONS

The values for the chain dimensions tabulated in Table 7.2 shows that with increasing metal alkoxide content in the TiOPr/PTMO ceramer system there is an increase in the mean square end to end distance of the chains. Figure 7.17 compares the computed chain dimensions (those calculated from the reduced data as well as the normal data) with the interdomain spacings measured from SAXS. From these results it can be seen that the interdomain spacings increase with metal alkoxide content. However, as seen from these computations, this increase in the interdomain spacing is contributed to partially by the increase in chain dimensions. The data calculated with the normal dimensions shows that the chain dimensions increase faster with

Table 7.2. Radius of gyration, chain end to end distances and interdomain spacings as measured for the TiOPr/PTMO ceramers.

wt. fraction TiOPr	$<R_g>$ Å	$<R>$ α Å	d Å
0	21.05	51.56	65
25	21.53	52.74	74
33	21.82	53.45	85
50	31.50	77.15	125
58	32.59	80.00	140

increasing metal alkoxide content (between 25 and 50 wt% TiOPr) than the data calculated with the reduced data. Both sets of data show that the end to end distance for the PTMO chains are always less than the interdomain spacings.

This increase in the chain dimensions is speculated to have profound implications for the structure-property relationships in these ceramer systems. These implications will be discussed shortly. The general morphological model for these ceramers described earlier in the literature review in chapter 2 was proposed by Huang (84) and subsequently verified and approved by Glaser (85) and Brennan (86). This model assumes that the increase in the interdomain spacing (as measured from SAXS) with the increase in the metal alkoxide content in the ceramers is primarily the result of increased inorganic

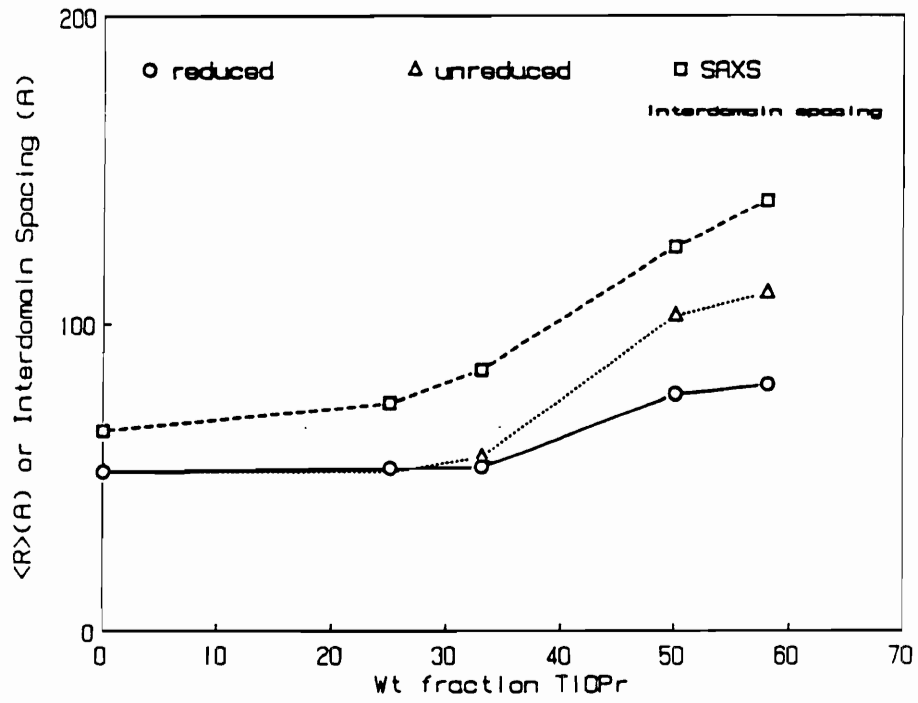


Figure 7.16. Plot shows PTMO chain end-to-end distance and interdomain spacing versus metal alkoxide content in the TiOPr/PTMO ceramers.

domain size. This, however, is not the case, as indicated by the results from Table 7.2. Thus the increase in the interdomain spacings with the metal alkoxide content (for only the more phase separated ceramer systems cast onto polystyrene petri dishes or any other substrate onto which they can adhere) is the result of both increased domain sizes as well as increased chain dimensions.

As stated above in order to verify the actual PTMO chain dimensions neutron scattering experiments would be desirable on these ceramers containing deuterated PTMO. In the meanwhile another set of experiments was performed on TEOS/PTMO ceramers reacted in DMF/IPA in order to further the arguments for increased chain dimensions. In these experiments the TEOS/PTMO reactants were cast onto two different surfaces - polystyrene and teflon. Since these TEOS/PTMO ceramers do not adhere to teflon the difference in scattering profiles as well as mechanical properties can be estimated, especially with respect to those ceramers cast onto a polystyrene surface. The reason for choosing the TEOS/PTMO system reacted in DMF/IPA is because this system displays a more phase separated behavior as does the TiOPr/PTMO ceramer system. Further this TEOS/PTMO ceramer system displays a sharp peak in the SAXS scattering profile and thus any additional effects caused by the reduced chain dimensions can also be evaluated from the scattering profiles. Two films (of different thicknesses) from the TEOS/PTMO ceramer cast onto the polystyrene (PS) surface, were examined using SAXS in order to determine the differences in the interdomain spacings

as a function of thickness. One film was ca. 3 mils thick while the other was ca. 12 mils thick. The film cast onto the teflon surface was approximately 20 mils thick.

The composition was chosen for this experiment was TEOS(60)-PTMO(2K)-100-0.048, reacted in DMF/IPA. Equal amounts of the reactants were cast into teflon and polystyrene petri dishes.

An examination of the SAXS profiles in Fig 7.18 shows that the peak scattering intensity of the samples cured in the PS petri dish is higher than the peak scattering intensity for the same material cured in teflon. Further the interdomain spacings for both the films cured on PS is larger than those cured on the teflon surface. The breadth of the scattering profiles for the film cured in teflon is also slightly greater than the same material cured in PS. Further, it can be seen that thinner film cast onto PS has a larger interdomain spacing (d = 142Å) than the thicker film (d = 120Å) cast onto the same surface. From these scattering results it can be seen that when a TEOS/PTMO ceramer film is cast onto a substrate to which it adheres there is an increase in the interdomain spacing (as measured from SAXS) which varies inversely with the thickness of the film. This increased interdomain spacing is caused in part by an extension of the PTMO chain as a result of adhesion of the film to the substrate. In the case of the film cast onto the Teflon substrate, the interdomain spacing is around 100Å There is also a greater amount of phase separation between the inorganic phase and the PTMO component (for

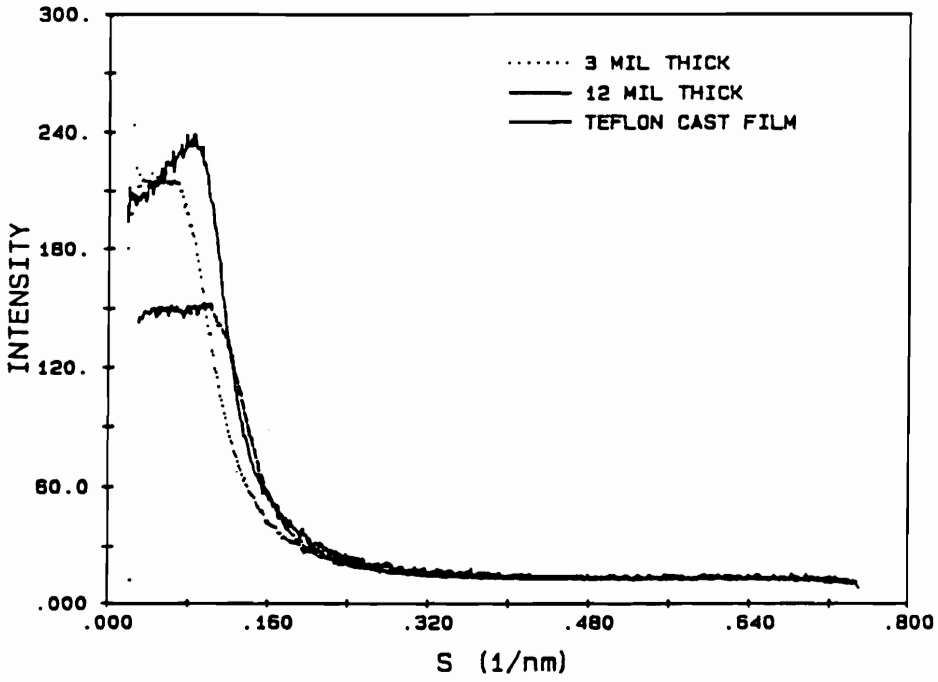


Figure 7.17. SAXS results for TEOS(60)-PTMO(2K)-100-0.048 ceramers reacted in DMF/IPA and cast onto teflon and PS petri dishes.

ceramers cast in polystyrene) which consequently allows for a greater extent of reaction and densification in the inorganic phase as indicated by the higher scattering intensity in the SAXS profiles. The result of this increased phase separation between inorganic and PTMO components and the consequent extension of the oligomeric chains in the system (as computed from the dielectric spectra) is an improvement in the mechanical properties, especially the elastic modulus. This however, will not be detailed in this chapter.

An extension of this reasoning can be therefore applied to the less phase separated systems such as the TEOS/PTMO ceramers reacted in THF/IPA and may help explain some of their mechanical properties. These TEOS/PTMO ceramer systems (reacted in THF/IPA) which have been previously described in chapter 5 have lower elastic modulii than their counterparts reacted in DMF/IPA. Their SAXS scattering profiles are much broader, the peak scattering intensity much lower and the interdomain spacing much smaller for the TEOS/PTMO components reacted in THF/IPA. The increased mixing between inorganic and oligomeric components in these (THF/IPA) systems and the fact that the inorganic phase in these ceramers is more ramified combine to allow the PTMO chains dimensions to be much smaller than than they are in their in the pure state. Thus when these chains are stretched in a tensile test the unravelling of these more coiled PTMO chains produce a lower elastic modulus and a higher elongation at break than the same ceramer produced in DMF/IPA where the oligomer chains are in a more extended conformation.

7.4.2 EFFECT OF SOLVENT ON THE CHAIN DIMENSIONS

For the dielectric storage spectra shown in Figs 7.12 and 7.14, a similar computational analysis outlined in equations (1), (2) and (3) was performed in order to gain a measure of the PTMO chain dimensions. These dielectric spectra in Figs 7.12 and 7.14 are for TEOS/PTMO ceramer films produced in THF/IPA and DMF/IPA repectively. The results are tabulated in Table 7.3 and show that the PTMO chain dimensions i. e. $<R_g>$ in the system reacted in THF/IPA are smaller than those for pure endcapped crosslinked PTMO (shown in Table 2). The PTMO dimensions shown for the TEOS/PTMO ceramers reacted in DMF/IPA are larger than those reacted in THF/IPA. The repeat units of the PTMO chain in its free unpeturbed state prefer the trans conformation (106, 107). In the more phase separated ceramers these repeat units of the PTMO chains are predominantly in the trans conformations as a result of chain extension during the process of adhesion to the substrate.

In the TEOS/PTMO ceramers reacted in THF/IPA the more open growth of the inorganic phase (the silicate chains are believed to be more linear in these systems as against the systems reacted in DMF/IPA where the silicate phase growth is believed to be more particulate like) produces a large number of adjacent (SiOH) sites to which the PTMO chains can be reacted to. Further these systems are known to be more mixed than their counterparts reacted in THF/IPA. The extensive mixing between the silicate and the PTMO components

Table 7.3. Radius of gyration, chain end to end distances and interdomain spacings as measured for the TEOS/PTMO ceramers.

Cosolvent system	$<R_g>$ Å	<R> Å	d Å
THF/IPA	13	33	106
DMF/IPA	41	101	142

in this ceramer system can force the oligomer chains to exist in a higher energy state than the trans conformation. This is because the silicate species in the ceramer is typically vitrified (as compared with the oligomer which is in the rubbery state) and can therefore serve as a template for the PTMO chains. Thus the repeat units of the PTMO chains in these ceramers have a greater probability of being in the gauche conformation (which is a higher energy state) than in the trans state. This would cause the PTMO chains to have lower end to end distances. The interdomain spacings for these ceramers as measured from SAXS is also lower than those measured for the TEOS/PTMO ceramers reacted in DMF/IPA as detailed earlier in chapters 4 and 5.

7.5 SUMMARY AND CONCLUSIONS

The dielectric spectroscopy certainly shows some very interesting features in these ceramers systems, not clearly understood before these experiments were performed. One such feature is the Maxwell Wagner Sillars behavior seen in all the more phase separated ceramers such as the TiOPr/PTMO, ZrOPr/PTMO and TEOS/PTMO ceramers reacted in DMF/IPA. This behavior is due to interfacial polarization in these systems and the existance of bimodal behavior in the MWS relaxations first gave the author a hint of the possible existance of porosity in the inorganic phase. This porosity which exists at low metal alkoxide concentrations of 40 wt% in these ceramers will be further discussed in the next chapter. It introduces the concept of a three phase system i. e. one containing metal oxide, PTMO and air.

The MWS behavior is found to be dependent upon the amount of phase separation in these ceramer systems. The more mixed systems do not show any MWS relaxation while for a given metal alkoxide content the intensity and breadth of the MWS behavior can be seen to increase with the the amount of phase separation in these ceramers. The MWS behavior typically manifests itself between 0°C and 100°C at lower frequencies. It is reduced in intensity at the higher frequencies. Further it does not shift to higher temperatures with increasing frequencies; behavior typically shown by the PTMO component in these systems. As seen with the TEOS/PTMO ceramer reacted in IPA, the

intensity of the MWS relaxation can be reduced with age or by annealing to higher temperatures.

The MWS behavior is metal alkoxide dependent and the intensity, shape and position of these relaxations are unique to each metal alkoxide. For a particular metal alkoxide the intensity of the MWS relaxation is dependent upon the initial metal alkoxide content in the ceramer formulation. The intensity of relaxation may be related to the reactivity of the metal alkoxide or the amount of water used in the initial reaction. It decreases with the reactivity of the metal alkoxide and typically increases with the amount of water used in a ceramer system.

From the computations performed on the dielectric storage spectra it can be seen that the PTMO chain dimensions expand with increasing metal alkoxide content when there is adhesion of the ceramer to the casting substrate. The increased chain dimensions are a result of less mixing between the inorganic and PTMO components which consequently improves mechanical properties of the ceramer by two means: a) a lower amount of mixing between two components permits for a greater densification of the inorganic phase because of less steric hindrance to the reacting inorganic. b) the extended PTMO chains seen in the more phase separated systems are in extended conformations and thus cannot be uncoiled during a tensile test and hence the mechanical properties are improved. In the less phase separated systems there is a greater amount of mixing which causes the oligomer chains to be

more coiled thereby producing lower elastic modulus. This is partly due to an unravelling of the PTMO chains during a tensile test.

CHAPTER 8

STRUCTURAL INVESTIGATIONS INTO CERAMERS DURING THE PROCESS OF GELATION

8.1 INTRODUCTION

Since the inception of the ceramer project almost six years ago, a wide variety of these novel hybrid inorganic organic networks have been produced and studied. The variations spawned in these ceramer materials, especially in the latter years, come primarily by changing one or more of the constitutive

components in any formulation. Changes in the metal alkoxide from TEOS to titanium isopropoxide to zirconium isopropoxide to aluminum secondary butoxide have been made, while at the same time the oligomeric component has been varied from hydroxyl terminated polydimethylsiloxane to isocyanatopropyltriethoxysilane endcapped polytetramethylene oxide, polyetherketone, polysulfone and polyimide. Through all these changes the morphological model proposed by Huang (84) has been quite successfully applied to these ceramer systems. While this model can be used qualitatively to successfully explain some of the structural features (as seen from SAXS only) of these ceramer systems, certain questions remain about other characteristics, especially mechanical properties displayed by these materials. For example, the TEOS/PTMO materials reacted in DMF/IPA as well as the TiOPr/PTMO ceramer systems reacted in IPA both display almost similar dynamic mechanical behavior but their SAXS scattering profiles are very different. The ceramer reacted in DMF/IPA shows a scattering profile with a rather sharp interference peak while the scattering profile for the TiOPr/PTMO ceramer is very broad suggesting a large distribution in interdomain spacings or sizes. Similarly, in the stress strain tests, the TiOPr/PTMO ceramers containing 60 wt% TiOPr show yield behavior while the 60 wt% TEOS/PTMO system reacted in DMF/IPA does not. This is but one of a large number of examples where the morphological model is inadequate and cannot account for distinctions and differences in behavior displayed by the various ceramer systems.

While the morphological model explains some of the general features of these ceramers, it does not give the reader any idea about the nature of the inorganic phase and the interaction of this phase with the organic component in the various ceramers. The growth of the inorganic phase and its interaction with the PTMO component is of vital importance in understanding the different mechanical properties displayed by these various ceramers. The experimental work described in this chapter is therefore focussed on developing a greater understanding of:

a) The nature of growth of the inorganic phase in some of these ceramer systems. This will be monitored using SAXS.

b) The phase separation characteristics of the inorganic component and PTMO component.

Some of the factors which influence this aspect in the various ceramers will be discussed. As will be seen, it is the nature of growth of the inorganic component which influence the phase separation characteristics in these ceramers.

Data obtained from SAXS and backscattered SEM will be used to qualitatively point out to some trends which may eventually help with the development of new ideas, means and ways to help gain some better understanding of the problem.

Only three ceramer materials were studied in order gain an understanding of the questions posed by sections (a) and (b) above. These three ceramers were TEOS/PTMO reacted in THF/IPA, TEOS/PTMO reacted in DMF/IPA and the TiOPr/PTMO ceramer reacted in IPA. Various metal alkoxide/PTMO compositions will be studied in each of the three ceramer systems. The reasons for choosing these three ceramers systems for further study is because the TEOS/PTMO system reacted in THF/IPA is known to be more phase mixed while the same system reacted in DMF/IPA is more phase separated. The TiOPr/PTMO ceramers show some phase separation in the DMA but as explained above, the SAXS profile is analogous to that displayed by the TEOS/PTMO ceramer reacted in THF/IPA.

8.2 FRACTALS: A BRIEF DISCUSSION ON THEIR FORM, SHAPE AND SIZE

It has been previously shown (65) that when the metal alkoxide tetraethylorthosilicate (TEOS) is reacted via the sol gel technique (no functionalized organic present), the resultant silicate particles display fractal behavior i. e. they display self similarity at different levels of magnification. The details of the fractal analysis on silicate particles (developed from acid and base catalyzed TEOS) from SAXS data have been provided by Brinker et

al (65). In the context of fractal behavior displayed by such silicate particles Brinker et al have stated that the acid catalysed systems display mass fractal behavior while species produced in a base catalysed reaction of TEOS are generally more colloidal and display surface fractal behavior. Fractal dimensions can be obtained from the slope in the Porod region of the SAXS profiles when the data are plotted in the form of log I(s) vs log s as seen in Fig 8.1; s being defined as $(2/\lambda)\sin\theta$ where θ is one half of the radial scattering angle and λ is the wavelength. Mass fractals have the property that the mass M varies as a power of the characteristic length or size i.e. $M \propto (length)^D$, D being the fractal dimension. Mass fractal dimensions are always less than the dimension of the space in which the fractal exists which implies that the mass of the particulate increases less rapidly than the volume it occupies (112). For mass fractals the Porod slope, x, is related to D as x = -D. Mass fractal structures therefore yield Porod slopes (x values) between -1 and -3 when the incident beam is of point geometry while for slit smeared intensity, the slopes for mass fractals lie between 0 and -2 because of the smearing effect (113). Fractal surfaces on the other hand have the property that the surface area S, varies as a non integer power of the length $S \propto (length)^{(D_s)}$, D_s being the surface fractal dimension. Fractal surfaces are characterized by a Porod slope x = $D_s - 6$. Surface fractals dimensions must therefore lie in the range of one less than the spatial dimensionality of the scattering unit up to the spatial dimensionality. Thus for surface fractals, data obtained from a pin hole collimation (point source) geometry will yield a Porod slope between -3 and -4

while after correction for slit smearing it will yield a slope between -2 and -3. Martin and Hurd (114) have also stated that in order for any material to display fractal behavior it must display a single slope in the Porod region over one decade of 's'. However in this chapter it will be seen that for the ceramers which display surface fractal behavior, this is not always the case and in some instances fractal dimensions were extracted from slopes extending over half a decade of 's'.

It should be noted that since all the data presented in this chapter were obtained in the infinite slit configuration, the slopes reported have been corrected to that which would be obtained from a point source by adding a factor of -1 to each slope. As shown by Brinker, both types of fractal structures are possible for silicate polymers. Therefore, in order to study the development and structure of the inorganic particles in these ceramer systems SAXS measurements were made on selected ceramer materials during gelation. These results were then analysed to determine the fractal dimensions as well as the radius of gyration of the dispersed inorganic particles. The radius of gyration is estimated in the Guinier region (116), shown in Fig 8.1 above. Guinier (117) showed that for a dilute monodisperse system in which the particles assume all orientations with equal probability the scattered intensity can be described by a series expansion as follows:

$$I(s) = I(0)\{1 - \frac{(S^2R^2)}{3} + ...\} \qquad (1)$$

The function I(0) is the intensity scattered at zero angle, which is proportional to the total number of electrons in the system irradiated, and R is the electronic radius of gyration, which is the root mean square of the distances of all the electrons from the electronic center of gravity of the representative particle.

When Guinier's law is actually obeyed by a system of scattering particles, then a plot of LN I(s) vs s^2 should yield a straight line over a significant scattering angle. However, this may not always be the case when the scattering particles are not monodisperse. The tangent to such a non-linear scattering profile as s^2 tends to zero angle is then taken as a measure of the mean radius of gyration of the scattering particles (115).

8.3 EXPERIMENTAL

The methodology of preparation of the TEOS/PTMO ceramers reacted in DMF/IPA and the TEOS/PTMO ceramers reacted in THF/IPA as well as the TiOPr/PTMO materials has been discussed previously in chapters 4, 5, and 6 respectively and hence will not be discussed once again. All these materials were cast into either polystyrene petri dishes and allowed to gel at room temperature under ambient conditions. When the materials were gelled i. e.

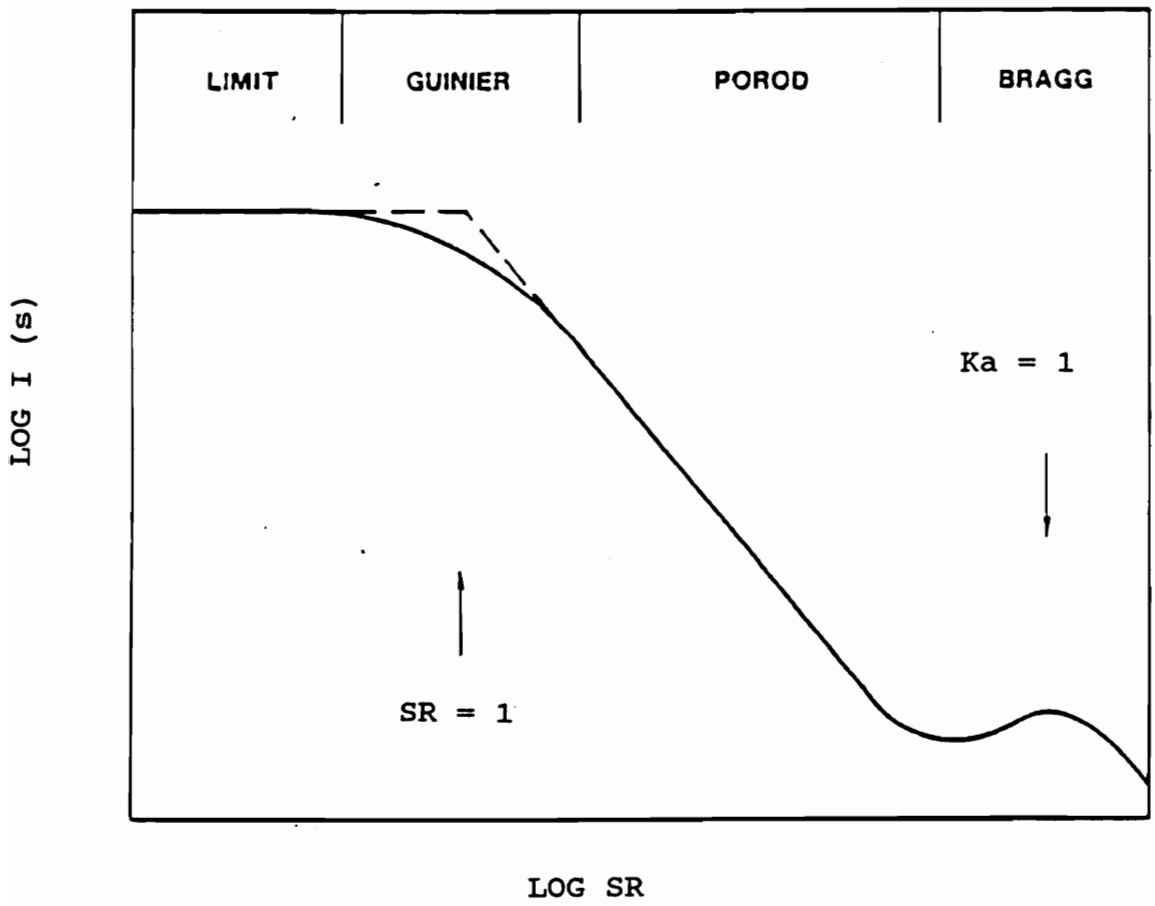


Figure 8.1. Schematic small angle xray scattering curve when plotted on log-log scales.

they ceased to flow, they were subjected to SAXS. However, even at this stage, they were too tacky and could not be handled. Hence they were examined by SAXS on the polystyrene substrate itself. The polystyrene which is amorphous scatters at the higher angles (at $s > 0.4$) and this scattering was later subtracted from the scattering profile of the gelling ceramer before analysis.

The time taken by the various ceramers to reach the point where they do not flow anymore depends upon the nature of the solvent used in the case of the TEOS/PTMO ceramer systems and the amount of solvent used in the case of the TiOPr/PTMO ceramers. Thus for the TEOS/PTMO ceramers reacted in DMF/IPA, after about 30 minutes it was possible to obtain a scattering profile while for the film reacted in THF/IPA it usually took a minimum of about two hours. For the TiOPr/PTMO ceramers, the minimum time for gelation to reach a stage where the network did not flow was approximately 6 hours.

8.4 RESULTS AND DISCUSSION

8.4.1 NATURE OF GROWTH OF THE SILICATE PHASES

8.4.1.1 TEOS/PTMO CERAMERS REACTED IN DMF/IPA

Various composition ratios of TEOS/PTMO were prepared ranging from 10 wt% TEOS to 100 wt% TEOS in steps of 10%. However, for this study on the nature of the inorganic component only the scattering behavior of the TEOS/PTMO gels containing 20wt%, 40wt% and 60wt% metal alkoxide will be described. Successive scans were made on the gel at 30 minutes, 2 hours, 12 hours, 1 day and 2 days. In some cases measurements were made after 2 weeks. As stated above the scattering profiles were then plotted on log I(s) versus log s plots (henceforth simply referred to as log-log plots) and the Porod region was analysed for trends in the fractal dimensions as well as on Log I vs s^2 plots (in the Guinier region) for trends in the radius of gyration.

The SAXS profiles TEOS/PTMO ceramer containing 20 wt% TEOS are displayed in Fig 8.2 on a plot of absolute Intensity vs s. This plot shows that with time the absolute scattering intensity at the peak position is increased from approximately 7 to 35 while the d spacing is decreased from 108Å to 78Å. The increased scattering intensity is a reflection of the increased reaction and

densification within the inorganic phase as well as increased phase separation between the inorganic and the PTMO components while the decrease in the d spacing reflects a contraction in the oligomer chains as the solvents which have swelled them evaporate from the film.

In the last chapter it was shown that the possibility existed for chain expansion in the more phase ceramers cast onto polystyrene. When the TEOS/PTMO reactants in DMF/IPA are cast in the polystyrene, the bottom layer of the forming ceramer film adheres to the surface of the petri dish. As the material begins to react and more of the sol is converted to a gel, the network tightens. At the same time the solvent evaporates from the network (IPA first and then DMF since the b. p. of the DMF is higher), thereby reducing the amount of swelling of the oligomer chains within the network. The PTMO chains thus begin to contract which causes the interdomain spacing (as measured from SAXS) to decrease with time. The amount of decrease in the interdomain spacing with time is dependent upon the PTMO content in the original ceramer composition as well as the thickness of the film.

Ceramers containing a greater PTMO content (60 - 100 wt%) in the initial composition show a greater tendency to undergo such chain shrinkage with consequent reduction in the measured interdomain spacing. This is because a larger percentage of shrinking PTMO chains within the ceramer impose a greater contractile force on the entire film causing it to reduce in diameter from the dimensions of the polystyrene petri dish into which it was cast. The

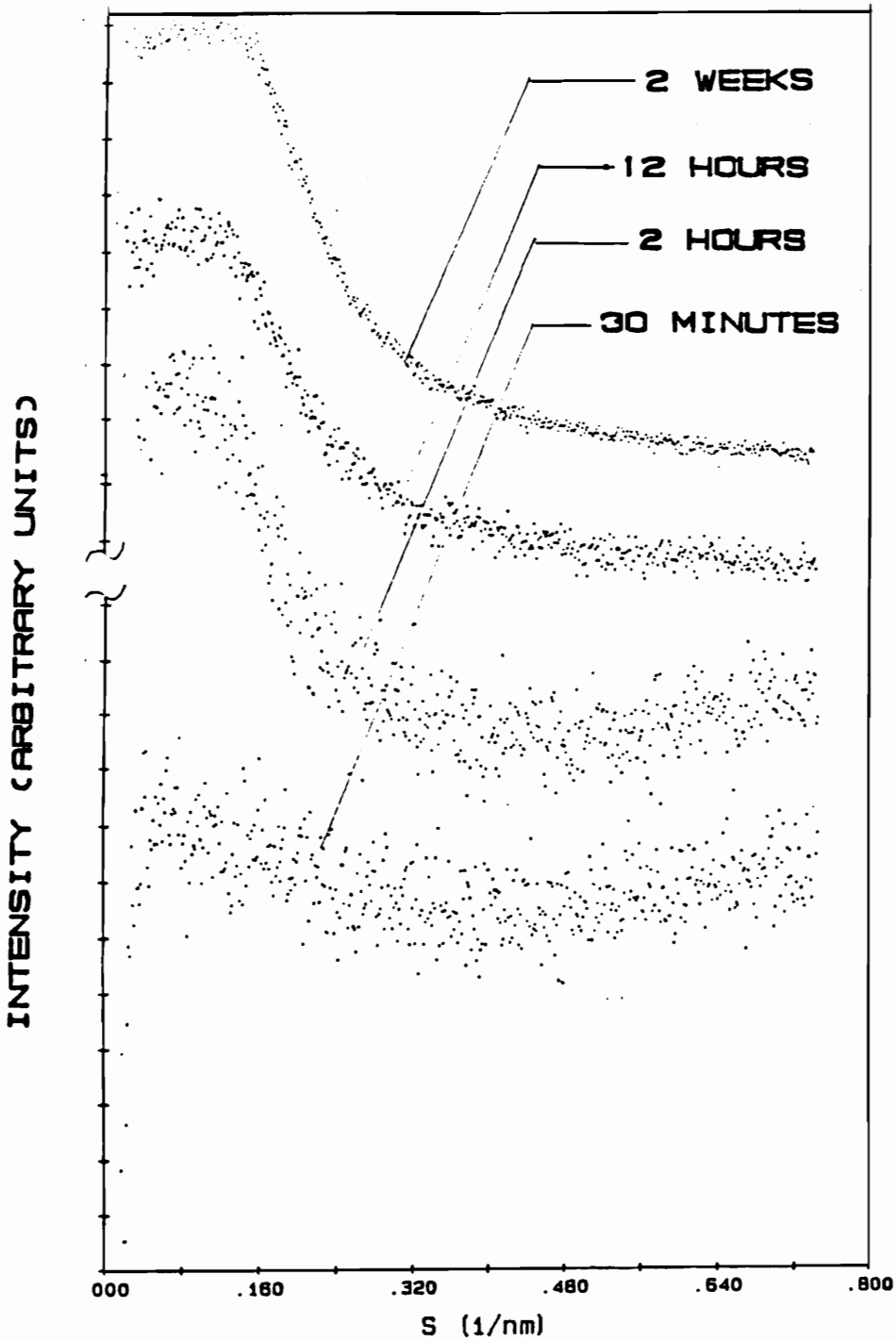


Figure 8.2. SAXS curves obtained from the TEOS(20)-PTMO(2K)-100-0.048 ceramers as a function of gelation time.

greater the PTMO content in the ceramer, the greater this reduction in diameter of the final film. This reduction in the diameter is as stated above, dependent upon the film thickness too. Thicker films cast onto polystyrene show a greater tendency to shrink than the thinner films. This is because while the bottom surface of the film adheres to the polystyrene the upper surface of the film is unhindered and consequently has a greater levity to shrink thus placing a radial stress on the film as shown in the Fig 8.3. This radial stress causes the thicker films of TEOS/PTMO (films greater than 10 mils) cast onto polystyrene to fracture during the process of gelation. In order to overcome this detrimental effect and produce monolithic thick films or even large bodies/structures of these ceramers the sol has to be cast onto a Teflon substrate or into teflon molds. This has important implication for the coating aspect of these ceramer systems where the thinner films would be expected to perform better than thicker ones because of the above mentioned effect, which is that the thinner films have higher elastic modulii than the thicker ones.

As stated above, evaporation of the IPA from the gelling TEOS/PTMO ceramer takes place before the evaporation of DMF because of the lower boiling point of IPA. This feature causes an increase in the phase separation of the PTMO from the inorganic component, since the remaining DMF drives the separation of these two components as documented in chapter 4. This phase separation behavior causes the scattering intensity at the peak position during the curing

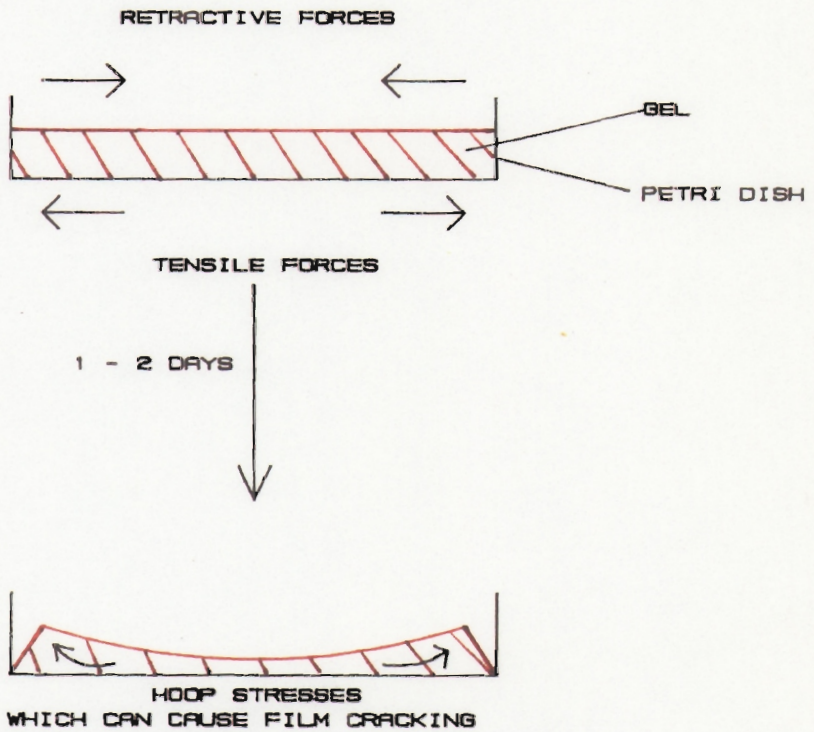


Figure 8.3. Stresses developed in the ceramer films cast onto substrates onto which they adhere.

process to increase as can be seen in the Fig 8.2. As stated earlier the scattering peak is produced by interparticle interference within the system.

In the introduction it was stated that one of the main aims of this work and hence of this chapter was to study the development of inorganic phase in these ceramers. In order to do this, the scattering profiles shown in Fig 8.2 were plotted in the form of a log I(s) vs log s plot as displayed in Fig 8.4. The slope of the scattering profile in the Porod region can be utilized to obtain an idea about the fractal dimensions of the inorganic component in these materials. As stated above the occurence of an interparticle interference peak in these ceramer systems may in some way influence the slope of the Porod plot which may cause these dimensions to be somewhat inaccurate. Nevertheless all scattering profiles plotted on log-log plots in this chapter should be considered for the trends they provide and indeed some useful information can be extracted from these trends.

From the log-log plot seen in Fig 8.4 for the TEOS(20)-PTMO(2K)-100-0.048 ceramer reacted in DMF/IPA, the Porod slope at 30 minutes is initially -1.28 which indicates that the mass of the scattering object may scale almost linearly with its length. This could be true only if the objects were very stiff (as in a liquid crystalline polymer) or if the length of the scattering object was very small i. e. one to two repeat units. Since these Si-O-Si linkages are typically not very stiff the only possibility is that the scattering may be produced by small objects of the size two to three repeat units in length. The radius of

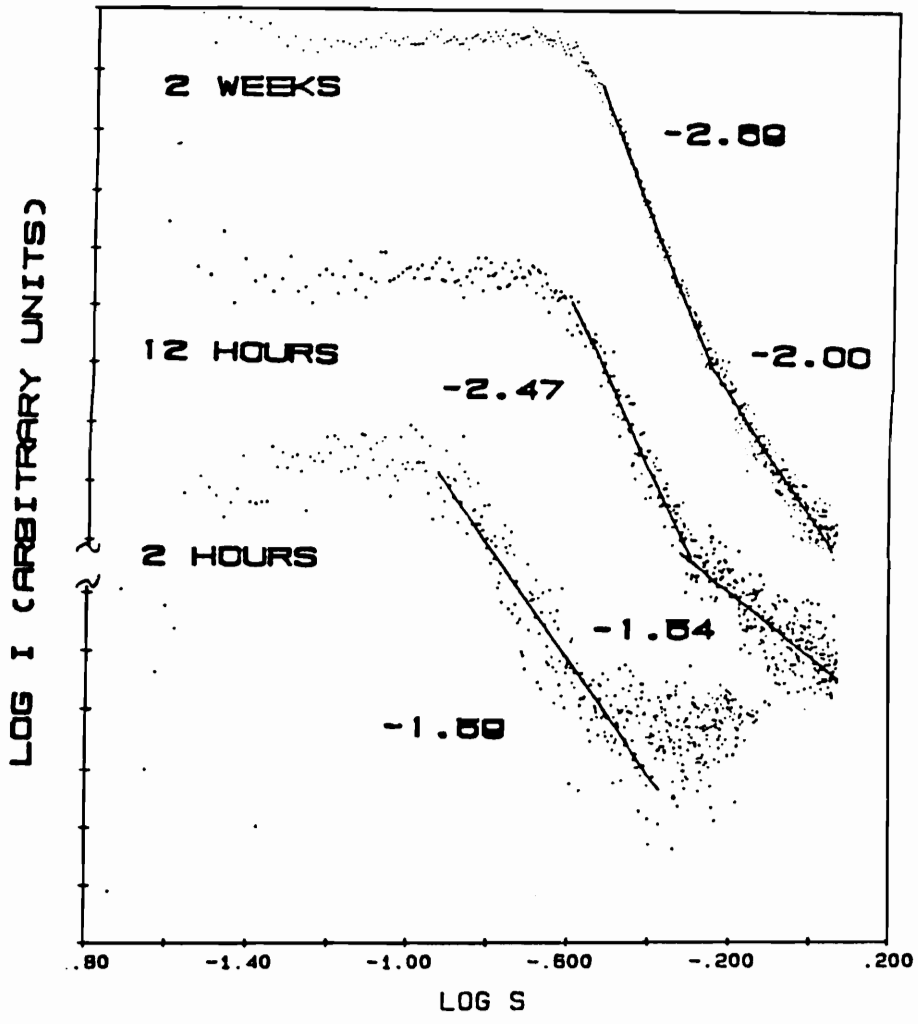


Figure 8.4. Scattering profiles for the TEOS(20)-PTMO(2K)-100-0.048 ceramer plotted on a log-log plot.

gyration as computed for these 20 wt% TEOS/PTMO ceramer systems with time is shown in Fig 8.5. At 30 minutes the measured electronic radius of gyration $<R_g>$ is approximately 6Å which corresponds very well with the assumption that the scattering particles are of the size of two or three repeat units.

At two hours the Porod slope as seen in Fig 8.4 is -1.59 and the radius of gyration is increased to around 10Å The fractal dimension of 1.59 indicates that these scattering particles are mass fractals. These results indicate that as the scattering silicate particles in this TEOS/PTMO ceramer grow larger they become more convoluted. At 12 hours the Porod plot displays two slopes in the Porod region, one at smaller angles having a value of -2.4 and the other having a value of-1.54. The radius of gyration is now increased to 12Å as seen from Fig 8.5. The existance of a larger Porod dimension at the smaller angles indicates that as phase separation between the inorganic and the PTMO in these ceramer systems increases, the scattering particles located at the PTMO chain ends become more convoluted. These silicate particles at the smaller scattering angles will hence forth be referred to as primary scattering particles.

After two weeks the Porod plot still possesses two slopes, the one at lower angles is approximately -2.69 while the one at lower angles is approximately -1.7. The radius of gyration is now 11.5Å This indicates that after a period of time these scattering silicate particles densify so that their radius of gyration

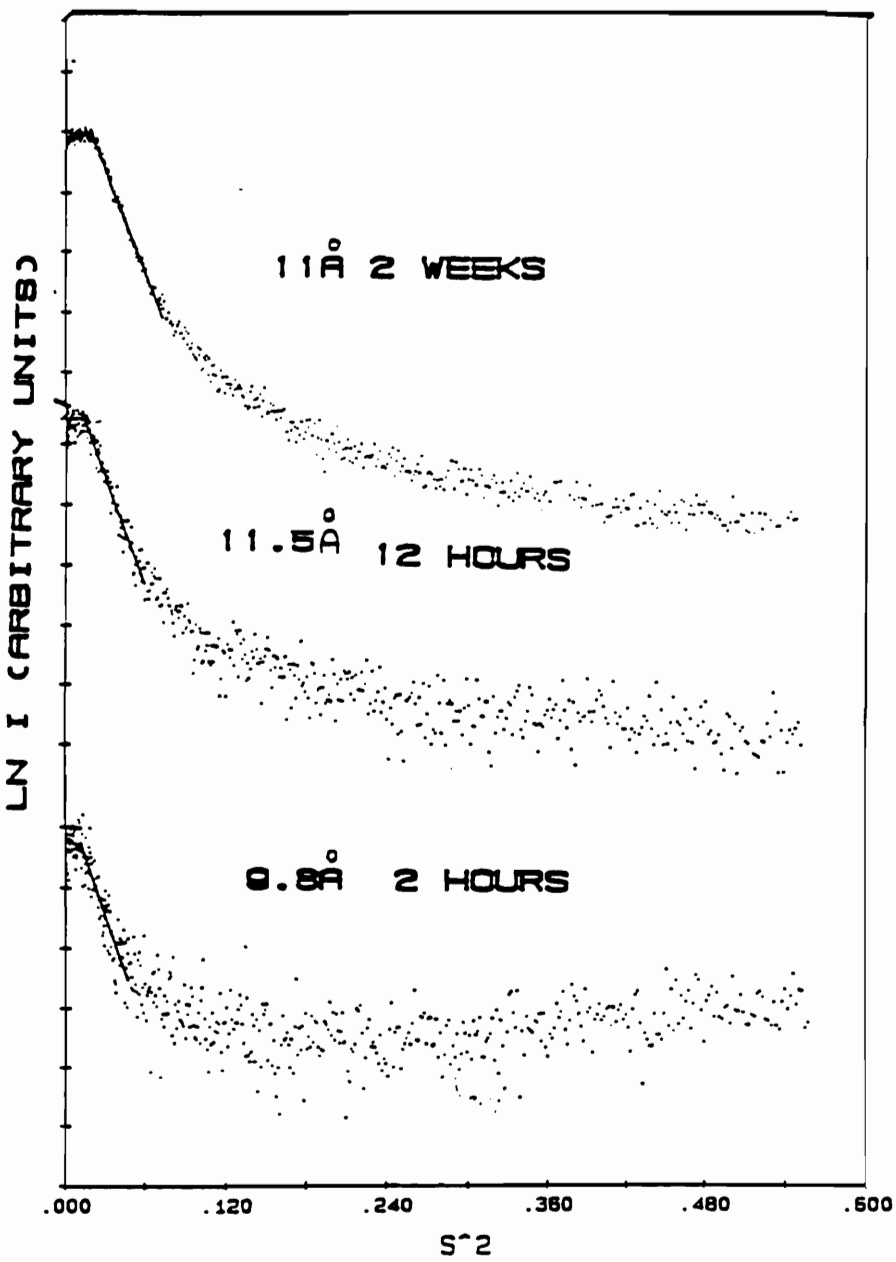


Figure 8.5. Radius of gyration as measured for the TEOS(20)-PTMO(2K)-100-0.048 ceramer plotted from a Log I vs S^2 plot.

decreases while at the same time the Porod slope at the smaller angles decreases. The decrease in the Porod slope (at the smaller angles) from -2.4 after 12 hours to -2.69 after 2 weeks may indicate that additional reaction has occurred in the primary silicate particles located at the chain ends. The decrease in the value of the Porod slope at the larger angles from -1.54 to -1.69 may indicate that some of the particles are physically trapped in the network thus providing for a more mixed system. Such particles which show scattering behavior at the higher scattering angles will hence forth be called secondary scattering particles. This phenomenon i. e. the development of a higher dimensionality at higher angles would be expected since systems containing larger PTMO contents (60-100 wt% initially) would quickly develop into a high molecular weight (because of the reacting PTMO) networks which would limit diffusion of these secondary silicate particles through them.

The increase in the size of the primary scattering particles at the expense of the secondary scatterers is a phenomenon typical of nucleation and growth. In these TEOS/PTMO ceramers reacted in DMF/IPA, the nucleating sites are the endcapped PTMO chain ends. Once these nucleii are formed, the system decomposes with a decrease in the free energy, and the nucleii grow in size. As the smaller secondary silicate species are transported to the nucleating centers they continue reacting with other species that they encounter along the way and hence they grow in size and also become more convoluted.

Meakin attributed the existance of self similarity in these silicate clusters to three key elements describing their growth processes (117). They are a) the nature of the reactants (either monomers and clusters - defined here as oligomers or polymers) b) their trajectories (Brownian or ballistic) and c) the relative rates of reaction and transport (diffusion or reaction limited conditions). Depending upon conditions, growth in silicate systems, may occur by the condensation of monomers with growing clusters or by the condensation reactions between clusters and other clusters. These two types of growth processes are identified as monomer-cluster and cluster-cluster growth processes. Monomer cluster growth processes may be either diffusion limited or reaction limited. Monomer-cluster growth requires a continual supply of monomers (65). Kelts, Effinger and Melpolder (118) have used ^{29}Si NMR to show that even at $t/t_g = 0.9$ (where t_g is the total time to gel) substantial concentrations of monomers exist in the reaction mixture for TEOS derived silicates when prepared at pH's between 5 and 7. It appears that the development of two slopes in the scattering profile (log- log plot) for this TEOS/PTMO ceramer system is due more to monomer-cluster type of growth. In other words monomers may be added to the primary silicate clusters growing at the nucleation sites (the pH for these TEOS/PTMO ceramers reacted in DMF/IPA is also around 5 as determined using litmus paper). This feature i. e. the addition of monomer to clusters is even more prominent in these TEOS/PTMO ceramers containing 60wt% and higher metal alkoxide contents as will be seen shortly.

As stated above monomer-cluster growth may be either diffusion limited or reaction limited. The diffusion limited monomer cluster aggregation model (DLMCA) model is so called because of the Brownian trajectories taken by the monomer as it approaches the cluster. This has nothing to do with the "diffusion limitation" term used in these TEOS/PTMO ceramers (reacted in DMF/IPA) containing high weight fractions of PTMO. In this model, the monomer sticks with the cluster on first contact. Growth in these systems occurs at mostly the exterior sites of the growing silicate species resulting in mass fractal (d_f = 2.45) objects whose density decreases radially from the center of mass. The reaction limited monomer-cluster aggregation model (RLMCA) is distinguished from DLMCA in that there is a barrier to bond formation. The effect of this barrier is to reduce the "sticking" probability (condensation rate), so that many collisions are required between monomer and cluster to form a bond. Since all possible reaction sites on the cluster are accessed with equal probability, this model leads to compact, smooth "Eden" clusters with d_f = 3 = dimension of space. As will be seen these TEOS/PTMO systems reacted in DMF/IPA are believed to produce smooth particulates as the weight fraction of TEOS is increased in these systems. Thus the silicate particulates in these systems may possibly be the result of reaction limited monomer-cluster growth.

Another factor to be taken into consideration in the more phase separated ceramer systems (TiOPr/PTMO and TEOS/PTMO reacted in DMF/IPA) is that the higher the weight fraction of PTMO (of a given molecular weight) in the

original ceramer composition the greater is the number of chain ends to which these silicate particles can migrate to. This would lead to a larger number of nucleation sites (in those materials containing a larger weight fraction of PTMO) which would cause the formation of a larger number of scattering particles of a smaller size. As the weight fraction of PTMO is decreased (the weight percent TEOS increases) the number of chain ends is reduced; thus there will be a smaller number of larger sized scattering particles.

The scattering profiles for the TEOS(40)-PTMO(2K)-100-0.048 ceramers reacted in DMF/IPA are presented in Fig 8.6. As in the 20 wt% TEOS/PTMO ceramer system, here too the scattering intensity at the peak position can be seen to increase with time. The interdomain spacing as measured from the peak position also decreases from 119Å (10 hours after casting) to 105Å (1 day after casting). The scattering profiles for the TEOS(40)-PTMO(2K)-100-0.048 ceramer shows no peak at 30 minutes and 2 hours after gelation. These scattering profiles appear more like profiles obtained from solution scattering. At 12 hours an interparticle interference peak appears in the scattering profile with an absolute intensity of 45. The intensity at the peak position increases to approximately 60 after 1 day (not shown in Fig 8.6) and further increases to around 120 after 2 weeks. This increase in the scattering intensity is typically associated with densification in the inorganic component in these ceramer systems. However, during the process of gelation it is better related to increased phase separation between the inorganic and the organic component in the ceramer.

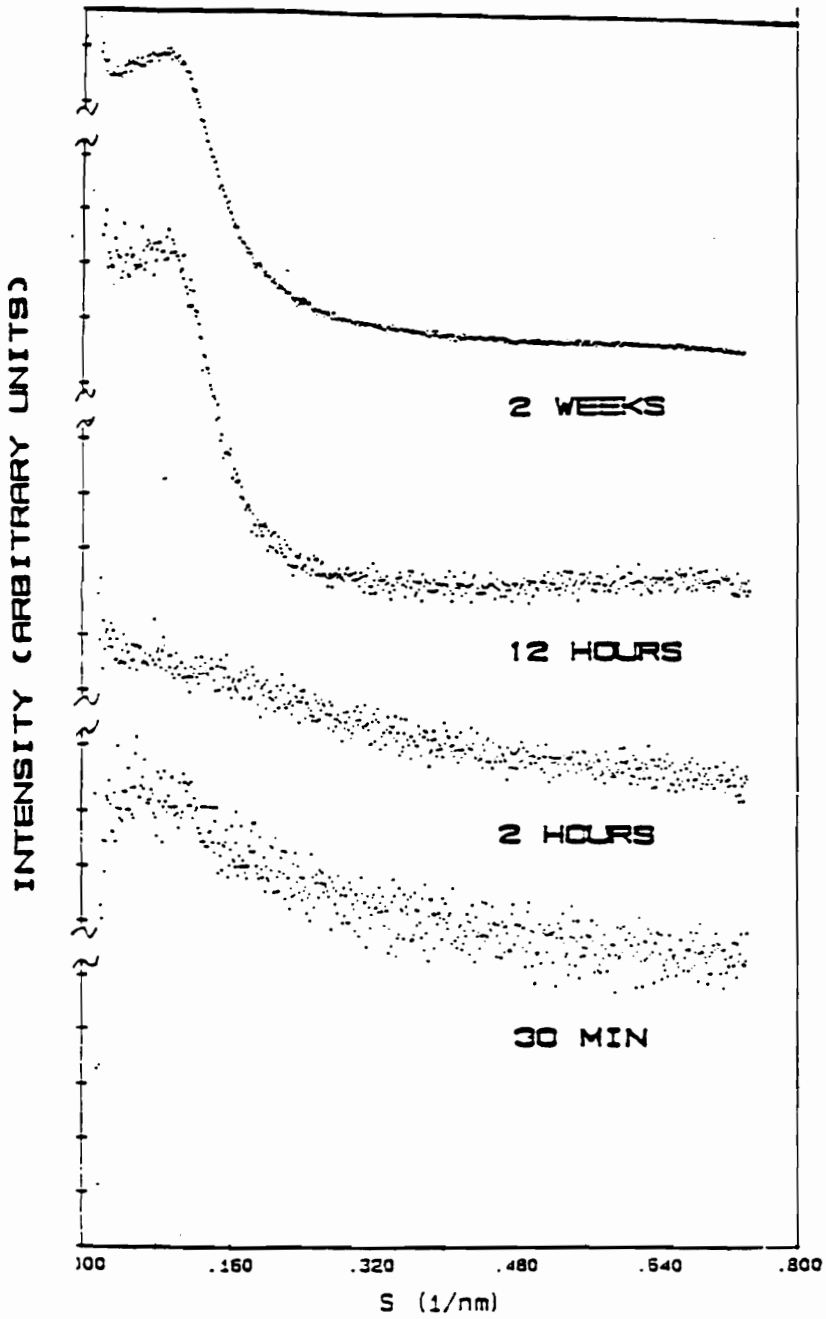


Figure 8.6. SAXS profiles measured for the TEOS(40)-PTMO(2K)-100-0.048 ceramer as a function of time.

The scattering profiles are plotted on a log-log plot in Fig 8.7 from which fractal dimensions for the silicate particles were measured. As can be seen from this figure the fractal dimensions measured after 30 minutes and 2 hours are both around 1.3 which again indicates that the scattering particles are very small i. e. of the size of two to three repeat units. After 12 hours and the appearance of an interparticle interference peak in the scattering profile as seen in Fig 8.6, there appear two slopes in the log-log plot in Fig 8.7. The slope at the lower scattering angle for the 40 wt% ceramer after 12 hours is approximately -2.3 while the slope at the higher scattering angle is -1.3. The measured radius of gyration at this time is around 12Å. At 1 day the slope at the smaller scattering angles is -2.95 while the slope at the higher scattering angles which corresponds to the secondary silicate particles is -2.30. The meausured radius of gyration after 1 day is 18.30Å Finally in the measurements taken after 2 weeks (Fig 8.7) for the slope at the smaller scattering angles is -3.14 while for the slope at the higher scattering angles it is still -2.30. The radius of gyration is now 17.30Å Thus, again there occurs a decrease in the radius of gyration of the scattering particles as measured from SAXS as can be seen in the Guinier plot in Fig 8.8. It should be noted that in all cases the decrease in the measured radius of gyration coincides with a tremendous increase in the scattering intensity at the peak position. In the case of the TEOS(40)-PTMO(2K)-100-0.048 ceramers reacted in DMF/IPA this increase in the absolute scattering intensity is almost 100% (from 60 at 1 day to 120 after 2 weeks). Further it may be seen that the dimensionality of the primary

scattering particles for the 40 wt% TEOS/PTMO ceramers indicates that these particles may be surface fractals, while those at higher angles i. e. the secondary particles may be mass fractals.

The two materials described above i. e. 20 and 40 wt% TEOS/PTMO ceramers show some similar features during their development from gels to films. For each ceramer material, two slopes were finally seen to exist in the log-log plots. The presence of two slopes is a feature that develops with time i.e. 10 hours to 1 day after casting of the reactants into the petri dish. Both slopes (those at higher angles as well as those at lower angles) indicate that the dimensionality of the scattering particles increases with time. The radius of gyration of the primary silicate particles increases with time initially but later decreases slightly as possible densification within the inorganic component occurs. The increase in the dimensionality of the primary scattering particles indicates that these particles become more convoluted with time. One difference that occurs between the particulates in the TEOS(20)-PTMO(2K)-100-0.048 and those seen in the TEOS(40)-PTMO(2K)-100-0.048 material is that those in the lower metal alkoxide content ceramer may be mass fractals while those in the 40 wt% ceramer display surface fractal behavior. All the TEOS/PTMO ceramers reacted in DMF/IPA, containing weight fractions of TEOS greater than 50 wt% display such surface fractal behavior. An explanation of this feature may be attempted on the basis of results generated by Keefer (112) who studied the growth of Eden clusters via computer modelling. Keefer simulated the growth

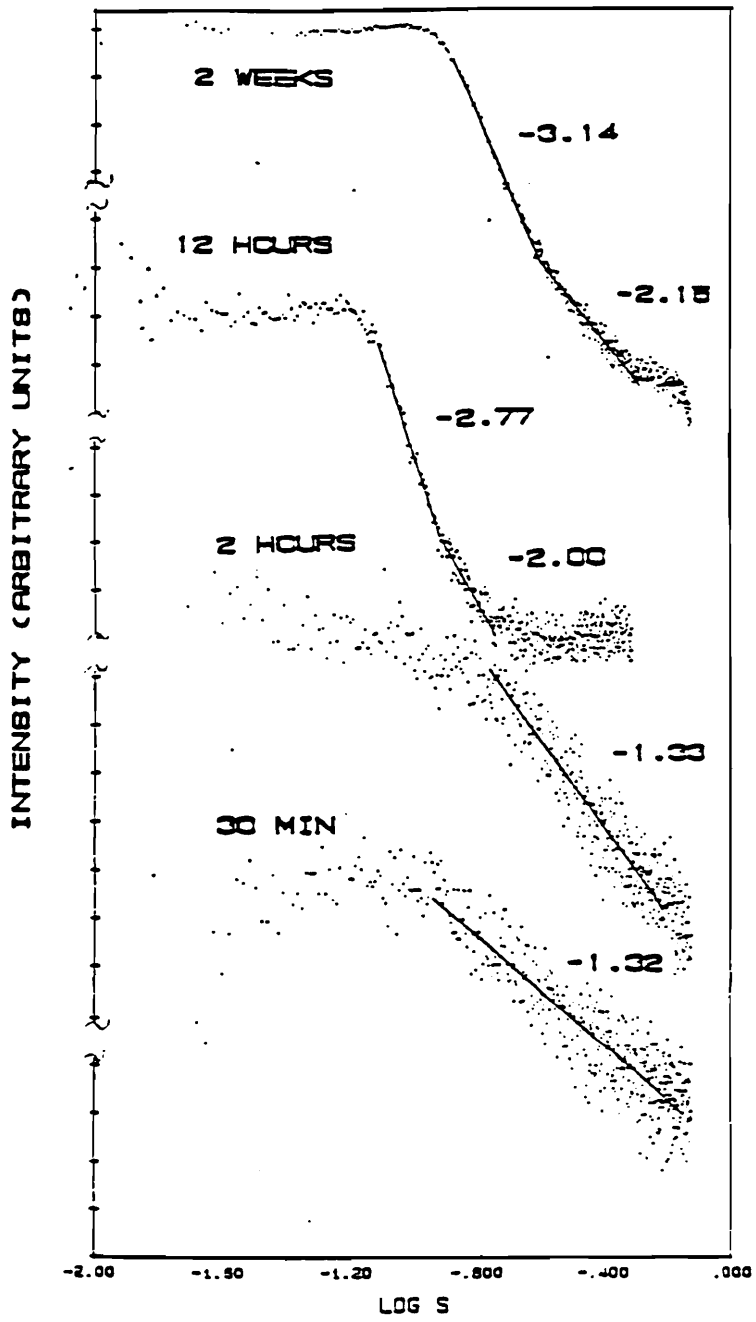


Figure 8.7. SAXS profiles measured for the TEOS(40)-PTMO(2K)-100-0.048 ceramer on a log-log plot.

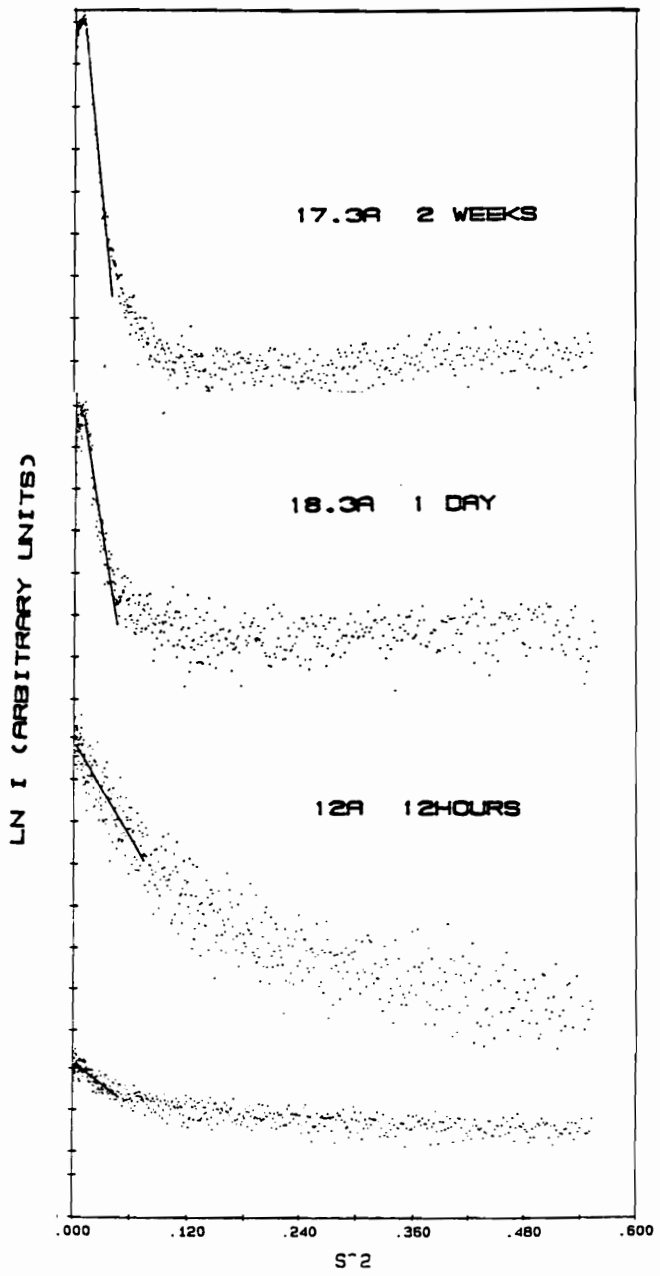


Figure 8.8. Guinier plot for the TEOS(40)-PTMO(2K)-100-0.048 ceramer.

of two dimensional Eden clusters by using tetrafunctional reactive sites (species) on a computer. Some of the sites were poisioned i.e. they were not permitted to react. Thus when a combination of bifunctional (two poisoned sites), trifunctional (one poisoned site) and tetrafunctional species were permitted to react a cluster of fractal dimension 1.8 was developed, while, when only bifunctional species were reacted with tetrafunctional species a fractal dimension of 1.67 was achieved. Thus using this Eden growth model Keefer was able to show that depending upon the sites chosen (for poisoning) structures could be generated which showed fractal behavior which varied from surface to mass fractal. Keefer (113) also used SAXS to to study silicate growth in base catalysed systems prepared from TEOS (r = 1 to 4, where r is the number of moles of water to the alkoxy functionalities). Studies conducted in the Porod region for these scattering profiles indicate that structures change from mass fractal to surface fractal as the value of r is increased, thus verifying his computer generated results.

In the TEOS/PTMO ceramer systems reacted in DMF/IPA, the primary silicate species can thus be poisoned in two ways. The first route consists of the reaction of an endcapped PTMO species with the growing polymeric silicate species. When a PTMO chain is covalently bonded to a silicate particulate, the site of attachment can be considered to be poisoned and hindered from further reaction with other silicate species. Since there are a larger percentage of PTMO chains in the 20 and 40 wt% TEOS/PTMO ceramer systems the probability of a hydrolysed TEOS species reacting with a PTMO species

initially (30 minutes - 2 hours) is much greater than later in the experiment i.e after 10 hours. Thus in the early stages of gelation the growth of the primary silicate species is likely hindered by the attachment of a large number of PTMO chains to them and in the later stages by the slow diffusion of other secondary silicate species to the nucleation sites. As a result of this combination of factors the dimensionality of the scattering silicate species is low. This behavior may also help explain the lower dimensionality of the silicate phase in the 20 wt% TEOS/PTMO ceramers when compared with the dimensionality of the silicate phase in the 40 wt% TEOS/PTMO ceramers. In other words the greater the PTMO content in a given ceramer of TEOS/PTMO (reacted in DMF/IPA) the less convoluted the silicate species will be. This trend will be seen to manifest itself further in the compositions containing higher initial weight fractions of TEOS i. e. greater than 40 wt%.

The second factor to be considered vis-a-vis poisoning, is that in reactive solutions containing low concentrations of water and catalyst (such as in these ceramers), hydrolysis is slow and incomplete. It is possible, then, that the silicate monomers are not fully hydrolyzed, that is, they still have alkoxy groups bonded to them. Due to steric hindrance, alkoxy groups on polymers tend not to hydrolyse as rapidly as those on monomers. Therefore the growing silicate polymer will have sites which are unavailable for further polymerization or become active only at a relatively slow rate (65). Thus these two features i. e. the higher probability of PTMO attachment to the growing primary silicate particle during the earlier stages of reaction as well as the

slow hydrolysis of the reactive sites on the polymeric silicate species help explain the lower dimensionality of the gels seen in the earlier stage of experiment (30 minutes to 2 hours).

As gelation proceeds, secondary silicate species attempt to diffuse to the nucleation sites located at the chain ends. This diffusion is brought about by the remaining DMF in the reaction mixture which drives the phase separation of the PTMO from the silicate components. As the secondary silicate species react with the primary silicate particles the dimensionality of the particulates (as measured from the Porod slope) at the smaller angles increases. Thus as more of these silicate particles make contact each other they react further thus becoming more convoluted (which gives a higher fractal dimension) and the radius of gyration of the primary scattering particles increases.

As stated above all these secondary silicate particles in the reactant mixture tend to diffuse towards the primary silicate particles or the nucleating sites located at the chain ends. However, in the case of these 20 and 40 wt% TEOS/PTMO ceramers, the existance of a second slope at higher angles in the Porod plot (after two days) indicates that not all these particles are capable of diffusing to the nucleating sites. These 20 wt% and 40 wt% TEOS/PTMO ceramers contain a relatively high PTMO content and these oligomer chains react rapidly to form a high molecular weight network. The formation of this network places diffusion limitations on the secondary silicate species. Thus these secondary silicate species which cannot diffuse to the chain ends are

trapped at non equilibrium positions along the PTMO backbone. They undergo additional reaction at these positions as indicated by the increase in the dimensionality seen in the Porod plot. They may also cause encapsulation of the PTMO chain. Thus as stated above these systems i.e. the 20 and 40 wt% TEOS/PTMO ceramers are more mixed than those containing a lower initial PTMO content such as the 60 wt% TEOS/PTMO systems which will be discussed shortly. Another important feature to be noted from this data is the occurence of an interparticle interference peak in the scattering profiles before the diffusion process of the silicate particles is completed. This indicates that the some PTMO chains may be connected to the core of the primary scattering particles rather than the surface of the silicate particles as indicated in the model proposed by Huang (84). This feature will become more evident as data for the 60 wt% TEOS/PTMO ceramer is examined.

The scattering profile for the TEOS(60)-PTMO(2K)-100-0.048 ceramer reacted in DMF/IPA is shown in the Fig 8.9. The first scattering profile taken at 30 minutes already shows the presence of an interparticle interference peak. The d spacing as measured from the peak position is 158Å. At 2 hours the scattering profile shows an increase in the intensity at the peak position and a decrease in the interdomain spacing to 148Å. As can be seen in the Fig 8.9 the increase in the scattering intensity continues for all meausurements made upto 2 weeks and the interdomain spacing as seen after 2 weeks is approximately 120Å These scattering profiles are plotted on a log-log plot in Fig 8.10. Here two distinct slopes can be seen initially at 30 minutes. The slope

at the smaller angle indicates that the primary silicate particles at the nucleation sites have a fractal dimensionality of 1.98 while the secondary particles have a fractal dimensionality of 1.27. With the passage of time the dimensionality of the scattering particles increases until after two weeks only a single slope is visible showing the existance of particles with a dimensionality of 3.40. The existance of a single slope in this ceramer may indicate that most secondary particles can diffuse to the nucleation sites located at the PTMO chain ends. This is because there is a smaller PTMO content in these ceramers. Further the presence of a larger TEOS content produces a larger amount of ethanol as the alkoxy groups are hydrolysed; this ethanol can plasticize the system and thus possibly offset any diffusion limitation which might occur as a result of the crosslinked PTMO. The increase in the dimensionality of the scattering particles from 3.14 in the TEOS(40)-PTMO(2K)-100-0.048 ceramers to 3.40 in the TEOS(60)-PTMO(2K)-100-0.048 ceramers may indicate that the scattering particulates are smoother as the TEOS weight fraction in the ceramer increases. This would be expected (since it appears that the PTMO chains are connected to the core of the primary silicate particle) fewer PTMO chains would distort the surface of the scattering particle in the 60 wt% TEOS/PTMO system as compared with the 40 wt% TEOS/PTMO system. Further as the radius of gyration of a particle gets larger for a given TEOS weight fraction the surface should become smoother because the distance between the PTMO chains intersecting the surface will be larger as depicted in Fig 8.11. The

radius of gyration in these systems further increases from 18Å to 25Å within two weeks after casting.

8.4.2 PHASE MIXING AND POROSITY IN TEOS/PTMO CERAMERS REACTED IN DMF/IPA

In the above section it was shown that the scattering particles changed from mass to surface fractals as the TEOS content in these (TEOS/PTMO films reacted in DMF/IPA) ceramers was increased. It was also stated that there was less mixing in the ceramers containing a higher weight fraction of TEOS as compared with those containing smaller weight fractions of the metal akoxide. In order to study and confirm these features, SAXS experiments were performed on a series of TEOS/PTMO materials reacted in DMF/IPA where the only variable was the TEOS content, which was changed from 10 wt% to 100 wt%. The scattering profiles are shown in Fig 8.12 for ceramers containing 10, 20, 40 and 60 wt% TEOS. The profiles were obtained two weeks after the casting of the reactants into the petri dishes. From these profiles it can be seen that with the increase in the weight fraction of the TEOS, there is a decrease in the breadth of the scattering profiles as well as an increase in the scattering intensity at the peak position. Further the interdomain spacings increases with the increase in the metal alkoxide content. The interdomain

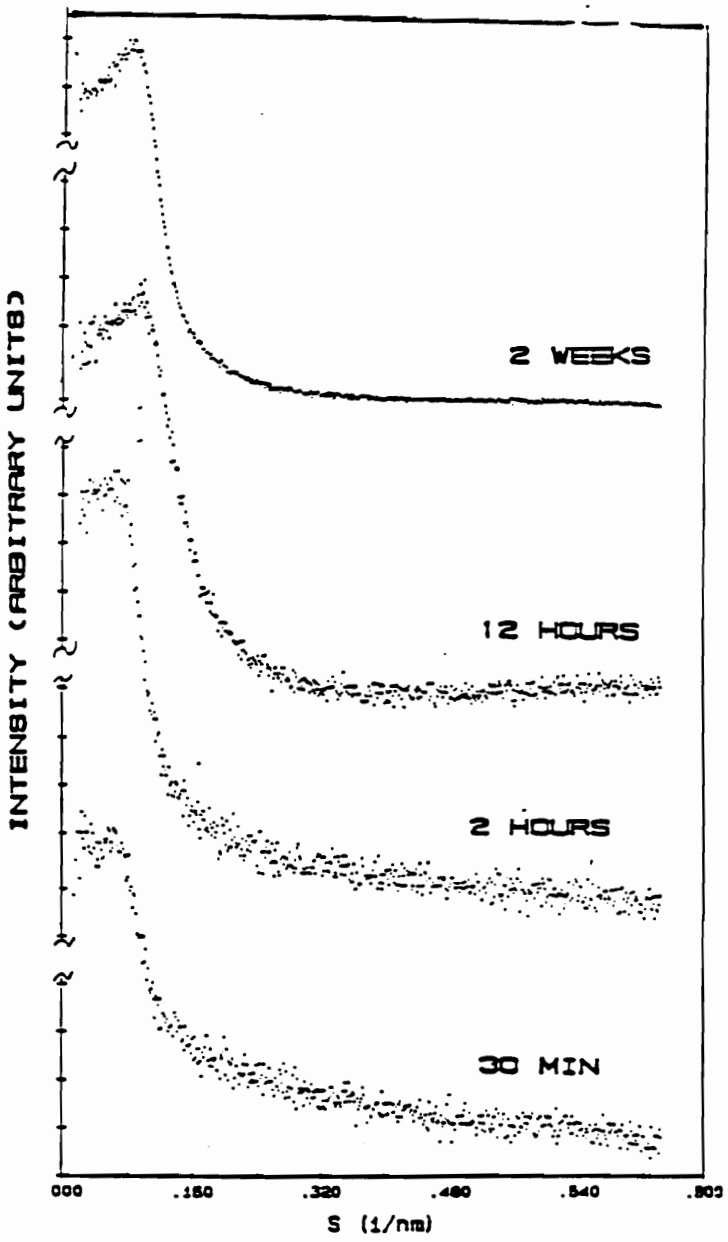


Figure 8.9. SAXS profiles measured for the TEOS(60)-PTMO(2K)-100-0.048 ceramer during curing

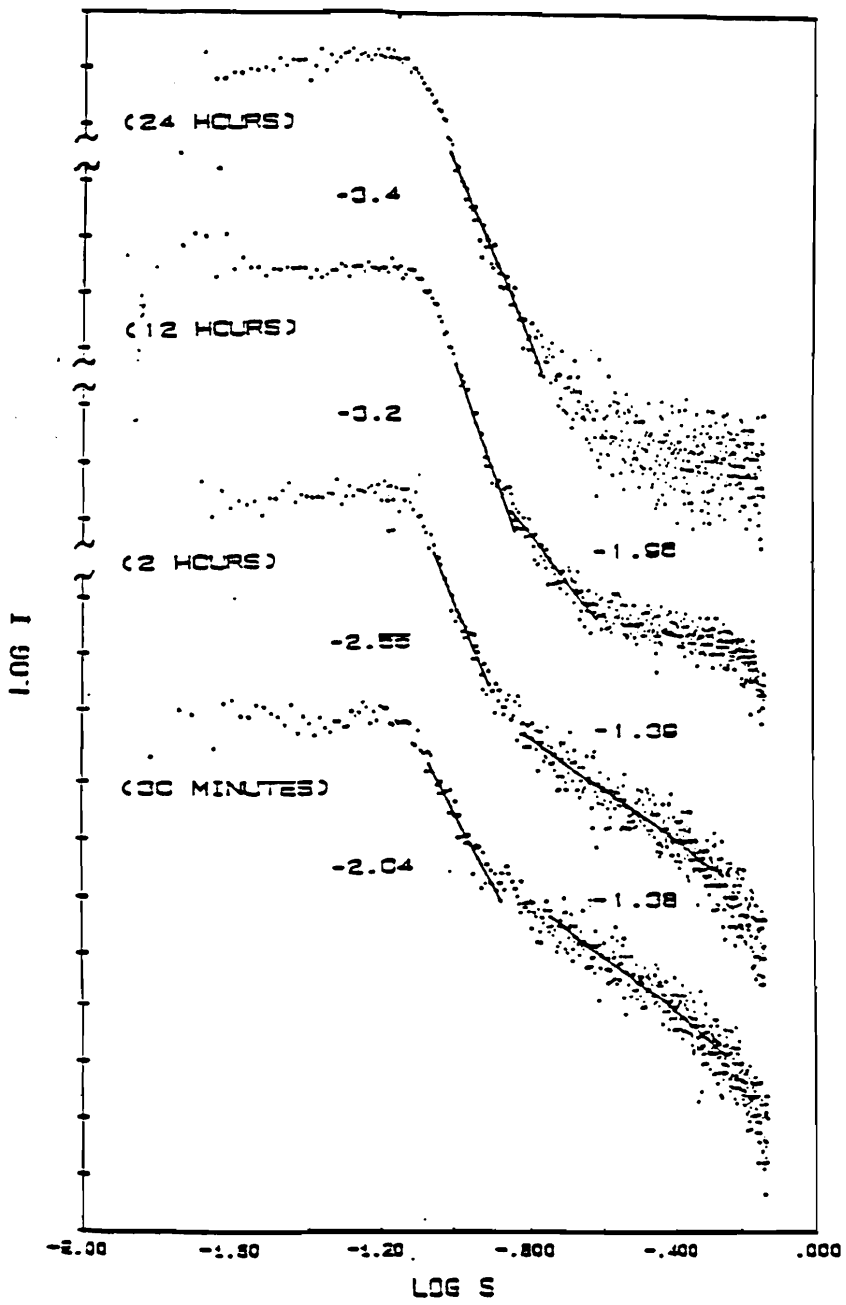


Figure 8.10. SAXS profiles measured for the TEOS(60)-PTMO(2K)-100-0.048 ceramer on a log-log plot.

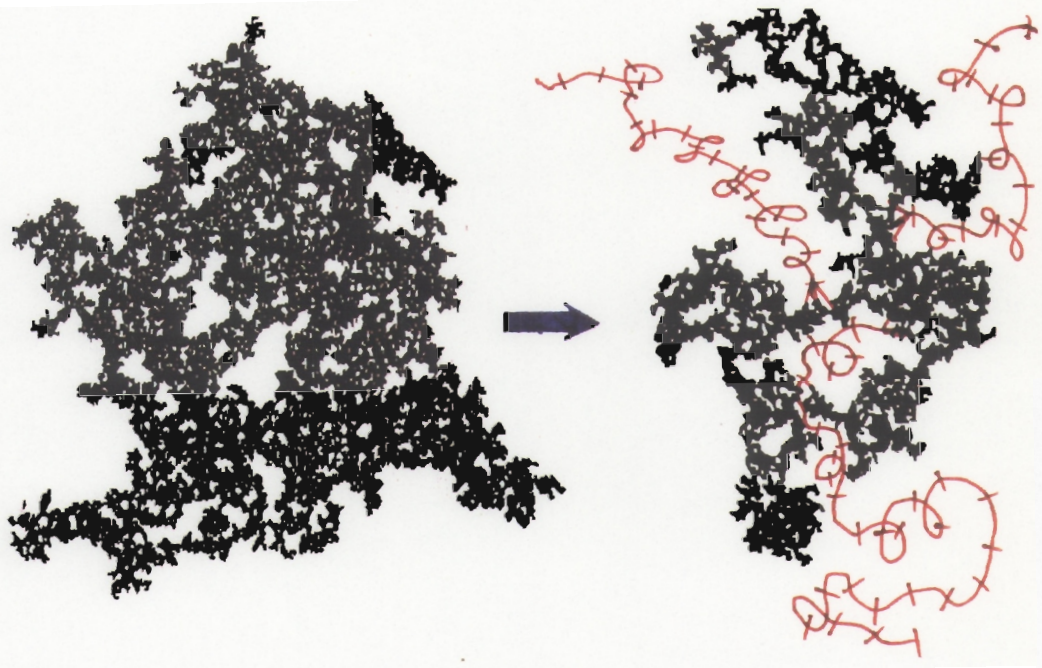


Figure 8.11. Schematic indicating how the PTMO chains can disrupt the surface texture of a scattering particle

spacing for the 10 wt% TEOS/PTMO ceramer is 70Å while the interdomain spacing for the 60 wt% TEOS/PTMO ceramer is around 120Å

The scattering profiles for the TEOS/PTMO ceramers containing 70 - 100 wt% TEOS are shown in the Fig 8.13. Here it can be seen that with the increase in metal alkoxide content there is an decrease in the scattering intensity at the regular peak position though the interdomain spacing increases upto 90wt% TEOS. The interdomain spacing for the 70 wt% TEOS/PTMO ceramer is around 125Å while it is 142Å for the 90wt% ceramer. There occurs, however, another broad peak at wider angles which corresponds to scattering from the porosity within the system. This porosity was alluded to in the last chapter and may have been responsible for the bimodal character of the Maxwell-Wagner-Sillars relaxation. For the 100% TEOS system reacted in DMF/IPA this peak which is due to intraparticle scattering from the pores is located at approximately 19Å. It should be stated at this point that the scattering intensity at the peak position for the 100 wt% TEOS material is much lower than that seen in the 70, 80 or 90 wt% TEOS/PTMO ceramers. Its position at the top of Fig 8.13, is only to maintain the trend (seen in Figs 8.12 and 8.13), where the scattering profiles are arranged in ascending with increasing metal alkoxide content. On closer examination of the scattering profiles (using a log I vs s^2 plot) it can be seen that this peak due to the porosity in the silicate phase manifests itself at TEOS concentrations as low as 40 wt% (Fig 8.14.) It is also around this composition (40 wt% TEOS/PTMO) that the MWS relaxation begins to manifest itself in the dielectric spectra.

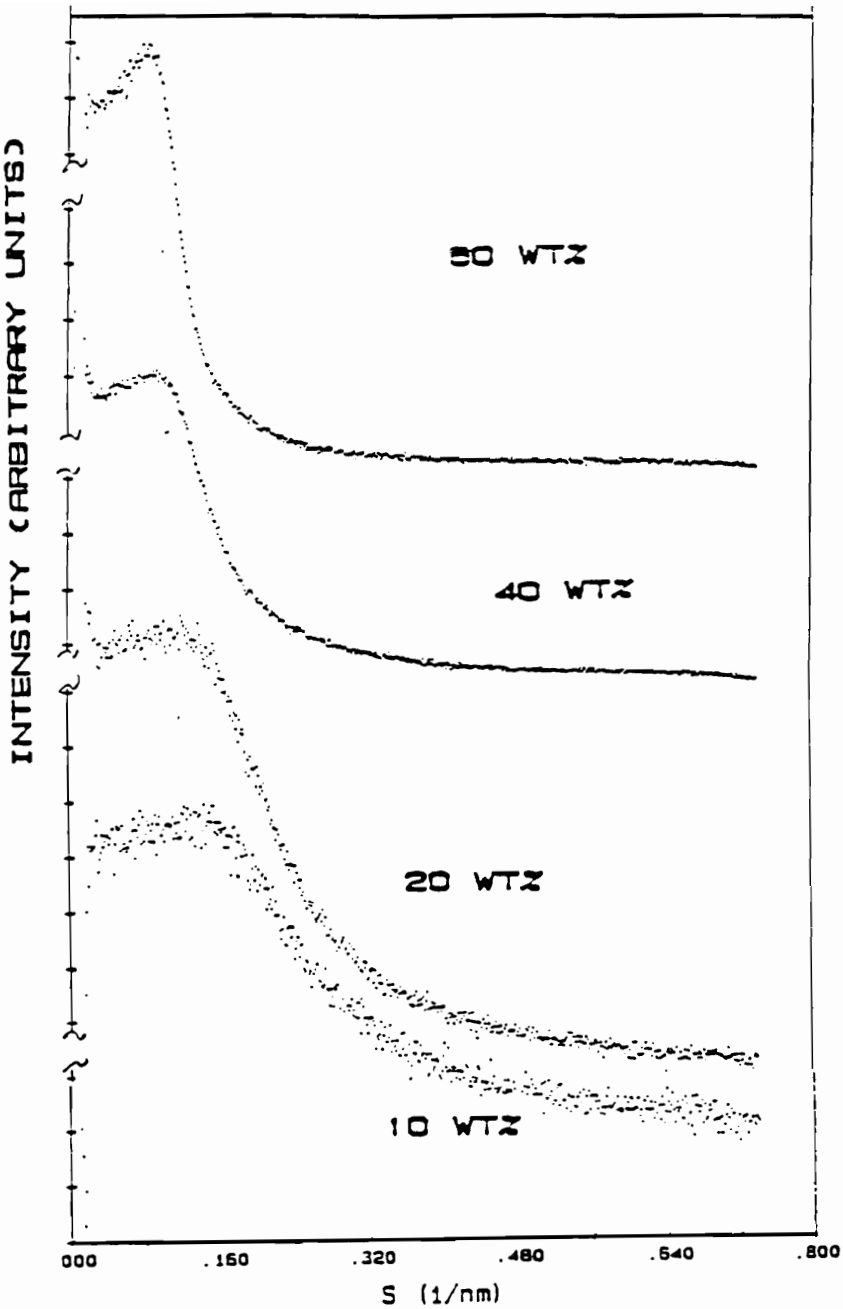


Figure 8.12. SAXS plots for the TEOS(X)-PTMO(2K)-100-0.048 ceramers, where X = 10, 20, 40 and 60 wt%.

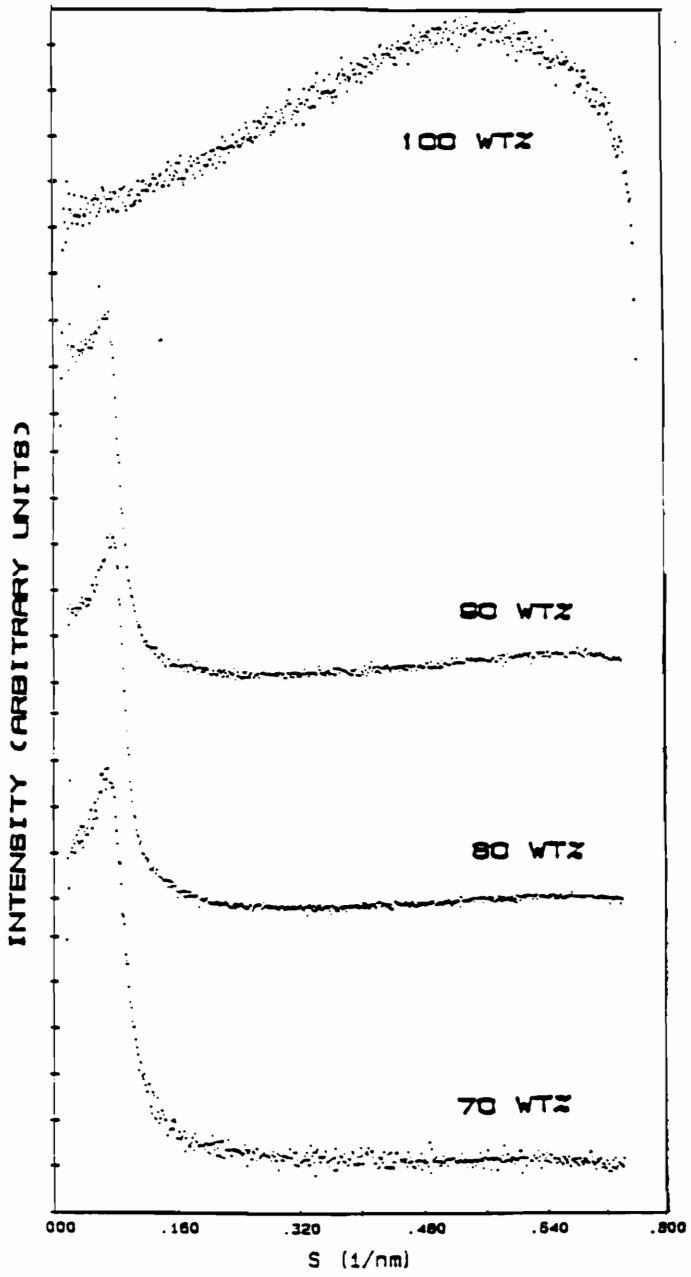


Figure 8.13. SAXS plots for the TEOS(X)-PTMO(2K)-100-0.048 ceramers, where X = 70, 80, 90 and 100 wt%.

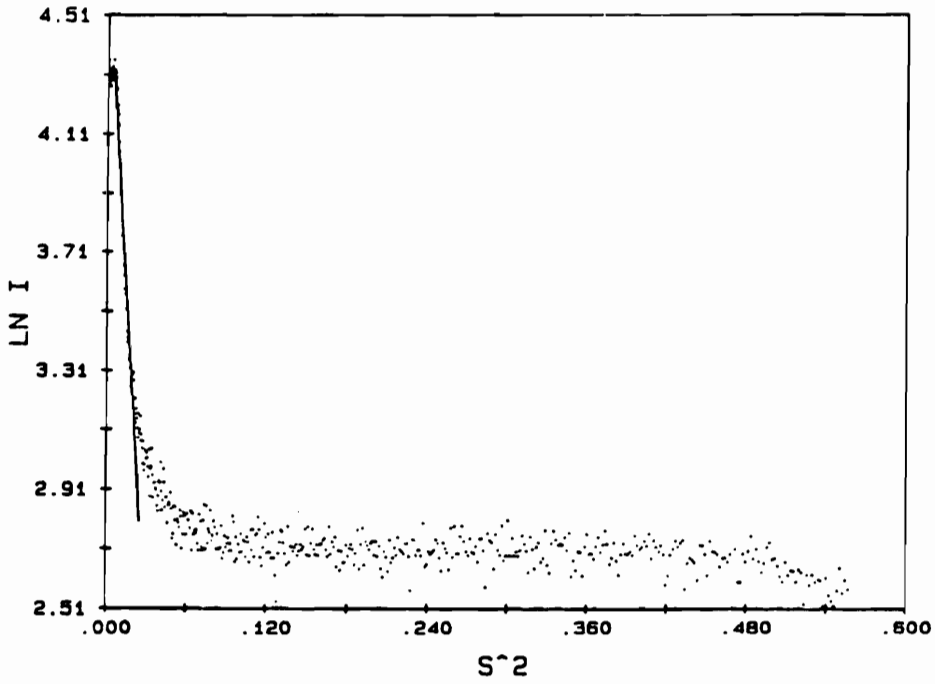


Figure 8.14. LN I vs s^2 plot for the TEOS(40)-PTMO(2K)-100-0.048 ceramer indicating the peak due to porosity at wider angles.

8.5 STRUCTURE OF THE INORGANIC PHASE IN THE TEOS/PTMO CERAMERS REACTED IN THF/IPA

The reaction between TEOS and PTMO in THF/IPA is conducted in a manner similar to that in DMF/IPA. As stated earlier, the minimum time required for this sample to gel (stop flowing) after casting was six hours. In this section only two sets of data will be discussed. They are the (Intensity vs s) scattering profiles obtained during the process of gelation of TEOS(60)-PTMO(2K)-100-0.048-THF/IPA as well as the fractal dimensions obtained on the 20, 40 and 60 wt% TEOS/PTMO ceramers. The reason for discussing the gelation scattering profiles of only the 60 wt% TEOS/PTMO ceramers is that all the other TEOS/PTMO systems (reacted in THF/IPA) studied show similar behavior unlike the ceramers reacted in DMF/IPA where the metal alkoxide content plays an important role in the type of structures formed.

Intensity vs s scattering profiles for the 60 wt% TEOS/PTMO reacted in THF/IPA were obtained at 6 hours, 24 hours and 48 hours after casting respectively and are shown in the Fig 8.15. At six hours the scattering profile resembles that which would be obtained from liquid scattering, while at 24

hours an interference peak due to interparticle scattering is clearly visible. The interdomain spacing as measured from the peak position is around 110Å At 48 hours the peak intensity is further increased from that seen at 24 hours while the interdomain spacing is around 100Å. These scattering profiles are very broad as compared with their TEOS/PTMO counterparts reacted in DMF/IPA. This indicates, as stated earlier, either a larger distribution in domain sizes or interdomain spacings.

The scattering profiles in Fig 8.15 were then plotted onto a log I(s) vs log s plot in Fig 8.16 to study the fractal dimensions of the scattering particles and also to try and understand the nature of formation of these scattering particles. The fractal dimension after two days is 1.95 indicating that the silicate species in these TEOS/PTMO ceramers are mass fractals rather than those seen in the TEOS/PTMO films produced in DMF/IPA, where they displayed more particulate like behavior. Brinker et al (65) measured fractal dimensions for TEOS derived silicates under acidic conditions (pH = 1) and determined the Porod exponent to be 1.93, which is very similar to the number obtained for these ceramers. Further, Brinker postulated that this fractal dimension corresponded to a linear silicate species with branches located on the backbone at every 20Å. As stated earlier in chapter 5, these TEOS/PTMO ceramers are suggested to be more phase mixed and the breadth of the scattering profiles in the intensity vs s plots indicates that this mixing produces a large distribution of interdomain spacings and interdomain distances.

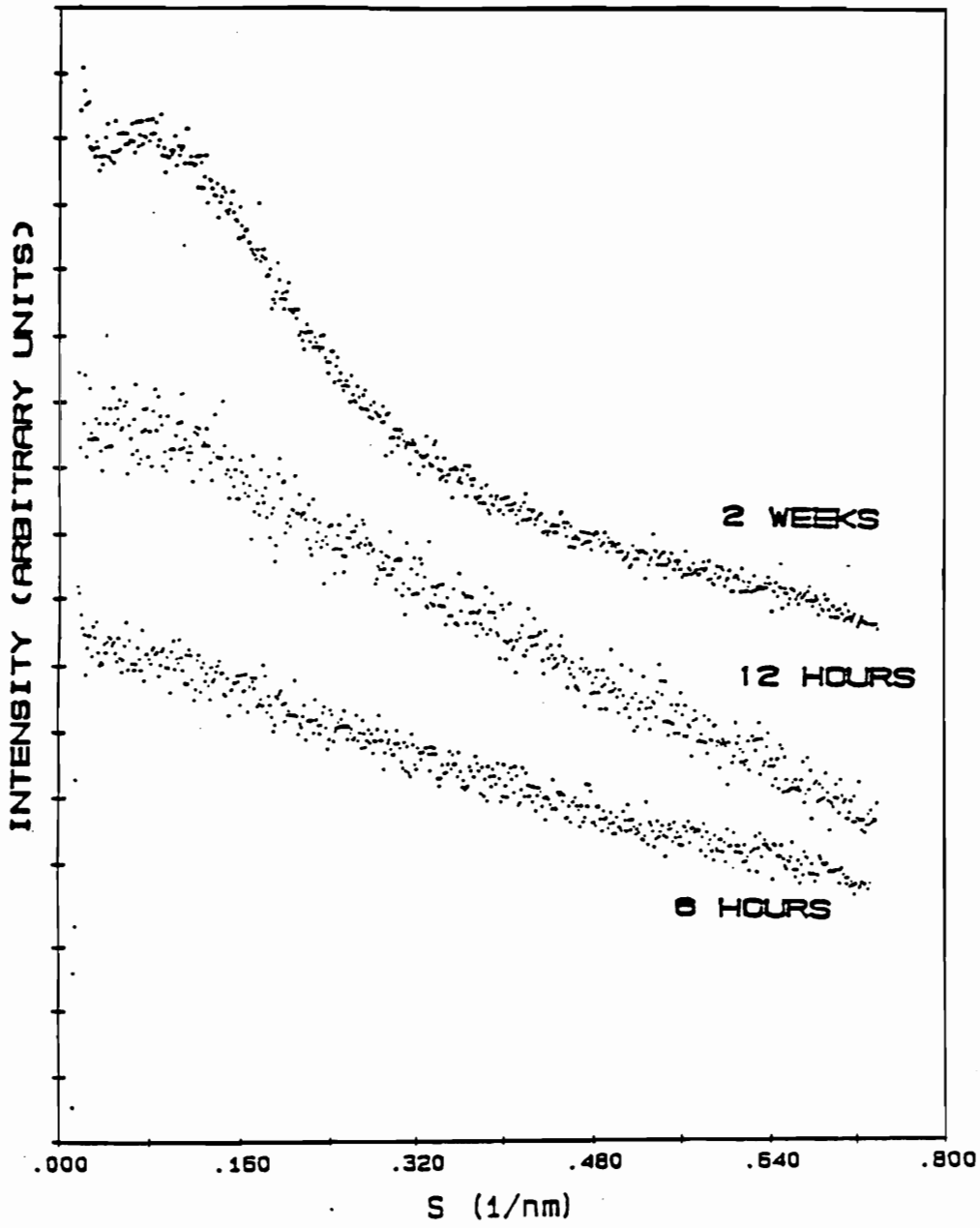


Figure 8.15. SAXS profiles for the TEOS(20)-PTMO(2K)-100-0.048 ceramer reacted in THF/IPA as a function of gelation.

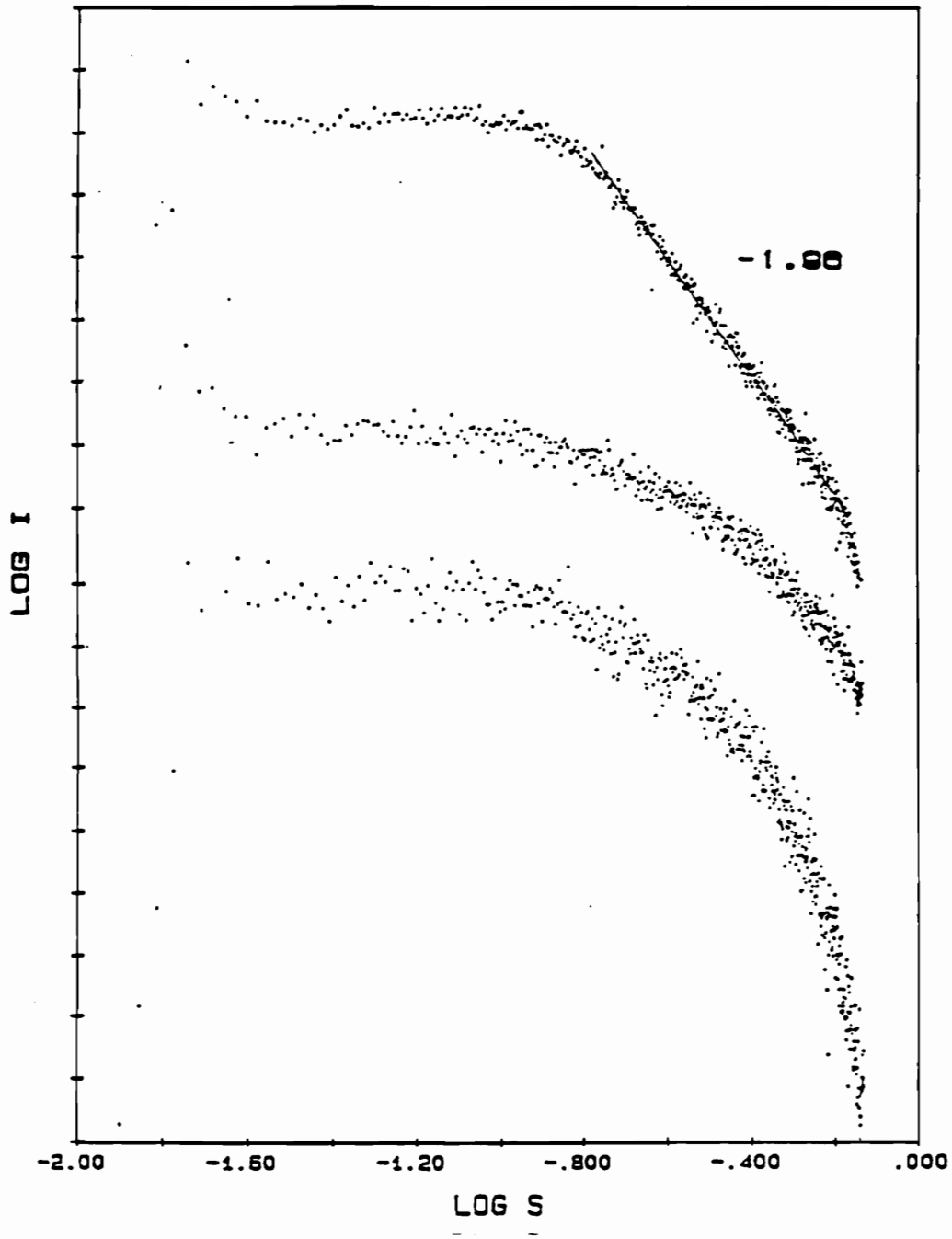


Figure 8.16. SAXS profiles for the TEOS(20)-PTMO(2K)-100-0.048 ceramer reacted in THF/IPA when plotted on a log-log plot.

The Porod slopes for the 20, 40 and 60 wt% TEOS/PTMO ceramers is shown in Fig 8.17. It can be seen that all three films show a single slope of around -2.0, indicating as stated above that these scatterers may be mass fractals. The fractal slopes are measured over one order of magnitude. It can also be seen that the knee in the scattering profiles plotted in the log-log plot, moves to smaller angles. This indicates that the size of the scattering particles is increasing as explained above.

Thus the formation and growth of a silicate domain in these TEOS/PTMO ceramer systems reacted in THF/IPA can take place at any position in the system with equal probability. In other words there is very little need for the presence of an endcapping group to act as a nucleating site for the growth of the silicate phase. Thus it is possible that there may be a greater concentration of silicate species in the system at regions other than at the chain ends. The occurence of a low intensity interference peak in scattering profiles for these ceramers is due to interparticle scattering. However, as indicated from the studies conducted with the unendcapped PTMO, the endcapping groups are necessary to prevent the macrophase separation of the silicate component from the PTMO component. This can be construed to mean that the high molecular weight PTMO network formed as a result of the condensation reaction can serve to physically trap some of the silicate chains in the ceramer film.

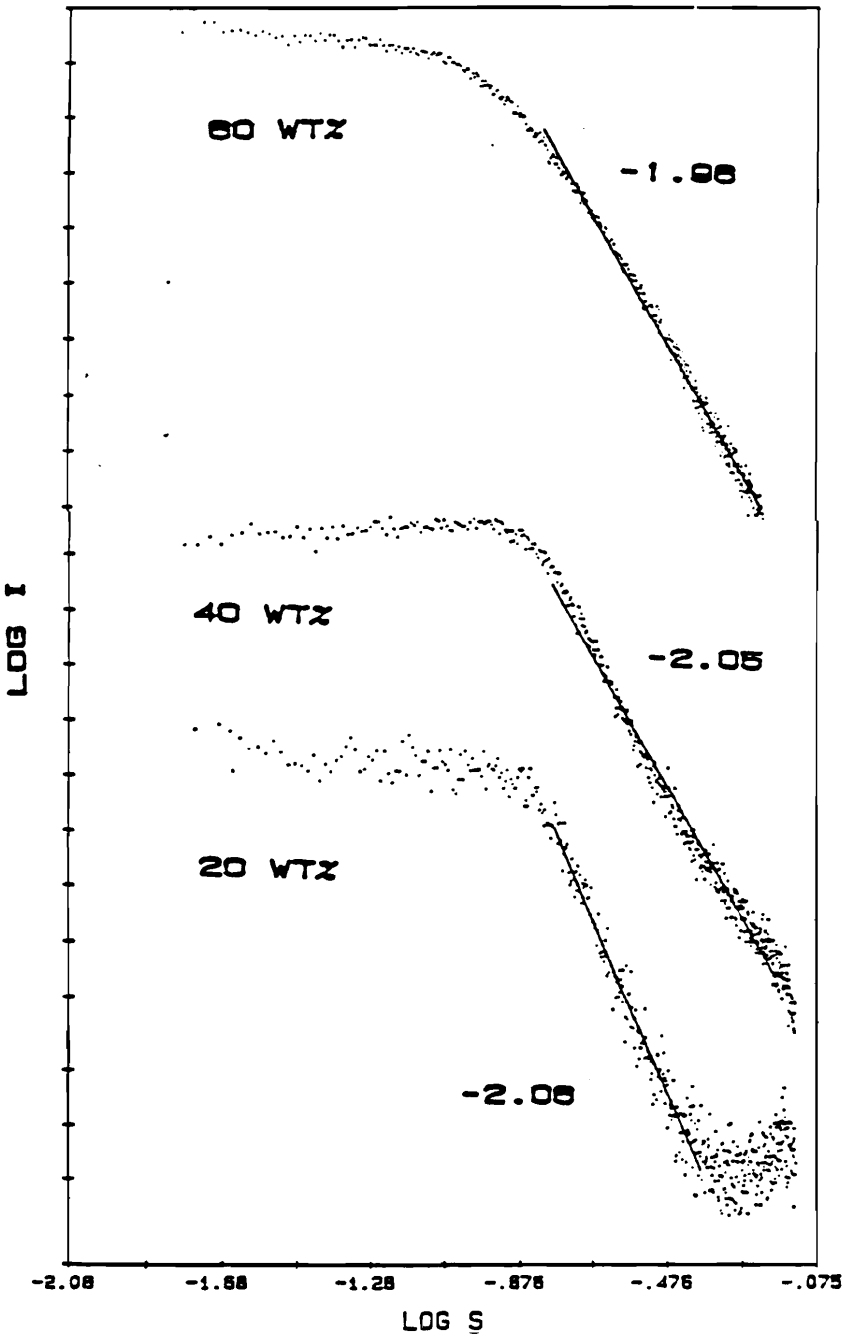


Figure 8.17. SAXS profiles for the TEOS(X)-PTMO(2K)-100-0.048 ceramer reacted in THF/IPA where X = 20, 40 and 60 wt%.

Under conditions of low pH, growth of the silicate clusters in TEOS derived gels has been found to be of the cluster-cluster aggregation variety. The cluster-cluster model describes growth when a "sea" of monomers undergoes random walks, forming a collection of clusters that continue to grow by condensing with each other and with other monomers (65). Cluster-cluster growth may also be diffusion limited or reaction limited as in the case of monomer-cluster growth. Compared to monomer-cluster growth, the strong screening between two contacting clusters causes their growth to be more open (fractally speaking!) even under reaction limited conditions. Thus the fractal dimensions for the DLCA cluster-cluster aggregation (114) is 1.8 while it is 2.09 for the RLCA aggregation (117). In cluster-cluster aggregation there is no necessity for a continuous source of monomers, as compared with the monomer-cluster growth. In these TEOS/PTMO ceramers reacted in THF/IPA the growth of the silicate clusters appear to be similar to cluster-cluster aggregation. As stated above these clusters do not require any special sites for nucleation and as has been shown in prior computer simulations (112, 119), they do not possess a center as is the case with particulates produced from monomer-cluster growth.

8.6 STRUCTURE OF THE INORGANIC PHASE IN THE TiOPr/PTMO CERAMERS

These ceramers were studied in order to gain an idea of how a prehydrolysed metal alkoxide i.e. TiOPr would change when incorporated into a ceramer. As previously described in chapter 6, TiOPr and ZrOPr are prehydrolysed in a solution of isopropanol in order to reduce their reactivity and thus prevent them from phase separating when incorporated into a ceramer. It therefore becomes obvious that two studies need to be conducted on these systems i. e. one on the TiOPr sol before the PTMO is added to it and a separate study on the ceramers containing different TiOPr contents in order to determine the effects of PTMO on the titania particulates. Such a study will also help the determination of the effect of interparticle interference on the Porod slopes. What follows is a discussion of these experiments.

8.6.1 STUDY OF THE TiOPr SOL USING SAXS

The study on the TiOPr sol will be described first. In this study TiOPr was first diluted with IPA as described in chapter 6. Following this, water, HCl and IPA were slowly added to the TiOPr/IPA mixture with plenty of stirring. Water was added in the stoichiometric amount necessary to hydrolyse 25 mole% of the

alkoxy functionalities present in the reaction mixture. When the stirring was complete the TiOPr sol was placed in a solution cell made of stainless steel and subjected to SAXS. The windows on the cell were made of Kapton film (thickness = 0.3 mils) which does not scatter in the small angle region. The scattering profiles were evaluated immediately after the preparation of the sol, 2hrs, 1, 2, 4 and 5 days after preparation of the sol. The total time for the scattering experiment was approximately 10 minutes. The liquid scattering was subtracted from the scattering profiles before the fractal dimensions and the radius of gyration were computed.

The scattering data plotted on a log I(s) vs log s plot are displayed in Fig 8.18. It can be seen that the transparent TiOPr sol displays a single slope in the Porod region with a fractal dimension of 1.6 within 10 minutes of preparing the sol. The measured radius of gyration from the Guinier region is about 10Å The sol turns to a gel very rapidly and within fifteen to twenty minutes the material ceases to flow. From this stage onwards the gel appears a translucent white which indicates that aggregation between the titania particles may have taken place. In the gelled state i. e. after 2 days, the log-log plot shows two slopes indicating that there may be two kinds of particles displaying self similarity. The Porod slope at the smaller angles which may represent the larger particles decreases with time from -1.9 after 2 days to -2.5, 4 days after preparation of the sol. The slope at the smaller angles does not change very much and remains essentially the same at -1.6. It is not possible to evaluate the radius

of gyration of the scattering particles once the material has gelled since the Guinier region at this stage lies outside the range of SAXS.

8.6.2 STUDY OF THE TiOPr/PTMO CERAMERS

The next stage of the experiment consisted of adding alkoxide functionalized PTMO diluted with IPA to the TiOPr sol and examining the gelling TiOPr/PTMO ceramer using SAXS in a manner analogous with that performed on the TEOS/PTMO materials described earlier. The scattering profiles for the TiOPr(20)-PTMO(2K)-100-0.048 ceramer is shown in Fig 8.19 and are plotted as intensity vs s. The first SAXS profile could be obtained only 6 hours after casting since these materials contain a large amount of solvent and hence tend to flow for extended periods of time as compared with their TEOS/PTMO counterparts which typically take less than two hours to gel. Subsequent scattering profiles were obtained at 12, 24 and 48 hours after the materials were cast. The scattering profile obtained at 6 hours does not display an interference peak due to interparticle scattering. The profile is more akin to that obtained from liquid scattering. At 12 hours there is an increase in the scattering intensity but still no interference peak is visible. At 24 hours the intensity of scattering is further increased from that seen at 12 hours and an interference peak is now visible in the scattering profile. The interdomain spacing as measured from the peak position in the scattering profile is 87.5Å

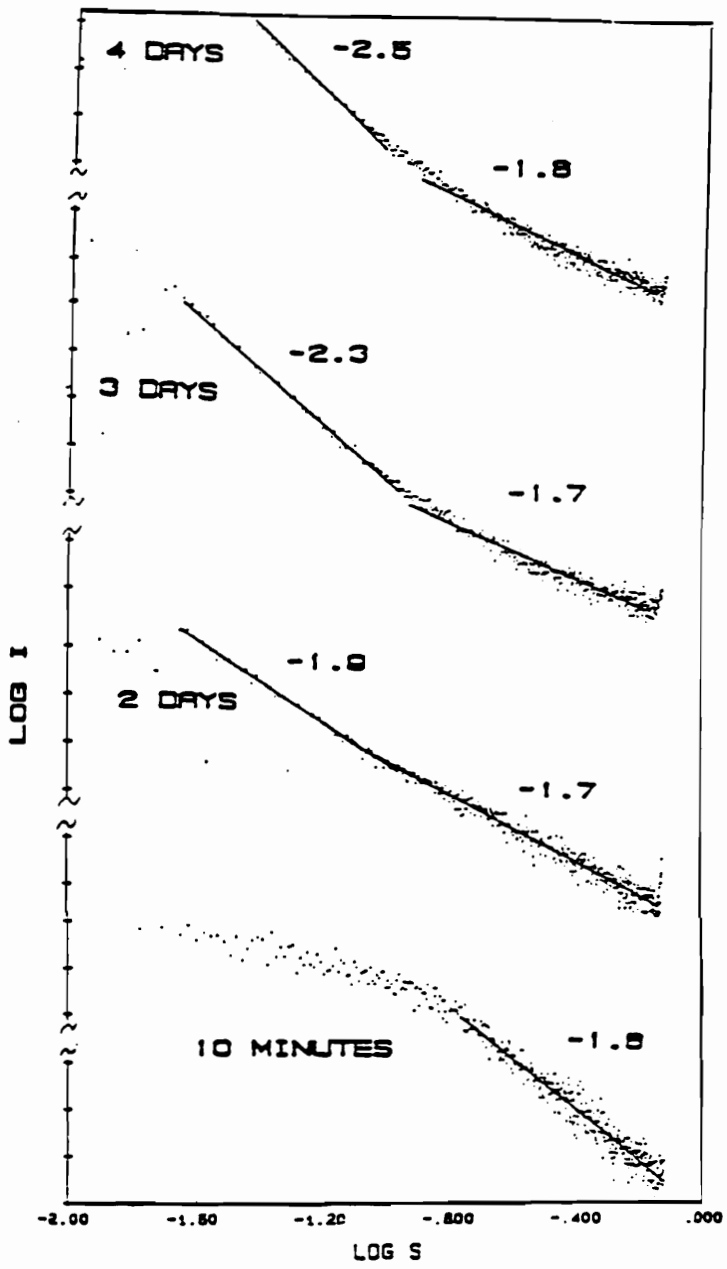


Figure 8.18. Porod slopes obtained from the TiOPr sol indicates that the scattering particles are mass fractals.

After two days the scattering intensity at the peak position is further increased to around 80 and the measured interdomain spacing is around 86Å. Thus from Fig 8.19 it can be seen that there is an increase in the scattering intensity at the peak position with time and little change in the interdomain spacing. The increase in the scattering intensity may be attributed to some densification in the inorganic component as well as the evaporation of solvent from the ceramer.

On plotting these scattering profiles for TiOPr(20)-PTMO(2K)-25-0.06 on a log-log plot as in Fig 8.20, it may be seen there exists only a single Porod slope with a fractal dimension which increases from 2.2 after 2 hours to 2.5 after 2 days. This increase in the fractal dimension parallels that seen for the slope seen at the lower angles seen in the TiOPr sol. Thus it appears that the titania particulates in these ceramer systems are mass fractals with a Porod slope between 2 and 2.5. The radius of gyration in these ceramers is around 10Å

The SAXS scattering profiles for the TiOPr(40)-PTMO(2K)-25-0.06 ceramers show similar trends to their 20 wt% counterparts during the period of gelation though the scattering profiles are not shown here. The intensity of scattering increases with time and the Porod slope decreases from -2.2 to -2.5. Thus the scattering particles are also mass fractals. The radius of gyration of the titania particles is again around 10Å

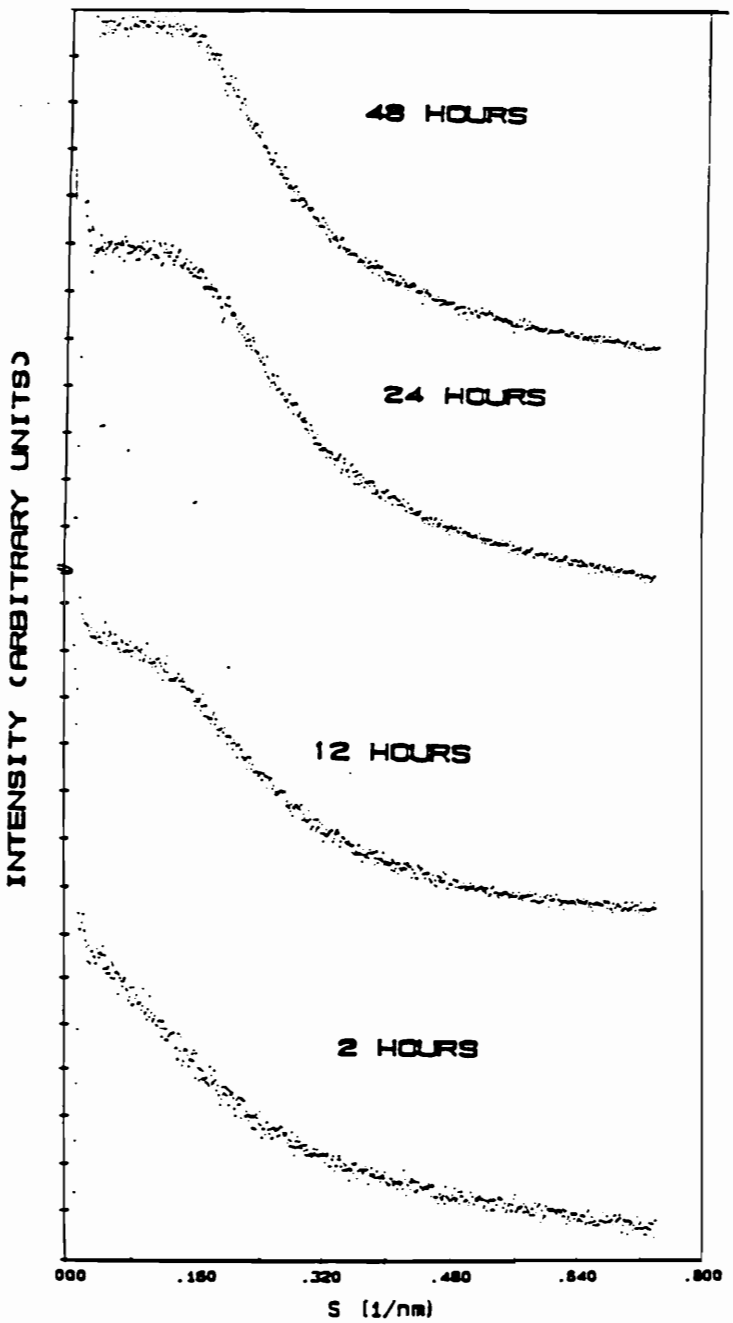


Figure 8.19. SAXS profiles for the TiOPr(20)-PTMO(2K)-25-0.06 ceramer as a function of curing time.

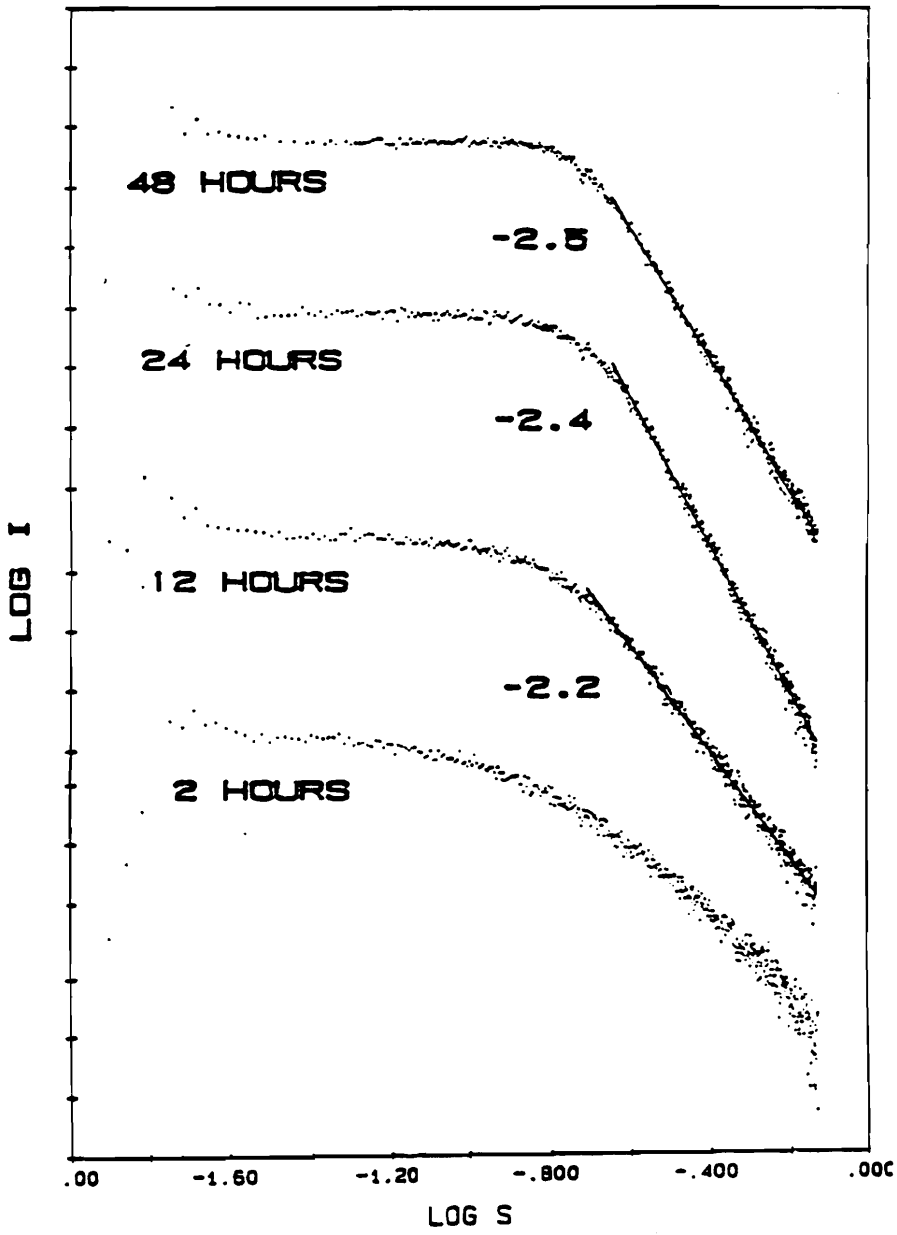


Figure 8.20. SAXS profiles for the TIOPr(20)-PTMO(2K)-25-0.06 ceramer as plotted on a log-log plot.

From the above discussion, the scattering particles seen in these TiOPr/PTMO ceramers appear to be mass fractals with dimensions in the range of 2.4 to 2.5. This was similar to the dimensionality of the particulates seen at the smaller scattering angles in the TiOPr sol. Further the radius of gyration in the sol was 10Å and remains around 10Å in the 20 and 40 wt% TiOPr/PTMO ceramers as well as in the 60 wt% TiOPr/PTMO ceramers which will be discussed shortly. It therefore appears that there may be little change in the basic structure of the titania particulates because of the addition of PTMO to the sol. It also does not appear that any significant encapsulation of the PTMO by the titania takes place as in the case of the TEOS/PTMO reacted in DMF/IPA. The lack of any significant change in the fractal dimensions of the titania particles with the addition of PTMO indicates that these oligomers may be attached to the outer surface of the titania particles. This has also been claimed by Brennan et al (96). The breadth of the scattering peaks in these systems may be related to the existance of scattering titania particulates throughout the system and not just at the chain ends as in the case of TEOS/PTMO ceramers reacted in DMF/IPA. This gives rise to the possibility that there may be an even greater concentration of titania dispersed amongst the PTMO chains (as against the chain ends) but which does not significantly encapsulate the PTMO chains. Thus it appears that the structure in the TiOPr/PTMO ceramers may be similar to the cluster-cluster growth seen in the TEOS/PTMO ceramers reacted in THF/IPA. The presence of the interference peak at around 100Å is only the

result of correlated interparticle scattering which occurs between the particulates located at the chain ends.

The TiOPr(60)-PTMO(2K)-25-0.06 ceramer also displays behavior typical of these gelling ceramer systems i. e. the scattering intensity increases with time. However, no scattering peak is seen in the scattering profiles. The Porod slopes for this ceramer are plotted in Fig 8.21 and shows a lower dimensionality than its 20 and 40 wt% counterparts discussed above. The Porod slope at 12 hours after casting is -1.84 and decreases to -2.1, 2 days after casting. This lower dimensionality occurs because of scattering from the porosity within the inorganic phase. This feature will be discussed in greater detail shortly. Again the radius of gyration for these ceramers is around 10Å thus indicating that there is no fundamental change in the shape or size of the TiOPr/PTMO particles developed in the the sol.

As the content of TiOPr is increased above 70 wt% in these TiOPr/PTMO ceramers, the scattering due to the electron density difference between the metal alkoxide and the PTMO (correlated scattering) is shifted to lower angles and cannot be observed by SAXS. However, scattering in the small angle region now occurs due to the existance of porosity within the inorganic phase as seen in Fig 8.22. This plot contains scattering profiles for 80, 90 and 100 wt% TiOPr/PTMO ceramers. The scattering intensity for all these materials is very low, in part, because the scattering is not due to interparticle scattering. In the 100 wt% TiOPr material, the scattering profile displays a maxima at ca.

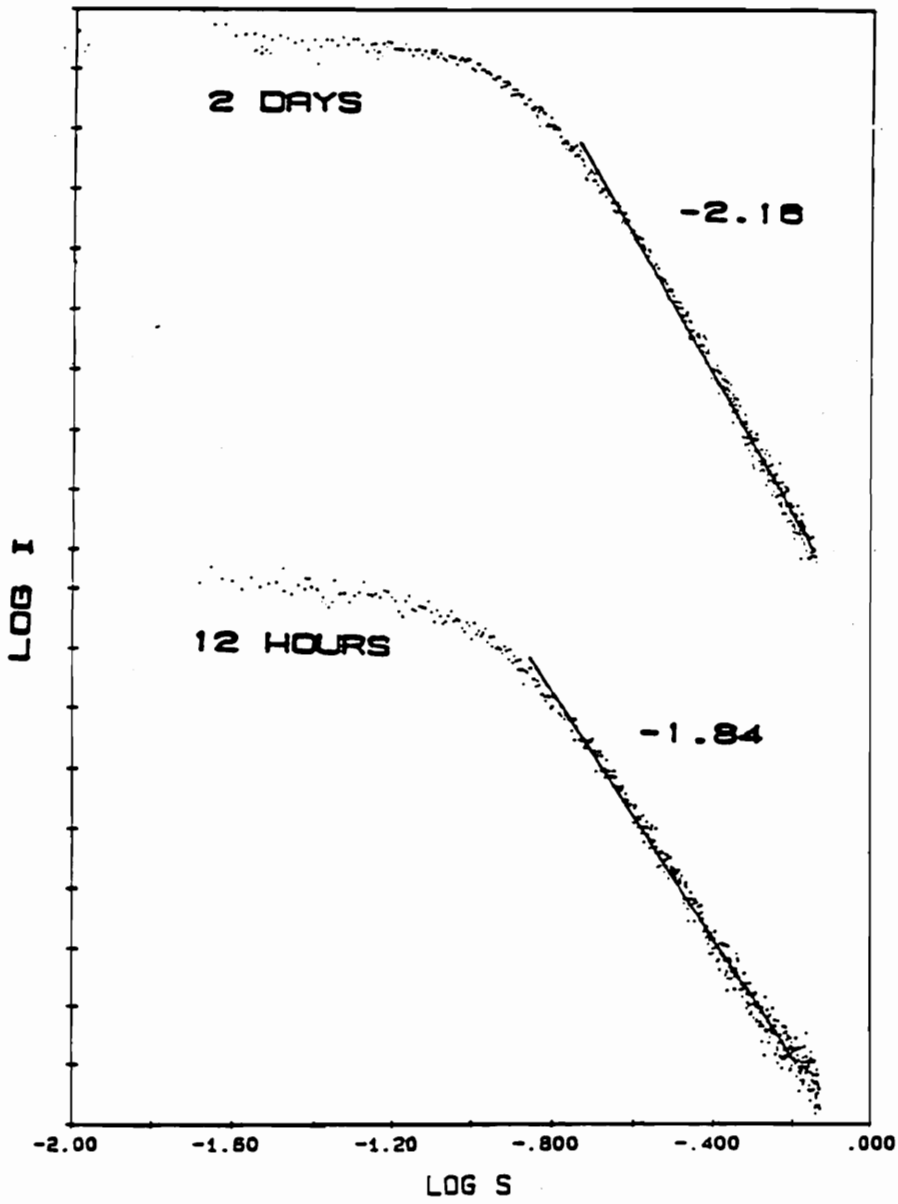


Figure 8.21. SAXS profiles for the TIOPr(60)-PTMO(2K)-25-0.06 ceramer as plotted on a log-log plot.

111Å which is typically in the range where correlated scattering occurs for most of the ceramer systems. Schmidt (120) has indicated that Porod exponents can also be measured from scattering by a polydisperse system of pores, platelets, spheres etc. The Porod exponent for the porous 100 wt% titania is 1.8. However, the presence of this scattering (due to the porosity) in the small angle region causes the scattering profiles for these TiOPr/PTMO (containing over 40 wt% TiOPr initially) ceramers to be a combination of scattering due to the electron density difference between the inorganic and PTMO as well as the electron density difference between the inorganic and air. Therefore the reduced fractal dimensions seen for the 60 wt% TiOPr/PTMO ceramers is because of the combined scattering from the two sources indicated above one of which (the titania particles) has a fractal dimension of around 2.5 and the other (porosity) which has a Porod exponent of 1.8.

8.7 CONCLUSIONS

For the TEOS/PTMO ceramers reacted in DMF/IPA the development of the primary silicate particles appears to be the result of nucleation and growth processes. The nucleation sites for the primary silicate particles are the PTMO chain ends. Thus the greater the number of chain ends in a give TEOS/PTMO composition the greater will be the number of such scattering particles. The

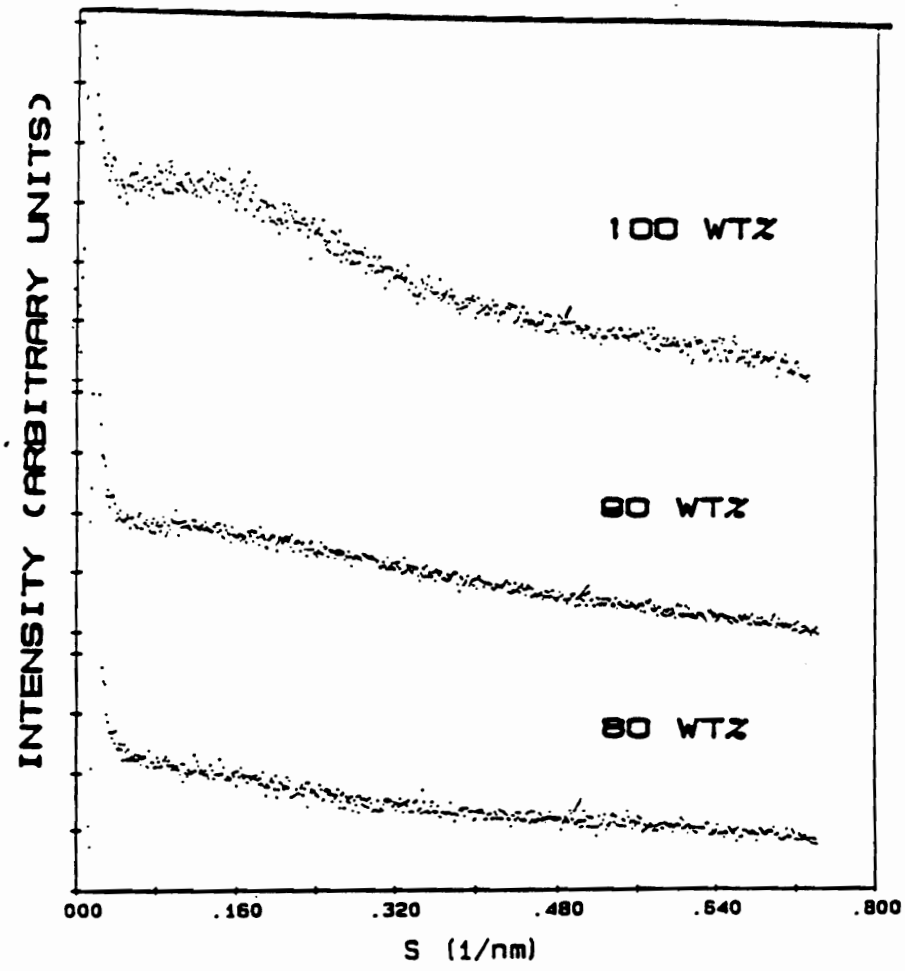


Figure 8.22. SAXS profiles for the TiOPr(X)-PTMO(2K)-25-0.06 ceramer where X = 80, 90 and 100 wt%.

growth of the silicate phase appears to occur by a monomer cluster mechanism initially. However, in the systems containing a large amount of PTMO it appears that in the later stages of gelation the growth occurs more by cluster-cluster growth because of diffusion limitations placed by the high molecular PTMO weight network on the diffusion of the secondary particulates to the nucleating sites.

From this work it has also been shown that for the TEOS/PTMO ceramers reacted in DMF/IPA the structure of inorganic component changes from mass fractal to surface fractal with the passage of time. This feature was attributed to the early attachment of the PTMO chains to the growing polymeric silicate species and the subsequent diffusion of smaller secondary silicate species to the primary silicate species located at the chain ends. The silicate phase in these ceramers was also found to change from mass to surface fractals depending upon the PTMO content in these materials. In other words the scattering particles at in these ceramers at TEOS contents above 40 wt% were found to display a smoother surface character as the weight fraction of metal alkoxide was increased. However, the TEOS/PTMO ceramers reacted in DMF/IPA and containing 40 wt% or more TEOS also show the existance of a weak interference peak at the very large angles due to scattering from porosity present in the inorganic phase.

From these studies it may also be seen that there is greater mixing between between TEOS and PTMO as the PTMO content is increased. This has been

related at least qualitatively to the number of chain ends present in the reaction mixture. Further, in the systems containing initial levels of PTMO, greater than 40 wt% there may be diffusion limitation during the later stages of gelation which prevent some of the secondary silicate particles from completely phase separating from the PTMO and thus being trapped in the midst of the PTMO network. This creates a situation where the xray scattering profiles become broader with increasing contents of PTMO. This does not include a 100 wt% PTMO network.

Another feature observed from these ceramers is that as the metal alkoxide content increases above 40 wt%, there is a new peak which occurs at larger s values, due to scattering from porosity present in the inorganic phase in these materials. This scattering due to the porosity is not due to interparticle scattering, and the peak due to such porosity is of a very low intensity. This feature i. e. porosity also manifests itself in the TiOPr/PTMO ceramer systems and results in a broadening of the scattering profiles seen in these ceramers.

In the case of the TEOS/PTMO ceramers reacted in THF/IPA, there appears to be extensive mixing between the silicate and the PTMO component. The silicate particles in these ceramers display mass fractal behavior and their dimensionality indicates that they are more open and linear structures as has earlier been shown by Brinker et al (65).

The TiOPr/PTMO ceramer systems show some unique behavior as compared with the TEOS/PTMO systems discussed above. In these systems the TiOPr was prehydrolyzed to form a titania sol which showed fractal dimensions of 1.6 for the titania particles and a radius of gyration of 10Å These fractal dimensions increase as the sol is converted to gel. The fractal dimensions after 4 days was approximately 2.5 which was the same as the measured Porod exponents for the TiOPr/PTMO ceramers containing lower extents of TiOPr. At higher TiOPr contents, the scattering profile has been shown to consist of two profiles one due to scattering from the electron density difference between the titania and the PTMO, while the other is believed to be due to the electron density difference between the titania and the air present in the pores in these titania particles. It appears that these titania particulates do not encapsulate any PTMO and the oligomer chains attach to these particulates at the surface rather than at the core as in the TEOS/PTMO ceramers reacted in DMF/IPA.

1.0 CHAPTER 9

RECOMMENDATIONS AND FUTURE WORK

Based on some the results obtained above and some of the speculations made in this dissertation the author considers it necessary to make a few propositions for future research which may help determine some more details of the structure property relationships of these ceramers in a more conclusive and decisive manner. From the chapters 3 to 6, it was proposed that the increase in the extent of curing as a result of microwave heating was due to the increased activation of the stronger dipoles in the reactive system. While this theory has been documented some time ago, it has not been verified, and on occasion has even been disputed, as indicated in the literature review in

this disseration. It therefore remains to put this theory to the test by performing some critical experiments using nuclear magnetic resonance (NMR). The results of such an experiment may help put an end to all controversy regarding this feature of microwave interactions with reactive dipolar molecules. One method by which this theory could be examined, would be to used pulsed microwaves to activate the molecules while simultaneously performing NMR on the reactive system to study the relaxation times of the dipoles. Dipoles with the shortest relaxation times (at 2.45 GHz) would be most susceptible to activation by the microwaves and hence could potentially attain higher temperatures than the bulk of the material. If such a dipole (with a shorter relaxation time) was reactive, then the potential for attaining a higher extent of reaction in the system would indeed be very possible.

From the research documented in chapter 7 on the dielectric spectroscopy of ceramers two features which are suitable candidates for further investigation are the Maxwell Wagner Sillars interfacial behavior and the effect of the casting surface on the structure property relationships in these materials. The MWS behavior has been documented extensively for a variety of two and three phase systems. This behavior has been modelled mathematically for most of these systems. However, this modelling has been performed with frequency as the independent variable while the temperature was kept constant. In the dielectric tests performed on the ceramers, the independent variable was the temperature, while the frequency was kept constant. Since the MWS interfacial polarization does not follow time temperature superposition, it is difficult to

apply these mathematical models to the ceramers. In view of the fact that a wealth of information (such as average pore size, pore volume etc) is available from such mathematical models it is imperative that a mathematical solution be developed to better describe the MWS behavior in these ceramers. Such a model would give a better idea of the interfacial thickness as well as the type of ionic species producing these interactions.

During the course of the work on dielectric spectroscopy it was seen that the end to end distance of the oligomer chains increased (in the more phase separated systems) with increasing metal alkoxide content, when the reactants were cast onto a substrate to which they adhered. These ceramers, with the larger chain dimensions were found to display higher elastic modulii than those in which the chain dimensions were not expanded (maybe even contracted as suggested by the results for the chain dimensions obtained on the TEOS/PTMO ceramers reacted in THF/IPA). A detailed set of experiments (such as DMA, DETA, SAXS and stress strain analysis), conducted with a variety of reactants which produce ceramers with varying degrees of phase separation, should be performed on these systems to determine the effect of the casting substrate on the properties of the ceramers. Films of different thickness should be cast onto polystyrene (onto which the films adheres) as well as teflon (where there is no adhesion) and the properties documented as a function of film thickness.

In order to verify the actual PTMO chain dimensions in these ceramers, neutron scattering experiments should be conducted. Deuterated PTMO should be utilized as the oligomeric component in the ceramers and the radius of gyration measured as a function of metal alkoxide content when the ceramers are cast onto different surfaces as explained above. The results of such an experiment would help verify some of the proposals made in the morphological model with regard to interdomain spacings in these ceramers. One potential problem in conducting such experiments is that the neutron scattering power of the inorganic phase needs to be neutralized so that the radius of gyration of the PTMO component can be obtained. This is easily achieved by using a combination of water and deuterated water whose scattering power can annul that of the inorganic phase thereby leaving only scattering contrast from the deuterated PTMO. A special solution cell containing aluminum windows should be used to hold the ceramer film as well as the water/deuterated water combination during the scattering experiments.

Finally the last proposal that this author would like to make is that these ceramers be made with an oligomeric segment that can be cleaved either thermally (at or below 70°C) or using an acid so that the fractal dimensions of the scattering particulates can be estimated accurately by solution scattering. The cleaved material can be extracted in a soxhlet extractor and after preciptation, it can be put into a solution upon which SAXS can be performed to obtain a more accurate picture of the fractal dimensions.

BLANK PAGE
(no text missing)

REFERENCES

1) Victor Veley, Modern Microwave Technology, Prentice Hall, N. J. (1987)

2) A. C. Metaxas and R. J. Meredith, Industrial Microwave Heating., peter Peregrinus Ltd. (1988).

3) Samuel V. Liao, Fundamentals of Microwave Technology, Wiley &Sons (1986).

4) Von Hippel, A. Dielectrics and Waves, MIT Press, (1954).

5) R. Coehlo, Physics of Dielectrics for the Engineer, Elsevier Publishing Co., Amsterdam, (1979)

6) H. Frolich., Theory of Dielectrics, Clarendon Press, Oxford (1949).

7) L. Onsager, J. Am. Chem. Soc., 58, 1486 (1936).

8) T. A. Johnk, Engineering Electromagnetic Fields and Waves, (1975).

9) A. F. Harvey., Microwave Engineering, Academic Press, New York (1963).

10) J. B. Hasted, Aqueous Dielectrics, Chapman and Hall, London (1973).

11) Ming Chen, Ph. D. Dissertation, VPI&SU (1988).

12) P. Debye, Polar Molecules, Chemical Catalogue, N. Y. (1929).

13) J. C. Maxwell, Electricity and Magnetism, Vol. 1, Clarendon, Oxford, (1892).

14) K. W. Wagner, Arch. Electrotech. 2, 378 (1914).

15) R. W. Sillars, J. Inst. Elect. Engr. 80, 378 (1937).

16) Dielectric Heating, Encyclopaedia of Polymer Science and Engineering, Wiley Interscience Publishers, N. Y. 1985.

17) N. Hill, W. E. Vaughan, A. H. Price and M. Davies, Dielectric Properties and Material Behavior., van Nostrand, N. Y. (1969)

18) A. L. McCLellan, Tables of Experimental Dipole Moments, W. H. Freeman and Co., San Francisco, 1963.

19) J. Aklonis and W. MacKnight, Polymer Viscoelasticity,

20) A. J. Burr, Polymer, 26, 963 (1985).

21) M. V. Volkenstein, Configurational Statistics of Polymer Chains,

22) V. Frossini and E. Butta., Journal of Applied Polymer Science 11, 527 (1967).

23) G. W. Chantry, J. W.Flemming, R. W. Cook, D. G. Moss, E. A. Nichol, H. A. Willis, M. E. A. Cudby, Journal of Infrared Physics 13, 157 (1973).

24) K. Nakagawa and T. Konaka, Polymer, 27, 1553 (1986)

25) Eva-Maria Amrhein, Annals of the New York Academy of Sciences, 179, (1972)

26) E. M. Amrhein, Physics Letters, 29A, 329 (1969).

27) M. Amano and K. Nakagawa, Polymer, 27, 1559 (1986)

28) M. Amano and K. Nakagawa, Polymer 28, 263 (1987).

29) H. F. Huang, Journal of Microwave Power 11(4), 305, (1976).

30) P. J. Hulls, Journal of Microwave Power 17, 29, (1982).

31) R. W. Bruce, MRS Symposium Proceedings, Volume 124, 3, (1988).

32) I. J. Chabinsky, MRS Symposium Proceedings, Volume 124, 17 (1988).

33) R. G. Raj, Polymer Material Science and Engineering, 537, 57 (1987).

34) R. G. Raj, Polymer Material Science and Engineering, 49, 53 (1986).

35) B. Silinski, C. Kuzcymz and A. Gourdenne, European Polymer Journal, 23(4), 273 (1987).

36) I. M. Thullier, H. Jullien and M. F. G. Lousfalot, Polymer Communications 27, 206 (1986).

37) Q. L. Van and A. Gourdenne, European Polymer Journal, 23(10), 777 (1987).

38) N. Beldjoudi, A. Bouazzi, D. Douibi and A. Gourdenne, European Polymer Journal, 24(1), 49 (1988).

39) N. Beldjoudi and A. Gourdenne, European Polymer Journal, 24(1), 53 (1988).

40) N. Beldjoudi and A. Gourdenne, European Polymer Journal, 24(3), 265 (1988).

41) D. A. Lewis, J. C. Hedrick, J. E. McGrath and T. C. Ward, ACS Polymer Preprints 28(2), 330, (1987).

42) J. C. Hedrick, D. A. Lewis, T. C. Ward and J. E. McGrath, ACS Polymer Preprints 29(1), 363, (1988).

43) D. A. Lewis, T. C. Ward, J. D. Summers and J. E. McGrath, ACS Polymer Preprints 29(1), 174, (1988)

44) G. Lyle, J. C. Hedrick, D. A. Lewis, J. S. Senger, D. H. Chen, S. D. Wu and J. E. McGrath, Polyimides: Materials, Chemistry and Characterization, Elsevier Publishers, B. V., Amsterdam (1989).

45) E. Jabbari, M. S. Thesis, VPI&SU, (1989)

46) C. L. Lee, ACS Symposia Series, 107, 45 (1978).

47) H. F. Scharwz, R. G. Bosisio, M. R. Wertheimer and D. Couderc, Journal of Microwave Power, 8(3/4), 303, (1973).

48) H. F. Scharwz, R. G. Bosisio, M. R. Wertheimer and D. Couderc, Rubber Age, 107(11), 27, (1975).

49) R. N. Gedye, F. E. Smith and K. C. Westaway, Canadian Journal of Chemistry, 66(1), 17 (1988).

50) R. K. Iler, The Chemistry of Silica, Wiley, New York, 1979.

51) J. E. McGrath et al, Ultrastructure and Processing of Ceramics

52) I. Artaki, T. W. Zerda and J. Jonas, Journal of Non-Crystalline Solids 81,381 (1986).

53) S. Wallace and L. L. Hench, Materials Research Society Symposia Proceedings 32, 47 (1984).

54) S. H. Wang and L. L. Hench, Materials Research Society Symposia Proceedings 32, 71 (1984)

55) Artaki et al Ultrastructure book in press

56) R. T. Morrison and R. N. Boyd, Organic Chemistry, Allyn and Bacon, Boston, 1966.

57) M. G. Voronkov, V. P. Mileshkevish and Y. A. Yuzhelevski, The Siloxane Bond, (Consultants Bureau, N. Y. 1978)

58) F. A. Carey and R. J. Sundberg, Advanced Organic Chemistry, Plenum, N. Y. 1984.

59) I. Artaki, M. Bradley, T. W. Zerda and J. Jonas, Journal of Physical Chemistry 89, 4399 (1985).

60) A. H. Boonstra, T. N. M. Bernards and J. J. T. Smits, Journal of Non-Crystalline Solids 109, 141 (1989).

61) W. G. Klemperer, V. V. Mainz, S. D. Ramamurthy and F. S. Rosenberg, in Better Ceramics Through CHemistry III, eds, C. J. Brinker, D. E. Clark and D. R. Ulrich, (Mat. Res. Soc., Pittsburgh, Pa., 1988) pp 15 - 24.

62) T. Adachi and S. Sakka, Journal of Materials Science 22, 4407 (1987).

63) M. Nogami and Y. Moriya, Journal of Non-Crystalline Solids 37, 191 (1980)

64) C. J. Brinker, K. D. Keefer, D. W. Schaefer, R. A. Assink, B. D. Kay and C. S. Ashley, Journal of Non-Crystalline Solids, 45, 63 (1984).

65) C. J. Brinker and G. W. Scherer, Sol Gel Science, Academic Press, (1990).

66) I. M. Strawbridge,

67) E. J. A. Pope and J. D. Mackenzie, Journal of Non-Crystalline Solids 198, 101 (1988)

68) C. J. Brinker and G. W. Scherer, Journal of Non-Crystalline Solids 301, 70 (1985).

69) T. A. Witten and L. A. Sander, Physics Review Letters, 47 1400 (1981)

70) J. Zarzycki, M. Prassas and J. Phalippou, Journal of Material Science 17, 3371 (1982)

71) A. Paul, Chemistry of Glasses, Chapman and Hall, N. Y. 1990.

72) G. W. Scherer, Journal of Non-Crystalline Solids, 87, 199 (1986).

73) G. W. Scherer, Journal of Non-Crystalline Solids, 89, 217 (1987).

74) G. W. Scherer, Journal of Non-Crystalline Solids, 91, 83 (1987).

75) G. W. Scherer, Journal of Non-Crystalline Solids, 91, 101 (1987).

76) G. W. Scherer, Journal of Non-Crystalline Solids, 92, 375 (1987).

77) G. W. Scherer, Journal of Non-Crystalline Solids, 99, 122 (1987).

78) G. W. Scherer, Journal of Non-Crystalline Solids, 99, 324 (1987).

79) D. P. Partlow and B. E. Yoldas, Journal of Non-Crystalline Solids 46, 153 (1981).

80) H. Huang and G. L. Wilkes, Polym. Prep. 28(2) 244, (1987)

81) H. Huang, R. H. Glaser and G. L. Wilkes, Macromolecules 20(6), 1322 (1987)

82) H. Huang, and G. L. Wilkes, Polymer Bulletin, 18, 455, (1987)

83) H. Huang, R. H. Glaser, A. B. Brennan, D. E. Rodrigues and G. L. Wilkes, Symposium on Ultrastructure Processing of Materials, Tucson 1989 in press.

84) H. Huang, Ph. D. Dissertation, VPI&SU, (1988).

85) R. H. Glaser, Ph. D. Dissertation, VPI&SU, (1988).

86) R. W. Lenz, Organic Chemistry of Synthetic High Polymers, Interscience Publishers, (1967).

87) J. Asmussen, H. H. LIn, B. Manring and R. Fritz, Rev. Sci. Instrum., 58 (8), 1987, pp. 1477 - 86

88) J. Jow, M. E. Hawley, M. C. Finzel, J. Asmussen, H. H. Lin and B. Manring, IEEE Transactions on Microwave Theory and Techniques, MTT - 35(12), 1987, pp 1435 - 43.

89) K. A. Wikersheim and M. H. Sun, J. Microwave Power, 85 (1987).

90) K. A. Wickersheim and M. H. Sun, Medical Electronics, 84, February (1987).

91) K. A. Wickersheim and M. H. Sun, Reprint from Research and Development, November (1985).

92) O. Kratky and I. Pilz, J. Appl. Cryst.,

93) C. G. Vonk, J. Appl. Cryst., 6, 81 (1973).

94) A. Guinier and G. Fournet in "Small Angle Scattering of Xrays" J. Wiley and Sons Inc. London (1955).

95) O. Glatter and O. Kratky, in "Small Angle Xray Scattering" Academic Press, New York (1982).

96) A. B. Brennan, VPI &SU Dissertation, (1990).

97) C. U. Ko, VPI & SU Dissertation (1988).

98) J. Volger, J. M. Stevels and C. van Amerongen, Philips Res. Rep. 8, 452 (1953).

99) J. M. Stevels, The Glass Industry, 69, 35(2), (1954).

100) J. M. Stevels, The Glass Industry, 135, 35(3) (1954).

101) K. A. Mauritz and R. M. Warren, Macromolecules 22 (1989) 1730.

102) G. A. York, VPI & SU Dissertation, (1990).

103) P. Dreyfuss, Polytetrahydrofuran, POLYMER MONOGRAPHS, Vol. 8, Gordon and Breach Science Publishers, NY. (1982).

104) B. Wang and G. L. Wilkes, J. Polym. Sci., Polym. Lett., submitted for publication.

105) C. S. Parkhurst, W. F. Doule, L. A. Silverman, S. Singh, M. P. Anderson, D. McClurg, G. E. Wnek and D. R. Ulhmann, Better Ceramics Through Chemistry II, eds C. J. Brinker, D. E. Clark and D. R. Ulrich (Mat. Res. Soc. Pittsburgh, Pa 1986) 769.

106) B. E. Read, Transactions of the Faraday Society, 61, (1965).

107) R. E. Wetton and G. Williams, Transactions of the Faraday Society, 61, 2132, (1965).

108) Polyethylene, Encyclopaedia of Polymer Science and Engineering, Wiley Interscience Publishers, 1985.

109) R. W. Sillars, Journal of the Institute of Electrical Engineers 80, 378 (1937).

110) Bergna and Simpko, in article by K. D. Keefer in Science of Ceramic Chemical Processing, eds. L. L. Hench and D. R. Ulrich (Wiley, New York, 1986).

111) P. C. Hiemenz, Polymer Chemistry, Marcal and Dekker, N. Y. (1984).

112) K. D. Keefer in Better Ceramics Through Chemistry II, eds. C. J. Brinker, D. E. Clark, and D. R. Ulrich (Mat. Res. Soc. Pittsburgh, Pa.)

113) K. D. Keefer in Science of Ceramic Chemical Processing, eds. L. L. Hench and D. R. Ulrich (Wiley, New York, 1986).

114) J. E. Martin and A. J. Hurd, J. Appl. Cryst., 20, (1987) 61.

115) L. E. Alexander, Xray Diffraction Methods in Polymer Science, Robert E. Krieger Publishing Co, Fl (1985).

116) A. Guinier, Ann. Phys. (Paris), 12, 161 (1939).

117) P. Meakin in On Growth and Form, eds., H. E. Stanley and N. Ostrowsky, Martinus-Nijhoff, (1986).

118) L. W. Kelts, N. J. Effinger and S. M. Melpolder, J. Non-Cryst. Solids, 83, (1986) 353.

119) D. W. Schaefer, MRS Bulletin, 8, (1988) 22.

120) P. W. Schmidt, J. Appl. Cryst., 15 (1982) 567.

The author David E. Rodrigues was born in India on the 7th of July 1961. He graduated from B. V. B. Engineering College, India, following which he worked as a quality control engineer in a valve manufacturing firm for one year. He completed his Masters in Materials Engineering at VPI&SU in 1987 and started working towards his Ph. D. immediately afterwards. He will be working on a post doctorate for a couple years and then hopes to find a faculty position in a University in the U. S. A.